WOMEN IN HEPATO PANCREATIC BILIARY (HPB) TUMORS: 2021, VOLUME I

EDITED BY: Nadia M. Hamdy and Bhawna Sirohi
PUBLISHED IN: Frontiers in Oncology

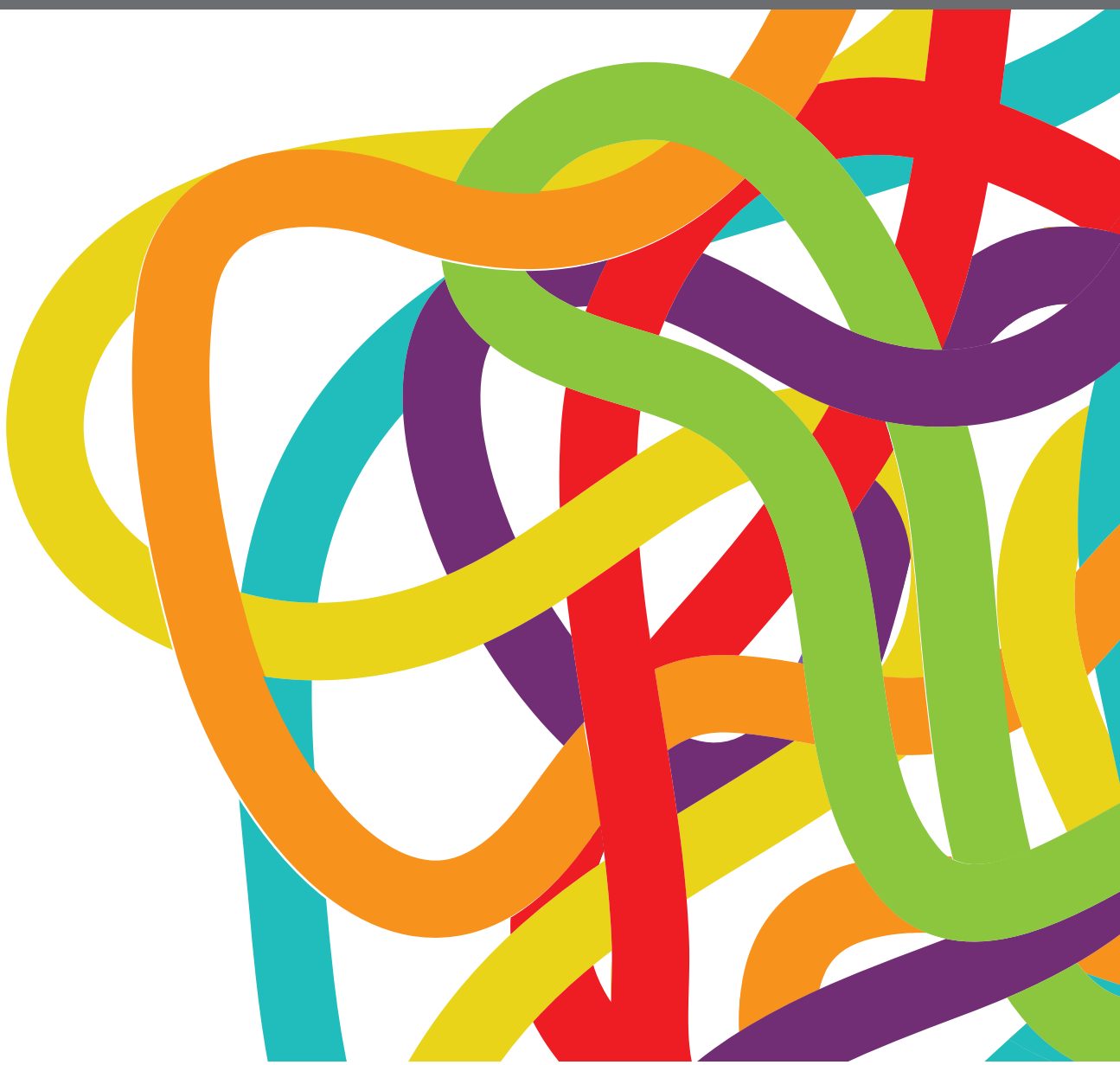

frontiers Research Topics

ISSN 1664-8714
ISBN 978-2-88976-600-0
DOI 10.3389/978-2-88976-600-0

About Frontiers

Frontiers is more than just an open-access publisher of scholarly articles: it is a pioneering approach to the world of academia, radically improving the way scholarly research is managed. The grand vision of Frontiers is a world where all people have an equal opportunity to seek, share and generate knowledge. Frontiers provides immediate and permanent online open access to all its publications, but this alone is not enough to realize our grand goals.

Frontiers Journal Series

The Frontiers Journal Series is a multi-tier and interdisciplinary set of open-access, online journals, promising a paradigm shift from the current review, selection and dissemination processes in academic publishing. All Frontiers journals are driven by researchers for researchers; therefore, they constitute a service to the scholarly community. At the same time, the Frontiers Journal Series operates on a revolutionary invention, the tiered publishing system, initially addressing specific communities of scholars, and gradually climbing up to broader public understanding, thus serving the interests of the lay society, too.

Dedication to Quality

Each Frontiers article is a landmark of the highest quality, thanks to genuinely collaborative interactions between authors and review editors, who include some of the world's best academicians. Research must be certified by peers before entering a stream of knowledge that may eventually reach the public - and shape society; therefore, Frontiers only applies the most rigorous and unbiased reviews.
Frontiers revolutionizes research publishing by freely delivering the most outstanding research, evaluated with no bias from both the academic and social point of view. By applying the most advanced information technologies, Frontiers is catapulting scholarly publishing into a new generation.

What are Frontiers Research Topics?

Frontiers Research Topics are very popular trademarks of the Frontiers Journals Series: they are collections of at least ten articles, all centered on a particular subject. With their unique mix of varied contributions from Original Research to Review Articles, Frontiers Research Topics unify the most influential researchers, the latest key findings and historical advances in a hot research area! Find out more on how to host your own Frontiers Research Topic or contribute to one as an author by contacting the Frontiers Editorial Office: frontiersin.org/about/contact

WOMEN IN HEPATO PANCREATIC BILIARY (HPB) TUMORS: 2021, VOLUME I

Topic Editors:
Nadia M. Hamdy, Ain Shams University, Egypt
Bhawna Sirohi, Apollo Proton Cancer Centre, India

Citation: Hamdy, N. M., Sirohi, B., eds. (2022). Women in Hepato Pancreatic Biliary (HPB) Tumors: 2021, Volume I. Lausanne: Frontiers Media SA.
doi: 10.3389/978-2-88976-600-0

Table of Contents

frontiers | Frontiers in Oncology

EDITORIAL
published: 23 June 2022
doi: 10.3389/fonc.2022.927775

Editorial: Women in Hepato Pancreatic Biliary (HPB) Tumors: 2021, Volume I

Nadia M. Hamdy[1], Yuming Jiang[2], Sumit Sahni[3], Wenchuan Wu[4], Yuelun Zhang[5], Bhawna Sirohi[6] and Jiang Chen[7]*

[1] Department of Biochemistry and Molecular Biology, Faculty of Pharmacy, Ain Shams University, Cairo, Egypt, [2] Radiation Oncology Department, Stanford University, Stanford, CA, United States, [3] Kolling Institute of Medical Research, Royal North Shore Hospital, Sydney, NSW, Australia, [4] Department of General Surgery, Zhongshan Hospital, Fudan University, Shanghai, China, [5] Medical Research Center, Peking Union Medical College Hospital, Chinese Academy of Medical Sciences and Peking Union Medical College, Beijing, China, [6] Apollo Proton Cancer Centre, Chennai, India, [7] Department of General Surgery, Sir Run-Run Shaw Hospital, Zhejiang University, Hangzhou, China

Keywords: women in oncology, Hepato-pancreatic biliary cancer, HPB tumors, HCC, pancreatic cancer, cholangiocarcinoma

Editorial on the Research Topic:

Women in HPB Tumors: 2021

OPEN ACCESS

Edited and reviewed by:
Khurum Hayat Khan, University College London, United Kingdom

****Correspondence:***
Nadia M. Hamdy
nadia_hamdy@pharma.asu.edu.eg

Specialty section:
This article was submitted to Gastrointestinal Cancers: Hepato Pancreatic Biliary Cancers, a section of the journal Frontiers in Oncology

Received: *25 April 2022*
Accepted: *09 May 2022*
Published: *23 June 2022*

Citation:
Hamdy NM, Jiang Y, Sahni S, Wu W, Zhang Y, Sirohi B and Chen J (2022) Editorial: Women in Hepato Pancreatic Biliary (HPB) Tumors: 2021, Volume I. Front. Oncol. 12:927775. doi: 10.3389/fonc.2022.927775

This editorial presents the inaugural Frontiers in Oncology 'Women in HPB Tumors" series of article collections. The Research Topic collection highlights the diversity of research performed across the entire breadth of oncology research by women scientists pursuing STEM careers. Research articles published under this Research Topic aimed to present advances in theory, experiment, and methodology, with applications to compelling problems related to hepato pancreatic biliary cancers.

Exploring the tumor-immune interactions in the tumor microenvironment (TME) and identifying new prognostic and therapeutic biomarkers will assist in decoding the novel mechanism of tumor immunotherapy.

Clinical and *in vitro* work was done by authors contributing to articles published in the Research Topics using serum for ELISA, comet assay, qRT-PCR, IHC, Western, and genotyping, performed using allelic discrimination and confirmed by sequencing, or using various cancer cell lines followed by microscopy, assays for MTT, migration, colony and sphere formation, qRT-PCR, FACS, Western blot, tissue microarray, IHC and bioinformatics, and *in silico* analysis using the online databases.

The works explored by the research articles were based on *in-silico* and advanced bioinformatics analysis for evaluation of targets by The Cancer Genome Atlas (TCGA), which is a publicly available online database (https://www.cancer.gov/about-nci/organization/ccg/research/structural-genomics/tcga).

The freely available online database resource KEGG (Kyoto Encyclopedia of Genes and Genomes (https://www.genome.jp/kegg/) was used for the selection of relevant biological functions and pathways with enrichment scores of $P<0.05$, and the liver hepatocellular carcinoma (LIHC) dataset was downloaded from the Broad Institute TCGA Genome Data Analysis Center, https://doi.org/10.7908/C11G0KM9.

Also, STRING database (http://string-db.org) was utilized to construct PPI networks of coexpressed genes with interaction scores > 0.4. For visualization, CytoHubba, a plugin from the open-source platform Cytoscape (version 3.8.2) (http://www.cytoscape.org/), was employed to analyze and calculate the network structure.

Several concepts have been demonstrated or proved in the published articles (i) standard-of-care diagnostic biopsies and (ii) personalized therapy, and more.

HCC was addressed in 5 articles, while one presented colorectal cancer, however, pancreatic cancer was studied in 4 articles, by 89 authors.

The emerging importance of cancer personalized treatment plans is addressed in 3 research articles. As each human tumor creates its own unique microenvironment, He et al. claimed that assessment of BGN expression represents a promising approach for identifying patients with the greatest potential to benefit from immunotherapy and is a new venture into personalized therapy for colon cancer patients. BGN (a typical extracellular matrix (ECM) protein, validated as a signaling molecule regulating multiple processes of tumorigenesis), could serve as a valid biomarker for diagnosis, prognosis, and immunotherapy response prediction in patients with colon cancer.

Lundy et al.'s study demonstrates proof-of-principle feasibility to molecularly screen patients with pancreatic ductal adenocarcinoma for targeted therapies, and confirms diagnostic endoscopic ultrasound-guided fine-needle aspiration (EUS-FNA) biopsies. Single agent panitumumab was safe and tolerable but led to no objective tumor responses in the population tested.

In another study, Ren et al. revealed the clinicopathological features and identified risk factors of prognosis among patients with pancreatic cancer bone metastasis (PCBM), to be six independent predictors of prognosis, including age, pathological type, chemotherapy, liver metastasis, lung metastasis, and marital status. Knowledge of these survival predictors is helpful for clinicians to accelerate clinical decision process and design personalized treatment for patients with PCBM.

The crucial role of non-coding microRNAs (miRNAs) in pathogenesis of different diseases, including cachexia of strong pro-inflammatory environments, occurring in pancreatic and non-small cell lung cancer patients, was studied by Yehia et al. Where high levels of miR-155 in the cachectic group lead to negative feedback inhibition of both SOCS1 and the transcription factor Foxp3 in both the pancreatic and NSCL cancer patients.

Studies are also included on the roles of exosomes (Exo) in cancer development *via* mediating communication between tumor and its microenvironment. Hedgehog ligands undergo complicated post-translational modifications that result in lipid attachment and multimerization. Mutations in Hedgehog pathway components or induced Hedgehog signaling pathway components including Shh are found during injury or severe stress, or HBV or HCV infection and in HCC, as Li et al.'s group studied. They found higher plasma cancer cell-derived Exo-Shh levels associated with higher recurrence, suggesting Exo-Shh could serve as a prognostic biomarker and points to the possibility of tumor-secreted exosome being a therapeutic target.

As the demand for potential molecular biomarker(s) that can effectively predict prognosis and progression of HCC has increased, Ouyang et al. studied the anti-silencing function 1B (ASF1B) expression and function in HCC. They provided multi-level evidence for the significance of oncogenic gene *ASF1B* in HCC development and could be a target for inhibiting HCC cell growth, *via* inducing apoptosis and cell cycle arrest, reduced the expression of proliferating cell nuclear antigen (PCNA), cyclinB1, cyclinE2 and CDK9. These findings proposed a potential target for the development of anti-cancer strategies in HCC.

One of the major risk factors for HCC is hepatitis C virus (HCV) infection. The epithelial cell adhesion molecule (EpCAM) is a stem cell marker involved in the tumorigenesis and progression of many malignancies, including HCC, and was studied by Motawi et al. Serum EpCAM levels may hold promise for HCC diagnosis and for improving the diagnostic accuracy of α-fetoprotein.

Currently, there is a lack of tumor-selective and efficacious therapies for HCC. Zhao et al. studied the effect of the new chemotherapeutic agent β-Lapachone (β-lap; ARQ761 in clinical form) as a novel NADPH:quinone oxidoreductase 1 (NQO1) bioactivatable drug, selectively kills HCC cells expressing NQO1, through inducing ROS and PAR formation, NAD^+ and ATP depletion and lethal DNA damage. High *NQO1:CAT* ratios in HCC tumors but low ratios in normal tissues offer an optimal therapeutic window and an ideal therapeutic target for β-lap.

Jin et al. studied the role of response to antiviral therapies on survival of patients with intermediate-stage HBV-related HCC undergoing transarterial chemoembolization (TACE). They proved the importance of regular HBV DNA surveillance and durable viral suppression during antiviral treatment.

Finally, Bai et al. studied the combination of the well-tolerated modalities tumor treating fields (TTFields) with mild hyperthermia of 38.5°C, as a novel supporting therapy combination for pancreatic cancer, more effective than each single treatment, with greater efficacy results without increased toxicity.

Great potential and efforts in cancer prognosis and therapeutics still need to be worked on. Therefore, we still need to do more and more research for efficient predictive and prognostic molecular-biomarkers. Moreover, we still need to address (epi)genetic profiling for precision medicine implementation, and (epi)genetic new novel potential targets identification and characterization for cancer treatment and/or control. Let us move ahead with drug design and discovery as well as drug repurposing for HPB tumors, with special emphasis on nano-bio-medicine.

AUTHOR CONTRIBUTIONS

NMH was an associate editor of the Research Topic and wrote the paper text. YJ, SS, WW, YZ are guest associate editors for FIO and acted as editor for one paper in the Research Topic. BS was co-associate editor of the Research Topic. JC is a guest associate editor for FIO and acted as editor for two papers in the Research Topic. All authors contributed to the article and approved the submitted version.

ACKNOWLEDGMENTS

We thank authors of the papers published in this research topic for their valuable contributions and the referees for their rigorous review. We also thank the editorial board of the Frontiers in Oncology j. Gastrointestinal Cancers: Hepato Pancreatic Biliary Cancers section, for their support.

Conflict of Interest: The authors declare that the research was conducted in the absence of any commercial or financial relationships that could be construed as a potential conflict of interest.

Publisher's Note: All claims expressed in this article are solely those of the authors and do not necessarily represent those of their affiliated organizations, or those of the publisher, the editors and the reviewers. Any product that may be evaluated in this article, or claim that may be made by its manufacturer, is not guaranteed or endorsed by the publisher.

frontiers in Oncology

ORIGINAL RESEARCH
published: 05 October 2021
doi: 10.3389/fonc.2021.747282

β-Lapachone Selectively Kills Hepatocellular Carcinoma Cells by Targeting NQO1 to Induce Extensive DNA Damage and PARP1 Hyperactivation

Wenxiu Zhao[1,2†], Lingxiang Jiang[1†], Ting Fang[2], Fei Fang[2], Yingchun Liu[3], Ye Zhao[3], Yuting You[2], Hao Zhou[1], Xiaolin Su[3], Jiangwei Wang[1], Sheng Liu[4], Yaomin Chen[5], Jun Wan[4,6] and Xiumei Huang[1]*

[1] Department of Radiation Oncology, Melvin and Bren Simon Comprehensive Cancer Center, Indiana University School of Medicine, Indianapolis, IN, United States, [2] Fujian Provincial Key Laboratory of Chronic Liver Disease and Hepatocellular Carcinoma, Zhongshan Hospital, Xiamen University, Xiamen, China, [3] Departments of Biochemistry and Molecular Biology, Melvin and Bren Simon Comprehensive Cancer Center, Indiana University School of Medicine, Indianapolis, IN, United States, [4] Department of Medical and Molecular Genetics, Indiana University School of Medicine, Indianapolis, IN, United States, [5] Indiana University Health Pathology Laboratory, Indiana University School of Medicine, Indianapolis, IN, United States, [6] Center for Computational Biology and Bioinformatics, Indiana University, School of Medicine, Indianapolis, IN, United States

Hepatocellular carcinoma (HCC) is the second leading cause of cancer-related death globally. Currently there is a lack of tumor-selective and efficacious therapies for hepatocellular carcinoma. β-Lapachone (ARQ761 in clinical form) selectively kill NADPH: quinone oxidoreductase 1 (NQO1)-overexpressing cancer cells. However, the effect of β-Lapachone on HCC is virtually unknown. In this study, we found that relatively high NQO1 and low catalase levels were observed in both clinical specimens collected from HCC patients and HCC tumors from the TCGA database. β-Lapachone treatment induced NQO1-selective killing of HCC cells and caused ROS formation and PARP1 hyperactivation, resulting in a significant decrease in NAD^+ and ATP levels and a dramatic increase in double-strand break (DSB) lesions over time *in vitro*. Administration of β-Lapachone significantly inhibited tumor growth and prolonged survival in a mouse xenograft model *in vivo*. Our data suggest that NQO1 is an ideal potential biomarker, and relatively high *NQO1:CAT* ratios in HCC tumors but low ratios in normal tissues offer an optimal therapeutic window to use β-Lapachone. This study provides novel preclinical evidence for β-Lapachone as a new promising chemotherapeutic agent for use in NQO1-positive HCC patients.

Keywords: beta-lapachone, NQO1, hepatocellular carcinoma, DNA damage/reactive oxygen species, NAD^+/ATP depletion

OPEN ACCESS

Edited by:
Wenchuan Wu,
Fudan University, China

Reviewed by:
Haijie Hu,
Sichuan University, China
Mi Deng,
Peking University, China

****Correspondence:***
Xiumei Huang
xiuhuang@iu.edu

†These authors have contributed equally to this work and share first authorship

Specialty section:
This article was submitted to Gastrointestinal Cancers: Hepato Pancreatic Biliary Cancers, a section of the journal Frontiers in Oncology

Received: *26 July 2021*
Accepted: *16 September 2021*
Published: *05 October 2021*

Citation:
Zhao W, Jiang L, Fang T, Fang F, Liu Y, Zhao Y, You Y, Zhou H, Su X, Wang J, Liu S, Chen Y, Wan J and Huang X (2021) β-Lapachone Selectively Kills Hepatocellular Carcinoma Cells by Targeting NQO1 to Induce Extensive DNA Damage and PARP1 Hyperactivation. Front. Oncol. 11:747282. doi: 10.3389/fonc.2021.747282

INTRODUCTION

As the most common primary liver cancer and the second leading cause of cancer-related deaths worldwide (1), hepatocellular carcinoma (HCC) patients are usually diagnosed with advanced disease, resulting in only 15% of HCC patients being eligible for surgical resection or liver transplantation and the median survival time for HCC patients in intermediate to advanced stages being only 1-2 years (2). Moreover, chemotherapy against HCC has limited benefits because of the high resistance to currently available chemotherapeutic agents. Sorafenib, the first-line drug used for patients with advanced HCC, has been used for over 10 years, but the overall outcomes are unsatisfactory (3). These have led to more extensive research focusing on personalized medicine with increased selectivity and efficacy.

A growing body of data demonstrates that NADPH:quinone oxidoreductase 1 (NQO1), a phase II two-electron reductase that can bioactivate certain quinone molecules and shows a protective effect against natural and exogenous quinones, is abnormally upregulated in many solid cancers, such as lung, pancreatic, breast, prostate, and colon cancers (4–11). In liver cancer, it has been reported that NQO1 was increased 18-fold in HCC versus normal livers (12). Recently, NQO1 overexpression was reported to be a potent independent biomarker for prognostic evaluation of HCC (13) and enhanced apoptosis inhibition of liver cancer cells *via* the SIRT6/AKT/XIAP signaling pathway (14, 15). NQO1 overexpression in tumors has the advantage of preferentially killing cancer cells and sparing normal cells when anticancer drugs that are bioreductively activated by NQO1, such as β-Lapachone (β-lap), are used (5).

β-lap has gained increasing attention for its tumor-selective and antitumor effects in many cancers, including lung cancer, breast cancer, prostate cancer, pancreatic cancer, and leukemia (4–7, 9–11, 16, 17). Its toxicity is closely correlated with NQO1 expression and activity. Our studies suggest that NQO1 metabolizes β-lap through a futile redox cycle in which β-lap is converted into a highly unstable hydroquinone form and then spontaneously reacts with oxygen to revert back to the parent compound, causing rapid NAD(P)H oxidation. This process generates high levels of reactive oxygen species (ROS) (e.g., H_2O_2), resulting in genomic instability and DNA damage (6, 11). In addition, catalase (*CAT*) can bypass β-lap toxicity by neutralizing hydrogen peroxide produced by β-lap (18). We have previously reported that β-lap alone or combined with other inhibitors had profound toxicity in pancreatic cancer and non-small-cell lung cancer (NSCLC) (11, 19–21). However, the effect of β-lap on HCC is virtually unknown.

Here, we demonstrate that HCC patient samples have significantly elevated levels of NQO1 but concomitantly low catalase levels compared with associated normal tissues. HCC cells were efficiently killed by β-lap, along with increases in ROS production and PARP1 hyperactivation, severe NAD^+/ATP depletion and DNA damage. NQO1-dependent HCC killing was confirmed in HCC cells with stable NQO1 overexpression and knockout. Furthermore, a human HCC subcutaneous xenograft mouse model exhibited efficient β-lap-induced control of tumor growth and prolonged mouse survival.

Abbreviations: HCC, hepatocellular carcinoma; β-lap, β-Lapachone; NQO1, NADPH:quinone oxidoreductase 1; *CAT*, catalase; TCGA, The Cancer Genome Atlas; DSB, double-strand break; ROS, reactive oxygen species; NSCLC, non-small-cell lung cancer; H_2O_2, Hydrogen peroxide; DIC, dicoumarol; PAR, poly (ADP-ribosyl)ated protein; NOD/SCID, nonobese diabetic/severe combined immunodeficiency; LIHC, liver hepatocellular carcinoma.

MATERIALS AND METHODS

Human HCC Cell Lines and Clinical Samples

Human HCC cell lines (SNU-182, PLC/PRF/5, Huh7, Hep3B, HepG2, and Li7) were purchased from Guangzhou Cellcook Biotechnology Co., Ltd. (Guangzhou, China), and PLC/PRF/5 and SK-HEP1 cells were purchased from ATCC. The authentication of these cell lines was performed *via* comparisons with the STR database. Cells were cultured in Dulbecco's modified Eagle's medium (DMEM) supplemented with 10% fetal bovine serum (FBS; HyClone), 100 U/ml penicillin, and 100 U/ml streptomycin at 37°C and 5% CO_2.

Reagents and Chemicals

β-lap, synthesized by Dr. Bill Bornmann (M.D. Anderson, Houston, TX) was dissolved in DMSO for *in vitro* experiments or 20% HPβCD for *in vivo* experiments, and the concentrations were verified by spectrophotometry. Hydrogen peroxide (H_2O_2) and dicoumarol (DIC) were purchased from Sigma-Aldrich. HPβCD (>98% purity) was purchased from Cydodextrin Technologies Development, Inc. The ROS-Glo™ H_2O_2 assay kit, NAD/NADH-Glo kit, and CellTiter-Glo® 2.0 kit for the ATP assay were obtained from Promega Corporation. An alkaline comet assay kit was purchased from Trevigen, Inc.

NQO1 Knockout/Knockin Cells

CRISP/Cas9 NOQ1 knockout PLC/PRF/5 cells and NQO1-overexpressing SK-HEP1 cells were generated by our lab. Vectors of guide RNA sensing human NQO1 or nontarget control (LV04) and Cas9 expression (CAS9NEO) were provided by Sigma-Aldrich, and the guide RNA targeting sequences were AGGATACTGAAAGTTCGCAGGG and CACAATATCTGG GCTCAGATGG. Vectors with NQO1 or empty control (EX-Z0563-Lv205, EX-NEG-Lv205) were purchased from Sigma-Aldrich, and transfection of SK-HEP1 with these vectors was performed with Lipofectamine 3000 reagent (Thermo Fisher) according to the manufacturer's protocol.

Cell Survival Assay

A total of 10,000 cells/well were seeded on 48-well plates 24 h prior to treatment. Varying doses of β-lap dissolved in DMSO ± DIC were added and incubated for 2 h at 37°C and 5% CO_2. After treatment, the media were replaced with fresh complete media and allowed to grow for 7 days. After 7 days, the cells were washed with 1x PBS, 200 µl of H_2O was added, and the cells were frozen at -80°C for at least 2 h. After thawing, 200 µl/well TNE

buffer (50 mM Tris–HCl (pH 7.4), 100 mM NaCl, 0.1 mM EDTA) with 1 μg/ml Hoechst 33258 was added and incubated for 1 h at room temperature in the dark. Cell growth was determined by absorbance at 560 nM with a multilabel plate reader (PerkinElmer). Percentage of cell growth = (100× (cell experimental – blank)): (cell control).

Antibodies

Antibodies used for immunofluorescence and western blotting included NQO1 (A180, Santa Cruz, La Jolla, CA), PARP1 (F-2, Santa Cruz), β-actin (C4, Santa Cruz), α-tubulin (B-7, Santa Cruz), PAR (Trevigen, Gaithersburg, MD), γH2AX (JBW301, Millipore, Temecula, CA), H2AX (938CT5.1.1, Cell Signaling, Danvers, MA), and catalase (12980S, Cell Signaling, MA).

Western Blotting Analysis

Cells were seeded on plates at approximately 70% confluence 24 h in advance and then treated with/without β-lap for 2 h. Next, the cells were lysed in lysis buffer. Approximately 40 μg of protein was resolved by SDS-PAGE, transferred onto PVDF membranes, and probed with antibodies. The protein-antibody complexes were detected by using Super Signal West Femto Substrate (Thermo Fisher, Waltham, MA) and exposure to film.

Real-Time PCR

Assays were performed as previously described (22). The primer sequences were as follows: GAPDH-sense: 5'-CTGCTGATG CCCCCATGTTC-3'; GAPDH- antisense: 5'-CATCCACAGTC TTCTGGGTGG-3'; NQO1-sense: 5'-GCCATGTATGAC AAAGGA CCC-3'; NQO1-antisense: 5'-ACTTGGAAGCC ACAGAAATGC-3'; CAT-sense: 5'-CTTCGACCCAAG CAACATGC-3'; CAT-antisense: 5'-GCGGTGAGTGTC AGGATA GG-3'. $2^{-\Delta\Delta Ct}$ was used to calculate the fold change of mRNA expression.

NQO1 and Catalase Activity Assays

Extracts were obtained from different HCC cell lines. Then NQO1 and catalase enzyme activities were assayed by NQO1 Activity Assay (Abcam) and CheKine™ catalase Activity Assay Kit (Abbkine), respectively, according to the manufacturer's manual.

ATP, NAD^+ and Hydrogen Peroxide (H_2O_2) Assays

Cells were cultured (1×10^4 cells/well) 24 h in advance in 96-well white-walled clear-bottom tissue culture plates (Sigma) and treated with β-lap with or without DIC for 2 h. Then, ATP (CellTiter-Glo), hydrogen peroxide (H_2O_2) (ROS-Glo), and NAD/NADH (NAD/NADH-Glo) were assayed at the indicated time points after treatments using specific assays (Promega).

Comet Assay

Total DNA damage was measured by the alkaline comet assay (Trevigen) according to the manufacturer's manual. Slides were stained with SYBR green, and images were acquired with a Leica DM5500 fluorescence microscope. Comet tail lengths were quantified by NIH ImageJ.

Immunofluorescence Staining of γH2AX

The treated cells were fixed with 4% paraformaldehyde for 30 min, permeabilized with 0.2% Triton-X 100 for 10 min at 4°C, blocked with 3% bovine serum albumin for 30 min at room temperature, and incubated overnight at 4°C with γH2AX antibody (diluted at 1:1000). Cells were washed 3 times for 5 min in PBS and then incubated for 2 h with AlexaFluor secondary antibody (diluted 1:1000 in blocking buffer). DAPI was used to stain nuclei. γH2AX foci were visualized with a laser scanning confocal microscope (LSM 510 Meta), and the number of H2AX foci per nucleus was quantified.

In Vivo Antitumor Study

All animal procedures were approved by the IU IACUC committee. For the *in vivo* xenograft model, PLC/PRF/5 cells (5×10^6) were subcutaneously inoculated into the right flank of nonobese diabetic/severe combined immunodeficiency (NOD/SCID) male mice (6~8 weeks old). Tumor volumes were measured with a caliper and calculated by the formula $0.5\times\text{length}\times\text{width}^2$. When tumor volumes reached ~150 mm^3, mice were randomly divided into vehicle (n=7) and treatment (n=8) groups with no significant differences in tumor sizes. Then, the mice were treated with HPβCD or HPβCD-β-lap (12.5 mg/kg) by intratumor injection every other day for a total of five injections. When the tumor volume reached ~1200 mm^3, the mice were sacrificed, and a survival curve was plotted.

Bioinformatic Analysis

The liver hepatocellular carcinoma (LIHC) dataset was downloaded from the Broad Institute TCGA Genome Data Analysis Center, https://doi.org/10.7908/C11G0KM9. Only samples with both tumor and matched normal samples were selected for further analysis of *NQO1* and *CAT* levels. The differences in gene expression levels for individual genes or fold changes of two genes between normal and tumor tissues were identified by paired t test.

Statistical Analysis

All the experimental results were analyzed using two-tailed Student's *t* tests for independent measures with Holm-Sidak correction for multiple comparisons if >1 comparison was performed. The minimum replicate size for experiment was n=3. Statistical analysis were performed in GraphPad Prism 8 (GraphPad Software, Inc. CA, USA). Images are representative of the results of experiments or staining repeated 3 times. Data are presented as the mean ± SD. The survival rate was analyzed by Kaplan-Meier survival curves. A p value of < 0.05 was considered statistically significant between the compared groups. $^*p < 0.05$; $^{**}p < 0.01$ and $^{***}p < 0.001$.

RESULTS

High Expression of NQO1 in Hepatocellular Carcinoma Patients

Our previous studies and other reports have shown that NQO1 enzyme levels were elevated, whereas catalase (gene: *CAT*) levels

were lower in NSCLC and pancreatic cancers than in associated normal tissues, suggesting that the *NQO1*/*CAT* ratios in tumor tissue versus associated normal tissue are an important and highly exploitable therapeutic window (8, 11, 23). To investigate whether the *NQO1:CAT* ratios are a potential therapeutic window in liver cancer, we analyzed *NQO1* and *CAT* expression in liver hepatocellular carcinoma (LIHC) from The Cancer Genome Atlas (TCGA). Our analysis revealed that the mRNA levels of *NQO1* were significantly elevated (**Figure 1A**, $p = 1.5\times10^{-7}$), while *CAT* levels were notably lower (**Figure 1B**, $p = 7.8\times10^{-8}$) in tumor tissues than in matched normal tissues. Consistently, markedly higher *NQO1:CAT* ratios were observed in these tumor samples than in normal samples (**Figure 1C**, $p = 1.5\times10^{-9}$). Moreover, we also found that patients with high NQO1 expression had a significantly lower overall survival rate than those with low *NQO1* expression (**Figure 1D**, $p = 0.0075$). Together, these results indicate that the *NQO1:CAT* ratio is an ideal therapeutic window in liver cancer for *NQO1* bioactivatable drugs.

Elevation of NQO1 Expression and Enzyme Activity in Hepatocellular Carcinoma Patients and Cell Lines

To further confirm the above observations, we collected 62 pairs of clinical HCC patient samples and associated normal tissues to detect the mRNA levels of *NQO1* and *CAT*. Indeed, 69.4% (43/62) of HCC patient samples showed relatively higher *NQO1* mRNA levels than associated normal tissues (p = 0.0005, **Figure 2A**). In contrast, notably lower *CAT* mRNA levels (54/62 = 87.0%, $p < 0.0001$, **Figure 2B**) were observed in tumor tissues than in associated normal tissues. Concomitant high *NQO1* and low *CAT* mRNA levels (high NQO1:CAT ratios (**Figure 2C**, $p < 0.0001$) in HCC tumor tissue offer an ideal target for NQO1 bioactivatable drugs. Consistently, our western blotting analysis revealed that NQO1 protein levels were obviously elevated in 43.8% (28/64) of HCC tumor tissues, while catalase levels were repressed significantly in most HCC tumor tissues (**Figure 2D** and **Supplementary Figures S1A, B**). These results confirm our above observations that the relatively high *NQO1:CAT* ratios in HCC patients might be an exploitable therapeutic target in liver cancer. On the other hand, similar to the analysis in HCC patient samples, we observed that the liver cancer cell lines HepG2, Huh7 and Li7 showed high NQO1 levels; PLC/PRF/5 cells exhibited moderate NQO1 expression; and Hep3B, SNU-182, and SK-HEP1 cells expressed low or undetectable NQO1 (**Figure 2E**). Consistently, the NQO1 enzyme activity assay exhibited similar NQO1 activity in these cell lines (**Figure 2F**). Meanwhile, relatively high catalase protein levels accompanied by relative high catalase enzyme activities were observed in HepG2, Huh7 and Hep3B liver cancer cells (**Figures 2E, G**).

Selective and Effective Killing of Hepatocellular Carcinoma Cells by β-Lapachone

It has been reported that NQO1 is a promising therapeutic target in multiple solid tumors, and the anticancer efficacy of β-lap is mainly mediated and promoted by NQO1 (7, 11, 17). Based on our above findings, we hypothesized that β-lap could effectively control cell growth in NQO1$^+$ HCC cells. To this end, we treated

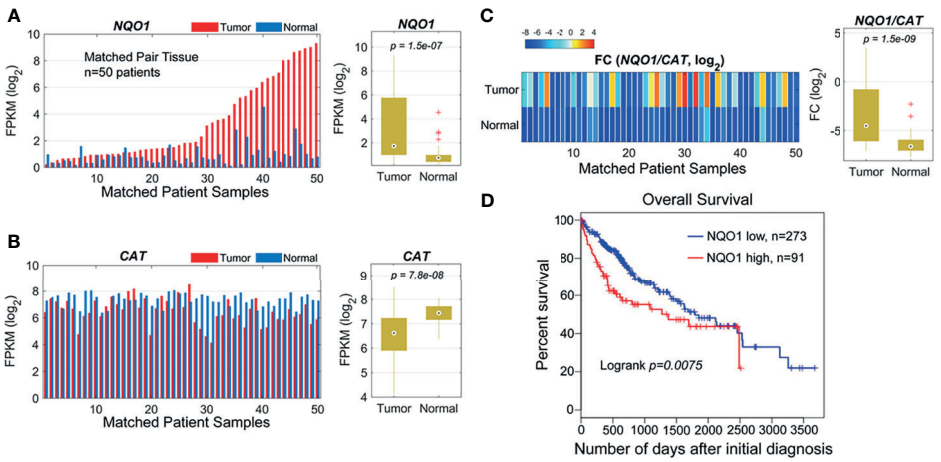

FIGURE 1 | NQO1 and CAT expression profile in matched hepatocellular carcinoma patient samples (n = 50) in the TCGA cohort. **(A)** Left panel: NQO1 mRNA levels (FPKM, in $\log_2$ scale) in paired HCC tumor and normal liver tissues. The samples were sorted by NQO1 expression levels in tumors. Right panel: Distributions of FPKMs of NQO1 in liver tumor and normal tissues. **(B)** CAT gene expression in tumor and normal tissues (left panel) and FPKM distributions (right panel). **(C)** Left panel: The gene expression difference between two genes, NQO1 and CAT (fold change, FC, in $\log_2$ scale), for tumor and normal tissues, respectively. Right panel: Distributions of FCs in tumor and normal tissues. The orders of samples in **(B, C)** were exactly matched with that in **(A)**. **(A–C)** patient samples are 50 total. **(D)** Kaplan-Meier survival analysis of all HCC patients (low NQO1, N=273; high NQO1, n=91) according to NQO1 mRNA expression in the TCGA database. Days to death: the number of days from the date of the initial pathological diagnosis to the date of death for the case in the investigation.

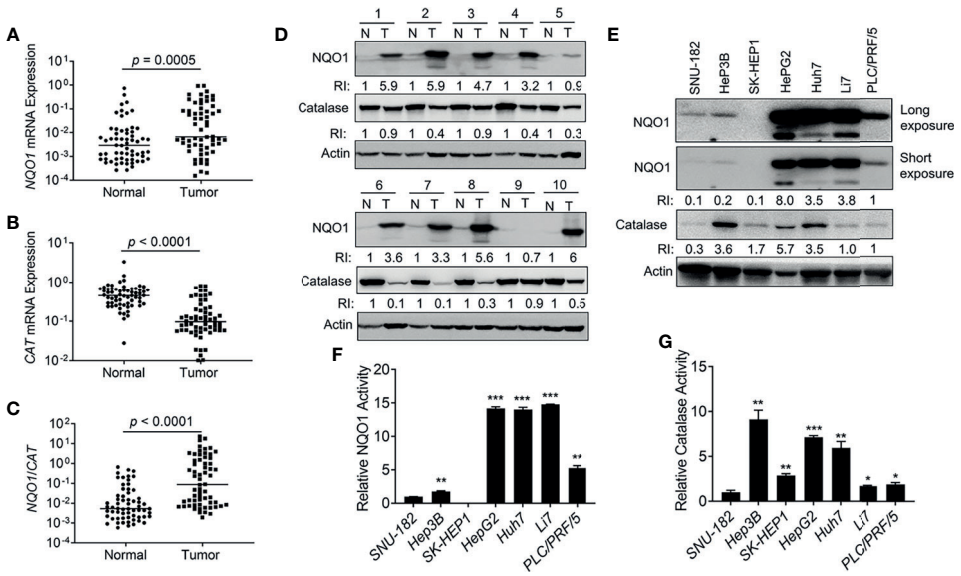

FIGURE 2 | NQO1 and catalase expression in hepatocellular carcinoma patients and cell lines. **(A–C)** mRNA expression of *NQO1* **(A)**, *CAT* **(B)**, and *NQO1/CAT* Ratio **(C)** in 62 pairs of HCC patient tumor samples and associated normal tissues. **(D)** Representative western blotting analysis of NQO1 and catalase protein expression in HCC patient tumor samples and adjacent normal tissues. N, Normal; T, Tumor; RI, Relative Intensity. Data were measured as relative intensity (RI) of NQO1/Actin, and catalase/Actin. The protein expression in normal tissues was defined as 1. **(E)** NQO1 and catalase protein expression in HCC cell lines. Data were measured as RI of NQO1/Actin, and catalase/Actin. The protein expression in PLC/PRF/5 (last lane) was defined as 1. **(F, G)** Relative NQO1 and catalase enzyme activities in various HCC cell lines were detected by the NQO1 and catalase activity assay kit respectively, all error bars are means ± SDs. ***$p < 0.001$, **$p < 0.01$, *$p < 0.05$ (t tests).

HCC cells with β-lap or β-lap + dicoumarol (DIC, an NQO1-specific inhibitor). As expected, HepG2, Huh7, Li7 and PLC/PRF/5 cells, which endogenously express different levels of NQO1 (**Figure 2D**), showed significant sensitivity to β-lap (**Figures 3A–D**), while SK-HEP1, SNU-182 and Hep3B cells, which have undetectable or very low NQO1 expression, were resistant to β-lap exposure (**Figures 3E–G**). Next, we established stable NQO1-expressing SK-HEP1 cells and NOQ1 knockout PLC/PRF/5 cells to examine the lethality of β-lap. Consistently, SK-HEP1 cells were rendered hypersensitive to β-lap treatment after NQO1 expression, and DIC spared lethality (**Figure 3H**). Stable NQO1 knockout PLC/PRF/5 cells were much more resistant to β-lap than parental PLC/PRF/5 cells (**Figure 3I**). NQO1 expression in SK-HEP1 or knockout PLC/PRF/5 cells was confirmed by western blotting analysis (inset, **Figures 3H, I**). Together, these results demonstrate that β-lap efficiently kills HCC cells in an NQO1-mediated manner.

β-Lapachone Induces NQO1-Dependent PARP1 Hyperactivation, ROS Formation and NAD$^+$/ATP loss

Accumulating evidence suggests that exposure to β-lap causes DNA lesions in NQO1$^+$ NSCLC, breast cancer, and pancreatic cancer cells, resulting in PARP hyperactivation in terms of the accumulation of poly(ADP-ribose)-PARP (PAR-PARP) posttranslational protein modification (11, 18, 24). To investigate whether PARP1 is involved in β-lap-induced cell death in HCC cells, we examined the effect of β-lap on poly(ADP-ribosyl)ated protein (PAR) accumulation, which is an indicator of PARP1 hyperactivation. First, β-lap-treated PLC/PRF/5 and Huh7 cells were analyzed for PAR formation using western blotting analysis. As shown, a lethal dose of β-lap (10 μM for PLC/PRF/5, 4 μM for Huh7 cells) significantly induced PARP1 hyperactivation, as indicated by a rapid rise in PAR formation and then an increase in DNA damage, as indicated by γH2AX expression over time (**Figure 4A** and **Supplementary Figure S2A**). To confirm that the β-lap-induced hyperactivation of PARP1 is NQO1-dependent, we next examined PAR formation in NQO1 knockout PLC/PRF/5 and NQO1-expressing SK-HEP1 cells. As expected, PAR formation was significantly inhibited by β-lap after NQO1 was stably knocked out in PLC/PRF/5 cells, accompanied by no detectable γH2AX expression (**Figure 4B**). A rapid increase and continuous level of PAR was detected after NQO1 re-expression in β-lap-resistant SK-HEP1 cells (**Figure 4C**). Consistently, DNA damage was observed in these SK-HEP1 cells. In addition, no significant change of catalase levels were noted in these β-lap-treated cells (**Figures 4A–C**). Taken together, these data indicate that β-lap induces PARP1 hyperactivation and DNA damage in NQO1$^+$ HCC cells.

Intracellular ROS production is crucial for cancer cell death (25), and our previous studies show that NQO1 metabolizes β-lap in a futile redox cycle manner to generate ROS in other solid cancer cells (6, 26). Therefore, we investigated whether ROS are involved in β-lap-induced HCC cell death. We examined the levels of hydrogen peroxide (H_2O_2) as an indicator of intracellular ROS. After 2 h of exposure to a sublethal dose (4 or 8 μM) of β-lap, PLC/PRF/5 cells exhibited a significantly higher level of H_2O_2 ($p < 0.001$) than the untreated group (**Figure 4D**), while NQO1 KO cells showed no

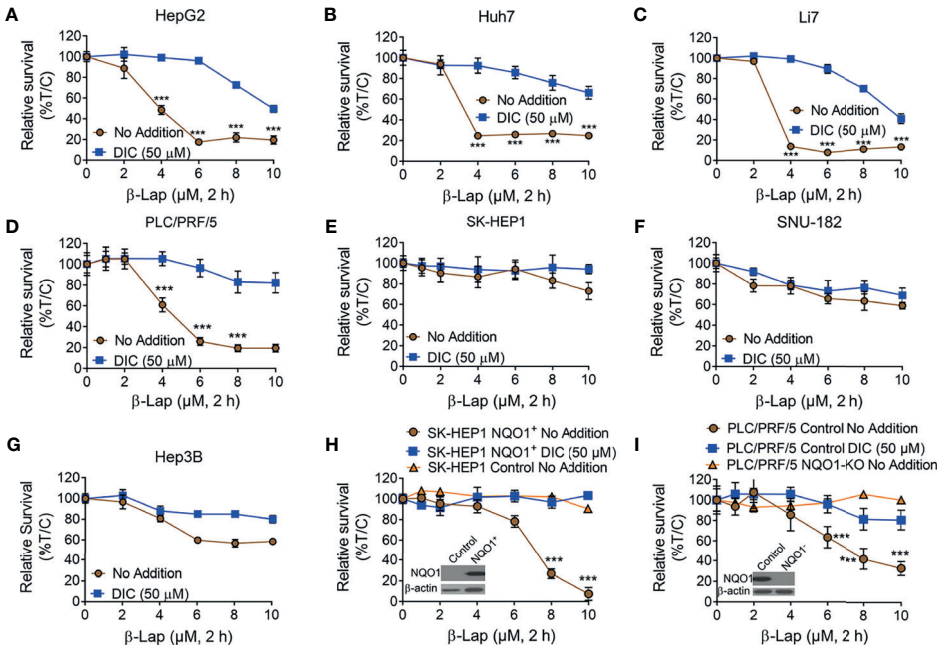

FIGURE 3 | The cytotoxicity of β-Lapachone in hepatocellular carcinoma cells is NQO1-dependent. **(A–F)** HCC cells (HepG2 **(A)**, Huh7 **(B)**, Li7 **(C)**, PLC/PRF/5 **(D)**, SK-HEP1 **(E)**, SNU-182 **(F)**, and Hep3B **(G)**, were exposed to β-lap (0-10 μM), ± dicoumarol (DIC, 50 μM) for 2 h, and then relative survival was assessed. **(H, I)** NQO1-overexpressing SK-HEP1 cells **(H)** and stable NQO1 knockout PLC/PRF/5 cells **(I)** were treated as in **(A)**, and then cell viability was assessed. All error bars are means ± SDs. ***$p < 0.001$ (t tests). No addition, DMSO alone; DIC, dicoumarol; β-lap, β-Lapachone. Inset, NQO1 expression in NQO1-overexpressing SK-HEP1 and NQO1 knockout PLC/PRF/5 cells was confirmed by western blotting. %T/C, the mean of %Treated/Control.

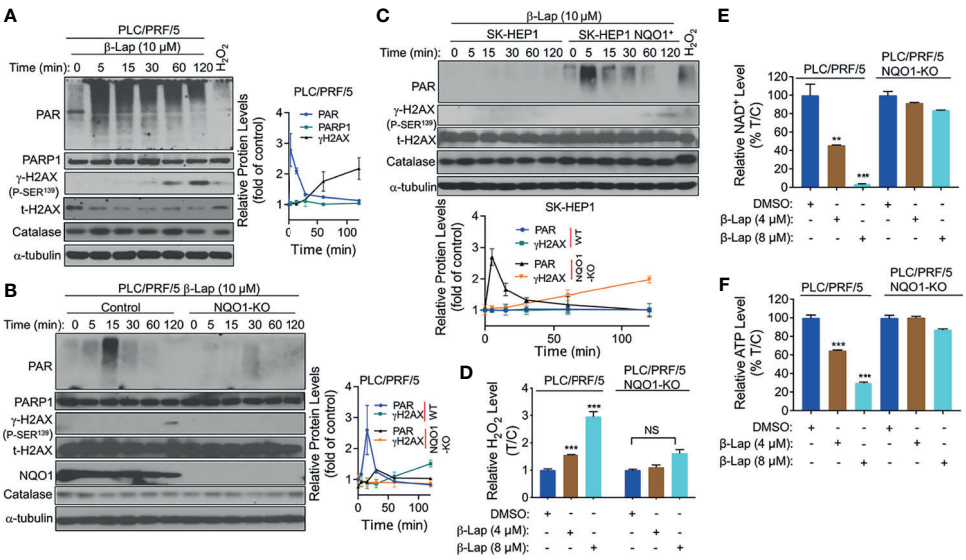

FIGURE 4 | β-Lapachone induces NQO1-dependent PARP1 hyperactivation, ROS formation and NAD^+/ATP loss. **(A–C)** PLC/PRF/5 **(A)**, NQO1 knockout PLC/PRF/5, **(B)** and NQO1-overexpressing SK-HEP1, (SK-HEP1 $NQO1^+$) **(C)** cells were exposed to 10 μM β-lap for the indicated times. Cells were then harvested, and western blotting analysis was performed to detect the levels of PAR (PARP1 hyperactivation), PARP1, NQO1, catalase and γH2AX. The protein levels of PAR and γH2AX were quantified by Image J and normalized to α-tubulin, which was used as a loading control. **(D–F)** PLC/PRF/5 cells were treated with or without β-lap (4 or 8 μM) ± DIC (50 μM) for 2 h. Then, cells were subjected to measurement of H_2O_2 levels **(D)**, NAD^+ levels **(E)** and ATP levels **(F)**. Data represent at least three independent sets of experiments. Error bars are means ± SDs. ***$p < 0.001$, **$p < 0.01$ (t tests). T/C, the mean of Treated/Control in **(D)** %T/C: the mean of %Treated/Control in **(E, F)**. NS, Not Statistically Significant

changes in H_2O_2 levels. Moreover, no obviously increase of H_2O_2 levels was observed in SK-HEP1 cells that have undetected NQO1 expression, while a significant increase of H_2O_2 levels was noted after reconstitution with NQO1 (**Supplementary Figure S2B**). Similarly, a significant increase in H_2O_2 levels in the β-lap-treated group was observed in NQO1$^+$ Huh7 cells, and DIC blocked this increase (**Supplementary Figure S2C**). As reported previously by us and others (11, 27), β-lap-induced PAR-PARP1 formation consumes NAD^+ and ATP, and together with our above results that PAR is induced rapidly and then decreases over time. Therefore, we examined NAD^+ and ATP levels in β-lap-treated HCC cells. As shown in **Figures 4E, F** and **Supplementary Figures S2D, E**, dramatic NAD^+ and ATP depletion was observed after NQO1$^+$ cells were exposed to β-lap for 2 h. All these depletions were blocked in the NQO1 KO cells or DIC-treated group. When NQO1 expression was restored in SK-HEP1 cells, markedly increase of NAD^+ and ATP levels were observed after treatment with β-lap (**Supplementary Figures S2F, G**). Together, these results demonstrate that β-lap induces cell stress in HCC cells by generating ROS, and disrupts essential metabolic nucleotides.

β-Lapachone Causes Dramatic NQO1-dependent Total DNA Damage and Double-Strand Breaks in Hepatocellular Carcinoma Cells

According to previous reports, ROS release can mediate and promote DNA damage (28, 29), and our above results show that β-lap generates ROS in HCC cells. Therefore, we investigated total DNA damage under β-lap treatment *via* an alkaline comet assay in PLC/PRF/5 cells. In NQO1-expressing PLC/PRF/5 wild-type cells, a sublethal dose of β-lap (4 μM) caused total DNA damage, as indicated by the comet tail, as early as 30 min, and a lethal dose of β-lap (10 μM) markedly increased DNA damage (**Figure 5A**). In contrast, when *NQO1* was knocked out, no obvious DNA tails were observed even at a lethal dose of β-lap (10 μM) (**Figure 5A**). Consistently, quantification of the comet tail length confirmed these observations. On the other hand, our previous study suggested that when PARP hyperactivity is exhausted, cells attempt to replicate despite the damage to AP sites or the presence of SSBs, and the damage becomes hypersensitive to the oxidative stress caused by β-lap and then induces DSBs (21). In fact, we observed γH2AX expression after β-lap treatment in NQO1$^+$ HCC cells, especially when PAR levels were exhausted (**Figure 4**). To further confirm whether β-lap induces DSBs in HCC cells, we examined γH2AX expression *via* immunofluorescence staining. As shown in **Figure 5B**, dramatic increases in DNA DSB formation were noted in the PLC/PRF/5 cells that were treated with a sublethal or lethal dose of β-lap compared to the untreated cells as early as 30 min. Even at a lethal dose of β-lap (10 μM), NQO1 knockout cells showed no obvious increase in γH2AX foci. The observations were confirmed by the quantification of γH2AX foci formation (**Figure 5B**). Taken together, these data suggest that exposure of NQO1$^+$ HCC cells to β-lap results in cell death due to significant DNA DSBs.

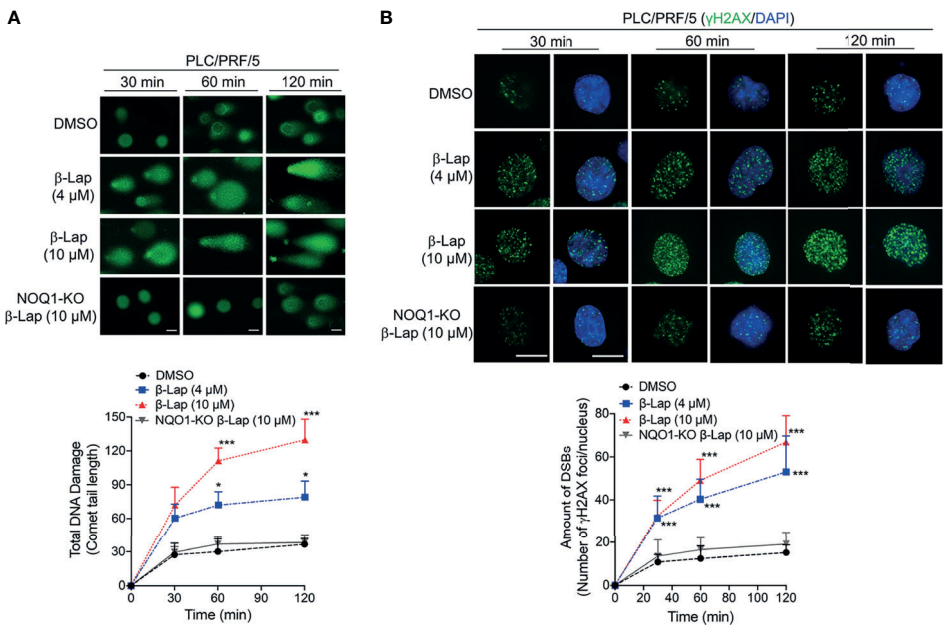

FIGURE 5 | β-Lapachone induces NQO1-dependent DSB formation in hepatocellular carcinoma cells. Wild-type or NQO1 knockout PLC/PRF/5 cells were treated with a sublethal (4 μM) or lethal (10 μM) dose of β-lap for the indicated time (min), and then total DNA lesions were assessed using the alkaline comet assay. **(A)** Comet tail lengths were imaged under an immunofluorescence microscope. **(B)** DSBs were quantified by γH2AX foci/nuclei. Data represent the means ± SDs. Student's t tests were performed. Scale bar = 10 μm, $^{***}p < 0.001$, $^{*}p < 0.05$.

β-Lapachone Significantly Suppresses Tumor Growth and Prolongs Survival in HCC Mouse Models

Relatively high NQO1 and low catalase expression in various HCC patients and cell lines indicates a potent therapeutic window in liver carcinoma for β-lap, and our above data confirmed that β-lap efficiently represses tumor cell growth *in vitro*. To address the antitumor efficacy of β-lap *in vivo*, we established xenograft liver cancer models. First, 5×10^6 PLC/PRF/5 cells/mouse were implanted subcutaneously into NOD/SCID mice. When the tumor size reached 150 mm^3, the mice were grouped and treated with vehicle (HPβCD, intratumor (i.t.)) or HPβCD-β-lap (hereafter referred to as β-lap, at 12.5 mg/kg, i.t.) every other day for a total of five injections. Tumor volume and survival were scored to monitor tumor growth and response (**Figures 6A–C**). Exposure to β-lap resulted in a dramatic decrease in tumor growth compared with vehicle group mice, confirmed by the quantification of tumor volume (**Figures 6A, B**). Moreover, overall survival also showed significant antitumor efficacy of β-lap (**Figure 6C**). This model suggests that β-lap is a good candidate agent to kill $NQO1^+$ HCC *in vivo*.

DISCUSSION

Here, we show a potential antitumor effect of β-lap in HCC and reveal that β-lap efficiently killed NQO1-overexpressing HCC cells without affecting NQO1-low-expressing cells or tissues. As the most common type of primary liver cancer, HCC often occurs in people with long-term liver diseases and is generally diagnosed with advanced disease, leading to systemic therapy (30, 31). At present, there are only a few efficacious drugs for HCC treatment or the drugs cause severe side effects (32, 33). Thus, exploiting new drugs and identifying differences between carcinomas and healthy tissue are critical for HCC treatment. Previous reports suggest that β-lap is a competent tumor-selective agent against many $NQO1^+$ solid cancers, such as NSCLC, pancreatic and breast cancers (6, 11, 34–36), while the antitumor effect of this drug in liver cancer is still unknown. Except the expression and activity of NQO1, the cytotoxicity of β-lap is also driven by ROS-metabolizing enzymes catalase and SOD1 expression and activity. catalase is an important resistance factor in β-lap-induced cytotoxicity and this resistance could be enhanced by superoxide dismutase (SOD) (37). The *NQO1:CAT* ratios are suggested to be a therapeutic window in NSCLC, pancreatic and breast cancers (11, 18). In our study, analysis of 64 clinical patient samples of HCC revealed that 43.8% of patients exhibited NQO1 overexpression, and the majority of patients showed low CAT levels in tumors compared with adjacent normal tissues. Moreover, LIHC data from TCGA demonstrated that patient overall survival significantly correlated with *NQO1* expression. These results suggest that relatively high NQO1:CAT ratios in tumor tissues could provide a therapeutic window for using NQO1 bioactivatable

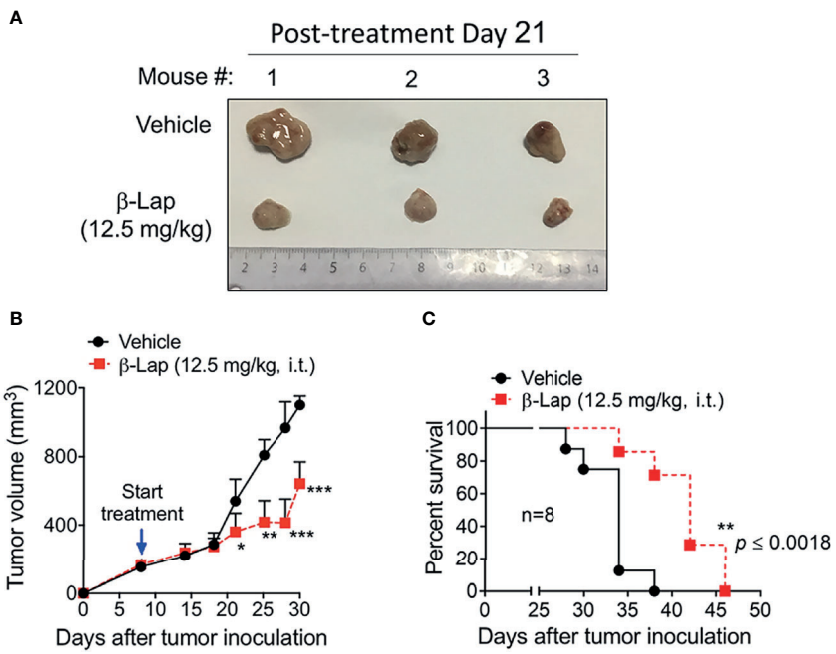

FIGURE 6 | Antitumor efficacy of β-Lapachone in a mouse xenograft model. The subcutaneous xenograft tumor model was established by injection of 5×10^6 PLC/PRF/5 cells into male NOD/SCID mice. After 8 days, mice were treated with vehicle (HPβCD) or HPβCD-β-Lap (12.5 mg/kg) by intratumor injections every other day for five injections. **(A)** Representative tumors at day 21 post-treatment. **(B)** Tumor volume at the indicated time (days). **(C)** Kaplan-Meier survival curves. ***$p < 0.001$, **$p < 0.01$, *$p < 0.05$.

drugs such as β-lap to kill HCC. In fact, cell viability showed that β-lap efficiently killed PLC/PRF/5, Huh7, and Li7 cells, which have high NQO1 expression, but did not affect NOQ1$^-$ cell growth (**Figure 2**).

β-lap was reported to induce cancer cell death *via* an NQO1-dependent programmed necrotic pathway, which caused robust ROS elevation and PARP1 hyperactivation (6, 38). In HCC cells, we observed β-lap-induced NQO1-selective elevated H_2O_2 and a rapid and transient increase in PAR formation, followed by DNA damage over time. On the other hand, PARP1 uses NAD^+ as a substrate to perform PAR posttranslational modification of proteins, resulting in NAD^+ and ATP losses (27, 39). Our β-lap-treated HCC cells indeed exhibited NQO1-dependent NAD^+ and ATP depletion. Collectively, our investigation of clinical patient samples of HCC and *in vitro* results offer a therapeutic window and potential use of β-lap in HCC.

β-lap has an apparently broader NQO1-dependent therapeutic window in HCC. NQO1 is overexpressed in numerous human cancers, and our previous studies together with others demonstrate that β-lap has efficacy in tumor-selective cell growth control and produced promising preclinical results (6, 11, 19, 34, 36). Our preclinical model exhibited an efficient antitumor effect of β-lap in HCC in which β-lap-treated mice had dramatically decreased tumor growth and prolonged survival compared to control mice. Together with our *in vitro* results, we anticipate that β-lap would be an extremely efficacious tumor-selective therapy against HCC and other kinds of liver cancer. Furthermore, the data presented in this study reveal that NQO1 and the *NQO1:CAT* ratio could be used as biomarkers to examine the efficacy of NQO1 bioactivatable drugs in HCC or other kinds of liver cancers. In addition, our *in vitro* and *in vivo* data could translate our findings regarding β-lap in HCC to the clinic. Moreover, because β-lap alone induces tumor programmed necrotic cell death that could induce many cytokines or other side effects *in vivo*, our recent report revealed that low-dose β-lap combined with a PARP inhibitor switched the pathway to apoptosis (11), which implies that combination therapy between β-lap and other clinical drugs would be worth exploring. Finally, immunotherapy with immune checkpoint inhibitors such as PD-1 inhibitors has shown promise in HCC (40). Clinical data showed that only approximately 15-20% of HCC patients exhibited a response, and a fraction of HCC patients could benefit from this therapy (41, 42). We recently revealed that β-lap not only directly kills tumor cells but also increases tumor immunogenicity by triggering immunogenic cell death and overcoming immunotherapy resistance (43). Thus, we propose that β-lap could exert a synergistic effect with immune checkpoint inhibitors and enhance the antitumor immune response in HCC.

Taken together, our study demonstrated that β-lap, a novel NQO1 bioactivatable drug, selectively kills HCC cells expressing NQO1 through inducing ROS and PAR formation, NAD^+ and ATP depletion and lethal DNA damage. High *NQO1:CAT* ratios in HCC tumors but low ratios in normal tissues offer an optimal therapeutic window and an ideal therapeutic target for β-lap.

DATA AVAILABILITY STATEMENT

The original contributions presented in the study are included in the article/**Supplementary Material**. Further inquiries can be directed to the corresponding author.

ETHICS STATEMENT

The studies involving human participants were reviewed and approved by Zhongshan Hospital of Xiamen University. The patients/participants provided their written informed consent to participate in this study. The animal study was reviewed and approved by the IU IACUC committee.

AUTHOR CONTRIBUTIONS

LJ, WZ, and XH designed the experiments, analyzed the data, and wrote the manuscript. XH supervised the project. SL, YY, HZ, and JW. analyzed the bioinformatic data. TF, FF, YL, YZ, XS, and JWW provided help with the experiments. LJ, WZ, YC, JW, and XH reviewed and edited the manuscript. All authors contributed to the article and approved the submitted version.

FUNDING

This work was supported by NIH R01 grants CA221158, CA224493 and CA240952 to XH. This work was also supported by the IU Simon Comprehensive Cancer Center (Grant P30CA082709), the Purdue University Center for Cancer Research (Grant P30CA023168) and the Walther Cancer Foundation.

SUPPLEMENTARY MATERIAL

The Supplementary Material for this article can be found online at: https://www.frontiersin.org/articles/10.3389/fonc.2021.747282/full#supplementary-material

Supplementary Figure S1 | NQO1 and catalase expression in hepatocellular carcinoma patients. **(A, B)** Western blotting analysis of NQO1 and catalase protein expressions in 54 pairs of HCC patient tumor samples and adjacent normal tissues. N, Normal; T, Tumor.

Supplementary Figure S2 | β-Lapachone induces NQO1-dependent PARP1 hyperactivation, ROS formation and NAD^+/ATP loss in Huh7 cells. **(A)** Huh7 cells were exposed to 4 μM β-lap at the indicated time, then cells were harvested and western blotting analysis was to detect the levels of PAR (PARP1 hyperactivation) and γH2AX. **(B–G)** SK-HEP1, SK-HEP1 NQO1$^+$, and Huh7 cells were treated with or without β-lap ± DIC (50 μM) for 2 h. Then cells were measured for H_2O_2 levels **(B, C)**, NAD^+ levels **(D, F)**, and ATP levels **(E, G)**. Data represent at least three independent sets of experiments. Error bars are means ± SD. ***$p < 0.001$, **$p < 0.01$, *$p < 0.05$ (t tests).

REFERENCES

1. Llovet JM, Zucman-Rossi J, Pikarsky E, Sangro B, Schwartz M, Sherman M, et al. Hepatocellular Carcinoma. *Nat Rev Dis Primers* (2016) 2:16018. doi: 10.1038/nrdp.2016.18
2. Marrero JA, Kulik LM, Sirlin CB, Zhu AX, Finn RS, Abecassis MM, et al. Diagnosis, Staging, and Management of Hepatocellular Carcinoma: 2018 Practice Guidance by the American Association for the Study of Liver Diseases. *Hepatology* (2018) 68:723–50. doi: 10.1002/hep.29913
3. Lee SH, Song IH, Noh R, Kang HY, Kim SB, Ko SY, et al. Clinical Outcomes of Patients With Advanced Hepatocellular Carcinoma Treated With Sorafenib: A Retrospective Study of Routine Clinical Practice in Multi-Institutions. *BMC Cancer* (2015) 15:236. doi: 10.1186/s12885-015-1273-2
4. Siegel D, Ross D. Immunodetection of NAD(P)H:quinone Oxidoreductase 1 (NQO1) in Human Tissues. *Free Radical Biol Med* (2000) 29:246–53. doi: 10.1016/S0891-5849(00)00310-5
5. Zhang K, Chen D, Ma K, Wu X, Hao H, Jiang S. NAD(P)H:Quinone Oxidoreductase 1 (NQO1) as a Therapeutic and Diagnostic Target in Cancer. *J Medicinal Chem* (2018) 61:6983–7003. doi: 10.1021/acs.jmedchem.8b00124
6. Bey EA, Bentle MS, Reinicke KE, Dong Y, Yang CR, Girard L, et al. An NQO1- and PARP-1-Mediated Cell Death Pathway Induced in Non-Small-Cell Lung Cancer Cells by Beta-Lapachone. *Proc Natl Acad Sci USA* (2007) 1041:1832–7. doi: 10.1073/pnas.0702176104
7. Cao L, Li LS, Spruell C, Xiao L, Chakrabarti G, Bey EA, et al. Tumor-Selective, Futile Redox Cycle-Induced Bystander Effects Elicited by NQO1 Bioactivatable Radiosensitizing Drugs in Triple-Negative Breast Cancers. *Antioxid Redox Signaling* (2014) 21:237–50. doi: 10.1089/ars.2013.5462
8. Chakrabarti G, Silvers MA, Ilcheva M, Liu Y, Moore ZR, Luo X, et al. Tumor-Selective Use of DNA Base Excision Repair Inhibition in Pancreatic Cancer Using the NQO1 Bioactivatable Drug, Beta-Lapachone. *Sci Rep* (2015) 5:17066. doi: 10.1038/srep17066
9. Dong Y, Chin SF, Blanco E, Bey EA, Kabbani W, Xie XJ, et al. Intratumoral Delivery of Beta-Lapachone *via* Polymer Implants for Prostate Cancer Therapy. *Clin Cancer Res: an Off J Am Assoc Cancer Res* (2009) 15:131–9. doi: 10.1158/1078-0432.CCR-08-1691
10. Dong Y, Bey EA, Li LS, Kabbani W, Yan J, Xie XJ, et al. Prostate Cancer Radiosensitization Through Poly(ADP-Ribose) Polymerase-1 Hyperactivation. *Cancer Res* (2010) 70:8088–96. doi: 10.1158/0008-5472.CAN-10-1418
11. Huang X, Motea EA, Moore ZR, Yao J, Dong Y, Chakrabarti G, et al. Leveraging an NQO1 Bioactivatable Drug for Tumor-Selective Use of Poly (ADP-Ribose) Polymerase Inhibitors. *Cancer Cell* (2016) 30:940–52. doi: 10.1016/j.ccell.2016.11.006
12. Cheng ML, Lu YF, Chen H, Shen ZY, Liu J. Liver Expression of Nrf2-Related Genes in Different Liver Diseases. *Hepatobiliary Pancreatic Dis International: HBPD Int* (2015) 14:485–91. doi: 10.1016/S1499-3872(15)60425-8
13. Lin L, Sun J, Tan Y, Li Z, Kong F, Shen Y, et al. Prognostic Implication of NQO1 Overexpression in Hepatocellular Carcinoma. *Hum Pathol* (2017) 69:31–7. doi: 10.1016/j.humpath.2017.09.002
14. Li WY, Zhou HZ, Chen Y, Cai XF, Tang H, Ren JH, et al. NAD(P)H: Quinone Oxidoreductase 1 Overexpression in Hepatocellular Carcinoma Potentiates Apoptosis Evasion Through Regulating Stabilization of X-Linked Inhibitor of Apoptosis Protein. *Cancer Lett* (2019) 451:156–67. doi: 10.1016/j.canlet.2019.02.053
15. Zhou HZ, Zeng HQ, Yuan D, Ren JH, Cheng ST, Yu HB, et al. NQO1 Potentiates Apoptosis Evasion and Upregulates XIAP *via* Inhibiting Proteasome-Mediated Degradation SIRT6 in Hepatocellular Carcinoma. *Cell Communication Signal: CCS* (2019) 17:168. doi: 10.1186/s12964-019-0491-7
16. Planchon SM, Wuerzberger S, Frydman B, Witiak DT, Hutson P, Church DR, et al. Beta-Lapachone-Mediated Apoptosis in Human Promyelocytic Leukemia (HL-60) and Human Prostate Cancer Cells: A P53-Independent Response. *Cancer Res* (1995) 55:3706–11.
17. Chakrabarti G, Moore ZR, Luo X, Ilcheva M, Ali A, Padanad M, et al. Targeting Glutamine Metabolism Sensitizes Pancreatic Cancer to PARP-Driven Metabolic Catastrophe Induced by ss-Lapachone. *Cancer Metab* (2015) 3:12. doi: 10.1186/s40170-015-0137-1
18. Bey EA, Reinicke KE, Srougi MC, Varnes M, Anderson VE, Pink JJ, et al. Catalase Abrogates Beta-Lapachone-Induced PARP1 Hyperactivation-Directed Programmed Necrosis in NQO1-Positive Breast Cancers. *Mol Cancer Ther* (2013) 12:2110–20. doi: 10.1158/1535-7163.MCT-12-0962
19. Beg MS, Huang X, Silvers MA, Gerber DE, Bolluyt J, Sarode V, et al. Using a Novel NQO1 Bioactivatable Drug, Beta-Lapachone (ARQ761), to Enhance Chemotherapeutic Effects by Metabolic Modulation in Pancreatic Cancer. *J Surg Oncol* (2017) 116:83–8. doi: 10.1002/jso.24624
20. Huang X, Dong Y, Bey EA, Kilgore JA, Bair JS, Li LS, et al. An NQO1 Substrate With Potent Antitumor Activity That Selectively Kills by PARP1-Induced Programmed Necrosis. *Cancer Res* (2012) 72:3038–47. doi: 10.1158/0008-5472.CAN-11-3135
21. Motea EA, Huang X, Singh N, Kilgore JA, Williams NS, Xie XJ, et al. NQO1-Dependent, Tumor-Selective Radiosensitization of Non-Small Cell Lung Cancers. *Clin Cancer Res: an Off J Am Assoc Cancer Res* (2019) 25:2601–9. doi: 10.1158/1078-0432.CCR-18-2560
22. Zhao B, Zhao W, Wang Y, Xu Y, Xu J, Tang K, et al. Connexin32 Regulates Hepatoma Cell Metastasis and Proliferation *via* the P53 and Akt Pathways. *Oncotarget* (2015) 6:10116–33. doi: 10.18632/oncotarget.2687
23. Li Z, Zhang Y, Jin T, Men J, Lin Z, Qi P, et al. NQO1 Protein Expression Predicts Poor Prognosis of Non-Small Cell Lung Cancers. *BMC Cancer* (2015) 15:207. doi: 10.1186/s12885-015-1227-8
24. Zhang F, Xie R, Munoz FM, Lau SS, Monks TJ. PARP-1 Hyperactivation and Reciprocal Elevations in Intracellular Ca2+ During ROS-Induced Nonapoptotic Cell Death. *Toxicol Sci: An Off J Soc Toxicol* (2014) 140:118–34. doi: 10.1093/toxsci/kfu073
25. Zou Z, Chang H, Li H, Wang S. Induction of Reactive Oxygen Species: An Emerging Approach for Cancer Therapy. *Apoptosis: An Int J Programmed Cell Death* (2017) 22:1321–35. doi: 10.1007/s10495-017-1424-9
26. Li LS, Reddy S, Lin ZH, Liu S, Park H, Chun SG, et al. NQO1-Mediated Tumor-Selective Lethality and Radiosensitization for Head and Neck Cancer. *Mol Cancer Ther* (2016) 15:1757–67. doi: 10.1158/1535-7163.MCT-15-0765
27. Pieper AA, Blackshaw S, Clements EE, Brat DJ, Krug DK, White AJ, et al. Poly (ADP-Ribosyl)Ation Basally Activated by DNA Strand Breaks Reflects Glutamate-Nitric Oxide Neurotransmission. *Proc Natl Acad Sci USA* (2000) 97:1845–50. doi: 10.1073/pnas.97.4.1845
28. Moloney JN, Cotter TG. ROS Signalling in the Biology of Cancer. *Semin Cell Dev Biol* (2018) 80:50–64. doi: 10.1016/j.semcdb.2017.05.023
29. Srinivas US, Tan BWQ, Vellayappan BA, Jeyasekharan AD. ROS and the DNA Damage Response in Cancer. *Redox Biol* (2019) 25:101084. doi: 10.1016/j.redox.2018.101084
30. Yu SJ. A Concise Review of Updated Guidelines Regarding the Management of Hepatocellular Carcinoma Around the World: 2010-2016. *Clin Mol Hepatol* (2016) 22:7–17. doi: 10.3350/cmh.2016.22.1.7
31. Qadan M, Kothary N, Sangro B, Palta M. The Treatment of Hepatocellular Carcinoma With Portal Vein Tumor Thrombosis. *Am Soc Clin Oncol Educ book Am Soc Clin Oncol Annu Meeting* (2020) 40:1–8. doi: 10.1200/EDBK_280811
32. Nie J, Lin B, Zhou M, Wu L, Zheng T. Role of Ferroptosis in Hepatocellular Carcinoma. *J Cancer Res Clin Oncol* (2018) 144:2329–37. doi: 10.1007/s00432-018-2740-3
33. Al-Salama ZT, Syed YY, Scott LJ. Lenvatinib: A Review in Hepatocellular Carcinoma. *Drugs* (2019) 79:665–74. doi: 10.1007/s40265-019-01116-x
34. Li LS, Bey EA, Dong Y, Meng J, Patra B, Yan J, et al. Modulating Endogenous NQO1 Levels Identifies Key Regulatory Mechanisms of Action of Beta-Lapachone for Pancreatic Cancer Therapy. *Clin Cancer Res: an Off J Am Assoc Cancer Res* (2011) 17:275–85. doi: 10.1158/1078-0432.CCR-10-1983
35. Silvers MA, Deja S, Singh N, Egnatchik RA, Sudderth J, Luo X, et al. The NQO1 Bioactivatable Drug, Beta-Lapachone, Alters the Redox State of NQO1+ Pancreatic Cancer Cells, Causing Perturbation in Central Carbon Metabolism. *J Biol Chem* (2017) 292:18203–16. doi: 10.1074/jbc.M117.813923
36. Yang Y, Zhou X, Xu M, Piao J, Zhang Y, Lin Z, et al. Beta-Lapachone Suppresses Tumour Progression by Inhibiting Epithelial-to-Mesenchymal Transition in NQO1-Positive Breast Cancers. *Sci Rep* (2017) 7:2681. doi: 10.1038/s41598-017-02937-0
37. Torrente L, Prieto-Farigua N, Falzone A, Elkins CM, Boothman DA, Haura EB, et al. Inhibition of TXNRD or SOD1 Overcomes NRF2-Mediated

Resistance to Beta-Lapachone. *Redox Biol* (2020) 30:101440. doi: 10.1016/j.redox.2020.101440
38. Pink JJ, Planchon SM, Tagliarino C, Varnes ME, Siegel D, Boothman DA. NAD(P)H:Quinone Oxidoreductase Activity Is the Principal Determinant of Beta-Lapachone Cytotoxicity. *J Biol Chem* (2000) 275:5416–24. doi: 10.1074/jbc.275.8.5416
39. Kim MY, Zhang T, Kraus WL. Poly(ADP-Ribosyl)Ation by PARP-1: 'PAR-Laying' NAD+ Into a Nuclear Signal. *Genes Dev* (2005) 19:1951–67. doi: 10.1101/gad.1331805
40. Sia D, Jiao Y, Martinez-Quetglas I, Kuchuk O, Villacorta-Martin C, Castro de Moura M, et al. Identification of an Immune-Specific Class of Hepatocellular Carcinoma, Based on Molecular Features. *Gastroenterology* (2017) 153:812–26. doi: 10.1053/j.gastro.2017.06.007
41. Wehrenberg-Klee E, Goyal L, Dugan M, Zhu AX, Ganguli S. Y-90 Radioembolization Combined With a PD-1 Inhibitor for Advanced Hepatocellular Carcinoma. *Cardiovasc Interventional Radiol* (2018) 41:1799–802. doi: 10.1007/s00270-018-1993-1
42. Zhu AX, Finn RS, Edeline J, Cattan S, Ogasawara S, Palmer D, et al. Pembrolizumab in Patients With Advanced Hepatocellular Carcinoma Previously Treated With Sorafenib (KEYNOTE-224): A Non-Randomised, Open-Label Phase 2 Trial. *Lancet Oncol* (2018) 19:940–52. doi: 10.1016/S1470-2045(18)30351-6
43. Li X, Liu Z, Zhang A, Han C, Shen A, Jiang L, et al. NQO1 Targeting Prodrug Triggers Innate Sensing to Overcome Checkpoint Blockade Resistance. *Nat Commun* (2019) 10:3251. doi: 10.1038/s41467-019-11238-1

Conflict of Interest: The authors declare that the research was conducted in the absence of any commercial or financial relationships that could be construed as a potential conflict of interest.

Publisher's Note: All claims expressed in this article are solely those of the authors and do not necessarily represent those of their affiliated organizations, or those of the publisher, the editors and the reviewers. Any product that may be evaluated in this article, or claim that may be made by its manufacturer, is not guaranteed or endorsed by the publisher.

frontiers in Oncology

ORIGINAL RESEARCH
published: 07 October 2021
doi: 10.3389/fonc.2021.756205

Cancer Cell-Derived Exosomes Promote HCC Tumorigenesis Through Hedgehog Pathway

Li Li [1,2†], Jing Zhao [1†], Quanbao Zhang [1,2†], Yifeng Tao [1,2], Conghuan Shen [1,2], Ruidong Li [1,2], Zhengyu Ma [1,2], Jianhua Li [1,2] and Zhengxin Wang [1,2]*

[1] Department of General Surgery, Huashan Hospital, Fudan University, Shanghai, China, [2] Institute of Organ Transplantation, Fudan University, Shanghai, China

Purpose: Hepatocellular carcinoma (HCC) accounts for more than 80% of primary liver cancers and is one of the leading causes of cancer-related death in many countries. Cancer cell-derived exosomes are shown to mediate communications between cancer cells and the microenvironment, promoting tumorigenesis. Hedgehog signaling pathway plays important roles in cancer development of HCC.

Methods: Exosomes were isolated from culture medium of HCC cell lines PLC/PRF/5 and MHCC-97H and were found to promote cancer cell growth measured with cell proliferation and colony formation assay. HCC cells cultured with cancer cell-derived exosome had increased cancer stem cell (CSC) population demonstrated by increased cell sphere formation CSC marker expressions. Hedgehog protein Shh was found to be highly expressed in these two HCC cell lines and preferably carried by exosomes. When Shh was knocked down with shRNA, the resulting exosomes had a reduced effect on promoting cancer cell growth or CSC population increase compared to normal cell-derived exosomes.

Results: The ability of PLC/PRF/5 cells to form tumor in a xenograft model was increased by the addition of the exosomes from control cancer cells but not the exosomes from Shh knocked down cancer cells. Finally, the higher plasma Exo-Shh levels were associated with later tumor stages, higher histological grades, multiple tumors, and higher recurrence rates.

Conclusion: This study demonstrated that HCC cells secreted Shh *via* exosome and promote tumorigenesis through the activated Hedgehog pathway.

Keywords: hepatocellular carcinoma, exosome, sonic hedgehog, tumorigenesis 3, cancer stem cell

OPEN ACCESS

Edited by:
Nadia M. Hamdy,
Ain Shams University, Egypt

Reviewed by:
Roger Leng,
University of Alberta, Canada
Kan Toriguchi,
Hyogo College of Medicine, Japan

***Correspondence:**
Zhengxin Wang
wangzhengxin@huashan.org.cn

[†]These authors have contributed equally to this work

Specialty section:
This article was submitted to Gastrointestinal Cancers: Hepato Pancreatic Biliary Cancers, a section of the journal Frontiers in Oncology

Received: *10 August 2021*
Accepted: *16 September 2021*
Published: *07 October 2021*

Citation:
Li L, Zhao J, Zhang Q, Tao Y, Shen C, Li R, Ma Z, Li J and Wang Z (2021) Cancer Cell-Derived Exosomes Promote HCC Tumorigenesis Through Hedgehog Pathway. Front. Oncol. 11:756205. doi: 10.3389/fonc.2021.756205

INTRODUCTION

Hepatocellular carcinoma (HCC), accounting for nearly 80% of the total number of liver cancers, is the fourth most common cause of death related to cancer (1). Surgical resection is still the primary choice for treatments. The nonoperative treatments include transcatheter arterial chemoembolization (TACE), radiofrequency ablation (RFA), and systematic administration of

targeted therapy represented by sorafenib. However, despite the advancement in therapeutics, the median survival time for HCC is still only 6–20 months (2). Better understanding the biology of HCC and developing more therapeutic targets are still needed for improving the outcome.

The Hedgehog signaling pathway is a master regulator in animal development. First discovered in *Drosophila*, Hedgehog is a conserved morphogen secreted to regulate differentiation process in many metazoans. Subsequently, it is also found to play roles in maintenance of adult stem cells and in the progression of various diseases. The canonical Hedgehog pathway involves the binding of Hedgehog protein to a 12-transmembrane receptor PTCH1, releasing the G-protein-coupled receptor smoothened (SMO) from its inhibitory effect. Activated SMO in turn releases transcription factor GLI1 (glioma-associated oncogene family members) from its inhibitors SUFU and KIF7. The released GLI1 is translocated into nucleus and activates transcription of a number of genes, including GLI1, PTCH1, Cyclin D, Cmyc, and VEGF. In mammals, three homologs of Hedgehog proteins, sonic (Shh), Indian (Ihh), and desert (Dhh) have been identified, of which Shh is the most broadly expressed and asserts its function through paracrine or autocrine fashion.

Evidence for the role of Hedgehog signaling in cancer development has been revealed in many studies. Mutations in Hedgehog pathway components are often found in cancer. Ligand-independent activation of Hedgehog signaling due to inactivation mutations on negative regulator PTCH or hyperactivation of SMO or GLI1 was found in various cancers (3, 4).

Healthy adult hepatocytes do not express Hedgehog ligand. During injury or severe stress, liver epithelial cells would produce Hedgehog protein to activate the pathway. It was found that partial hepatectomy activates Hedgehog signaling in mice and that individuals with primary biliary cirrhosis have also upregulated signaling (5, 6). HBV or HCV infection would induce Hedgehog expression (7). The activated Hedgehog pathway is found associated with hepatocarcinogenesis (8). Aberrant activation of Hedgehog signaling pathway components including Shh, PTCH1, GLI, and SMO has been found in HCC (9–12). Shh is the most highly expressed Hedgehog ligand in HCC, expressed in about 60% of HCC patients and its presence is concentrated in and around tumor (13).

Extracellular vesicles (EVs) are lipid-bound particles derived from cells. They can be characterized into two types based on their size, content, biogenesis, and release pathways: microvesicles (MVs) and exosomes. MVs, usually at a diameter greater than 100 nm, are secreted by cells in the form of budding from the plasma membrane. Exosomes, usually at a diameter of 30–150 nm, are derived from intraluminal vesicles in polycystic bodies and are released by cells through the fusion of polycystic bodies and cell membranes. Both MVs and exosomes carry cargos including lipid, RNA, and proteins, and play important roles in regulating various biological processes.

Studies on the roles of EVs in cancer development have demonstrated its versatile functions in mediating communication between tumor and its microenvironment (14). EVs secreted by cancer cells have been subjects of studies as biomarkers and targets of therapy (15). In HCC, it has been found that exosome can induce various cellular biological changes in promoting cell proliferation, migration, angiogenesis, and immune suppression during tumorigenesis (16).

It is known that Hedgehog ligands undergo complicated post-translational modifications that results in lipid attachment and multimerization (17). It can be released in various forms, such as lipoproteins (17), or in association with extracellular vesicles (EVs) (18, 19). In the Drosophila model, the Hedgehog ligand carried on the surface of MV and exosome can activate the Hedgehog signaling pathway in promoting embryonic development (18).

In this presented study, we investigated the effect of exosomes secreted by HCC cell lines and demonstrated the evidence that HCC released Shh through exosome to promote cell proliferation and tumor formation.

MATERIALS AND METHODS

All human subjects involved in the study have signed informed consent for participation. The experimental protocol was reviewed and approved by the ethics committee of Fudan University. Peripheral blood samples were collected in tubes containing EDTA anticoagulation, stored at 4°C for no more than 8 h before centrifuging at 1,000 *g* for 10 min to obtain plasma. The plasma samples were stored at −80°C before further analysis. HCC tissue specimens were obtained during surgical resection. Samples were fixed in 4% paraformaldehyde and subjected to subsequent immunohistochemical analysis. Patients' medical data were obtained through patients' medical record with permission, and the post-surgical follow-ups were carried out in line with patients' routine medical visit.

Animal

Male NOD/SCID mice age of 6 weeks were obtained from SLAC Laboratory Animal Corporation (Shanghai, China). All animal experiments were performed according to animal protocol approved by animal care ethic committee of Fudan University. The xenograft tumor model was established by inoculating PLC/PRF/5 with or without Exo treatment subcutaneously into the groin of mice. Animals were continually monitored for 4 weeks before being euthanized. Tumors were collected and fixed in 4% paraformaldehyde. The tumors were weighted and measured, and the volumes were calculated based on the formula: $V = 0.5*\text{long diameter}*\text{short diameter}^2$.

Cell Lines

Hepatic carcinoma cell lines PLC/PRF/5 and MHCC-97H (abbreviated as PLC and 97H in figure label) and normal hepatic cell line L02 were obtained from Cancer Institute of Fudan University (Shanghai, China) and were maintained in DMEM cell culture medium (Gibco, New York, USA) supplemented with 10% FBS (Gemini, West Sacramento, USA) and 1% ampicillin and streptomycin in the incubator at 37°C

with 5% CO_2. The EV free FBS was obtained by centrifuging the purchased FBS at 120,000 *g* 4°C for 16 h, and filtering the supernatant through a 0.22-μm filter.

Reagents

Primary antibodies used in the Western blot studies are as follows: anti-human Grp75, CD9, OCT4 (CST, Danvers, USA), anti-human ALDH, CD44, CD133 (GeneTex, Irvine, USA), anti-human sytenin1 (Abcam, Cambridge, UK), anti-human CD64 (Proteintech, Wuhan, China), and anti-human GAPDH [Beyotime Institute of Biotechnology (Nanjing, China)]. HRP conjugated secondary antibodies are from Beyotime Institute of Biotechnology (Nanjing, China). Growth factors bFGF and EGF were purchased from Gibco. MicroBCA protein quantification kit was purchased from Thermo Scientific (USA). Cell Counting Kit-8 (CCK-8) was purchased from Dojindo Laboratories (Kumamoto, Japan).

Conditioned Medium

Cells grown to 60% confluency were washed three times with PBS before they are placed in the new medium supplemented with EV free FBS and continued to grow for another 24 h at 37°C with 5% CO_2. The medium is collected and centrifuged at 300 g for 10 min, and the supernatant was further centrifuged at 2,000 *g* for 20 min. The resulting supernatant is the conditioned medium.

Exosome Purification

EV and subsequent Exo and MV isolation from CM are based on Kowal et al. (20). Briefly, CM was centrifuged at 10,000 *g* for 40 min at 4°C. After supernatant was removed, the pellet, which was the MV fraction, was washed with PBS and resuspended in 50–100 μl of PBS. The supernatant from previous centrifugation was centrifuged again at 100,000 *g* for 90 min at 4°C. After the supernatant was discarded, the pellet, which was the Exo fraction, was washed with PBS and resuspended in 50–100 μl of PBS.

Sphere Formation Assessment

A total of 250 PLC/PRF/5 or 500 MHCC-97H cells were seeded in 24-well plates in 1 ml of DMEM/F12 medium supplemented with 20 ng/ml epidermal growth factor (EGF), 20 ng/ml fibroblast growth factor (FGF), 2% B27, and 1% penicillin. The plate was shaken well before sealed with parafilm and cultured at 37°C, 5% CO2. Replenishment of the medium was made at 0.2 ml per well after 1 week of culture. Sphere count was carried out under the microscope after 2 weeks of culture. Each condition has three triplicate wells.

Cell Proliferation Assay

PLC/PRF/5 and MHCC-97H cells were seeded in a 96-well plate at 1,000 or 2,000/well respectively, and incubated at 37°C and 5% CO_2 for 24 h before various stimulus conditions were applied. Cells were continued to culture for another 48 h before the Cell Counting Kit-8 (CCK8) working solution, made by diluting CCK8 reagent in culture medium at 1:9 ratio, was added at 100 μl/well. Absorbance at 450 nm was measured by a spectrometer after 2 h. Five replicates were included for each culture condition.

Clone Formation Assay

PLC/PRF/5 and MHCC-97H cells were seeded in 24-well plates at 125 or 250/well respectively, and incubated at 37°C, 5% CO_2 for 24 h before various stimulus conditions were applied. Cells were continued to culture for another 10 days before the culture medium was removed. Cells were washed with PBS twice before fixed with 4% paraformaldehyde for 10 min and stained with crystal violet. After the plates were washed and air dried, the number of clones with more than 50 cells was counted.

Protein Analysis

Total protein levels of extracted samples were determined with the Micro BCA Protein Assay Kit (Thermo Scientific). Protein samples were resolved with SDS-PAGE and transferred onto PVDF membrane for Western blot analysis. Primary antibodies were diluted according to the manufacturer's instruction and incubated with membrane at 4°C, overnight with constant agitation. Secondary antibody incubations were carried out at room temperature for 1.5 h. ECL was used for visualization. Shh ELISA (Abcam) was performed as specified by the manufacturer.

Lentivirus Infection

shRNA was introduced by shRNA carrying lentivirus made by GenePharma (Shanghai, China). The shRNA was cloned into GenePhama Supersilencing vector under CMV promoter/enhancer. The vector carries GFP gene for visualization and puromycin resistance gene for selection. Cells were grown in a six-well plate for 24 h to about 50% confluency. Cells were washed with PBS, and viral transfection solution was added together with 3 μl of Polybrene. Cells were incubated at 37°C, 5% CO_2 for 24 h before changing into normal medium. Transfection efficiency was estimated by observing green fluorescence under a fluorescence microscope at 48 h post transfection. Puromycin were added at 48 h post transfection to maintain stable transfected cells. ShRNA sequences were as follows: Shh-shRNA1: GCTCGGTGAAAGCAGAGAACT, Shh-shRNA2: GCCAAGAAGGTCTTCTACGTG.

RNA Analysis

Total RNA was extracted from cells using Trizol/chloroform method, and precipitated with isopropanol. Reverse transcription was performed according to the manufacturer's instruction (Takara, Japan). Primers for qPCR (Takara, Japan) are listed in **Table 1**.

Statistical Analysis

Statistical analysis was performed using SPSS 20 and GraphPad Prism 8 software. All experiments were performed with three biological replicates. Chi-square test was used in the comparison of the count data. Student's *t*-test was used in the comparison of the measurement data between the two groups, while one-way ANOVA was used in the comparison of the measurement data among multiple groups. p-value < 0.05 indicates statistical difference, *<0.05, **<0.01, and ***<0.001.

TABLE 1 | Sequence of primers in quantitative PCR analysis.

Primer name	Primer sequence
Actin-F	5'-AATCGTGCGTGACATTAAGGAG-3'
Actin-R	5'-CAGGAAGGAAGGCTGGAAGAG-3'
Oct4-F	5'-ACCGAGTGAGAGGCAACC-3'
Oct4-R	5'-TGAGAAAGGAGACCCAGCAG-3'
CD133-F	5′-AGTCGGAAACTGGCAGATAGC-3′
CD133-R	5′-GGTAGTGTTGTACTGGGCCAAT-3′
CD44-F	5'-CTGCCGCTTTGCAGGTGTA-3'
CD44-R	5'-CATTGTGGGCAAGGTGCTATT-3'
ALDH1-F	5'-CCGTGGCGTACTATGGATGC-3'
ALDH1-R	5'-GCAGCAGACGATCTCTTTCGAT-3'
GLI1-F	5'-AGCGTGAGCCTGAATCTGTG-3'
GLI1-R	5'-CAGCATGTACTGGGCTTTGAA-3'
PTCH1-F	5'-CCAGAAAGTATATGCACTGGCA-3'
PTCH1-R	5'-GTGCTCGTACATTTGCTTGGG-3'
Cmyc-F	5'-GTCAAGAGGCGAACACACAAC-3'
Cmyc-R	5'-TTGGACGGACAGGATGTATGC-3'
CyclinD1-F	5'-TGGAGCCCGTGAAAAAGAGC-3'
CyclinD1-R	5'-TCTCCTTCATCTTAGAGGCCAC-3'

RESULTS

Exosome Purification

Exosome can be isolated based on its physical, chemical, and biological property, with methods mainly including ultracentrifugation, polymer precipitation, ultrafiltration, chromatography, and immunoaffinity capture. Among them, ultracentrifugation is more time-consuming. However, with relatively high purity in extraction, it is still a widely used method.

To understand whether EVs would play a role in HCC development, we extracted and separated EVs secreted by HCC cell lines PLC/PRF/5 and MHCC-97H, as well as the normal human liver cell line L02 using ultracentrifugation. Cells were cultured in DMEM supplemented with 10% exosome-free FBS before the isolation process. After a separation protocol containing ultracentrifugation at 10,000 *g* and 100,000 *g*, the EV was separated into MV and exosome (Exo) fractions.

The nanoparticle tracking analysis showed that the average particle sizes of the MV fractions from the three cell lines were between 135 and 150 nm in diameter, while the average sizes of the particles from the Exo fractions were between 99 and 114 nm in diameter (**Figure 1A**). Electron microscopy analysis showed that the extracted MV and Exo particles were in typical cup-shape morphology (**Figure 1B**). Analysis of particles and protein levels revealed that both PLC/PRF/5 and MHCC-97H cells secreted more particles as Exo than MVs, and these particles contained more protein in Exo than MVs (**Supplementary Figure S1**).

The purity of the fractions was analyzed by Western blot using protein markers specific for each fraction. It is shown that MV marker Grp75 was predominantly presented in the cell extract and MV fractions, while the Exo markers CD9,

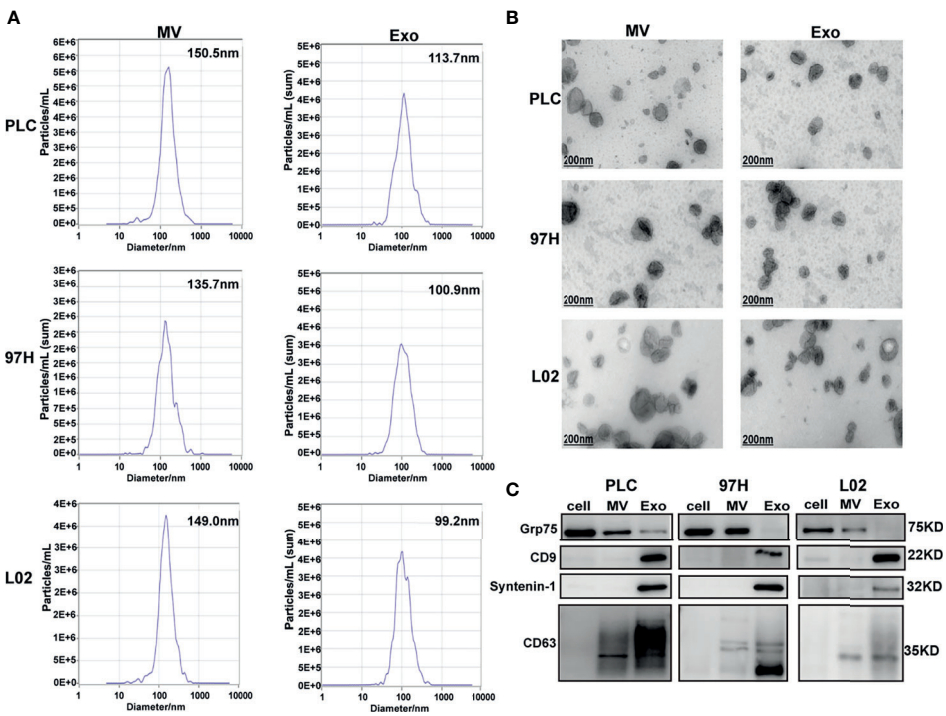

FIGURE 1 | Examine the extracellular vesicles (EVs) isolated from HCC cell lines PLC/PRF/5 and MHCC-97H, as well as normal hepatic cell line L2. **(A)** Nanoparticle tracking analysis of the sizes of the EVs isolated from the three cell lines. **(B)** Electron microscope images of isolated EVs isolated from the three cell lines. **(C)** Western blot analysis of extracellular vesicle markers on the EVs isolated from the three cell lines.

Syntenin-1, and CD63 were predominantly presented in the Exo fractions (**Figure 1C**). These results indicated that we successfully separated Exo and MV fractions through ultracentrifugation process, and this provided us the tools in studying the effect of Exo in subsequent experiments.

Exosome Effect on Cancer Cell Growth

To determine whether exosome secreted by cancer cells has any effect on cell growth, we cultured PLC/PRF/5 and MHCC-97H cells in the presence of additional exosome isolated from their respective culture medium. As shown in **Figure 2A**, addition of Exo into the culture medium promoted PLC/PRF/5 and MHCC-97H growth in a dose-dependent manner. When the Exo concentration was above 5 μg/ml, the cell proliferations were significantly increased. We then studied the colony formation ability. When Exo is added at a concentration of 10 μg/ml in culture medium, the numbers of colonies formed were significantly increased in both PLC/PRF/5 and MHCC-97H (**Figure 2B**). We then investigated whether the addition of exosomes could lead to an increased subpopulation of cancer stem-like cells in culture. The morphology of cells cultured in medium supplemented with Exo were compared with those cultured in normal medium, and we found that the number of spheres in culture increased significantly in both cell lines when isolated Exo was added into culture medium (**Figure 2C**). The expression levels of several cancer stem cell (CSC) markers, CD55, CD133, OCT4, and ALDH1 were also increased at both transcription and protein level (**Figures 2D, E**) when cells were cultured with additional cancer cell-derived exosomes. These findings suggested that the exosome secreted by cancer cells was responsible for promoting cell growth and inducing CSC.

Shh Signaling Is Responsible for the Effect Seen With Exosome

Several studies have shown that Hedgehog signaling pathway plays an important role in HCC growth and development. We decided to investigate whether the effect of exosome on cell growth was through the activation of the Hedgehog pathway.

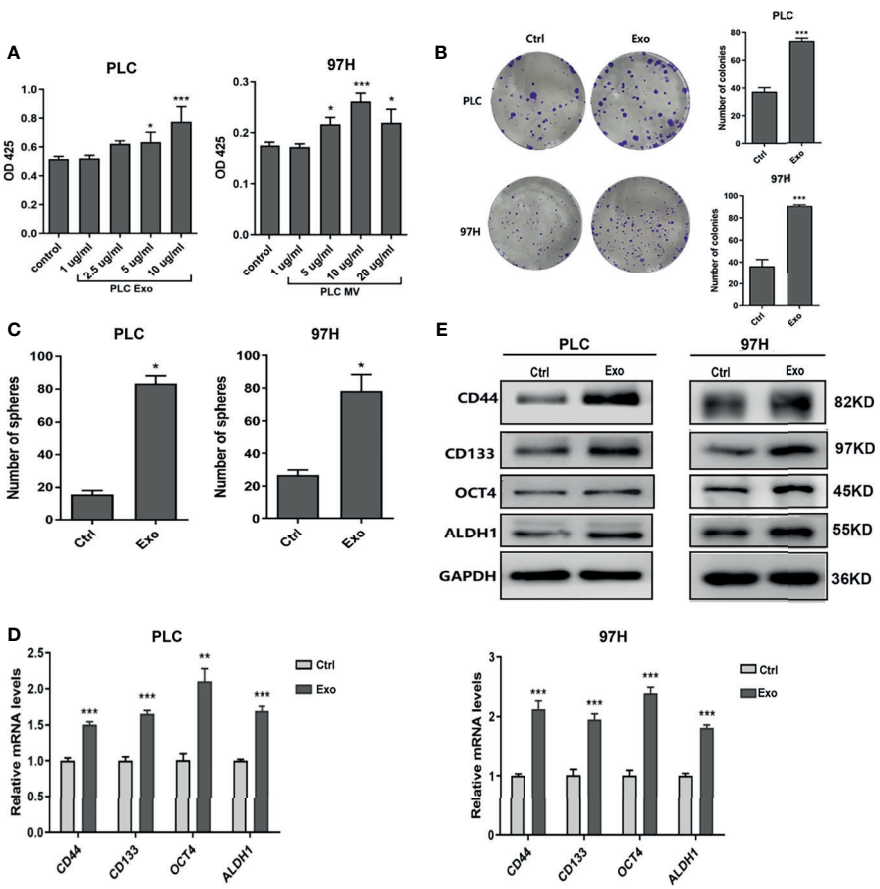

FIGURE 2 | Effect of exosomes on HCC cell growth. **(A)** Proliferation of PLC/PRF/5 and MHCC-97H in the presence of various concentrations of exosomes isolated from culture medium of the same cell line as measured by CCK8 assay. **(B)** Colony formation assay and **(C)** count of sphere formed in PLC/PRF/5 and MHCC-97H with and without exosomes (10 μg/ml) isolated from the culture medium of the same cell line. **(D)** Quantitative PCR analysis of the mRNA levels, and **(E)** Western blot analysis of the protein levels of stem cell marker genes in PLC/PRF/5 and MHCC-97H cells cultured with and without exosomes (10 μg/ml) isolated from the culture medium of the same cell line. The data are presented as an average of three biological replicates. $^{*}p < 0.05$, $^{**}p < 0.01$, $^{***}p < 0.001$.

Two inhibitors of the Hedgehog pathway, Gant-61, which inhibits GLI transcription factor, and Vismodegib, which inhibits SMO receptor, were added into the cell culture, and the effects of these inhibitors on Exo stimulation were studied. Both inhibitors, while themselves had minimal effects on cell proliferation or cell sphere formation, could significantly reverse the stimulating effects of the Exo on cell proliferation and sphere formation on both HCC cell lines (**Figures 3A, B**).

This promoted us to examine the expressions of Hedgehog protein in the two cancer cell lines. Two forms of Hedgehog proteins Shh and Ihh were expressed in these cell lines, with Shh being expressed at a higher level in both cells (**Figure 3C**). Hedgehog proteins were also found in EVs isolated from the cell culture, in which Exo contained much higher levels of both Shh and Ihh than MV. Both cancer cell lines expressed significantly higher Hedgehog protein in the secreted exosomes than the normal hepatocyte cell line L2 (S2), suggesting that the Hedgehog signaling was preferably activated in cancer development. Our results indicated that PLC/PRF/5 and MHCC-97H might use Shh as the main Hedgehog pathway ligand, and Exo would be the preferable way for the cells to secrete the protein.

We performed immunogold labeling with anti-Shh antibody on the exosomes isolated from PLC/PRF/5 and MHCC-97H cells, and as shown in **Figure 3D**, Shh was localized on the surface of Exo secreted by cancer cells. This indicated that Shh carried by exosome may directly interact with its receptor on cell membrane.

To study whether these Shh carrying exosomes can activate the Hedgehog pathway, we assess the expressions of the Hedgehog pathway target genes in cells stimulated with cancer cell-derived exosomes. We found that in both PLC/PRF/5 and MHCC-97H cells, the mRNA and protein levels of several target genes, including GLI1, PTCH1, Cmyc, and CyclinD1, were all elevated when Exo was added in the culture medium (**Figures 3E, F**).

To determine whether the Shh protein carried in these exosomes was responsible for the stimulating effect, we used shRNA to knock down the expression of Shh, and observed its impact. The Western blot analysis demonstrated that two different shRNA-containing lentivirus constructs successfully reduced the expression of Shh in both PLC/PRF/5 and MHCC-97H cells (**Figure 4A**). As a consequence, the Shh

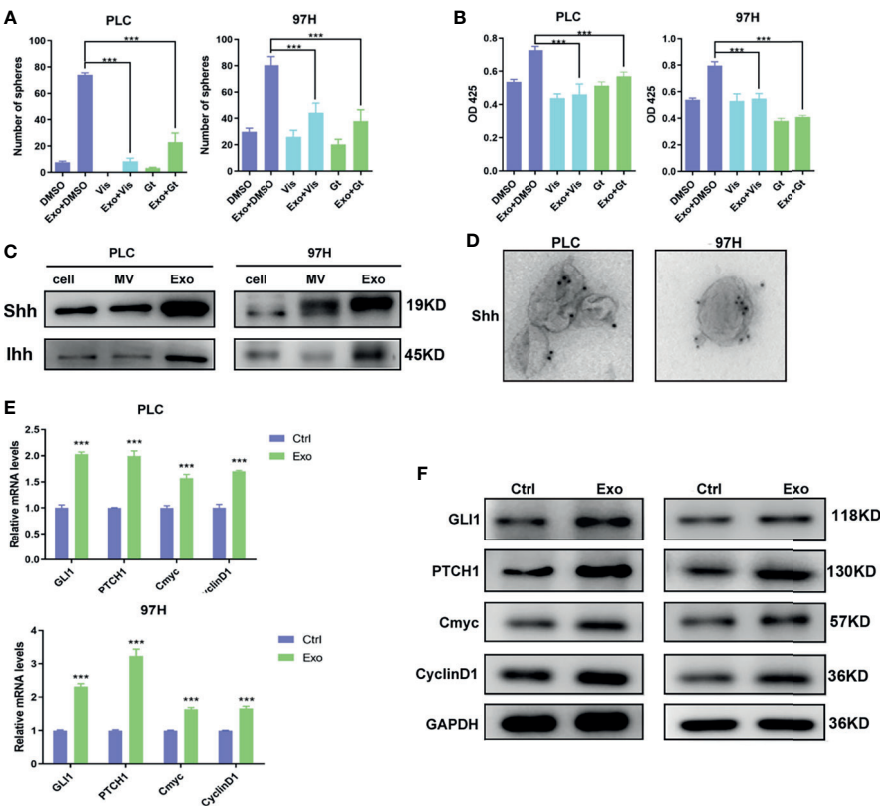

FIGURE 3 | The role of Shh and hedgehog signaling pathway in promoting cell growth. The effect of hedgehog inhibitors on the stimulating effect of Exo (10 μg/ml) on **(A)** sphere formation and **(B)** cell proliferation. The inhibitors were added at the concentrations of 5 μM for GANT61 or 10 μM for Vismodegib. **(C)** The expressions of hedgehog ligands in PLC/PRF/5 and MHCC-97H as analyzed by Western blot. **(D)** Electron microscope image of immunogold staining of Shh on MV and Exo of PLC/PRF/5 and MHCC-97H. **(E)** Quantitative PCR analysis of the mRNA levels, and **(F)** Western blot analysis of the protein levels of hedgehog signaling pathway target genes in PLC/PRF/5 and MHCC-97H cells cultured with and without exosomes (10 μg/ml) isolated from the culture medium of the same cell line. The data are presented as an average of three biological replicates. ***$p < 0.001$.

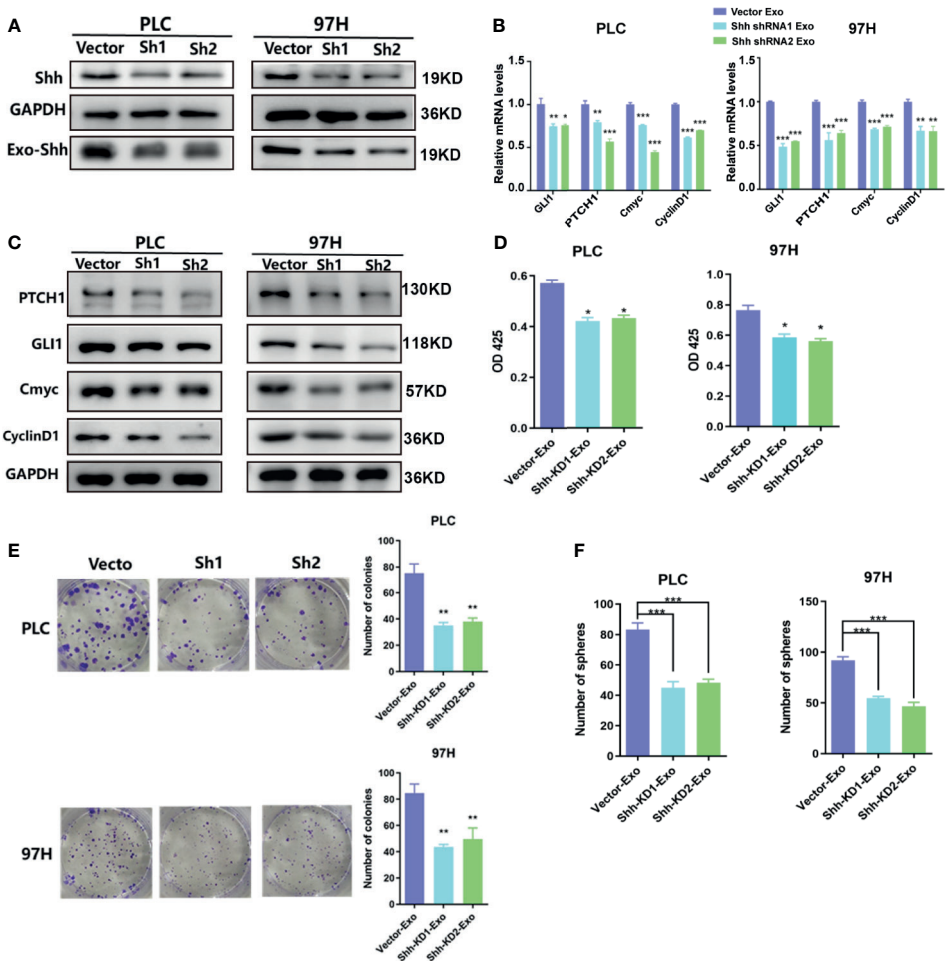

FIGURE 4 | The effect of exosomes isolated from Shh knockdown cells. **(A)** Western blot analysis on the transfection of Shh shRNA lentivirus on the expression of cellular Shh and Exo Shh. **(B)** Quantitative PCR analysis of the mRNA levels, and **(C)** Western blot analysis of the protein levels of hedgehog signaling pathway target genes in PLC/PRF/5 and MHCC-97H cells cultured with exosomes isolated from the culture medium of the same cell line that were transfected with vector or shRNA containing lentivirus. **(D)** Cell proliferations as measured by CCK8 assay, **(E)** colony formation assay, and **(F)** count of sphere formed in PLC/PRF/5 and MHCC-97H cells cultured with exosomes isolated from the culture medium of the same cell line that were transfected with vector or shRNA containing lentivirus. The data are presented as an average of three biological replicates. $^{*}p < 0.05$, $^{**}p < 0.01$, $^{***}p < 0.001$.

levels in the isolated Exo from respective culture medium were also reduced when shRNA-containing lentivirus was transfected into the cells. We isolated the exosomes from the Shh knockdown cells and compared their effect on the Hedgehog pathway and cell growth with the exosomes isolated from the Shh intact cells (vector transfected). As shown in **Figures 4B, C**, when the exosomes isolated from the Shh knockdown cells were added to the culture of the PLC/PRF/5 or MHCC-97H cells, they did not stimulate the expression of Hedgehog pathway target genes as the exosomes isolated from the control cells did in both mRNA and protein levels. Moreover, exosomes from the Shh knockdown cells had reduced ability in stimulating the cell proliferation, colony formation, and sphere formation, compared to the exosome isolated from the control cells (**Figures 4D–F**). These studies indicated that Shh played an important role in PLC/PRF/5 and MHCC-97H cancer development, and the cells secreted the protein into exosome to assert regulation.

In Vivo Experiment

We demonstrated that PLC/PRF/5 and MHCC-97H could secrete Shh containing exosome to regulate the growth of cells. We decided to investigate whether these exosomes influenced tumor formation *in vivo*. PLC/PRF/5 was inoculated subcutaneously into NOD/SCID mice at various numbers mixed with PBS or 5 μg/ml of exosome from its own culture; the tumor formation was observed continuously for 4 weeks. The mice were then euthanized and tumors were removed, measured, and weighted. At the inoculation doses of 1×10^6/mouse and 3×10^5/mouse, tumor was formed in all five mice with cells co-injected with PBS or isolated exosomes. However, the average tumor volumes and weights formed by cells mixed with isolated

exosomes were significantly higher than those formed by cells mixed with PBS (**Figure 5A**). At the lowest inoculation of 1×10^5/mouse, however, tumor only formed in 40% (2/5) of the mice when cells were mixed with PBS before injection, while it formed in 100% (5/5) of the mice when cells were mixed with cancer cell-derived exosomes (**Figure 5A**). Similarly, the average weight and volume of the tumors were significantly higher formed by cells mixed with exosome than those formed by control cells.

We then studied whether the exosomes isolated from cells with Shh knockdown would abolish the stimulating effect on tumor formation of the exosomes. We inoculated the NOD/SCID mice with PLC/PRF/5 cells mixed with either exosomes isolated from control or Shh knockdown cells. As shown in **Figure 5B**, at the inoculation doses of 1×10^6 and 3×10^5, PLC/PRF/5 mixed with either exosomes form tumor in all (5/5) mice tested. However, the average volume and weight of the tumors formed by cells mixed with exosomes isolated from untreated cells were significantly higher than those by cells mixed with exosomes isolated from Shh knockdown cells. When mice were inoculated with PLC/PRF/5 at 1×10^5, tumor formed in 60% (3/5) of the mice injected with cells mixed with exosomes derived from normal cells, but none (0/5) with cells mixed with exosomes derived from Shh knockdown cells.

Clinical Manifestation

Finally, we explored the clinical relevance of circulating Shh levels in HCC patients. We first compared the plasma Shh levels and plasma Exo-Shh levels from 30 HCC patients to 10 normal healthy donors. We found that the average plasma Shh and plasma Exo-Shh levels were both significantly higher in HCC patients than those in healthy donors (**Figure 6A**).

To understand if there is a correlation between circulating Shh levels and the activation of the Hedgehog pathway in HCC, we performed immunostaining on the sections of the tumor tissue for the expression of GLI-1 and PTCH1. Based on the quantitation of the staining, we categorized them into a low-expression and a high-expression group (S3). We then studied correlation between plasma Exo-Shh levels and the expression levels of GLI-1 and PTCH1. As shown in **Figure 6B**, plasma Exo-Shh levels were significantly higher in patients with higher expression levels of GLI-1 and PTCH1 than those with lower levels.

We then analyzed the correlations between the plasma Exo-Shh levels with the clinical characteristics, in terms of TNM stages, number of tumors, and histological grades. As shown in **Figure 6C**, patients with later TMN stages of cancer, multiple tumors, or higher histological tumor grades had significantly higher levels of plasma Exo-Shh than patients with earlier stages of cancer, single tumor, or lower histological grade.

Finally, these 30 HCC patients were followed up for the tumor recurrence after surgery within 18 months. We found that patients with plasma Exo-Shh levels that were higher than 110 pg/ml (n = 15) had a recurrence rate of 46.7% within 18 months after surgery, while patients with plasma Exo-Shh levels lower than 110 pg/ml (n = 15) had a recurrence rate of 13.3%. Recurrence between the two groups reached a statistical difference at the time point of 14th month post-surgery (46.7% vs 6.7%) (**Figure 6D**).

DISCUSSION

Exosomes, double-layer membrane-bound EVs, have been the subject of extensive study since its discovery because of its role in the biological process. Many studies have focused on its miRNA contents and their regulatory functions in biological processes

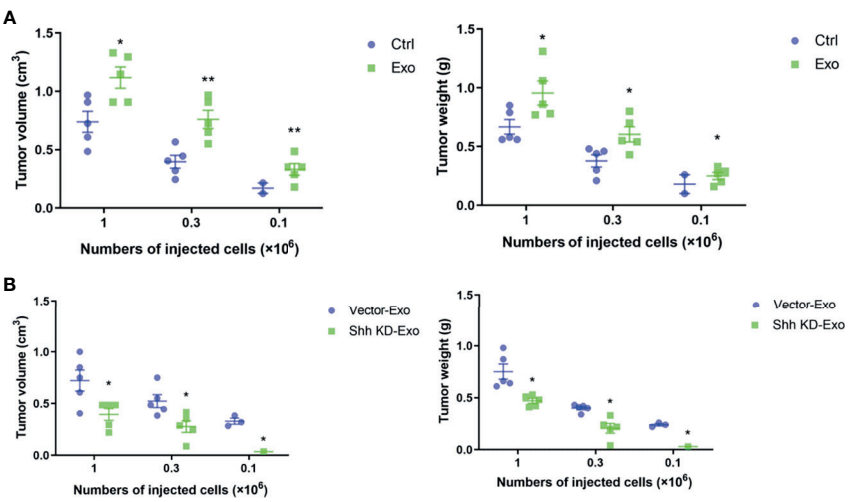

FIGURE 5 | Tumor formations in NOD/SCID mice by PLC/PRF/5. **(A)** The volume and weight of the tumor formed by PLC/PRF/5 subcutaneously injected into NOD/SCID mice with or without mixed with isolated Exo (5 μg/ml) from the same cell culture medium. **(B)** The volume and weight of the tumor formed by PLC/PRF/5 subcutaneously injected into NOD/SCID mice mixed with Exo (5 μg/ml) isolated from culture medium of the vector or Shh shRNA containing lentivirus transfected cells. *$p < 0.05$, **$p < 0.01$.

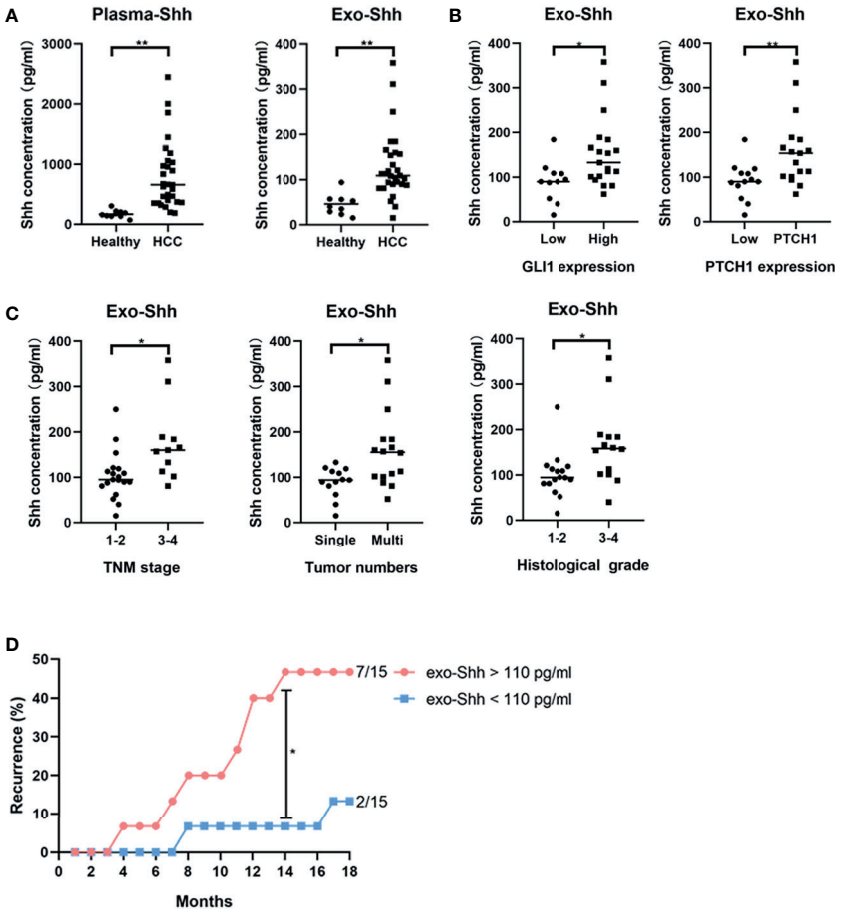

FIGURE 6 | **(A)** Levels of plasma Shh and Exo-Shh isolated from plasma from healthy donors and HCC patients as determined by ELISA. **(B)** Levels of Exo-Shh isolated from plasma of HCC patients grouped based on tissue GLI-1 and PTCH1 levels. **(C)** Levels of Exo-Shh isolated from plasma of HCC patients grouped based on cancer TNM stage, tumor numbers, and histological grade. **(D)** Recurrence of HCC after surgical sections grouped by the Exo-Shh levels. $^{*}p < 0.05$, $^{**}p < 0.01$.

and cancer development, including HCC (21, 22). A number of microRNAs (miRNAs), long noncoding RNAs (lncRNAs), and even messenger RNAs (mRNAs) have been shown to be carried by exosomes, asserting regulatory functions to neighboring cells, and can potentially serve as biomarkers for diagnosis and prognosis in HCC (21). Recent studies have also uncovered evidence that proteins can be transported through exosomes and play a role in HCC tumorigenesis. For example, exosomes released from metastatic HCC cell lines, such as MHCC-97L and HKCI-8, have been found to contain pro-tumorigenic RNAs and proteins, which can promote cell migration and invasion upon internalization by hepatocytes (23). Recently, it was reported that lysyl oxidase-like 4 was transferred by exosomes and promoted cell migration *via* the FAK/Src pathway (24). Another protein, alpha-enolase (ENO1), can be transferred by exosomes between HCC cells and upregulates integrin α6β4 through the FAK/Src pathway (25).

In this study, we focused our investigations on the effect of exosome secreted by HCC cells on tumor development through the Shh protein it carried. We demonstrated that HCC cell lines PLC/PRF/5 and MHCC-97H secreted Shh through EVs, preferably in exosome. The Shh containing exosome promoted cell growth, colony formation, and sphere formation. It upregulated the expression of a number of CSC markers. We found that the Hedgehog signaling pathway was activated when the culture medium was supplemented with additional cancer cell-derived exosomes. We demonstrated that when we reduced the Shh levels by shRNA knockdown, the exosomes derived from knockdown cells did not induce Hedgehog signaling pathway or promote cell growth, as the exosomes derived from the untreated cells did. We provided convincing evidence that Shh carried by exosomes was the main signaling molecule in activating the Hedgehog pathway in HCC cells. This is the first illustration of the role of exosome on Hedgehog signaling in HCC tumorigenesis.

Activating the Hedgehog pathway through overexpression of Shh in HCC tissues was confirmed by many studies (10, 26). Cancer cells secreting Hedgehog ligands to activate autocrine signaling of the pathway has also been found in lung cancer (27), prostate cancer (28), and gastrointestinal cancer (29). Some

studies also found that cancer cells or stromal cells in cancer microenvironment can secrete Hedgehog protein to promote cancer development in a paracrine fashion (30, 31). Our study provided insights into how Shh can be transported within the tumor to confer its activity, i.e., cancer cells could secrete Shh *via* exosomes that may transport the signaling molecule to a site of greater distance to activate the pathway.

CSC theory has become more attractive in recent years. It is proposed that there exists a small population of tumor cells that carry the characteristics of somatic stem cells and are capable of evolved into different cell types within a tumor. These CSCs are capable of self-renewal, differentiation, metastatic dissemination, and are resistant to traditional therapy. The self-renewal of CSCs is tightly regulated by several signaling pathways, including Wnt/β-catenin, Notch, Hippo, and Hedgehog pathways, although they may be alerted to suit the need for malignancy (32). The origin of these CSCs is not well understood. One theory is that they may originate from a more differentiated cancer cell that acquires stem cell properties through an epithelial-to-mesenchymal transition (EMT) process (33). There is also evidence for a normal stem cell undergoing malignant transformation (34).

Our study showed that HCC cell lines PLC/PRF/5 and MHCC-97H, when cultured with additional Shh containing exosome, had increased sphere formation in cell culture. At the same time, expression levels of several CSC marker proteins also increased. These observations suggested that ligand-dependent activation of the Hedgehog pathway could lead to increased proportion of HCC cells that exhibit the property of CSCs, consistent with the model of cancer cell acquiring stem cell properties. Other studies have also found that activation of the Hedgehog pathway induces the expression of CSC marker CD133 and cytokine IL-6, contributing an important function in the liver acute phase response and in HCC development (35). This may explain the increased ability of PLC/PRF/5 to form tumor in the xenograft model when cells were inoculated with Shh containing exosome. Not only was the inoculation required to form a tumor in mice smaller when PLC/PRF/5 was injected with exosome, the volume and weight of the tumor formed with the same inoculations were also on average larger than those formed with cells injected without exosome.

Transforming growth factor (TGF)-β plays a critical role in the induction of EMT, and it has been found that its expression is elevated in 40% of human HCC tissues (36). A recent study has demonstrated that MHCC-97L and MHCC-97H cell-derived exosomes can induce EMT through the TGF-β/Smad signaling pathway (37). In fact, studies have shown that activated the Hedgehog pathway may induce EMT *via* a number of signaling cascades, including WNT, EGF/FGF, Notch, and TGF-β in a variety of tumors (38). It would be of future interest to investigate cross talk of Hedgehog signaling with other pathways in modulating HCC CSCs.

Lastly, we found that circulating Shh levels in HCC patients were significantly higher than those in healthy people. However, it is the plasma Exo-Shh levels, not total plasma Shh levels (data not shown), that had a positive correlation with the tumor stage and histological grade, as well as the expression levels of Hedgehog pathway components in tumor tissue. Higher plasma Exo-Shh levels were also associated with higher recurrence. These findings suggest that Exo-Shh could serve as a prognostic biomarker.

CONCLUSION

In summary, our study provided the first evidence that HCC cells secreted Shh through exosome and this exosome that carried Shh played an important role in HCC tumorigenesis. As shown in **Figure 7**, we proposed that HCC cells secrete Shh protein *via* exosome and Exo-Shh interact with cellular receptor PTCH and induce the activation of Hedgehog signaling in HCC cells to promote tumorigenesis. At present, two Hedgehog pathway-targeted drugs that act on SMO protein, Vimodji and Songyib, have been approved for clinical treatment of basal cell carcinoma. However, in ligand dependently activated tumors, such as gastric cancer, pancreatic cancer, and lung cancer, no clinical benefit has been achieved (39–41). Our findings may point to the possibility of tumor-secreted exosome being a therapeutic target.

Future studies are needed to validate the clinical value of the plasma Exo-Shh as a biomarker for HCC prognosis. The complexity of cancer cell-derived exosomes also requires further analysis to better understand the cross talk of the Hedgehog pathway and other signaling pathways and their roles in tumor progression.

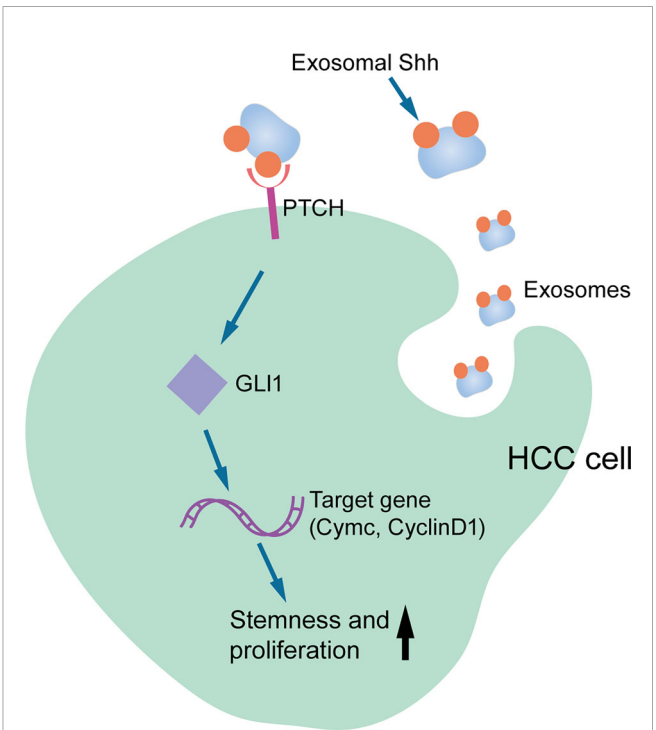

FIGURE 7 | Diagram for the Exo-Shh activating Hedgehog signaling in HCC cells.

DATA AVAILABILITY STATEMENT

The original contributions presented in the study are included in the article/**Supplementary Material**. Further inquiries can be directed to the corresponding author.

ETHICS STATEMENT

All human subjects involved in the study have signed informed consent for participation. The experimental protocol was reviewed and approved by the ethics committee of Fudan University. The patients/participants provided their written informed consent to participate in this study. The animal study was reviewed and approved by the ethics committee of Fudan University.

AUTHOR CONTRIBUTIONS

LL, JZ, and QZ contributed to the study conception and design, performed main experiments, analyzed data, and drafted this article. YT and CS participated in the other experiments, such as Western blotting. RL, ZM, and JL provided assistance in creating figures and tables. ZW supervised experiments and revised the manuscript. All authors contributed to the article and approved the submitted version.

FUNDING

This work was supported by the National Natural Science Foundation of China (81873874 and 82071797), the National Science and Technology Major Project (2017ZX10203205) and Clinical Research Plan of SHDC (No. SHDC2020CR2021B). The funder did not make any substantive contributions to the article.

SUPPLEMENTARY MATERIAL

The Supplementary Material for this article can be found online at: https://www.frontiersin.org/articles/10.3389/fonc.2021.756205/full#supplementary-material

REFERENCES

1. Fitzmaurice C, Allen C, Barber RM, Barregard L, Bhutta ZA, Brenner H, et al. Global, Regional, and National Cancer Incidence, Mortality, Years of Life Lost, Years Lived With Disability, and Disability-Adjusted Life-Years for 32 Cancer Groups, 1990 to 2015: A Systematic Analysis for the Global Burden of Disease Study. *JAMA Oncol* (2017) 3(4):524–48. doi: 10.1001/jamaoncol.2016.5688
2. Forner A, Llovet JM, Bruix J. Hepatocellular Carcinoma. *Lancet* (2012) 379 (9822):1245–55. doi: 10.1016/s0140-6736(11)61347-0
3. Kudchadkar R, Lewis K, Gonzalez R. Advances in the Treatment of Basal Cell Carcinoma: Hedgehog Inhibitors. *Semin Oncol* (2012) 39(2):139–44. doi: 10.1053/j.seminoncol.2012.01.011
4. Wang X, Venugopal C, Manoranjan B, McFarlane N, O'Farrell E, Nolte S, et al. Sonic Hedgehog Regulates Bmi1 in Human Medulloblastoma Brain Tumor-Initiating Cells. *Oncogene* (2012) 31(2):187–99. doi: 10.1038/onc.2011.232
5. Jung Y, McCall SJ, Li YX, Diehl AM. Bile Ductules and Stromal Cells Express Hedgehog Ligands and/or Hedgehog Target Genes in Primary Biliary Cirrhosis. *Hepatology* (2007) 45(5):1091–6. doi: 10.1002/hep.21660
6. Mangold K, Chang YJ, Mathews C, Marien K, Hendricks J, Bailey G. Expression of Ras Genes in Rainbow Trout Liver. *Mol Carcinog* (1991) 4 (2):97–102. doi: 10.1002/mc.2940040204
7. Pereira Tde A, Witek RP, Syn WK, Choi SS, Bradrick S, Karaca GF, et al. Viral Factors Induce Hedgehog Pathway Activation in Humans With Viral Hepatitis, Cirrhosis, and Hepatocellular Carcinoma. *Lab Invest* (2010) 90 (12):1690–703. doi: 10.1038/labinvest.2010.147
8. Jeng KS, Jeng CJ, Jeng WJ, Sheen IS, Li SY, Leu CM, et al. Sonic Hedgehog Signaling Pathway as a Potential Target to Inhibit the Progression of Hepatocellular Carcinoma. *Oncol Lett* (2019) 18(5):4377–84. doi: 10.3892/ol.2019.10826
9. Lu JT, Zhao WD, He W, Wei W. Hedgehog Signaling Pathway Mediates Invasion and Metastasis of Hepatocellular Carcinoma *via* ERK Pathway. *Acta Pharmacol Sin* (2012) 33(5):691–700. doi: 10.1038/aps.2012.24
10. Sicklick JK, Li YX, Jayaraman A, Kannangai R, Qi Y, Vivekanandan P, et al. Dysregulation of the Hedgehog Pathway in Human Hepatocarcinogenesis. *Carcinogenesis* (2006) 27(4):748–57. doi: 10.1093/carcin/bgi292
11. Zhang D, Cao L, Li Y, Lu H, Yang X, Xue P. Expression of Glioma-Associated Oncogene 2 (Gli 2) Is Correlated With Poor Prognosis in Patients With Hepatocellular Carcinoma Undergoing Hepatectomy. *World J Surg Oncol* (2013) 11:25. doi: 10.1186/1477-7819-11-25
12. Zheng X, Vittar NB, Gai X, Fernandez-Barrena MG, Moser CD, Hu C, et al. The Transcription Factor GLI1 Mediates Tgfβ1 Driven EMT in Hepatocellular Carcinoma *via* a SNAI1-Dependent Mechanism. *PLoS One* (2012) 7(11):e49581. doi: 10.1371/journal.pone.0049581
13. Arzumanyan A, Sambandam V, Clayton MM, Choi SS, Xie G, Diehl AM, et al. Hedgehog Signaling Blockade Delays Hepatocarcinogenesis Induced by Hepatitis B Virus X Protein. *Cancer Res* (2012) 72(22):5912–20. doi: 10.1158/0008-5472.can-12-2329
14. Bebelman MP, Smit MJ, Pegtel DM, Baglio SR. Biogenesis and Function of Extracellular Vesicles in Cancer. *Pharmacol Ther* (2018) 188:1–11. doi: 10.1016/j.pharmthera.2018.02.013
15. Urabe F, Kosaka N, Ito K, Kimura T, Egawa S, Ochiya T. Extracellular Vesicles as Biomarkers and Therapeutic Targets for Cancer. *Am J Physiol Cell Physiol* (2020) 318(1):C29–39. doi: 10.1152/ajpcell.00280.2019
16. Wang H, Lu Z, Zhao X. Tumorigenesis, Diagnosis, and Therapeutic Potential of Exosomes in Liver Cancer. *J Hematol Oncol* (2019) 12(1):133. doi: 10.1186/s13045-019-0806-6
17. Ryan KE, Chiang C. Hedgehog Secretion and Signal Transduction in Vertebrates. *J Biol Chem* (2012) 287(22):17905–13. doi: 10.1074/jbc.R112.356006
18. Matusek T, Wendler F, Polès S, Pizette S, D'Angelo G, Fürthauer M, et al. The ESCRT Machinery Regulates the Secretion and Long-Range Activity of Hedgehog. *Nature* (2014) 516(7529):99–103. doi: 10.1038/nature13847
19. Vyas N, Walvekar A, Tate D, Lakshmanan V, Bansal D, Lo Cicero A, et al. Vertebrate Hedgehog Is Secreted on Two Types of Extracellular Vesicles With Different Signaling Properties. *Sci Rep* (2014) 4:7357. doi: 10.1038/srep07357
20. Kowal J, Arras G, Colombo M, Jouve M, Morath JP, Primdal-Bengtson B, et al. Proteomic Comparison Defines Novel Markers to Characterize Heterogeneous Populations of Extracellular Vesicle Subtypes. *Proc Natl Acad Sci U S A* (2016) 113(8):E968–77. doi: 10.1073/pnas.1521230113
21. Li LM, Liu ZX, Cheng QY. Exosome Plays an Important Role in the Development of Hepatocellular Carcinoma. *Pathol Res Pract* (2019) 215 (8):152468. doi: 10.1016/j.prp.2019.152468

22. Liu H, Li B. The Functional Role of Exosome in Hepatocellular Carcinoma. *J Cancer Res Clin Oncol* (2018) 144(11):2085–95. doi: 10.1007/s00432-018-2712-7
23. He M, Qin H, Poon TC, Sze SC, Ding X, Co NN, et al. Hepatocellular Carcinoma-Derived Exosomes Promote Motility of Immortalized Hepatocyte Through Transfer of Oncogenic Proteins and RNAs. *Carcinogenesis* (2015) 36 (9):1008–18. doi: 10.1093/carcin/bgv081
24. Li R, Wang Y, Zhang X, Feng M, Ma J, Li J, et al. Exosome-Mediated Secretion of LOXL4 Promotes Hepatocellular Carcinoma Cell Invasion and Metastasis. *Mol Cancer* (2019) 18(1):18. doi: 10.1186/s12943-019-0948-8
25. Silva DA, de Aguiar GB, Jory M, Conti MLM, Veiga JCE. "Whiplash" Cervical Trauma With Fracture and Migration of Carotid Stent Fragments. *Surg Neurol Int* (2020) 11:329. doi: 10.25259/sni_550_2020
26. Che L, Yuan YH, Jia J, Ren J. Activation of Sonic Hedgehog Signaling Pathway Is an Independent Potential Prognosis Predictor in Human Hepatocellular Carcinoma Patients. *Chin J Cancer Res* (2012) 24(4):323–31. doi: 10.3978/j.issn.1000-9604.2012.10.10
27. Singh S, Wang Z, Liang Fei D, Black KE, Goetz JA, Tokhunts R, et al. Hedgehog-Producing Cancer Cells Respond to and Require Autocrine Hedgehog Activity. *Cancer Res* (2011) 71(13):4454–63. doi: 10.1158/0008-5472.can-10-2313
28. Chung MK, Kim HJ, Lee YS, Han ME, Yoon S, Baek SY, et al. Hedgehog Signaling Regulates Proliferation of Prostate Cancer Cells *via* Stathmin1. *Clin Exp Med* (2010) 10(1):51–7. doi: 10.1007/s10238-009-0068-7
29. Saqui-Salces M, Merchant JL. Hedgehog Signaling and Gastrointestinal Cancer. *Biochim Biophys Acta* (2010) 1803(7):786–95. doi: 10.1016/j.bbamcr.2010.03.008
30. Tian H, Callahan CA, DuPree KJ, Darbonne WC, Ahn CP, Scales SJ, et al. Hedgehog Signaling Is Restricted to the Stromal Compartment During Pancreatic Carcinogenesis. *Proc Natl Acad Sci U S A* (2009) 106(11):4254–9. doi: 10.1073/pnas.0813203106
31. Dierks C, Grbic J, Zirlik K, Beigi R, Englund NP, Guo GR, et al. Essential Role of Stromally Induced Hedgehog Signaling in B-Cell Malignancies. *Nat Med* (2007) 13(8):944–51. doi: 10.1038/nm1614
32. Saygin C, Matei D, Majeti R, Reizes O, Lathia JD. Targeting Cancer Stemness in the Clinic: From Hype to Hope. *Cell Stem Cell* (2019) 24(1):25–40. doi: 10.1016/j.stem.2018.11.017
33. Espinoza I, Miele L. Deadly Crosstalk: Notch Signaling at the Intersection of EMT and Cancer Stem Cells. *Cancer Lett* (2013) 341(1):41–5. doi: 10.1016/j.canlet.2013.08.027
34. Krivtsov AV, Twomey D, Feng Z, Stubbs MC, Wang Y, Faber J, et al. Transformation From Committed Progenitor to Leukaemia Stem Cell Initiated by MLL-Af9. *Nature* (2006) 442(7104):818–22. doi: 10.1038/nature04980
35. He G, Karin M. NF-κb and STAT3 - Key Players in Liver Inflammation and Cancer. *Cell Res* (2011) 21(1):159–68. doi: 10.1038/cr.2010.183
36. Fabregat I, Caballero-Díaz D. Transforming Growth Factor-β-Induced Cell Plasticity in Liver Fibrosis and Hepatocarcinogenesis. *Front Oncol* (2018) 8:357. doi: 10.3389/fonc.2018.00357
37. Qu Z, Feng J, Pan H, Jiang Y, Duan Y, Fa Z. Exosomes Derived From HCC Cells With Different Invasion Characteristics Mediated EMT Through TGF-β/Smad Signaling Pathway. *Oncol Targets Ther* (2019) 12:6897–905. doi: 10.2147/ott.s209413
38. Katoh Y, Katoh M. Hedgehog Signaling, Epithelial-to-Mesenchymal Transition and miRNA (Review). *Int J Mol Med* (2008) 22(3):271–5. doi: 10.3892/ijmm_00000019
39. Catenacci DVT, Bahary N, Nattam SR, Marsh RDW, Wallace JA, Rajdev L, et al. Final Analysis of a Phase IB/randomized Phase II Study of Gemcitabine (G) Plus Placebo (P) or Vismodegib (V), a Hedgehog (Hh) Pathway Inhibitor, in Patients (Pts) With Metastatic Pancreatic Cancer (PC): A University of Chicago Phase II Consortium Study. *J Clin Oncol* (2013) 31(15_suppl):4012–. doi: 10.1200/jco.2013.31.15_suppl.4012
40. Cohen DJ, Christos PJ, Kindler HL, Catenacci DVT, Bekaii-Saab TB, Tahiri S, et al. Vismodegib (V), a Hedgehog (HH) Pathway Inhibitor, Combined With FOLFOX for First-Line Therapy of Patients (Pts) With Advanced Gastric and Gastroesophageal Junction (GEJ) Carcinoma: A New York Cancer Consortium Led Phase II Randomized Study. *J Clin Oncol* (2013) 31 (15_suppl):4011–. doi: 10.1200/jco.2013.31.15_suppl.4011
41. Belani CP, Dahlberg SE, Rudin CM, Fleisher M, Chen HX, Takebe N, et al. Three-Arm Randomized Phase II Study of Cisplatin and Etoposide (CE) Versus CE With Either Vismodegib (V) or Cixutumumab (Cx) for Patients With Extensive Stage-Small Cell Lung Cancer (ES-SCLC) (ECOG 1508). *J Clin Oncol* (2013) 31(15_suppl):7508–. doi: 10.1200/jco.2013.31.15_suppl.7508

Conflict of Interest: The authors declare that the research was conducted in the absence of any commercial or financial relationships that could be construed as a potential conflict of interest.

Publisher's Note: All claims expressed in this article are solely those of the authors and do not necessarily represent those of their affiliated organizations, or those of the publisher, the editors and the reviewers. Any product that may be evaluated in this article, or claim that may be made by its manufacturer, is not guaranteed or endorsed by the publisher.

frontiers in Oncology

ORIGINAL RESEARCH
published: 22 October 2021
doi: 10.3389/fonc.2021.751777

Association of Virological Response to Antiviral Therapy With Survival in Intermediate-Stage Hepatitis B Virus-Related Hepatocellular Carcinoma After Chemoembolization

Meng Jin[1†], Yong Chen[1†], Shuifang Hu[1†], Meiyan Zhu[1], Yan Wang[1], Minshan Chen[2] and Zhenwei Peng[1,3,4,5*]*

[1] Department of Radiation Oncology, The First Affiliated Hospital of Sun Yat-sen University, Guangzhou, China, [2] Department of Liver Surgery, Sun Yat-sen University Cancer Center, Guangzhou, China, [3] Clinical Trials Unit, The First Affiliated Hospital of Sun Yat-sen University, Guangzhou, China, [4] Institute of Precision Medicine, The First Affiliated Hospital of Sun Yat-sen University, Guangzhou, China, [5] Cancer Center, The First Affiliated Hospital of Sun Yat-sen University, Guangzhou, China

OPEN ACCESS

Edited by:
Yuelun Zhang,
Peking Union Medical College Hospital (CAMS), China

Reviewed by:
Zhu-Ting Fang,
Fujian Provincial Hospital, China
Wei-Zhong Zhou,
Nanjing Medical University, China

***Correspondence:**
Zhenwei Peng
pzhenw@mail.sysu.edu.cn
Minshan Chen
Chminsh@mail.sysu.edu.cn

[†]These authors have contributed equally to this work

Specialty section:
This article was submitted to Gastrointestinal Cancers: Hepato Pancreatic Biliary Cancers, a section of the journal Frontiers in Oncology

Received: 02 August 2021
Accepted: 11 October 2021
Published: 22 October 2021

Citation:
Jin M, Chen Y, Hu S, Zhu M, Wang Y, Chen M and Peng Z (2021) Association of Virological Response to Antiviral Therapy With Survival in Intermediate-Stage Hepatitis B Virus-Related Hepatocellular Carcinoma After Chemoembolization. Front. Oncol. 11:751777. doi: 10.3389/fonc.2021.751777

Introduction: Role of response to antiviral therapies on survival of patients with intermediate-stage hepatitis B virus-related hepatocellular carcinoma (HBV-HCC) undergoing transarterial chemoembolization (TACE) remains unknown. We aimed to determine whether virological response (VR) or prolonged maintained virological response (MVR) to nucelos(t)ide analogues (NA) therapy could result in improved survival in HBV-HCC patients receiving TACE.

Methods: Between January 2012 and October 2018, data of patients with intermediate HBV-HCC who underwent TACE and started NA therapy within one week prior to TACE treatment at our institution were reviewed. Overall survival (OS) was compared using the Kaplan-Meier method with log-rank test between different VR status groups. Univariable and multivariable Cox regression analyses were used to determine the association between achievement of VR or MVR and OS. VR was defined as an undetectable HBV DNA level (<100 IU/ml) on two consecutive measurements during NA treatment. MVR was defined as a persistently undetectable HBV DNA level after achieving a VR.

Results: A total of 1265 patients undergoing TACE with a median follow-up time of 18 months (range, 2-78 months) were included in the analysis. Of 1265 NA-treated patients [1123 (88.8%) male, median (range) age, 56 (18-75) years], 744 patients (58.8%) achieved VR and the remaining patients (41.2%) did not. Patients with achievement of VR showed a significantly longer OS than those without VR (median OS: 21 *vs* 16 months; HR, 0.707; 95% CI, 0.622-0.804; $P<0.001$). Among patients with VR, MVR was present in 542 patients (72.8%), while the other 202 patients (27.2%) in the non-MVR group. The OS for the MVR group was significantly higher than the non-MVR group (median OS: 23.2 *vs* 18 months; HR, 0.736; 95% CI, 0.612-0.885; $P=0.001$). Additionally, patients with MVR status more than two years showed a better OS than those with just one-year (HR, 0.719;

95% CI, 0.650-0.797; *P*<0.001) or one-to-two-year MVR (HR, 0.612; 95% CI, 0.471-0.795; *P*=0.024). On multivariable analyses, splenomegaly and up-to-seven criteria were independent prognostic factors of OS in both VR and MVR cohorts.

Conclusions: In patients with intermediate-stage HBV-HCC, both VR to antiviral therapy and prolonged response are associated with prolonged OS after TACE, especially for those within up-to-seven criteria.

Keywords: hepatocellular carcinoma, hepatitis B, nucelos(t)ide analogues, virological response, transarterial chemoembolization

INTRODUCTION

Hepatitis B virus (HBV) infection accounts for over 50% of hepatocellular carcinoma (HCC) which makes it the leading etiology of HCC (1–3). HBV can promote development of HCC both directly by integration of HBV DNA into the host genome or truncated HBV proteins and indirectly *via* chronic necro-inflammation, induced apoptosis, and regenerative activity (4). Antiviral therapy using oral nucelos(t)ide analogues (NAs) have changed the outcome of HBV infection by inhibiting HBV replication, thereby reducing instead of eliminating the risk of HCC in chronic hepatitis B patients (5, 6). For HBV-related HCC (HBV-HCC), NA therapy is significant in HBV DNA inhibition and liver function preservation for increasing the chance of treatment interventions.

According to the Barcelona Clinic Liver Cancer staging system, transarterial chemoembolization (TACE) has been recognized as a standard treatment for intermediate-stage HCC (7, 8). High viral replication of HBV indicated a poorer overall survival (OS) of HBV-HCC after anti-tumor treatment including radical hepatectomy, systemic chemotherapy and TACE (9–11). NA therapy has been shown to reduce tumor recurrence and improve survival outcomes after curative resection or radiofrequency ablation in patients with HBV-HCC in the large cohort study or randomized controlled trials (9, 12–15). In addition, HCC patients undergoing TACE can benefit from NA therapy as reported in the previous studies (16, 17). Recently, a large-scale study has revealed that prophylactic antiviral therapy is associated with better long-term survival among HBV-HCC patients undergoing TACE (18).

To date, achievement of virological response (VR) after antiviral therapy has been demonstrated to be associated with a reduced HCC risk in patients with chronic hepatitis B (19, 20). Furthermore, chronic hepatitis B cirrhotic patients with maintained undetectable HBV DNA levels after NA therapy had better transplant-free survival outcomes (21). These findings highlight the importance of VR status after NA therapy on survival outcomes of HCC patients with anti-tumor treatment, but only one recent research has proposed that survival differed with antiviral response in HBV-HCC patients after TACE (18). However, it remains less clear whether the status of maintained virological response (MVR) when compared to low-level viremia or persistent detectable HBV DNA level has benefits for postponing HCC progression after TACE. Therefore, the purpose of this study was to evaluate the impact of VR status and duration of MVR on survival of HBV-HCC in patients undergoing TACE.

Abbreviations: CI, confidence interval; HBV, hepatitis B virus; HBV-HCC, hepatitis B virus related hepatocellular carcinoma; HCC, hepatocellular carcinoma; HR, hazard ratio; MVR, maintained virological response; NA, nucelos(t)ide analogues; OS, overall survival; TACE, transarterial chemoembolization; VR, virological response.

MATERIALS AND METHODS

Study Design and Participants

The Ethics Committee of Sun Yat-sen University Cancer Center approved this retrospective study (B2019061), and the requirement to obtain informed consent was waived. The study consists of 2915 patients with primary intermediate-stage HBV-HCC who underwent TACE at the Sun Yat-sen University Cancer Center between January 2012 and October 2018. The inclusion criteria were as follows: (a) aged 18 years or above; (b) with intermediate-stage HCC according to the Barcelona Clinic Liver Cancer staging system; (c) no previous antiviral or anti-tumor treatment; (d) underwent TACE as initial treatment and achieved complete response; (e) HBV DNA level ≥2000 IU/ml before TACE; (f) liver function scored by Child-Pugh A; (g) patients' performance status scored by Eastern Cooperative Oncology Group: 0-1; (h) absence of simultaneous carcinoma. Among them, 1650 patients were excluded for the following reasons: HBV DNA levels <2000 IU/ml (n = 843), coinfection with hepatitis C virus or other viral hepatitis (n = 46) and human immunodeficiency virus (n = 16), presence of chronic alcohol intake (n = 89), metabolic syndrome (n = 13), Child-Pugh B or C (n=412), Eastern Cooperative Oncology Group performance status score >1 (n=153) and presence of simultaneous carcinoma (n = 78). The workflow of the present study was shown in **Figure 1**.

Study Variables and Definitions

HCC was diagnosed by imaging techniques according to the American Association for the Study of Liver Diseases guideline (8). Data of the following variables were collected at baseline before TACE treatment (within one week): age; sex; history of diabetes, arterial hypertension, obesity, viral hepatitis, and human immunodeficiency virus. Routine examination included complete blood count (white blood cells, hemoglobin, platelet

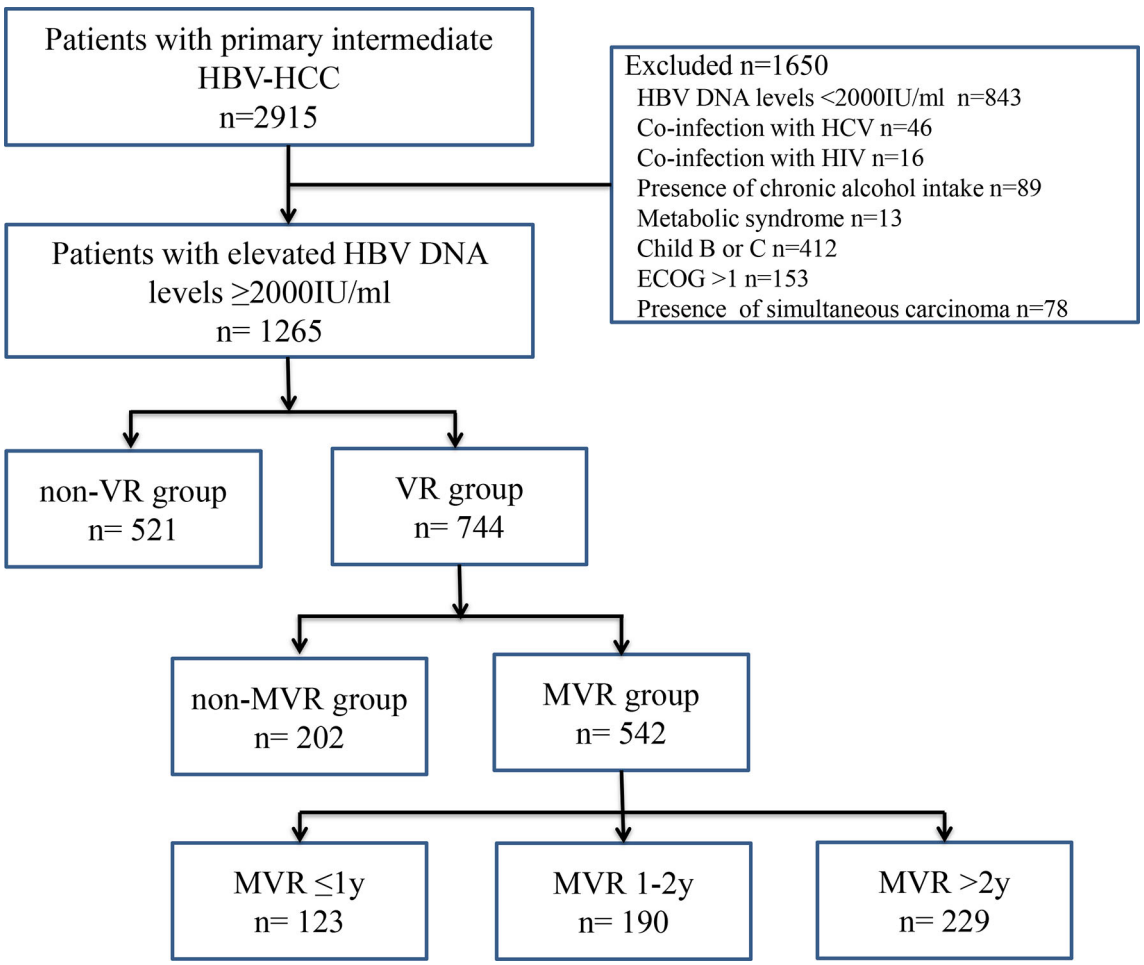

FIGURE 1 | Workflow chart of patient enrollment in the present study. ECOG, Eastern Cooperative Oncology Group; HBV, hepatitis B virus; HBV-HCC, hepatitis B virus-related hepatocellular carcinoma; HCV, hepatitis C virus; HIV, human immunodeficiency virus; MVR, maintained virological response; VR, virological response.

count); serum liver function tests (alanine aminotransferase, aspartate aminotransferase, gamma-glutamyl transferase, albumin, total bilirubin) and kidney function tests; alpha fetoprotein; prothrombin time and serum HBV DNA level. Serum HBV DNA level was quantified using a real-time polymerase chain reaction assay with a limit of detection of 100 IU/ml. Thus, an HBV DNA level lower than 100 IU/mL was considered undetectable in our study.

According to the European Association for the Study of the Liver clinical practice guidelines (22), VR was defined as an undetectable HBV DNA level on two consecutive measurements during NA treatment. The VR group was allocated with patients who had achieved a VR after NA therapy throughout the follow-up period. Meanwhile, those who never achieved a VR were assigned to the non-VR group. MVR was defined as a persistently undetectable HBV DNA level after achieving a VR during the follow-up period (23). Non-MVR was defined as intermittent or persistent period of detectable HBV DNA levels after achieving a VR throughout the follow-up period.

Cirrhosis was clinically defined by ultrasonographical features, including small-sized liver, nodular liver surface or caudate lobe hypertrophy, and splenomegaly (by imaging) or by the presence of varices (by upper endoscopy or imaging test) (24). Tumor burden was evaluated by the up-to-seven criteria (25).

TACE Procedure and Nucelos(t)ide Analogues Administration

TACE was performed by 2 radiologists with at least 5 years of interventional therapy experience as described in the previous research (26, 27). Briefly, visceral angiography of the superior mesenteric and hepatic artery was performed to assess arterial blood supply of the liver and to confirm patency of the portal vein *via* inserting a selective catheter into the segmental or subsegmental tumor-feeding arteries. And 300 mg of carboplatin (Bristol-Myers Squibb, New York, NY) was used in hepatic artery infusion chemotherapy. Then, chemolipiodolization was conducted *via* using 30-50 mg epirubicin (Pharmorubicin; Pfzer, Wuxi, China) and 6-8 mg mitomycin C (Zhejiang Hisun

Pharmaceutical, Taizhou, China) mixed with 5-20 mL lipiodol (Lipiodol Ultra-Fluide; André Guerbet Laboratories, Aulnay-Sous-Bois, France). Finally, embolization was performed using absorbable gelatin sponge particles of 1-2 mm in diameter (Gelfoam, Hangzhou Alc, China) or with polyvinyl alcohol particles of 350-560 μm in diameter (Alicon Pharmaceutical, Hangzhou, China) until achieving blood static for more than 10 successive cardiac beats. Angiography was conducted again to detect the extent of vascular occlusion and to evaluate blood flow in other arterial vessels after embolization. TACE therapies were performed until achieving complete response. Tumor response to TACE was evaluated 4-week after each TACE cycle. The modified Response Evaluation Criteria in Solid Tumors were applied at contrast-enhanced computed tomography or magnetic resonance imaging to evaluate treatment response (28). NAs using entecavir (0.5mg per day; Sino-American Squibb, Shanghai, China) were applied within 1 week prior to the first TACE treatment.

Follow-Up and Endpoints

Followed up assessments were performed every 3 months during the first 2 years, every 6 months for years 3-5 and then every 12 months thereafter. The follow-up examinations included the above-mentioned biochemical tests, HBV DNA level, alpha fetoprotein, ultrasonography and contrast-enhanced computed tomography or magnetic resonance imaging.

The endpoint of the study was overall survival (OS), which was measured from the date of initiation of TACE to the date of patient death or the last follow-up (December 31, 2020).

Statistical Analysis

The study variables were presented as median (range) for continuous data and numbers or percentage for categorical data. Differences in medians were compared using Mann-Whitney *U* test, and differences in percentages were evaluated by the Chi-square test. Survival rates were plotted using Kaplan-Meier method and differences between various VR status or MVR duration groups were analyzed using log-rank test. The associations between clinicopathological factors and survival outcomes were assessed by univariate and multivariate analyses using the Cox proportional hazard regression models. The variables significant on univariate analysis ($P<0.05$) were subjected in the multivariate Cox regression model. The proportional hazards assumption was checked based on the scaled Schoenfeld residuals. All statistical analyses were performed using Statistical Product and Service Solutions software version 19.0. A value of two-sided $P<0.05$ was considered statistically significant.

RESULTS

Baseline Characteristics of Patients Receiving NA Therapy

A total of 1265 HBV-HCC patients treated with TACE receiving NA therapy were included in final analyses. The baseline characteristics of study patients were shown in **Table 1**. Overall, the median follow-up time was 18 months (range, 2-78 months) and the median cycles of receiving TACE was 3 (range, 1-6) for all subjects. VR was observed in 744 patients (58.8%), while the remaining 521 subjects (41.2%) did not achieve VR. For patients achieving VR, a total of 250 patients undergoing other treatment including sorafenib (n=174), radiofrequency ablation (n=38), hepatectomy (n=19), radiotherapy (n=13) and chemotherapy (n=6). While 151 patients received other treatment in non-VR group, including sorafenib (n=104), radiofrequency ablation (n=24), hepatectomy (n=11), radiotherapy (n=8) and chemotherapy (n=4). There was no significant difference in demographic and clinical characteristics, such as median age, sex, proportion of patients with cirrhosis, ascites, splenomegaly, or tumor capsule and percentage of participants beyond the up-to-seven criteria, as well as laboratory tests including blood routine examination and liver and kidney function tests, and other treatment after TACE between the VR and non-VR groups ($P>0.05$). As shown in **Table 2**, splenomegaly, up-to-seven criteria, alpha fetoprotein, total bilirubin, platelet count and sorafenib treatment after TACE were associated with OS in VR group. In the multivariable Cox regression analysis, splenomegaly (hazard ratio (HR), 1.340; 95% confidence interval (CI), 1.095-1.641; $P=0.005$), up-to-seven criteria (HR, 1.298; 95% CI, 1.048-1.607; $P=0.017$), total bilirubin (HR, 1.505; 95% CI, 1.104-2.052; $P=0.010$), platelet count (HR, 1.326; 95% CI, 1.088-1.617; $P=0.005$) and sorafenib treatment after TACE (HR, 0.605; 95% CI, 0.494-0.742; $P<0.001$) were identified as independent factors of OS in patients with NA therapy achieving VR.

Baseline Characteristics of Patients With VR

Among patients with VR, MVR was present in 542 patients (72.8%), while the other 202 patients (27.2%) were in the non-MVR group. No significant differences in baseline characteristics were found between the MVR and non-MVR groups (**Table 3**). Additionally, splenomegaly, up-to-seven criteria, sorafenib treatment after TACE and radical therapy after TACE were correlated with OS in the univariable Cox regression analysis. Similarly, in the multivariable analysis, the prognostic factors included splenomegaly (HR, 1.339; 95% CI, 1.059-1.692; $P=0.015$), tumor burden beyond up-to-seven criteria (HR, 1.430; 95% CI, 1.110-1.844; $P=0.006$), receiving sorafenib treatment after TACE (HR, 0.668; 95% CI, 0.533-0.838; $P<0.001$) and receiving radical therapy after TACE (HR, 0.586; 95% CI, 0.392-0.877; $P=0.009$) (**Table 4**).

Survival According to VR

For patients achieving VR, the 1-, 3-, and 5-year OS rates were 69.8%, 17.7%, and 13.6%, respectively. In comparison, in the non-VR group, the corresponding OS rates were 51.0%, 14.1%, and 8.0%, respectively (**Figure 2A**). Thus, patients in the VR group had better OS than patients in the non-VR group (median OS: 21 *vs* 16 months; HR, 0.707; 95% CI, 0.622-0.804; $P<0.001$). As shown in **Table 5**, without controlling for other factors, VR was associated with increased OS in patients undergoing TACE ($P<0.001$). After

TABLE 1 | Baseline characteristics of patients received NA therapy (VR *versus* non-VR).

Variables	VR group (n = 744)	non-VR group (n = 521)
Age, y	55.4 (18-75)	56.5 (18-75)
Sex		
Male	657 (88.3)	466 (89.4)
Female	87 (11.7)	55 (10.6)
Cirrhosis		
Yes	475 (63.8)	343 (65.8)
No	269 (36.1)	178 (34.2)
Ascites		
Yes	35 (4.7)	28 (5.4)
No	709 (95.3)	493 (94.6)
Splenomegaly		
Yes	591 (79.4)	410 (78.7)
No	153 (20.6)	111 (21.3)
ICGR 15		
≤10%	622 (83.6)	451 (86.6)
>10%	122 (16.4)	70 (13.4)
Tumor capsule		
Yes	223 (30.0)	140 (26.9)
No	521 (70.0)	381 (73.1)
Up-to-seven criteria		
Within	544 (73.1)	396 (76.0)
Beyond	200 (26.9)	125 (24.0)
AFP, ug/L		
≤20	220 (29.6)	134 (25.7)
>20	524 (70.4)	387 (74.3)
GGT, u/L	210 (45.6-989.3)	242 (40.6-896.8)
AST, u/L	36 (10-116)	35 (10-123)
ALT, u/L	24 (10-120)	21 (10-120)
Albumin, g/L	37 (33-47)	36 (34-49)
TBIL, umol/L	12.4 (5.2-25.0)	11.3 (3.8-26.3)
PT, sec	9.3 (7.4-15.4)	8.7 (6.8-17.5)
WBC, 10^9/L	6.1 (4-10)	5.4 (4-10.0)
HB, g/L	13.4 (11.3-14.6)	12.8 (11.7-14.7)
Platelet count, 10^9/L	115 (90-450)	112 (90-456)
Treatment cycles, n	3 (1-6)	3 (1-6)
Other treatment after TACE		
None	494 (66.4)	370 (71.0)
Sorafenib	174 (23.4)	104 (20.0)
Radical therapy	57 (7.7)	35 (6.7)
Radiotherapy or chemotherapy	19 (2.5)	12 (2.3)

Data are presented as median (range) or number (percentage).

AFP, alpha fetoprotein; ALT, alanine aminotransferase; AST, aspartate aminotransferase; GGT, gamma-glutamyl transferase; HB, hemoglobin; ICGR, indocyanine green retention rate; NA, nucelos(t)ide analogue; PT, prothrombin time; TACE, transarterial chemoembolization; TBIL, total bilirubin; VR, virological response; WBC, white blood cells.

adjusting splenomegaly, up-to-seven criteria, alpha fetoprotein and platelet count as confounders, VR remained as an independent factor for OS in patients received NA therapy undergoing TACE (HR, 0.772; 95% CI, 0.615-0.916), *P*=0.003).

Survival According to MVR

The 1-, 3-, and 5-year OS rates were 75.1%, 19.2%, and 15.3%, respectively, for the MVR group and 55.3%, 15.4%, and 11.2%, respectively, for the non-MVR group (**Figure 2B**). Thus, patients achieving MVR to NA therapy had significantly longer OS than patients in the non-MVR group (median OS: 23.2 *vs* 18 months; HR, 0.736; 95% CI, 0.612-0.885; *P*=0.001).

Moreover, survival analyses were separately performed for each subgroup of interest stratified by presence of splenomegaly and up-to-seven criteria for HCC. As a result, MVR again showed significantly improved OS than the non-MVR group, irrespective of patients with or without splenomegaly (HR, 0.758; 95% CI, 0.616-0.931; *P*=0.005 and HR, 0.553; 95% CI, 0.363-0.843; *P*=0.008, respectively) (**Figures 3A, B**). In addition, a consistent survival benefit of achieving MVR was observed among patients within the up-to-seven criteria. Among these patients with relative low tumor burden, the 1-, 3-, and 5-year OS rates for patients with MVR were 77.0%, 20.5%, and 16.9%, compared to 57.3%, 13.6%, and 0% among patients in the non-MVR group (HR, 0.707; 95% CI, 0.575-0.869; *P*=0.001). For patients beyond the up-to-seven criteria, there was no significant difference in OS between the MVR and non-MVR groups (median OS, 17.7 *vs* 11.5 months; HR, 0.906; 95% CI, 0.598-1.373; *P*=0.639) (**Figures 3C, D**).

Subgroup Analysis of OS for Patients With MVR

In the MVR cohort, patients were classified into three subgroups (1 year, 1-2 years, ≥2 years) according to the duration of MVR

TABLE 2 | Univariable and multivariable analysis of OS in the VR group.

Variables	Univariable analysis	Multivariable analysis	
	P value	HR (95% CI)	*P* value
Age, y (≤60/>60)	0.971		
Sex (Male/Female)	0.667		
Cirrhosis (yes/no)	0.060		
Ascites (yes/no)	0.144		
Splenomegaly (yes/no)	0.007	1.340 (1.095-1.641)	0.005
ICGR 15 (≤10%/>10%)	0.751		
Tumor capsule (yes/no)	0.151		
Up-to-seven criteria (beyond/within)	0.002	1.298 (1.048-1.607)	0.017
AFP, ug/L (≤20/>20)	0.030		
GGT, u/L (≤50/>50)	0.956		
AST, u/L (≤40/>40)	0.700		
ALT, u/L (≤40/>40)	0.511		
Albumin, g/L (≤30/>30)	0.158		
TBIL, umol/L (>20.5/≤20.5)	0.049	1.505 (1.104-2.052)	0.010
PT, sec (≤14/>14)	0.431		
WBC, 10^9/L (≤4/>4)	0.771		
HB, g/L (≤120/>120)	0.626		
Platelet count, 10^9/L (≤100/>100)	0.019	1.326 (1.088-1.617)	0.005
Sorafenib after TACE (yes/no)	<0.001	0.605 (0.494-0.742)	<0.001
Radical therapy after TACE (yes/no)	0.606		

CI, confidence interval; HR, hazard ratio; OS, overall survival.

status. There were 123 (22.7%), 190 (35.1%), and 229 (42.2%) patients in the above three subgroups, respectively. As shown in **Figure 4** and **Table 6**, there was a significant difference in OS among different MVR duration subgroups (log-rank *P*<0.001). Particularly, patients with MVR status more than two years showed a better OS than those with just one-year (HR, 0.719; 95% CI, 0.650-0.797; *P*<0.001) or one-to-two-year MVR (HR, 0.612; 95% CI, 0.471-0.795; *P*=0.024). Meanwhile, patients in the one-to-two-year MVR duration subgroup had a significantly improved OS when compared to those did not achieve one-year MVR. Furthermore, in the MVR group, patients with high tumor burden showed obviously worse OS than those with low tumor burden, with respective OS at 1, 3 and 5 years (65.5%, 12.4%, 8.3% *vs*. 77.0%, 20.5%, 16.9%; HR, 1.491; 95% CI, 1.158-1.920; *P*=0.002). In addition, patients with splenomegaly had a worse OS compared to those without enlarged spleen (HR, 1.287; 95% CI, 1.109-1.626; *P*=0.034). The results of the subgroup survival analyses were summarized in **Table 6**.

DISCUSSION

This large retrospective study has demonstrated that both achievement of VR status and prolonged MVR during NA treatment are associated with a prolonged survival time of patients with HBV-HCC undergoing TACE. The findings of the current study indicate that longer maintenance of undetectable HBV-DNA should be pursued for those with high viral load pre-TACE treatment.

Antiviral therapy using NA has changed the outcome of HBV infection by inhibiting HBV replication and decreasing HBV DNA levels, thereby reducing instead of eliminating the risk of HCC in chronic hepatitis B patients *via* long-term NA treatment. TACE is a common form of locoregional therapy to treat intermediate HCC, which may induce HBV reactivation posttreatment in patients with HBV-HCC as reported in previous studies (29, 30). Another study has demonstrated that a high pre-TACE HBV DNA level has been correlated with poor OS and rapid disease progression after TACE (11), indicating the importance of long-term antiviral therapy for long-lasting suppression of HBV replication to prevent HCC progression. Furthermore, several studies have shown that NA therapy could reduce the risk of deterioration of hepatic function (16, 31, 32) or improve survival outcomes in patients with HBV-HCC undergoing TACE (17, 18).

Numerous studies have demonstrated that the achievement of VR to antiviral therapy is associated with improved clinical outcomes in patients with chronic hepatitis B, including reduced risk of liver disease progression and lower incidence of HCC (20, 33, 34). Additionally, achievement of sustained VR was reported to be important for the reduction of tumor recurrence and improvement of survival outcomes in patients with hepatitis C virus related HCC undergoing TACE treatment with complete remission (35). However, whether VR to NA therapy affects the clinical outcomes of patients with HBV-HCC undergoing TACE treatment is not well known. In the current study, we found that nearly 60% HBV-HCC patients with a high viral load pre-TACE achieved VR after NA therapy. Moreover, our findings suggest that NA therapy with achievement of VR improves OS after TACE for HBV-HCC, which is consistent with a recent study reported by Jang and colleagues (18).

Achieving maintenance of undetectable HBV DNA with NA therapy has been shown to significantly decreased the incidence

TABLE 3 | Baseline characteristics of patients received NA therapy achieving VR (MVR *versus* non-MVR).

Variables	MVR group (n = 542)	non-MVR group (n = 202)
Age, y	56.7 (18-75)	55.9 (18-75)
Sex		
Male	480 (88.6)	177 (87.6)
Female	62 (11.4)	25 (12.4)
Cirrhosis		
Yes	340 (62.7)	135 (66.8)
No	202 (37.3)	67 (33.2)
Ascites		
Yes	28 (5.2)	7 (3.5)
No	514 (94.8)	195 (96.5)
Splenomegaly		
Yes	422 (77.9)	169 (83.7)
No	120 (22.1)	33 (16.3)
ICGR 15		
≤10%	451 (83.2)	171 (84.7)
>10%	91 (16.8)	31 (15.3)
Tumor capsule		
Yes	375 (69.2)	146 (72.3)
No	167 (30.8)	56 (27.7)
Up-to-seven criteria		
Within	415 (76.6)	129 (63.9)
Beyond	127 (23.4)	73 (36.1)
AFP, ug/L		
≤20	167 (30.8)	53 (26.2)
>20	375 (69.2)	149 (73.8)
GGT, u/L	221 (45.0-945.5)	227 (42.5-869.0)
AST, u/L	35 (10-110)	35 (10-121)
ALT, u/L	24 (10-120)	22 (10-120)
Albumin, g/L	38.1 (34-45)	37.5 (34-48)
TBIL, umol/L	12.2 (5.0-25.0)	11.8 (4.1-26.2)
PT, sec	9.5 (7.8-15.0)	8.7 (6.8-17.0)
WBC, 10^9/L	6.2 (4-10)	6.0 (4-10.0)
HB, g/L	13.5 (11.4-14.5)	13.1 (11.6-14.0)
Platelet count, 10^9/L	116 (92-450)	152 (90-449)
Treatment cycles, n	3 (1-6)	3 (1-6)
Other treatment after TACE		
None	338 (62.4)	130 (64.4)
Sorafenib	154 (28.4)	54 (26.7)
Radical therapy	39 (7.2)	13 (6.4)
Radiotherapy or chemotherapy	11 (2.0)	5 (2.5)

Data are presented as median (range) or number (percentage).
MVR, maintained virological response.

of HCC in patients receiving entecavir treatment (23). In this study, according to the level of HBV-DNA during NA therapy, patients with VR achievement were further classified into MVR and non-MVR groups for evaluating the association between MVR status and OS. During follow-up period, 542 of 744 patients (72.8%) presented persistently undetectable HBV DNA levels (MVR), while the remaining subjects experienced episodes of detectable HBV DNA after achieving VR. Jang et al. (18) reported a maintained undetectable HBV-DNA level rate of 58.4% with antiviral therapy for TACE-treat HCC patients. The higher MVR rate of this study can be explained by the different antivirals and baseline characteristics. Only entecavir was used in the current study, while both low-potency NAs (lamivudine, telbivudine, clevudine or adefovir) and high-potency NAs (entecavir or tenofovir) were delivered for antiviral therapy in Jang's study, which may cause a higher rate of drug resistance leading to the HBV reactivation or increase of HBV DNA levels during the period of NA treatment. This indicates the significance of regular HBV DNA surveillance in patients receiving NA treatment, monitoring changes in viral load for timely adjustment of antivirals.

We further evaluated factors correlated with OS. Splenomegaly, tumor burden, total bilirubin and platelet count were independently associated with OS in NA-treated patients therapy achieving VR. In addition, with splenomegaly and tumor burden beyond up-to-seven criteria were the only two adverse factors related to OS in patients achieving MVR based on the multivariable analysis. More importantly, in the subgroup analyses, patients with MVR showed a significantly improved OS than those not achieving MVR, regardless of splenomegaly. We also found that OS was significantly higher among those who achieved MVR than in those without MVR, with a significant VR effect observed in the subgroup of HCC within up-to-seven criteria (P =0.001), but not in those out of up-to-seven criteria.

TABLE 4 | Univariable and multivariable analysis of OS in the MVR group.

Variables	Univariable analysis	Multivariable analysis	
	P value	HR (95% CI)	*P* value
Age, y (≤60/>60)	0.734		
Sex (Male/Female)	0.744		
Cirrhosis (yes/no)	0.202		
Ascites (yes/no)	0.295		
Splenomegaly (yes/no)	0.034	1.339 (1.059-1.692)	0.015
ICGR 15 (≤10%/>10%)	0.939		
Tumor capsule (yes/no)	0.153		
Up-to-seven criteria (beyond/within)	0.001	1.430 (1.110-1.844)	0.006
AFP, ug/L (≤20/>20)	0.100		
GGT, u/L (≤50/>50)	0.795		
AST, u/L (≤40/>40)	0.886		
ALT, u/L (≤40/>40)	0.532		
Albumin, g/L (≤30/>30)	0.303		
TBIL, umol/L (>20.5/≤20.5)	0.163		
PT, sec (≤14/>14)	0.762		
WBC, 10^9/L (≤4/>4)	0.721		
HB, g/L (≤120/>120)	0.336		
Platelet count, 10^9/L (≤100/>100)	0.158		
Sorafenib after TACE (yes/no)	0.001	0.668 (0.533-0.838)	<0.001
Radical therapy after TACE (yes/no)	0.013	0.586 (0.392-0.877)	0.009

Currently, there is lack of an evidence on the effect of MVR duration on survival of HBV-HCC patients receiving TACE. As reported in a Korean study, longer MVR was related to lower risk of HCC in HBV-related compensated cirrhosis patients with low viral load (36). Our findings above demonstrated that maintenance of VR conferred long-term clinical benefits for up to 5 years in HBV-HCC patients with NA therapy undergoing TACE. More importantly, achievement of longer duration of MVR under NA therapy was correlated with a better OS in patients with HBV-HCC following TACE. This highlights the importance of long-term NA therapy and durable viral suppression to improve survival of patients with intermediate HBV-HCC following TACE.

There are several limitations in the present study. First, this is a single-center retrospective study, which may cause inherent bias. Although the baseline characteristics and potential confounders were balanced with no obvious heterogeneity between the two comparison groups (VR and non-VR groups, MVR and non-MVR groups), a causal association between VR status or MVR duration and clinical outcomes of HBV-HCC

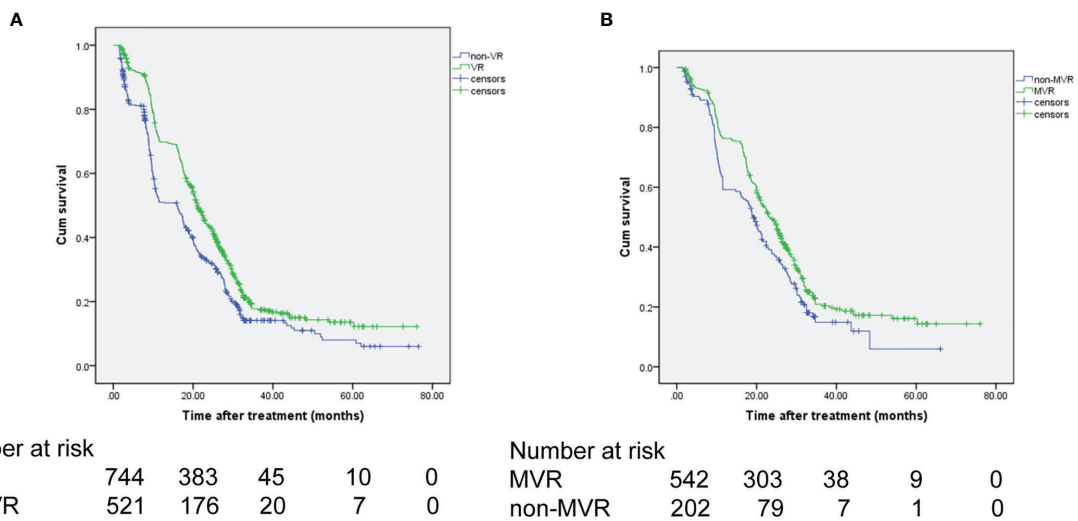

FIGURE 2 | OS of the patients receiving NA therapy. **(A)** OS comparison between the VR and non-VR groups. **(B)** OS comparison between the MVR and non-MVR groups. OS, overall survival; NA, nucelos(t)ide analogues.

TABLE 5 | Univariable and multivariable analysis of OS in patients with NA therapy.

Variables	Univariable analysis	Multivariable analysis	
	P value	HR (95% CI)	*P* value
VR (yes/no)	<0.001	0.772 (0.615-0.916)	0.003
Age, y (≤60/>60)	0.308		
Sex (Male/Female)	0.932		
Cirrhosis (yes/no)	0.872		
Ascites (yes/no)	0.182		
Splenomegaly (yes/no)	0.017	1.222 (1.047-1.426)	0.011
ICGR 15 (≤10%/>10%)	0.457		
Tumor capsule (yes/no)	0.164		
Up-to-seven criteria (within/beyond)	0.001		
AFP (≤20/>20)	0.036		
GGT, u/L (≤50/>50)	0.950		
AST, u/L (≤40/>40)	0.740		
ALT, u/L (≤40/>40)	0.988		
Albumin, g/L (≤30/>30)	0.950		
TBIL, umol/L (≤20.5/>20.5)	0.164		
PT, sec (≤14/>14)	0.096		
WBC, 10^9/L (≤4/>4)	0.438		
HB, g/L (≤120/>120)	0.341		
Platelet count, 10^9/L (≤100/>100)	0.001	1.277 (1.095-1.490)	0.002

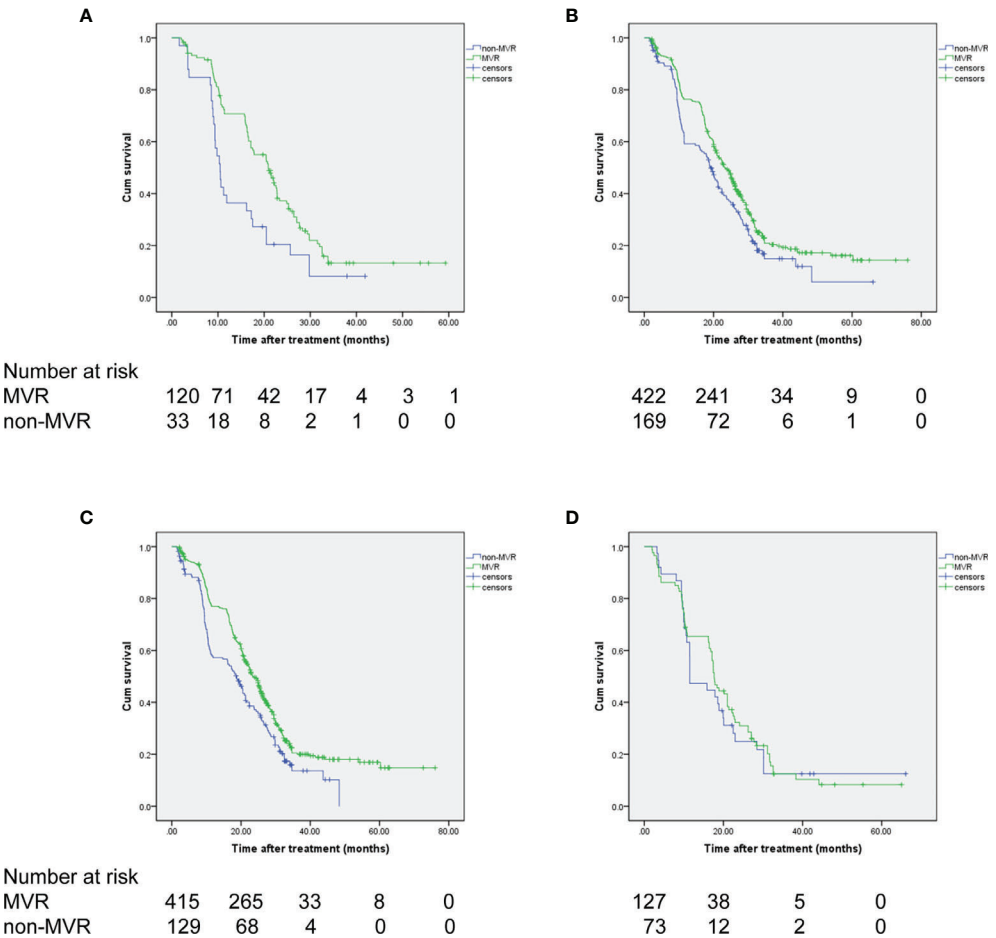

FIGURE 3 | OS of the patients achieving VR based on **(A, B)** splenomegaly status and **(C, D)** up-to-seven criteria. **(A)** without splenomegaly, **(B)** with splenomegaly, **(C)** within up-to-seven criteria, **(D)** beyond up-to-seven criteria.

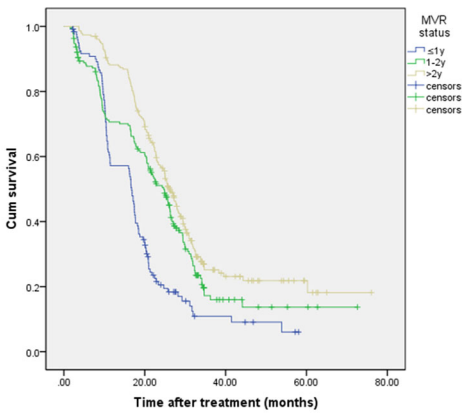

Number at risk

1y	123	38	6	0	0
1-2y	190	109	10	3	0
>2y	229	156	18	6	0

FIGURE 4 | Subgroup analysis of OS in patients with MVR stratified by durations of MVR status.

TABLE 6 | Survival analysis by duration of MVR, tumor burden or splenomegaly in the MVR group.

	OS rate (%)			*P* value
	1-year	3-year	5-year	
MVR status				<0.001
≤1y (n=123)	57.2	10.9	6	< 0.001
1-2y (n=190)	70.6	16.0	13.7	0.024
>2y (n=229)	88.2	25.2	21.8	reference
Tumor burden				0.002
Within up-to-7	77.0	20.5	16.9	
Beyond up-to-7	65.5	12.4	8.3	
Splenomegaly				0.034
No	76.3	20.9	16.1	
Yes	70.7	13.2	13.2	

treated with TACE cannot be directly inferred. On the other hand, few patients who died before achieving the second time of HBV DNA measurement were assigned to the non-VR group, which may lead to immortal time bias. Second, patients receiving TACE treatment with a pre-TACE HBV-DVA over 2000 IU/mL were included in the analysis. For those with a low viral load (baseline HBV-DNA level between 100 to 1999) or undergoing other anticancer treatments, the conclusions need further confirmed. Thus, findings in the present study need to be validated in the well-designed prospective studies.

In conclusion, both achievement of VR status and prolonged MVR receiving NA therapy are correlated with better OS in patients with intermediate-stage HBV-HCC undergoing TACE, indicating the importance of regular HBV DNA surveillance and durable viral suppression during antiviral treatment.

DATA AVAILABILITY STATEMENT

The original contributions presented in the study are included in the article/supplementary material. Further inquiries can be directed to the corresponding authors.

ETHICS STATEMENT

The studies involving human participants were reviewed and approved by Ethics Committee of Sun Yat-sen University Cancer Center. The ethics committee waived the requirement of written informed consent for participation.

AUTHOR CONTRIBUTIONS

ZP had full access to all the data in the study and takes responsibility for the integrity of the data and the accuracy of the data analysis. Concept and design: MC and ZP. Acquisition, analysis, or interpretation of data: MJ, YC, SH, MZ, YW, MC, and ZP. Drafting of the manuscript: MJ and SH. Critical revision of the manuscript for important intellectual content: YC, MC, and ZP. Statistical analysis: MJ and ZP. All authors contributed to the article and approved the submitted version.

FUNDING

This study was supported by the National Natural Science Foundation of China (No. 81770608, 82072029), the National high level talents special support plan-"Ten thousand plan"-Young top-notch talent support program.

REFERENCES

1. El-Serag HB. Epidemiology of Viral Hepatitis and Hepatocellular Carcinoma. *Gastroenterology* (2012) 142(6):1264–73.e1. doi: 10.1053/j.gastro.2011.12.061
2. Sung H, Ferlay J, Siegel RL, Laversanne M, Soerjomataram I, Jemal A, et al. Global Cancer Statistics 2020: GLOBOCAN Estimates of Incidence and Mortality Worldwide for 36 Cancers in 185 Countries. *CA Cancer J Clin* (2021) 71(3):209–49. doi: 10.3322/caac.21660
3. Global Burden of Disease Liver Cancer C, Akinyemiju T, Abera S, Ahmed M, Alam N, Alemayohu MA, et al. The Burden of Primary Liver Cancer and Underlying Etiologies From 1990 to 2015 at the Global, Regional, and National Level: Results From the Global Burden of Disease Study 2015. *JAMA Oncol* (2017) 3(12):1683–91. doi: 10.1001/jamaoncol.2017.3055
4. Fung J, Lai CL, Yuen MF. Hepatitis B and C Virus-Related Carcinogenesis. *Clin Microbiol Infect* (2009) 15(11):964–70. doi: 10.1111/j.1469-0691.2009.03035.x
5. Liaw YF, Sung JJ, Chow WC, Farrell G, Lee CZ, Yuen H, et al. Lamivudine for Patients With Chronic Hepatitis B and Advanced Liver Disease. *N Engl J Med* (2004) 351(15):1521–31. doi: 10.1056/NEJMoa033364
6. Wu CY, Lin JT, Ho HJ, Su CW, Lee TY, Wang SY, et al. Association of Nucleos(T)Ide Analogue Therapy With Reduced Risk of Hepatocellular Carcinoma in Patients With Chronic Hepatitis B: A Nationwide Cohort

Study. *Gastroenterology* (2014) 147(1):143–51.e5. doi: 10.1053/j.gastro.2014.03.048
7. European Association for the Study of the Liver, Electronic Address Eee and European Association for the Study of the L. EASL Clinical Practice Guidelines: Management of Hepatocellular Carcinoma. *J Hepatol* (2018) 69 (1):182–236. doi: 10.1016/j.jhep.2018.03.019
8. Marrero JA, Kulik LM, Sirlin CB, Zhu AX, Finn RS, Abecassis MM, et al. Diagnosis, Staging, and Management of Hepatocellular Carcinoma: 2018 Practice Guidance by the American Association for the Study of Liver Diseases. *Hepatology* (2018) 68(2):723–50. doi: 10.1002/hep.29913
9. Yin J, Li N, Han Y, Xue J, Deng Y, Shi J, et al. Effect of Antiviral Treatment With Nucleotide/Nucleoside Analogs on Postoperative Prognosis of Hepatitis B Virus-Related Hepatocellular Carcinoma: A Two-Stage Longitudinal Clinical Study. *J Clin Oncol* (2013) 31(29):3647–55. doi: 10.1200/JCO.2012.48.5896
10. Yeo W, Mo FK, Chan SL, Leung NW, Hui P, Lam WY, et al. Hepatitis B Viral Load Predicts Survival of HCC Patients Undergoing Systemic Chemotherapy. *Hepatology* (2007) 45(6):1382–9. doi: 10.1002/hep.21572
11. Yu SJ, Lee JH, Jang ES, Cho EJ, Kwak MS, Yoon JH, et al. Hepatocellular Carcinoma: High Hepatitis B Viral Load and Mortality in Patients Treated With Transarterial Chemoembolization. *Radiology* (2013) 267(2):638–47. doi: 10.1148/radiol.13121498
12. Wu CY, Chen YJ, Ho HJ, Hsu YC, Kuo KN, Wu MS, et al. Association Between Nucleoside Analogues and Risk of Hepatitis B Virus-Related Hepatocellular Carcinoma Recurrence Following Liver Resection. *JAMA* (2012) 308(18):1906–14. doi: 10.1001/2012.jama.11975
13. Huang G, Lau WY, Wang ZG, Pan ZY, Yuan SX, Shen F, et al. Antiviral Therapy Improves Postoperative Survival in Patients With Hepatocellular Carcinoma: A Randomized Controlled Trial. *Ann Surg* (2015) 261(1):56–66. doi: 10.1097/SLA.0000000000000858
14. Huang G, Li PP, Lau WY, Pan ZY, Zhao LH, Wang ZG, et al. Antiviral Therapy Reduces Hepatocellular Carcinoma Recurrence in Patients With Low HBV-DNA Levels: A Randomized Controlled Trial. *Ann Surg* (2018) 268 (6):943–54. doi: 10.1097/SLA.0000000000002727
15. Lee TY, Lin JT, Zeng YS, Chen YJ, Wu MS, Wu CY. Association Between Nucleos(T)Ide Analog and Tumor Recurrence in Hepatitis B Virus-Related Hepatocellular Carcinoma After Radiofrequency Ablation. *Hepatology* (2016) 63(5):1517–27. doi: 10.1002/hep.28266
16. Lao XM, Luo G, Ye LT, Luo C, Shi M, Wang D, et al. Effects of Antiviral Therapy on Hepatitis B Virus Reactivation and Liver Function After Resection or Chemoembolization for Hepatocellular Carcinoma. *Liver Int* (2013) 33 (4):595–604. doi: 10.1111/liv.12112
17. Zhou ZG, Zheng XR, Zhou Q, Shi M, Zhang YJ, Guo RP, et al. Impact of Oral Anti-Hepatitis B Therapy on the Survival of Patients With Hepatocellular Carcinoma Initially Treated With Chemoembolization. *Chin J Cancer* (2015) 34(5):205–16. doi: 10.1186/s40880-015-0017-7
18. Jang JW, Yoo SH, Nam HC, Jang BH, Sung Sung PS, Lee W, et al. Association of Prophylactic Anti-Hepatitis B Virus Therapy With Improved Long-Term Survival in Patients With Hepatocellular Carcinoma Undergoing Transarterial Therapy. *Clin Infect Dis* (2020) 71(3):546–55. doi: 10.1093/cid/ciz860
19. Cho JY, Paik YH, Sohn W, Cho HC, Gwak GY, Choi MS, et al. Patients With Chronic Hepatitis B Treated With Oral Antiviral Therapy Retain a Higher Risk for HCC Compared With Patients With Inactive Stage Disease. *Gut* (2014) 63(12):1943–50. doi: 10.1136/gutjnl-2013-306409
20. Kim SS, Hwang JC, Lim SG, Ahn SJ, Cheong JY, Cho SW. Effect of Virological Response to Entecavir on the Development of Hepatocellular Carcinoma in Hepatitis B Viral Cirrhotic Patients: Comparison Between Compensated and Decompensated Cirrhosis. *Am J Gastroenterol* (2014) 109(8):1223–33. doi: 10.1038/ajg.2014.145
21. Di Marco V, Marzano A, Lampertico P, Andreone P, Santantonio T, Almasio PL, et al. Clinical Outcome of HBeAg-Negative Chronic Hepatitis B in Relation to Virological Response to Lamivudine. *Hepatology* (2004) 40 (4):883–91. doi: 10.1002/hep.20381
22. European Association for the Study of the Liver, Electronic Address Eee and European Association for the Study of the L. EASL 2017 Clinical Practice Guidelines on the Management of Hepatitis B Virus Infection. *J Hepatol* (2017) 67(2):370–98. doi: 10.1016/j.jhep.2017.03.021
23. Kim JH, Sinn DH, Kang W, Gwak GY, Paik YH, Choi MS, et al. Low-Level Viremia and the Increased Risk of Hepatocellular Carcinoma in Patients Receiving Entecavir Treatment. *Hepatology* (2017) 66(2):335–43. doi: 10.1002/hep.28916
24. Tsochatzis EA, Bosch J, Burroughs AK. Liver Cirrhosis. *Lancet* (2014) 383 (9930):1749–61. doi: 10.1016/S0140-6736(14)60121-5
25. Mazzaferro V, Llovet JM, Miceli R, Bhoori S, Schiavo M, Mariani L, et al. Predicting Survival After Liver Transplantation in Patients With Hepatocellular Carcinoma Beyond the Milan Criteria: A Retrospective, Exploratory Analysis. *Lancet Oncol* (2009) 10(1):35–43. doi: 10.1016/S1470-2045(08)70284-5
26. Zhang Y, Zhang M, Chen M, Mei J, Xu L, Guo R, et al. Association of Sustained Response Duration With Survival After Conventional Transarterial Chemoembolization in Patients With Hepatocellular Carcinoma. *JAMA Netw Open* (2018) 1(6):e183213. doi: 10.1001/jamanetworkopen.2018.3213
27. Peng ZW, Zhang YJ, Chen MS, Xu L, Liang HH, Lin XJ, et al. Radiofrequency Ablation With or Without Transcatheter Arterial Chemoembolization in the Treatment of Hepatocellular Carcinoma: A Prospective Randomized Trial. *J Clin Oncol* (2013) 31(4):426–32. doi: 10.1200/JCO.2012.42.9936
28. Lencioni R, Llovet JM. Modified RECIST (mRECIST) Assessment for Hepatocellular Carcinoma. *Semin Liver Dis* (2010) 30(1):52–60. doi: 10.1055/s-0030-1247132
29. Jang JW, Choi JY, Bae SH, Kim CW, Yoon SK, Cho SH, et al. Transarterial Chemo-Lipiodolization can Reactivate Hepatitis B Virus Replication in Patients With Hepatocellular Carcinoma. *J Hepatol* (2004) 41(3):427–35. doi: 10.1016/j.jhep.2004.05.014
30. Jang JW, Choi JY, Bae SH, Yoon SK, Chang UI, Kim CW, et al. A Randomized Controlled Study of Preemptive Lamivudine in Patients Receiving Transarterial Chemo-Lipiodolization. *Hepatology* (2006) 43(2):233–40. doi: 10.1002/hep.21024
31. Nagamatsu H, Itano S, Nagaoka S, Akiyoshi J, Matsugaki S, Kurogi J, et al. Prophylactic Lamivudine Administration Prevents Exacerbation of Liver Damage in HBe Antigen Positive Patients With Hepatocellular Carcinoma Undergoing Transhepatic Arterial Infusion Chemotherapy. *Am J Gastroenterol* (2004) 99(12):2369–75. doi: 10.1111/j.1572-0241.2004.40069.x
32. Li X, Zhong X, Chen ZH, Wang TT, Ma XK, Xing YF, et al. Efficacy of Prophylactic Entecavir for Hepatitis B Virus-Related Hepatocellular Carcinoma Receiving Transcatheter Arterial Chemoembolization. *Asian Pac J Cancer Prev* (2015) 16(18):8665–70. doi: 10.7314/apjcp.2015.16.18.8665
33. Yang SC, Lee CM, Hu TH, Wang JH, Lu SN, Hung CH, et al. Virological Response to Entecavir Reduces the Risk of Liver Disease Progression in Nucleos(T)Ide Analogue-Experienced HBV-Infected Patients With Prior Resistant Mutants. *J Antimicrob Chemother* (2013) 68(9):2154–63. doi: 10.1093/jac/dkt147
34. Zoutendijk R, Reijnders JG, Zoulim F, Brown A, Mutimer DJ, Deterding K, et al. Virological Response to Entecavir Is Associated With a Better Clinical Outcome in Chronic Hepatitis B Patients With Cirrhosis. *Gut* (2013) 62 (5):760–5. doi: 10.1136/gutjnl-2012-302024
35. Teng W, Hsieh YC, Lui KW, Chen WT, Hung CF, Huang CH, et al. Eradication of Hepatitis C Virus Profoundly Prolongs Survival in Hepatocellular Carcinoma Patients Receiving Transarterial Chemoembolization. *J Viral Hepat* (2017) 24 (12):1160–7. doi: 10.1111/jvh.12745
36. Sinn DH, Lee J, Goo J, Kim K, Gwak GY, Paik YH, et al. Hepatocellular Carcinoma Risk in Chronic Hepatitis B Virus-Infected Compensated Cirrhosis Patients With Low Viral Load. *Hepatology* (2015) 62(3):694–701. doi: 10.1002/hep.27889

Conflict of Interest: The authors declare that the research was conducted in the absence of any commercial or financial relationships that could be construed as a potential conflict of interest.

The handling editor declared a past collaboration with one of the authors MJ.

Publisher's Note: All claims expressed in this article are solely those of the authors and do not necessarily represent those of their affiliated organizations, or those of the publisher, the editors and the reviewers. Any product that may be evaluated in this article, or claim that may be made by its manufacturer, is not guaranteed or endorsed by the publisher.

frontiers in Oncology

ORIGINAL RESEARCH
published: 03 November 2021
doi: 10.3389/fonc.2021.738801

Establishment of Tumor Treating Fields Combined With Mild Hyperthermia as Novel Supporting Therapy for Pancreatic Cancer

Liping Bai[1†], *Tobias Pfeifer*[1], *Wolfgang Gross*[1], *Carolina De La Torre*[2], *Shuyang Zhao*[3], *Li Liu*[1], *Michael Schaefer*[1‡] *and Ingrid Herr*[1*‡]

[1] Molecular OncoSurgery, Section Surgical Research, Department of General, Visceral and Transplantation Surgery, University of Heidelberg, Heidelberg, Germany, [2] Medical Research Center, Medical Faculty Mannheim, University of Heidelberg, Heidelberg, Germany, [3] Department of Hematology, Oncology and Rheumatology, Internal Medicine V, University Hospital of Heidelberg, Heidelberg, Germany

Pancreatic ductal adenocarcinoma (PDAC) is a highly malignant tumor with poor prognosis and limited therapeutic options. Alternating electrical fields with low intensity called "Tumor Treating Fields" (TTFields) are a new, non-invasive approach with almost no side effects and phase 3 trials are ongoing in advanced PDAC. We evaluated TTFields in combination with mild hyperthermia. Three established human PDAC cell lines and an immortalized pancreatic duct cell line were treated with TTFields and hyperthermia at 38.5°C, followed by microscopy, assays for MTT, migration, colony and sphere formation, RT-qPCR, FACS, Western blot, microarray and bioinformatics, and *in silico* analysis using the online databases *GSEA, KEGG*, Cytoscape-String, and Kaplan-Meier Plotter. Whereas TTFields and hyperthermia alone had weak effects, their combination strongly inhibited the viability of malignant, but not those of nonmalignant cells. Progression features and the cell cycle were impaired, and autophagy was induced. The identified target genes were key players in autophagy, the cell cycle and DNA repair. The expression profiles of part of these target genes were significantly involved in the survival of PDAC patients. In conclusion, the combination of TTFields with mild hyperthermia results in greater efficacy without increased toxicity and could be easily clinically approved as supporting therapy.

Keywords: pancreatic ductal adenocarcinoma, hyperthermia, tumor treating fields, alternative therapies, bioinformatics and computational biology

OPEN ACCESS

Edited by:
Jiang Chen,
Zhejiang University, China

Reviewed by:
Feng Zengyu,
Shanghai Jiao Tong University, China
Antonio Giovanni Solimando,
University of Bari Aldo Moro, Italy
Hop Tran Cao,
University of Texas MD Anderson Cancer Center, United States

***Correspondence:**
Ingrid Herr
i.herr@uni-heidelberg.de

***Present address:**
Liping Bai,
Department of Gastrointestinal Surgery, The Affiliated Zhongshan Hospital, and Institute of Gastrointestinal Oncology, School of Medicine, Xiamen University, Xiamen, China

*These authors share last authorship

Specialty section:
This article was submitted to Gastrointestinal Cancers: Hepato Pancreatic Biliary Cancers, a section of the journal Frontiers in Oncology

Received: *09 July 2021*
Accepted: *18 October 2021*
Published: *03 November 2021*

Citation:
Bai L, Pfeifer T, Gross W, De La Torre C, Zhao S, Liu L, Schaefer M and Herr I (2021) Establishment of Tumor Treating Fields Combined With Mild Hyperthermia as Novel Supporting Therapy for Pancreatic Cancer. Front. Oncol. 11:738801. doi: 10.3389/fonc.2021.738801

Abbreviations: ANOVA, One-way analysis of variance; CI, Confidence interval; HR, Hazard ratio; FDR, False discovery rate; GSEA, Gene set enrichment analysis; KEGG, Kyoto Encyclopedia of Genes and Genomes; MTT, 3-(4,5-dimethylthiazol-2-yl)-2,5-diphenyltetrazolium bromide; OS, Overall survival; RFS, Recurrence-free survival; SD, Standard deviation; PDAC, Pancreatic ductal adenocarcinoma; TCGA, The Cancer Genome Atlas; TTFs, Tumor Treating Fields.

INTRODUCTION

Pancreatic ductal adenocarcinoma (PDAC) has an exceptionally poor prognosis, high therapy resistance, and high rates of early metastasis (1). Currently, surgery remains the only chance to cure pancreatic cancer; however, >90% of patients relapse and die of their disease without additional treatment (2). For resectable tumors, surgery followed by adjuvant chemotherapy (gemcitabine plus capecitabine) is the standard of care. In the metastatic setting, FOLFIRINOX and nab-paclitaxel–gemcitabine are standard treatment options for patients with good performance status; both combinations have shown a survival advantage over the previous standard of gemcitabine monotherapy (2).

Tumor Treating Fields (TTFields) were first described in 2004 (3) and are low-intensity, intermediate-frequency, alternating electric fields delivered through noninvasive transducer arrays placed locoregionally around the anatomic region of the tumor (4). TTFields selectively target tumor cells or rapidly proliferating cells but not slowly proliferating tissues or cell cultures. The advantage of TTFields is that (1) the electrodes are noninvasive; (2) mainly cancer cells are targeted; (3) a thermal effect is not described due to the low intensity; and (4) nerves and muscles are not stimulated because of the high frequency of TTFields (3, 5, 6). Mechanistically, TTFields inhibit tumor cell division (7) by impairing the polymerization of microtubules and septin filaments during mitosis (7–9) and extending the duration of mitosis by the formation of defective mitosis structures (3, 7). This leads to aneuploidy and genomic instability, termed mitotic catastrophe, followed by cell death and senescence (7, 10).

Currently, the NovoTTF-100 or Optune system developed by Novocure Ltd. was approved by the FDA and EU for the treatment of therapy-refractory cancer entities such as glioblastoma and mesothelioma (11), and in Germany, a reimbursement mechanism has been in place since March 2020 (12). Phase 3 studies are currently underway for brain, lung, pancreas and uterine tumors, and a phase 2 study is being conducted for liver tumors. In addition, promising experimental data are available for numerous tumor entities (13), including the effects of TTFields on the PDAC cell lines AsPC-1 (14), CFPAC-I and HPAF-II (15). Upon treatment with TTFields at 150 kHz for 72 h, the cell number and viability were reduced, and the gemcitabine or radiation efficacy increased (14, 15). The PANOVA-2 trial recently demonstrated that the combination of TTFields and systemic chemotherapy is safe and tolerable in patients with advanced PDAC (16). Based on these results, the randomized PANOVA-3 trial is currently testing the efficacy of TTFields generated by the NovoTTF-100L(P) System in advanced PDAC in combination with palliative chemotherapy (17). However, TTFields remain controversial, e.g., in glioblastoma therapy, where the uptake of TTFields is increasing but remains limited (12).

Hyperthermia in oncology was first reported 5,000 years ago in a case of breast cancer (18). Today, the efficacy of locally applied, mild, moderate or severe hyperthermia, in the range from 39°C to 43°C was proven to be clinically effective in combination with radiotherapy and chemotherapy (19–21). Several applications at different temperatures are in clinical use, such as whole-body heating, or loco-regional hyperthermia. The latter also includes intraoperative superficial heating, hyperthermic intraperitoneal chemotherapy (HIPEC) and non-invasive deep regional heating (22). Moderate hyperthermia temperatures are used clinically in the form of whole-body hyperthermia e.g. in pain therapy. For this purpose, patients are heated for a duration of up to 1.5 h in insulated heat cabins. Alternatively, local application of mild hyperthermia in the tumor region can be achieved by infrared or microwave heating of the tissue. Randomized phase 2 and 3 clinical trials demonstrated that hyperthermia sensitizes tumors to cytotoxic therapy and thereby improved the outcome of cancers of the lung (23), breast (24), cervix (25), head and neck (26), skin (27), gastrointestinal tract (28), ovary (29), and sarcoma (30). For PDAC, the efficacy of hyperthermia has been demonstrated in the preclinical setting, e.g., in xenograft models in rats and mice, where the combination of gemcitabine and hyperthermia was more effective than single therapies (31). Mechanistically, hyperthermia alters the blood flow and nutrient distribution in tumors, induces a heat shock response followed by cell death in cancer cells (32), causes DNA damage (33), inhibits DNA repair (34), and induces cell cycle arrest (33, 35). However, the effective delivery of hyperthermia is often limited, and moderate to severe hyperthermia can have complications (36).

Our present study investigated whether a combination of mild hyperthermia of 38.5°C and TTFields of less than 1 V/cm would be more effective than each single treatment alone. We found a synergistic effect in PDAC cancer cells, whereas nonmalignant cells were not affected, and we identified the underlying signaling chains.

RESULTS

Hyperthermia Enhances TTField-Mediated Inhibition of Viability

To examine the effect of TTFields on the viability of PDAC cell lines, we cultured BxPc-3, BxGEM and AsPC-1 cells in specially manufactured 96-well culture plates with electrodes to induce TTFields at frequencies of 150 kHz by a generator (**Figure 1A**). The cells in these culture plates were incubated at 37°C or 38.5°C for up to six days. The plates were then evaluated daily by MTT assay, which measures the cellular metabolic activity as an indicator of cell viability, proliferation and cytotoxicity. The values of each group were set to 0 at the start of the experiment at day 1. Whereas the MTT signal of cells cultured at 37°C in the presence or absence of TTFields continuously increased, it was even higher when the cells were cultured at 38.5°C (**Figure 1B**). A pronounced inhibition of viability was only seen upon the combination of hyperthermia and TTFields. These results became even clearer upon setting the controls to 1 and presenting the data in bar charts. While TTFields tended to increase the viability at 37°C, they significantly decreased it at 38.5°C after 3 days (**Figure 1C**). After 6 days, however, TTFields largely decreased the viability even at 37°C and almost completely

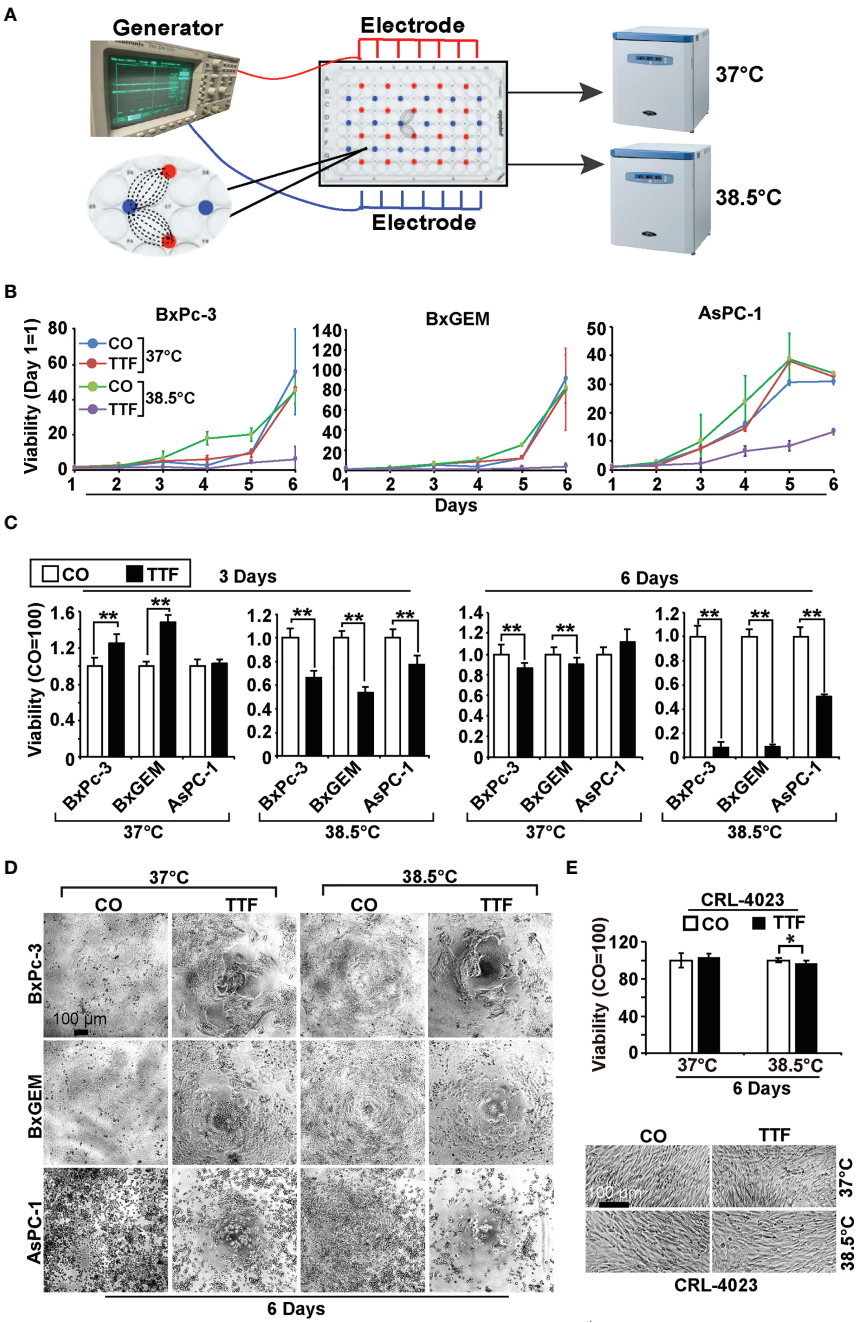

FIGURE 1 | TTField-mediated inhibition of viability is enhanced by hyperthermia. **(A)** The scheme illustrates the treatment of PDAC cells with TTFields at a regular incubation temperature of 37°C or mild hyperthermia at 38.5°C. **(B)** The human PDAC cell lines AsPC-1, BxPC-3 and BxGEM were incubated at 37°C or 38.5°C in the presence (TTF) or absence (CO) of TTFields at 150 kHz and an intensity of less than 0.7 V/cm. To measure TTField effects as a function of treatment duration, PDAC cells were treated for 1 to 6 days in separate experiments. The examination of all 6 days together in one large experiment was not possible because the availability of the cell culture plates with antenna wires was limited. At the end of each single experiment, the viability was measured by MTT assay, the results were accumulated as a total curve for each cell line, and the values of each curve were normalized to start at 0 on day 1. **(C)** The cells were treated as described above, and the viability was analyzed 3 or 6 days later by MTT assay. The controls were set to 1. **(D)** The morphology of the cells, which were treated as described above, was microscopically examined at 100× magnification 6 days after treatment, and representative images are shown. The scale bar indicates 100 μm. **(E)** Likewise, the viability of the human, nonmalignant pancreatic duct cell line CRL-4023 was evaluated by MTT assay and microscopic evaluation at 100× magnification. Representative images of each treatment group of CRL-4023 cells 6 days after treatment are shown. Three independent experiments were performed at least in triplicate, and the data are presented as the means ± SD; *P < 0.05, **P < 0.01.

at 38.5°C. Representative images of the cell morphology under microscopic magnification confirm the above results (**Figure 1D**). Interestingly, mild hyperthermia paired with TTFields failed to substantially inhibit the viability of the nonmalignant pancreatic ductal cell line CRL-4023, even 6 days after treatment (**Figure 1E**).

Hyperthermia Increases TTField-Mediated Inhibition of Cancer Progression

To obtain information on the influence of mild hyperthermia paired with TTFields on stem cell properties, we studied the ability to form colonies. BxPc-3, BxGEM and AsPC-1 cells were treated with TTFields at 37°C or 38.5°C for 72 h. Then, the cells were reseeded at clonal density in 6-well plates, and colony formation was evaluated 14 days later. Whereas TTFields at 37°C only marginally reduced colony formation, they strongly reduced it at 38.5°C (**Figure 2A**). In contrast, hyperthermia alone significantly increased colony formation. For examination of the long-term effect, the surviving cells of each group were collected and equal cell numbers were reseeded at clonal density without further treatment. The resulting, so-called "second-generation" colonies were analyzed 14 days later. TTFields at 37°C reduced colony formation to approximately 50% to 60%, and TTFields in the presence of 38.5°C nearly completely abolished colony formation. Additionally, hyperthermia alone did not enhance colony formation, as observed in the short-term treatment. Similar results were obtained when the cells were treated and grown as spheroids (**Figure 2B**). Under these conditions, the effects were more pronounced upon reseeding the cells for second-generation spheroid formation. Next, we examined the effect of TTFields combined with mild hyperthermia or of mild hypothermia alone on migration and performed scratch assays. The closure of the wounded region was examined 12 h and 24 h later. The gap was significantly larger upon combination of TTFields and 38.5°C compared to 38.5°C alone (**Figure 3**). In contrast, the same experiments at 37°C were largely ineffective (data not shown). This result suggests again that the combination therapy also inhibits migration more than each single treatment option alone.

Hyperthermia Increases TTField-Induced Differential Gene Expression

To further highlight gene expression changes, we treated BxGEM cells at 37°C and 38.5°C and used untreated cells cultured at 37°C as control. Seventy-two hours later, the RNA was harvested and a gene array analysis was performed. A heat map was generated and demonstrated well-separated gene clusters between the groups (**Figure 4A**). This finding was further highlighted by a volcano plot analysis of the array results, which exhibited a greater spreading of differentially regulated genes when TTFields plus were combined with 38.5°C compared to TTFields alone at 37°C (**Figure 4B**). Then, a KEGG enrichment analysis was performed, which led to the identification of 20 significantly up- or downregulated pathways closely related to tumorigenesis (**Figure 4C** and **Table 1**). Among the differentially regulated pathways were the ubiquitin proteasome system and autophagy, DNA repair, DNA replication, MAPK signaling and cell cycle regulation. Next, a GSEA analysis was performed and resulted in enrichment plots of autophagy, cell cycle and DNA replication (**Figure 5A**). The most significantly differentially regulated genes belonging to these pathways are shown in heat maps (**Figure 5B**). To identify the related signaling networks, the open source software platforms Cytoscape and String were utilized, which showed Tp53, PNCA, and MAD2L2 in the center of two cell cycle/DNA replication signaling networks and AKT1 in the center of an autophagy-related signaling network (**Figure 5C**). Thus, there is an interaction of the identified differentially regulated genes in biological signaling networks.

Hyperthermia and TTFields Enhance Autophagy and Cell Cycle Signaling

For validation of our previous results, BxPc-3, BxGEM and AsPC-1 cells were treated with TTFields plus hyperthermia at 38.5°C, whereas cells cultured at 37°C without further treatment served as control. Seventy-two hours later, RT-qPCR was performed to examine the expression of the before identified target genes CyclinB, CDK1, GADD45B, MAD2L2, MCM6, TP53, ATG5, TSC1 and AKT1. The expression of each gene was normalized to the expression of GAPDH, and the gene expression of the TTField plus 38.5°C group was evaluated relative to the 37°C control, which was set to 1. GADD45B, TP53, ATG5 and TSC1 were significantly upregulated in all cell lines, whereas MAD2L2, MCM6 and AKT1 were significantly downregulated (**Figure 6A**). In contrast, the expression levels of CyclinB and CDK1 did not appreciably change. Most importantly, the expression patterns largely confirmed the expression data from the microarray assay, which is underlined by comparison of the results of both assays (**Table 2**).

To investigate the effect of TTFields on the cell cycle, the cells were cultured at 37°C or 38.5°C in the presence or absence of TTFields. Seventy-two hours later, the cells were stained with propidium iodide and examined by flow cytometry. TTFields combined with mild hyperthermia led to an increase of the G2/M phase, and a decrease of the G1 phase, whereas a statistically significant S phase arrest was not observed (**Figure 6B**).

To examine the influence induction of autophagy, the cells were cultured at 37°C or 38.5°C in absence or presence of TTFields. Seventy-two hours later, the expression of the autophagic flux indicator p62 and the presence of the autophagy marker LC3-II were examined by Western blot analysis. Whereas p62 expression decreased upon TTField treatment at 37°C and 38.5°C, indicating autophagy signaling, LC3-II was only clearly visible after combining TTFields with mild hyperthermia, as shown by a representative Western blot, quantification by Image J and a diagram with the means and standard deviations; also, the crude Western blot images are provided (**Figure 6C** and **Supplementary Figure S1**, data not shown). These data indicate that autophagy signaling occurred and was strongest when TTFields were combined with mild hyperthermia.

Our Candidate Genes Are of Prognostic Relevance in PDAC

To demonstrate the clinical relevance of candidate genes, which we identified by gene array analysis, we utilized TCGA public database and identified the availability of expression data paired

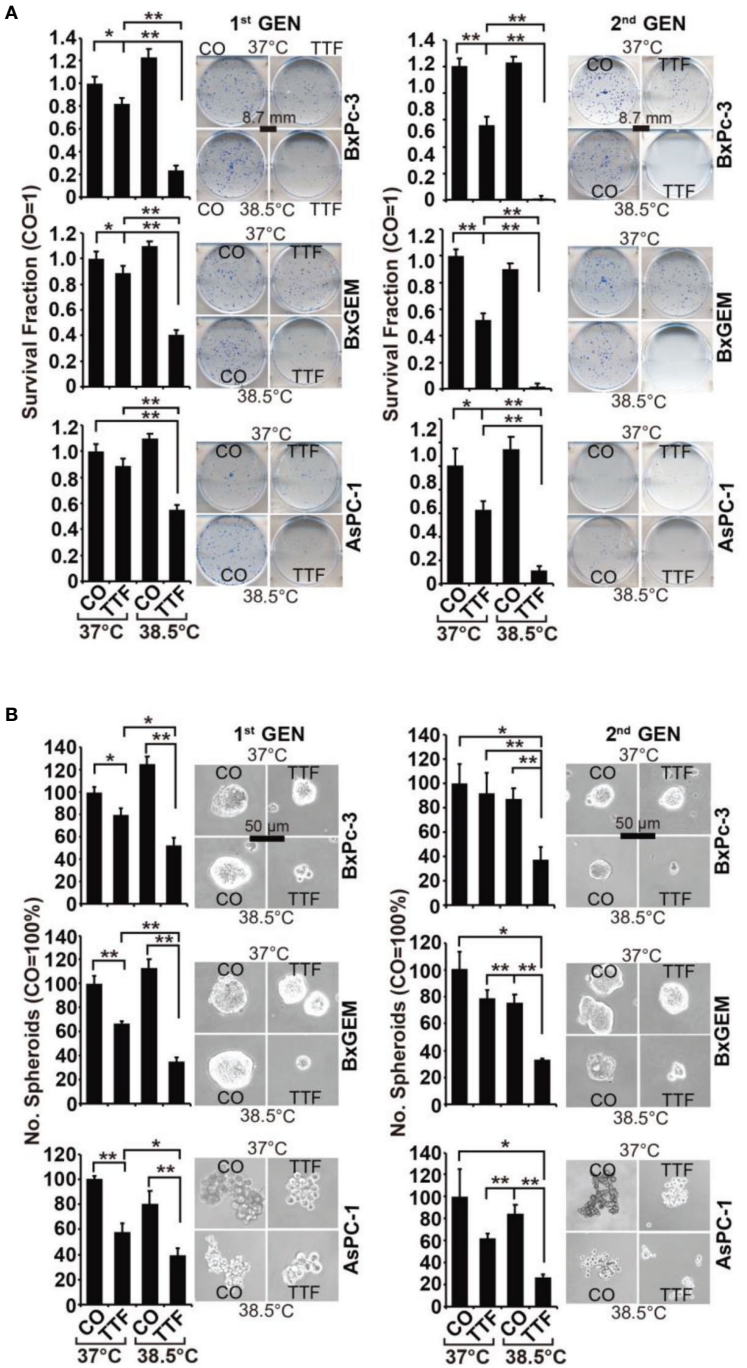

FIGURE 2 | TTField-mediated inhibition of cancer stem cell features is enhanced by hyperthermia. **(A)** The cells were treated as described in **Figures 1A, B**. **(B)** After 3 days, the cells were detached from the cell culture plates by trypsinization and reseeded at clonal density (AsPC-1: 1,500 cells/well; BxPC-3 and Bx-GEM: 1,000 cells/well) in 6-well plates. The cells were cultured under regular conditions at 37°C without a medium change for 2 weeks, resulting in first-generation colonies (1st GEN). The number of colonies was evaluated by fixing and Coomassie staining, followed by counting colonies with at least 50 cells using a dissecting microscope. The survival fraction and representative images are shown on the left. For the formation of second-generation (2nd GEN) colonies, surviving cells from each group of first-generation colonies were collected, reseeded and analyzed as described above. **(B)** After treatment, as described in **Figure 1A**, the cells were seeded at a clonal density of 500 cells/well in ultralow-attachment 24-well plates in cell growth factor-supplemented serum-free culture medium to induce spheroid formation. Six days later, the first generation of spheroids developed, and the percentage of viable spheroids was evaluated by microscopy at 100× magnification and counting. Representative photographs and the means are shown on the left. For the formation of second-generation spheroids (2nd GEN), surviving cells were collected from each group of first-generation spheroids and reseeded and analyzed as described above. The data are presented as the means ± SDs. *P < 0.05, **P < 0.01.

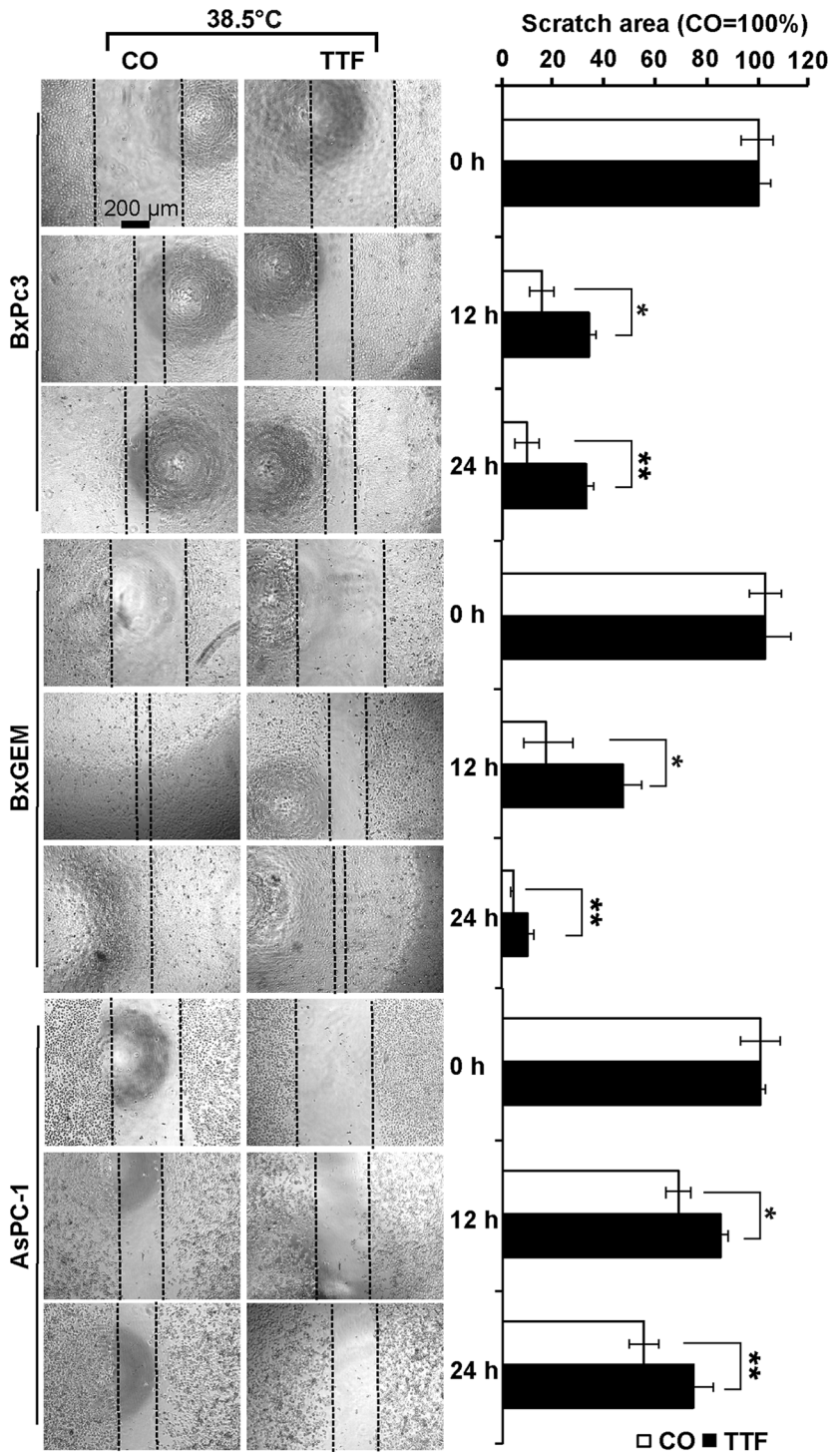

FIGURE 3 | TTField-mediated inhibition of migration is stronger upon combination with hyperthermia. AsPC-1, BxPC-3 and Bx-GEM cells were seeded at a density of 4,000 cells/well in 96-well plates and grown to 90% confluency overnight. The cell layer was scratched with the tip of a 100-μL pipet, followed by treatment of the cells with TTFields at 38.5°C for 24 h. The controls (CO) were incubated at 38.5°C without exposure to TTFields. The closure of the wounded region was evaluated by microscopy at 0, 12 and 24 h after scratching. The gap width was measured using ImageJ. Representative images are shown on the left, and the means are shown in bar graphs on the right. The data are presented as the means ± SD. *$P < 0.05$, **$P < 0.01$.

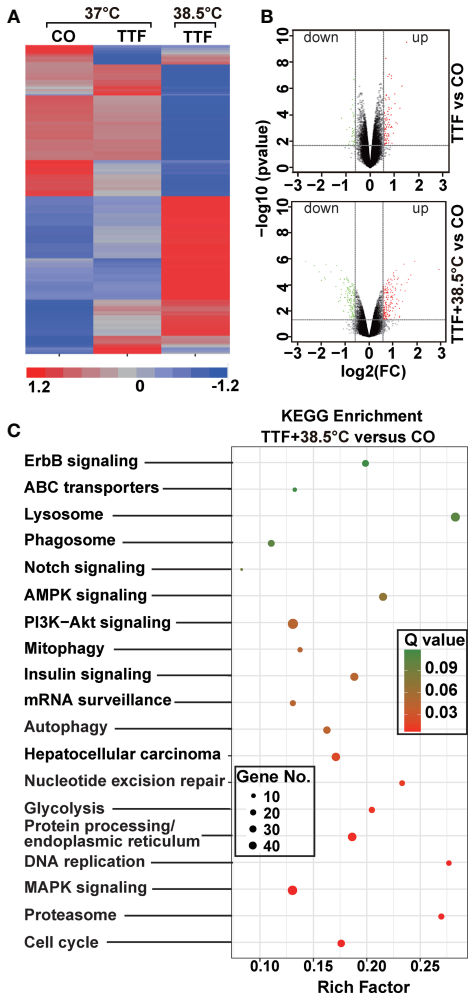

FIGURE 4 | Gene array analysis demonstrates that hyperthemia enhances TTField-induced differential gene expression. **(A)** BxGEM cells were cultivated at 37°C in the absence (CO) or presence of TTFields (TTF) or were cultured at 38.5°C in the presence of TTFields (TTF+38.5°C) for 72 hours. Then, the mRNA was isolated, and gene array analysis was performed, followed by analysis of differentially regulated genes with a fold change of at least 1.5 and a significance of $P < 0.05$. Hierarchical cluster analysis was performed to organize the genes into clusters based on their expression similarities. Red: gene upregulation; Lilac: gene downregulation within a scale of 1.2 to -1.2. **(B)** Volcano plots were created and show the distribution of differentially expressed mRNAs in BxPc-3 cells cultured at 37°C in the absence (CO) or presence of TTFields (TTF *vs* CO) or at 38.5°C in the presence of TTFields (TTF +38.5°C *vs* CO). Red: (upregulated genes); Green (downregulated genes). The X-axis represents the expression profiles of multiple genes. The Y-axis represents the magnitude of gene expression changes. FC = 1.5, $P < 0.05$. **(C)** A KEGG enrichment analysis was performed to compare differentially regulated pathways between cells treated with TTFields + 38.5°C and control cells, which were cultivated at 37°C. The X-axis represents the rich factor, and the Y-axis represents the KEGG terms. Rich factor: ratio of differentially expressed gene numbers annotated in this pathway term to all gene numbers annotated in this pathway term. The greater the Rich factor, the greater the degree of pathway enrichment. The size of the circles increases with the gene count. Different circle colors represent distinct Q values as indicated.

with clinical data for DDIT4/REDD1, which is involved in cell growth, proliferation and survival; TSC1, which acts as a tumor suppressor; MCM6, which is involved in the cell cycle and DNA replication; and ORC1, which is involved in the initiation of DNA replication. Kaplan-Meier plots were created to visualize the relevance of expression of these genes in PDAC tissue and the related clinical outcome of patients (**Figures 7A, B**). Whereas high expression levels of DDIT4, MCM6 and ORC1 were related to significantly shorter survival, high expression of the tumor suppressor TSC1 was related to significantly longer survival, as expected. Together, these data confirm the relevance of the identified TTField plus hyperthermia-induced candidate genes identified by gene array analysis.

DISCUSSION

Here we investigated the therapeutic effects of TTFields at a frequency of 150 kHz, mild hyperthermia at 38.5°C, or the combination thereof. We deliberately chose a temperature below 39°C to avoid side effects as far as possible. We found that the combination treatment of PDAC cells nearly completely abolished the viability, metabolism, clonogenicity, migratory capacity, cell cycle progression and induced autophagy, while each single treatment was largely ineffective. In contrast, a nonmalignant pancreatic duct cell line was less affected, as we found by examination of the viability by MTT-assay. Although the latter finding does not exclude sub-lethal toxicity of TTFields combined with mild hypoxia to non-malignant cells, we assume that this is rather improbable. It is true that alternating electric TTFields affect the electric dipole moments of molecules in both, malignant and non-malignant cells. However, the field strength of the applied TTFields is quite low. Thus, a selective damage to malignant cells can be achieved by appropriate adjustment of the TTFields frequency to control the cell geometry-dependent amplification of the electric field in the division furrow. Due to the different geometry of malignant and non-malignant cells and a higher division rate of malignant cells, TTFields are suggested to interfere mainly with the mitotic spindle apparatus of malignant cells (7–9), followed by extension of the duration of mitosis by the formation of defective mitosis structures (3, 7), aneuploidy and genomic instability, and finally cell death and senescence (7, 10). Together, non-malignant or resting cells are less affected, because the selective effect of TTFields on cancer cells depends on cell size, doubling time and the optimal high frequency of TTFields (3, 5–7). These facts may exclude a severe damage of the vascular system as a key in order to keep the homeostasis of oxygen tension. Whether our therapeutic approach may target cancer-associated angiogenesis and thereby the endothelial cell as a checkpoint for immunological patrolling, as described (37), is a matter of debate and future evaluation.

We used the optimal TTField frequency of 150 kHz for the treatment of PDAC cells as described before by Giladi et al. (14). The combination with mild hyperthermia seems to be important because we demonstrated that the single treatments were less

TABLE 1 | GSEA analysis based on KEGG biological processes.

Name	NES	P	FDR
hsa03040_Spliceosome	1.73	0.00095	0.01413
hsa04141_Protein_processing_in_endoplasmic_reticulum	1.73	0.00037	0.00801
hsa04137_Mitophagy	1.66	0.00680	0.04629
hsa04010_MAPK_signaling_pathway	1.64	0.00018	0.00599
hsa03015_mRNA_surveillance_pathway	1.62	0.00710	0.04629
hsa04330_Notch_signaling_pathway	1.57	0.01913	0.08623
hsa04012_ErbB_signaling_pathway	1.43	0.03195	0.11690
hsa04142_Lysosome	1.41	0.02714	0.10552
hsa04140_Autophagy	1.37	0.03673	0.12996
hsa04151_PI3K-Akt_signaling_pathway	1.35	0.00767	0.04629
hsa04152_AMPK_signaling_pathway	-1.47	0.01406	0.07054
hsa04910_Insulin_signaling_pathway	-1.48	0.00741	0.04629
hsa02010_ABC_transporters	-1.5	0.03101	0.11556
hsa05225_Hepatocellular_carcinoma	-1.56	0.00233	0.02202
hsa00010_Glycolysis:–Gluconeogenesis	-1.82	0.00061	0.01010
hsa04110_Cell_cycle	-1.84	0.00020	0.00599
hsa03420_Nucleotide_excision_repair	-1.87	0.00120	0.01445
hsa03030_DNA_replication	-2.05	0.00020	0.00599
hsa03050_Proteasome	-2.21	0.00020	0.00599

The TTF+38.5°C group was compared with the control group (P < 0.05, FDR < 0.15).

effective or even induced tumor growth upon short-term treatment. Thus, the viability of BxPc-3 and BxGEM cells was significantly increased 3 days after treatment with TTFields at 37°C, but inhibited after 6 days. Transferred to the treatment of patients with TTFields, which are delivered by a head hood or abdominal belt, these results suggest, that within the first days the tumor viability/metabolism may be stimulated, whereas later it is inhibited. Such a scenario of stimulation of cell proliferation by electric fields is e.g. described in the context of alternating fields with frequencies in the range between 60 kHz and 448 kHz, which excited nerve cells and heart muscle tissue by targeted depolarization of the membrane potential (38, 39). Likewise, improved fracture healing and increased bone growth seem to be stimulated by low-frequency alternating fields (40). These frequencies overlap with the frequency range of TTFields (41). We suspect that the field strength used by us also induced proliferation at the beginning of the treatment, whereas it may have induced perturbations in cell division at later time points and as described (7–9), and thereby inhibition of proliferation. The question is why we observed a stimulation of proliferation at an early time point in BxPc-3 and BxGEM cells, but not in AsPC-1 cells. This observation may be due to the 2-dimensiol growth of BxPc-3 and BxGEM cells and the 3-dimensional, spheroid-like growth of AsPC-1 cells and the accordant mitotic spindle orientation exposed to TTFields.

In our experimental setting, the treatment duration was a crucial factor because the observed therapeutic effects of single or combined TTFields plus mild hypothermia increased with time. Our experimental system is different from the Inovitro™ system provided by Novocure Ltd., which uses switching mechanisms to change the field direction to increase the efficiency (3). Patients are encouraged to wear the Novocure Ltd. device daily on the abdomen at the level of the pancreas to treat PDAC (17) or, in the case of glioblastoma, as a cap on the head (12). The TTFields that we induced were in one spatial direction, with no interaction with dividing cells oriented perpendicular to the electric field direction. Additionally, we were not able to use an optimal higher power due to the heat generated by the antenna wires; as a result, the electric field strengths in the middle of the wells were slightly less than 1 V/cm. Studies by Kirson et al. showed that starting at 1 V/cm with increasing electric field strength, the effect on mitotic cells increases during treatment (42). Recently, Ravin et al. developed a novel device to deliver TTFields to cell and tissue cultures, which solved the problem of unwanted heat production by continuous thermal regulation (43).

An important observation made in our study is that TTFields plus mild hyperthermia strongly inhibited the self-renewal potential by reducing the colony and spheroid formation abilities. Similar results were recently obtained in glioma cancer stem cell-like cells (44). In terms of the cancer stem cell hypothesis (45), these data suggest that the combination of TTFields with mild hyperthermia prevents tumor recurrence and therapy resistance, at least *in vitro*. However, the colonies and spheroids were not totally eliminated, suggesting that TTFields combined with mild hyperthermia should be rather seen as supporting approach in addition to standard cytotoxic therapy.

According to our gene array results, the combination of TTFields and mild hyperthermia inhibited pathways and signaling chains involved in DNA replication. We supported the gene array results by qRT-PCR analysis, Western blot analysis of candidate genes related to autophagy, FACS-analysis of cell cycle progression, as well as online database analysis including KEGG enrichment analysis, GSEA analysis, Cytoscape/String analysis, and Kaplan-Meier Plotter-based detection of the clinical relevance of the identified target genes for overall survival and relapse-free survival of patients suffering from pancreatic cancer.

Alterations in DNA replication have already been described for severe hyperthermia at a minimum temperature of 43°C, which damages DNA repair, increases DNA breaks, and

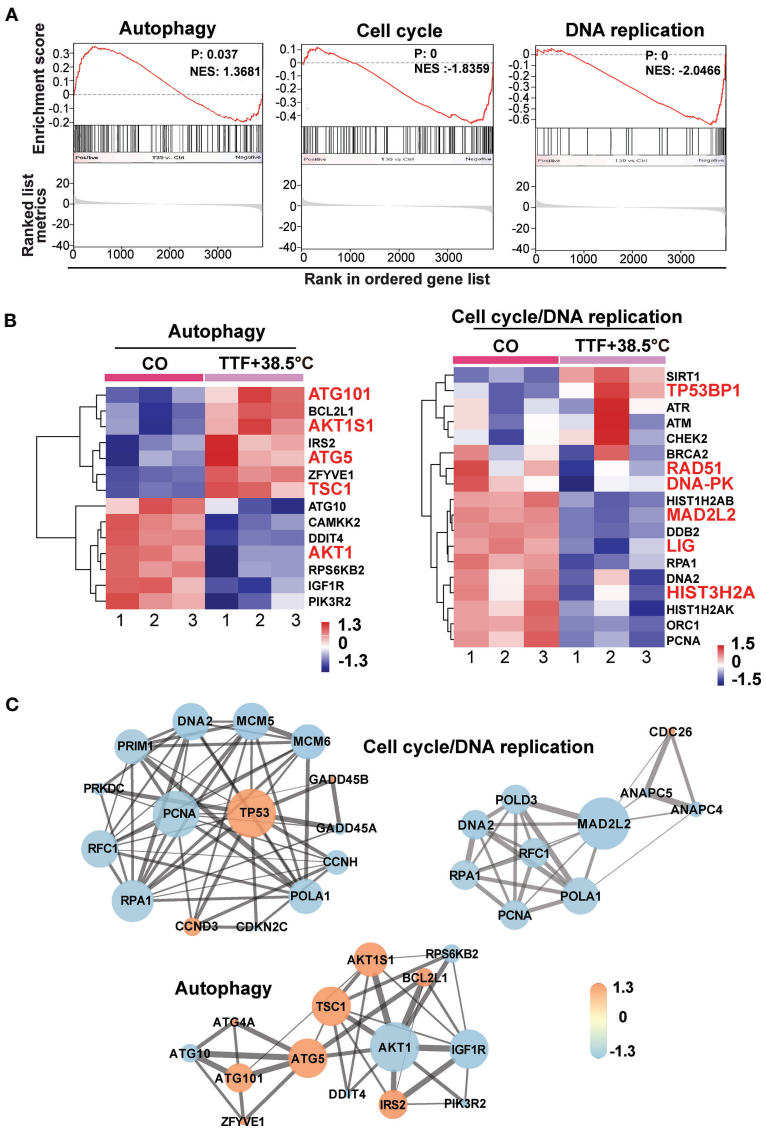

FIGURE 5 | GSEA suggests TTField plus hyperthermia-mediated regulation of autophagy, the cell cycle and DNA replication. **(A)** The biological pathways that are enriched in the gene array lists were identified by gene set enrichment analysis (GSEA). Differentially regulated genes in BxGEM cells cultivated at 37°C or at 38.5°C plus TTFields were evaluated. In this way, clustering of an autophagy-related gene set, which positively correlated with the treatment group, was detected (Normalized enrichment score (NES) = 1.3681, P = 0.037, False discovery rate (FDR) = 0.13). Likewise, the clustering of a cell cycle-related gene set was found to be negatively correlated with the treatment group (NES = -1.8359, p = 0, FDR = 0.005). Additionally, the clustering of a DNA replication-related gene set was found to be negatively correlated with the treatment group (NES = -2.0466, P = 0, FDR = 0.006). **(B)** The most relevant genes of each gene set are shown as heat maps. The name of genes, which were identified by a Cytoscape/String analysis in the following are enlarged and marked in red. **(C)** The mRNA array data were analyzed with the open source software platform Cytoscape, which resulted in the visualization of networks of co-expressed genes related to the cell cycle, DNA replication and autophagy. The sizes of the circles indicate the interaction degrees of proteins. The circle colors indicate different fold changes. Orange: upregulation, Lilac: downregulation within a scale from -1.3 to 1.3 as indicated.

ultimately converges into cell death (46–48). Although the temperature of 38.5°C tested here is far below the temperatures of severe hyperthermia, we observed an altered distribution of cells in the cell cycle and an accumulation of the G2/M population. Our results are similar to the findings of Giladi et al. (14) and Voloshin et al. (7, 49). Also, mild hyperthermia has increased the described spindle fiber damage known to be induced by TTFields (3, 7–9), which usually activates the spindle assembly checkpoint and induces cell cycle arrest in the G2/M-phase (50). This assumption is supported by our gene array results, where we found alterations in the expression levels of *MAD2L2*, *GADD45B*, *MCM5*, *MCM6* and *PRKDC*. All of these candidate genes indicate that the differential gene expression caused by TTFields in the presence of mild

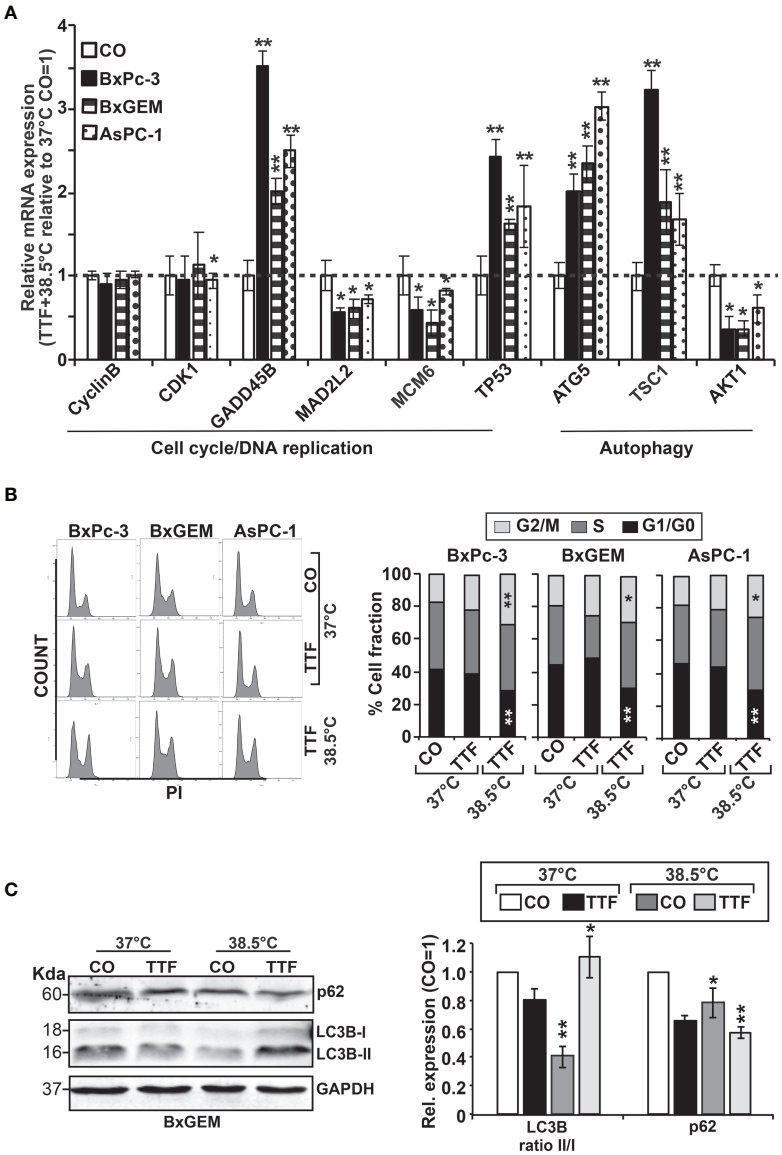

FIGURE 6 | Functional studies confirm TTField plus hyperthermia-mediated autophagy, the cell cycle and DNA signaling. **(A)** BxPc-3, BxGEM and AsPC-1 cells were cultivated at 38.5°C plus TTFields or at 37°C in the controls, followed by isolation of mRNA three days later and RT-qPCR analysis. The gene expression level of each gene was normalized to that of *GAPDH*, and the relative mRNA expression of hyperthermia/TTFields compared to control cells is shown. The primer sequences are given in **Supplementary Table S1**, and a comparison of the expression levels is provided in **Table 1**. The results are presented as relative gene expression. For calculation, the $2^{-\Delta\Delta Ct}$ method of relative quantification given in the equation was used. **(B)** PDAC cells were seeded in 96-well plates and cultivated at 37°C in the absence (CO) or presence of TTFields (TTF) or were cultivated at 38.5°C plus TTFields (TTF+38.5°C) for 72 h. Then, the progression of the cell cycle was analyzed by staining the cells with propidium iodide, followed by flow cytometry. The results are shown as flow cytometry profiles (left) and cell cycle quantification in bar graphs (right). **(C)** The cells were cultivated at 37°C in the absence (CO) or presence of TTFields (TTF) or at 38.5°C plus TTFields, as indicated, and 72 h later, the proteins were isolated, and the expression of p62 and LC3 was examined by the use of specific antibodies and Western blot analysis. GAPDH served as the control for equal conditions. Three independent experiments were performed at least in triplicate, and the data are presented as the means ± SD; *P < 0.05, **P < 0.01.

hyperthermia converges in the canonical pathways of cell cycle and DNA replication.

Moreover, we demonstrated that TTFields combined with mild hyperthermia induces autophagy in PDAC cells. This finding is consistent with published studies in glioblastoma cells (44, 51). However, autophagy is a double-edged sword and can induce cell death or prevent it, dependent on the cellular context, as we recently demonstrated in PDAC (52, 53). In the context of mild hyperthermia and TTFields, we found that the induction of autophagy supported cell death. Based on our gene array and *in*

TABLE 2 | Comparison of RT-qPCR and microarray results.

Gene	Name of Gene	Microarray		qPCR	
		Fold change	FDR	2-△△CT	*P value*
CCNB1	CyclinB1	-1.07	7.26E-1	0.93	7.20E-1
CDK1	cyclin dependent kinase 1	-1.10	4.59E-3	1.12	8.10E-1
GADD45B	growth arrest and DNA damage inducible beta	1.36	4.03E-2	2.49	2.33E-3
MAD2L2	mitotic arrest deficient 2 like 2	-1.27	3.99E-3	0.61	2.16E-2
MCM6	minichromosome maintenance complex component 6	-1.50	7.85E-4	0.44	2.02E-2
TP53	tumour protein p53	1.23	1.06E-1	1.62	1.54E-3
ATG5	autophagy related 5	1.27	2.89E-2	2.32	3.43E-3
TSC1	TSC complex subunit 1	1.28	1.17E-2	1.88	7.99E-3
AKT1	AKT serine/threonine kinase 1	-1.3	2.09E-2	0.36	2.52E-3

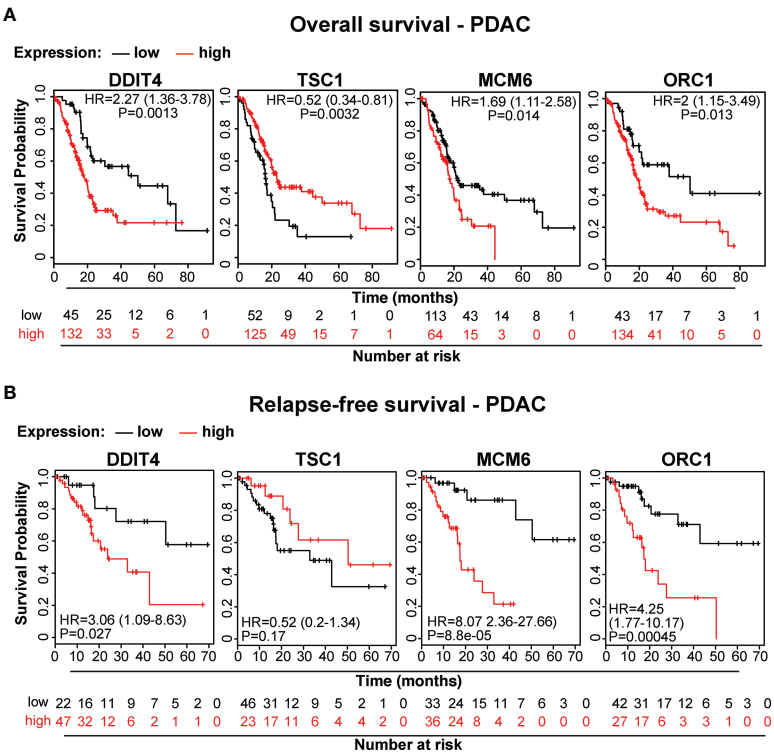

FIGURE 7 | The expression levels of the candidate genes MCM6, ORC1, DITT4 and TSC1 correlate to overall and relapse-free survival in PDAC. **(A)** We searched the online database TCGA for existing data of the identified target genes and found PDAC-related expression and clinical data for *MCM6*, *ORC1*, *DITT4* and *TSC1*. Using these online data, we performed Kaplan-Meier analysis of overall survival and **(B)** relapse-free survival in relation to gene expression (data from TCGA-PAAD, pH 000178, N = 185). HR, Hazard ratio and the significance P are given.

silico analysis, we speculate that the TTField-induced upregulation of autophagy is possibly dependent on the PIK3/AKT1 signaling pathway. This may be due to the cellular self-killing mechanism mediated by autophagy, or its protective effect in situations of cellular stress. Our data postulate that TTFields combined with mild hyperthermia induce DNA damage and delay DNA damage repair, which correlates with recent data showing that hyperthermia causes DNA damage (33) and/or interferes with DNA repair pathways (34). In this regard, hyperthermia has been reported to act as a radiosensitizer by interfering with DNA repair (54). Accordingly, we also observed alterations in important genes related to DNA repair, e.g., *53BP1*, *DNA-PK*, *MAD2L2*, *RAD51*, *H2A*, *LIG* and *DDB2*, upon combined treatment with TTFields and mild hyperthermia. We noted that the expression profiles of the identified candidate genes *MCM6*, *ORC1*, *DITT4* and *TSC1* directly correlated with the overall and recurrence-free survival of patients diagnosed with PDAC. These candidate genes may therefore be seen as novel progression markers in PDAC.

Conclusion

We combined for the first time TTFields and mild hyperthermia of 38.5°C and demonstrate that this combination is more

effective than each single treatment. Thus, the application of these two well-tolerated modalities may provide an efficient new treatment approach. A logical next step would now be the evaluation by *in vivo experiments* with mice, for which, however, the complex technical equipment would first have to be further developed. Then it would also have to be tested to apply the TTFields for quite short time in a repeated way with an interval time between repetitions of days, because such a protocol and its effects are interesting for the clinical application. As both individual treatments, TTFields and hyperthermia, are already in clinical use, their direct, combined application in patients, as co-treatment along with chemotherapy, would also be conceivable.

MATERIALS AND METHODS

Cell Lines

The established human pancreatic cancer cell lines BxPc-3 and AsPC-1 and the human hTERT-HPNE immortalized nonmalignant pancreatic duct cell line CRL-4023 were obtained from the American Type Culture Collection (ATCC, Manassas, VA, USA) and cultured as described (55). Gemcitabine-resistant BxPc-3 cells (BxGEM) were selected from parental cells by continuous gemcitabine treatment with increasing concentrations up to 200 nM for more than one year (56). Negative mycoplasma cultures were confirmed by monthly mycoplasma tests. The cell lines were recently authenticated by a commercial service (DSMZ, Braunschweig, Germany).

Generation of TTFields

Recently we developed in-house a device for applying TTFields to cells growing in 96-well flat-bottom plates and evaluated its functionality in control experiments (57). This TTField device enabled us to treat PDAC cells with an alternating voltage between two insulated wires. The antenna wires were arranged diametrically to each well within a 96-well plate and formed, together with a variable capacitor, the capacitive part of an electrical resonant circuit. The inductive part of the resonant circuit was the secondary coil of a transformer whose primary coil was connected to a function generator (HP 3310A, Hewlett Packard, USA) and a customized preamplifier. An alternating low-voltage signal with a fixed frequency between 100 and 300 kHz was generated in the primary coil, and the resonant circuit was tuned to resonance using the variable capacitor. At resonance, voltage amplitudes U_{eff} of up to 500 V were generated in the resonant circuit. We calculated the maximum value of the electric field strength in the area of the cells under highly simplified conditions. The antenna wires ended at the bottoms of the 96-well plates on which the cells grew. Considering only the 2-dimensional case on the bottom plane of the 96-well plates, the antenna wires can be approximated as point-like charges, and Coulomb's law in equation (1) was used for the calculation.

$$\vec{E}(\vec{r}) = \frac{Q}{4\pi\epsilon_0\epsilon_r}\frac{\vec{e}}{r^2} \tag{1}$$

In this equation, Q is the field-generating charge, $\vec{e}$ is the unit vector for the field direction, $\epsilon_0 = 8.85 * 10^{-12} As/Vm$ is the vacuum permittivity, ϵ_r is the relative permittivity and r is the distance to the charge. The total field is formed as a superposition of 2-point charges according to equation (1). The calculations were carried out only for the straight line connecting the two-point charges. The field effects of charges outside the calculation plane were ignored. With the applied voltage U_{eff} = 500 V, we calculated the charge Q with equation (2):

$$Q = CU_{eff} \tag{2}$$

with the capacitance C of the antenna wires.

The total capacitance C was calculated according to equation (3), taking into account, that there were different dielectric materials between the antenna wires: air, plastic, and the saline cell medium.

$$C = \left(\frac{2}{C_{air}} + \frac{2}{C_p} + \frac{1}{C_{Med}}\right)^{-1} \tag{3}$$

C_{air}, C_P, and C_{Med} were calculated with equation (4):

$$C_k = \epsilon_k\epsilon_0\frac{A}{d_k} \tag{4}$$

with $k = air, P, Med$ and $A = \pi d_w L_w/2$, $d_w = 0.5mm$, $L_w = 10mm$.

C_{air} is the capacitance of the air gap between the antenna wire and the adjacent well wall using $\epsilon_{air} = 1$ and $d_{air} = 3$ mm, C_P is the capacitance of the plastic well wall using $\epsilon_p = 2$ and $d_P = 1$ mm, and C_{Med} is the capacitance of the cell medium using $\epsilon_{Med} = 75$ and $d_{Med} = 5$ mm. Depolarization factors due to the geometry of the various dielectrics were not taken into account.

For treatment of cell lines with TTFields, the cells were seeded in 96-well plates at a density of 2000-4000 cells/ml in 200 µl of medium per well. After installation of the antenna wires for the treatment with TTFields, the plates were placed in the incubator. The cell culture medium was not changed during treatment.

Examination of Viability/Metabolic Activity by MTT Assay

PDAC cell lines were resuspended at a concentration of 2 to 4x 10^3 cells/ml, and 200 µl per well of a 96-well microplate were seeded. We minimized the counting errors by continuous shaking of the cell suspension and the use of a multi-head pipette for cell seeding. Also, the different cell concentrations from 2 to 4x 10^3 cells/ml per batch enabled us to took those for evaluation in which the control group grew to nearly 100% density after 6 days. After treatment, 20 µL of the 5 mg/mL yellow MTT tetrazolium salt (3-(4,5-dimethylthiazol-2-yl)-2,5-diphenyltetrazolium bromide) were added to each well. The plates were incubated for 3.5 h at 37°C. The principle of this assay is that viable, metabolically active cells, but not dead or dying cells, contain NAD(P)H-dependent oxidoreductase enzymes, which reduce the yellow MTT to purple formazan crystals. By microscopic inspection, we detected the formation of formazan crystals and subsequently the medium was carefully

removed, 200 µL DMSO was added and the cells were agitated on a shaker for 10 min at 37°C until the formazan crystals were completely dissolved. Finally, the optical density of the purple colour, which reflects mitochondrial activity, was measured at 570 nm by the use of an ELISA reader.

Western Blot Analysis

Proteins were harvested by the use of RIPA Lysis Buffer and the protein concentration was determined by the use of the BCA Protein Assay Kit (both from Abcam, Cambridge, UK). After denaturation by boiling for 5 min, the samples were incubated on ice and then separated along with a commercial protein ladder by SDS-PAGE. A semi-dry system was used for the transfer of separated proteins in the gel to a PVDF membrane. The membrane was blocked by shaking in 3% BSA solution, followed by incubation with primary antibodies and thereafter with IRDye® infrared.

Dye-conjugated secondary antibodies (LI-COR Biosciences GmbH, Bad Homburg, Germany). The infrared intensity was measured by the use of an Odyssey CLx Infrared Imaging System (LI-COR Biosciences GmbH). The primary antibodies were rabbit polyclonal anti-LC3B and anti-P62 (Abcam, Cambridge, UK) and rabbit monoclonal anti-GAPDH antibody (Abcam).

Cell Cycle Analysis

Seventy-two hours after treatment with TTFields at 37°C or 38.5°C as described above, the cells were harvested, washed and 5 ml ice-cold 70% EtOH was added drop-by-drop while vortexing. Subsequently, the samples were incubated at -20°C overnight. After PBS-washing, the cells were resuspended in 0.5 mL of the PI/RNase Staining Buffer (Becton Dickinson, Heidelberg, Germany) and stored for 15 min at room temperature. The cell cycle was analyzed by flow cytometry and the use of a FACSCalibur™ device (Becton Dickinson). The measured data were assessed with FLOWJO software (FLOWJO, LLC, Ashland, USA) to determine the cell fractions in the G1, S, and G2+M phases of the viable cell population.

Colony-Forming Assay

Seventy-two hours after treatment with TTFields at 37°C or 38.5°C as described above, the cells were detached by trypsinization and reseeded at low density in 6-well plates (BxPc-3 and BxGEM, 1000 cells/well; AsPC-1, 800 cells/well) in six-fold approaches. The cells were incubated in a 37°C incubator for 10-14 days without changing the cell culture medium until considerably appropriate colonies were observed under the microscope in plates containing untreated control cells. Subsequently, the cells were washed with 10 mL PBS and 2 mL of 3.7% paraformaldehyde (PFA), was added for 10 min at room temperature. The fixation solution was removed, and 2 mL of 70% EtOH were added for 10 min. Finally, the cells were stained with 0.05% Coomassie blue, followed by washing with water. The plates were dried overnight. Colonies consisting of a minimum of 50 cells were counted under a stereomicroscope. The percentage of plating efficiency was evaluated by normalising the values obtained for treated cells to the values of non-treated cells. After normalisation, the value of non-treated cultures was set to 1. For the analysis of the second generation of colony formation, living cells were harvested and re-plated at low density in 6-well plates.

Spheroid Assay

Seventy-two hours after treatment with TTFields at 37°C or 38.5° C as described above, the cells were seeded at a density of 1x 10^3 cells/mL in 500 µL NeuroCult™ NS-A basal serum-free medium supplemented with 20 ng/mL hEGF, 10 ng/mL bFGF and 2 µg/mL heparin (STEMCELL Technologies Cambridge, US) per well in 24-well Sphera Low-Attachment Surface plates (ThermoFisher Scientific, Waltham, MA, USA) for spheroid formation. The spheroids were photographed after 5 days, and cell spheroids were identified according to their typical shape and size and the percentage of spheroids was calculated. To evaluate secondary spheroid formation, equal numbers of surviving cells of the first round of spheroid-formation were reseeded. For quantification of the percentage of spheroid forming cells, the cells were seeded at one cell per well in 96-well plates. Wells with more than one cell were excluded from evaluation.

Wound Healing/Scratch/Migration Assay

The cells (1x 10^3/well) were seeded in 96-well plates and grown to >90% confluence overnight. The cell layer was scratched with the fine end of a 10 µL pipette tip (time 0). Then the cells were exposed to TTFields at 37°C or 38.5°C. The closure of the wounded region was evaluated 12 h and 24 h later. Pictures were taken by the use of a Nikon Eclipse TS 100-F inverted microscope equipped with a camera. The images and the closure of the gap were analyzed with the computer program Image J (58).

Real-Time Quantitative PCR

Seventy-two hours after treatment with TTFields at 37°C or 38.5°C as described above, the cells were harvested and total RNA was isolated by the use of the RNeasy® Mini Kit (Qiagen, Hilden, Germany) according to the manufacturer's instructions. The concentration was determined by the use of a Nanodrop 2000 spectrophotometer (ThermoFisher Scientific, Waltham, MA, USA) and the RNA was stored at -80°C until use. A total of 100 ng mRNA were reverse transcribed using the High Capacity RNA to cDNA™ Kit according to the instructions of the manufacturer (ThermoFisher Scientific, Waltham, MA, USA). The cDNA was diluted in 200 µl RNAse-free water and 1 µL cDNA was used immediately as template for real-time PCR, which was performed with 1 µL of forward and reverse primers for the genes of interest and SSoAdvanced SYBR Green Supermix (Qiagen, Hilden, Germany). The primer sequences were created by the use of PrimerBank, available for free online (https://pga.mgh.harvard.edu/primerbank/), and the primer sequences for *MAD2L2*, *GADD45B*, *MCM6*, Cyclin B1 (*CCNB1*), *CDK1*, *ATG5*, *TSC1*, *TP53* and *AKT1* are shown in **Table 3**. The PCR conditions were 10 min 95°C as initial denaturation step, followed by 40 cycles of 15 s denaturation at 95°C, 1 min annealing at 60°C, followed by cooling down to 4°C. All reactions were run in duplicate. Melt curve analysis for each pair of primers and agarose gel electrophoresis of the PCR products ensured the specificity of the primers. The gene expression level of each target gene was normalised to that of

TABLE 3 | Primer Sequences used for RT-qPCR.

Symbol	Sequence
MAD2L2	Fw 5′-CGAGTTCCTGGAGGTGGCTGTGCATC-3′
	Rev 5′- CTTGACGCAGTGCAGCGTGTCCTGGATA-3′
GADD45B	Fw 5′-ACGAGTCGGCCAAGTTGATG3′
	Rev 5′-GGATGAGCGTGAAGTGGATTT-3′
MCM6	Fw 5′- GAGGAACTGATTCGTCCTGAGA-3′
	Rev 5′- CAAGGCCCGACACAGGTAAG -3′
CCNB1	Fw 5′- AATAAGGCGAAGATCAACATGGC-3′
	Rev 5′- TTTGTTACCAATGTCCCCAAGAG -3′
CDK1	FW 5′- AAACTACAGGTCAAGTGGTAGCC-3′
	Rev 5′-TCCTGCATAAGCACATCCTGA -3′
ATG5	FW 5′- AAAGATGTGCTTCGAGATGTGT -3′
	Rev 5′- CACTTTGTCAGTTACCAACGTCA-3′
TSC1	FW 5′- CAACAAGCAAATGTCGGGGAG -3′
	Rev 5′- CATAGGGCCACGGTCAGAA 3′
TP53	FW 5′- CAGCACATGACGGAGGTTGT -3′
	Rev 5′- TCATCCAAATACTCCACACGC 3′
AKT1	FW 5′- ATGAACGACGTAGCCATTGTG-3′
	Rev 5′- TTGTAGCCAATAAAGGTGCCAT-3′
GAPDH	Fw 5′-GAAGGTGAAGGTCGGAGTC-3′
	Rev 5′-GAAGATGGTGATGGGATTTC-3′

GAPDH. The results are presented as relative expression value (REV) by using the $2^{-\Delta\Delta Ct}$ method of relative quantification given in equation (6).

$$REV = 2^{Ct\ value\ of\ GAPDH - Ct\ value\ of\ the\ gene\ of\ interest} \quad (5)$$

By referring to each REV value of the target gene, the fold change (FC) can be calculated using equation (7).

$$Fold\ change = \frac{REV\ treated\ cells}{REV\ untreated\ cells} \quad (6)$$

mRNA Microarray Analysis

mRNA was isolated from untreated or TTField-treated BxGEM cells grown at 37°C or 38.5°C using the RNeasy Kit (QIAGEN, Hilden, Germany) according to the manufacturer's instructions. Microarray analyses was performed at the Microarray-Analytic Center of the Medical Faculty Mannheim using Clariom™ D Assays (Thermo Fisher Scientific, Dreieich, Germany). Biotinylated antisense complementary DNA (cDNA) was prepared based on a standard Affymetrix labeling protocol with the GeneChip® WT Plus Reagent Kit and the GeneChip® Hybridization, Wash and Stain Kit. Thereafter, hybridization on the chip was performed in a GeneChip hybridization oven 640, staining was performed in the GeneChip Fluidics Station 450, and the chip was then scanned with a GeneChip Scanner 3000. The custom CDF version 22 with ENTREZ-based gene definitions was used to annotate the arrays (59). The raw fluorescence intensity values were normalized by applying quantile normalization and RMA background correction. One-way analysis of variance (ANOVA) was applied; a fold change of 1.5 was used for the selection of differentially expressed genes using commercial SAS JMP10 Genomics version 6 (SAS Institute, Cary, USA). A false positive rate/false discovery rate (FDR) <0.15 was considered to be the level of significance. The accession number of the gene array at ArrayExpress (https://www.ebi.ac.uk/arrayexpress/) is #E-MTAB-10270 (BxGEM, control, TTF, TTF+hyperthermia 38.5°C).

In Silico Analysis of the mRNA Microarray Results

The gene array-derived list of differentially expressed genes was further correlated for their biological function and involvement in signaling pathways. For the selection of differentially expressed genes, an absolute value of the logarithmic fold change (log FC) ≥1.3 and a cutoff of P<0.05 were chosen to identify statistically significant pathways.

Heat maps and volcano plots were created with the free software environment for statistical computing and graphics R (https://www.R-project.org/).

Gene set enrichment analysis (GSEA) was performed using the *fgsea* package available in the open-source software Bioconductor (https://bioconductor.org/packages/release/bioc/html/fgsea.html).

The freely available online database resource **KEGG (Kyoto Encyclopedia of Genes and Genomes,** https://www.genome.jp/kegg/) was used for the selection of relevant biological functions and pathways with enrichment scores of P<0.05.

The open source platform **String 11.0** (https://string-db.org) was used to collect, score and integrate publicly available sources of protein–protein interaction data and to supplement it with calculations and predictions. By the use of the **Cytoscape StringApp** (http://apps.cytoscape.org/apps/stringapp), we visualized the identified protein-protein-interaction network based on the obtained differentially expressed candidate genes.

Evaluation of Target Genes by TCGA and Kaplan-Meier Plotter Analysis

The Cancer Genome Atlas (TCGA) is a publicly available online database (https://www.cancer.gov/about-nci/organization/ccg/research/structural-genomics/tcga) with over 20,000 primary cancer and matched normal samples spanning 33 cancer types with matched molecular and clinicopathological data. TCGA was used for evaluation of the identified target genes DDIT4, TSC1, MCM6 and ORC1 by Kaplan-Meier analysis using the online available Kaplan-Meier Plotter (http://kmplot.com/analysis/index.php?p=service). mRNAs expression data of the above-mentioned target genes from human PDAC tumor tissue were available and used to analyze the overall survival (OS) and recurrence-free survival (RFS) of patients. The database divides patient samples into high expression groups and low expression groups according to the median values of mRNA expression and validates them by a Kaplan–Meier survival curve. Information on number of patients, median values of mRNA expression, 95% confidence interval (CI), hazard ratio (HR), and P-value can be found on the Kaplan–Meier Plotter web page (http://kmplot.com/analysis/index.php?p=service). A P-value <0.05 was considered as statistically significant. The log-rank test was

used to calculate the statistical significance of the differences observed among the Kaplan-Meier curves.

Statistical Evaluation

Statistical analyses were performed using JMP14.0.0 (SAS Institute, Cary, USA) or Prism 7.0 (GraphPad Software, San Diego, California, USA). For most of the experiments, Dunnett's tests were used to calculate the P values; nontreated cells at 37°C served as the control group. For cell migration, Student's t-tests of independent samples were used to calculate the P values. All experiments were repeated a minimum of three times, and the data are presented as the mean ± standard deviation (SD). The null hypothesis was rejected when $P < 0.05$ (*$P < 0.05$ and **$P < 0.01$).

DATA AVAILABILITY STATEMENT

The datasets presented in this study can be found in online repositories. The names of the repository/repositories and accession number(s) can be found in the article/**Supplementary Material**.

ETHICS STATEMENT

The studies involving human participants does not apply because we used anonymous patient data, which are available for free from online databases, such as The Cancer Genome Atlas Program. Written informed consent for participation was not required for this study in accordance with the national legislation and the institutional requirements.

AUTHOR CONTRIBUTIONS

LB, MS, IH: Concept and design. MS, LB; TP, LL, SZ: Development of methodology. LB, TP, CT, SZ: Acquisition of data. LB, MS, WG, CT, IH: Analysis and interpretation of data. LB, MS, IH: Writing, review and/or revision of the manuscript. All authors contributed to the article and approved the submitted version.

FUNDING

This study was supported by grants to IH from the German Research Council (DFG HE 3186/15-1), Hanns A. Pielenz-Stiftung, Heidelberger Stiftung Chirurgie, Dietmar Hopp-Stiftung, and Klaus Tschira Stiftung. The authors declare that this study received funding from Karsten Burmeister/BIMAG Bau- und Industriemaschinen GmbH. The funder was not involved in the study design, collection, analysis, interpretation of data, the writing of this article or the decision to submit it for publication.

ACKNOWLEDGMENTS

We are grateful to S. Bauer for excellent technical assistance and to S. Karakhanova for discussion regarding FACS analysis.

SUPPLEMENTARY MATERIAL

The Supplementary Material for this article can be found online at: https://www.frontiersin.org/articles/10.3389/fonc.2021.738801/full#supplementary-material

REFERENCES

1. Siegel RL, Miller KD, Fuchs HE, Jemal A. Cancer Statistics, 2021. *CA Cancer J Clin* (2021) 71:7–33. doi: 10.3322/caac.21654
2. Neoptolemos JP, Kleeff J, Michl P, Costello E, Greenhalf W, Palmer DH. Therapeutic Developments in Pancreatic Cancer: Current and Future Perspectives. *Nat Rev Gastroenterol Hepatol* (2018) 15:333–48. doi: 10.1038/s41575-018-0005-x
3. Kirson ED, Gurvich Z, Schneiderman R, Dekel E, Itzhaki A, Wasserman Y, et al. Disruption of Cancer Cell Replication by Alternating Electric Fields. *Cancer Res* (2004) 64:3288–95. doi: 10.1158/0008-5472.CAN-04-0083
4. Mun EJ, Babiker HM, Weinberg U, Kirson ED, Von Hoff DD. Tumor-Treating Fields: A Fourth Modality in Cancer Treatment. *Clin Cancer Res* (2018) 24:266–75. doi: 10.1158/1078-0432.CCR-17-1117
5. Castellvi Q, Ginesta MM, Capella G, Ivorra A. Tumor Growth Delay by Adjuvant Alternating Electric Fields Which Appears Non-Thermally Mediated. *Bioelectrochemistry* (2015) 105:16–24. doi: 10.1016/j.bioelechem.2015.04.006
6. Davies AM, Weinberg U, Palti Y. Tumor Treating Fields: A New Frontier in Cancer Therapy. *Ann N Y Acad Sci* (2013) 1291:86–95. doi: 10.1111/nyas.12112
7. Giladi M, Schneiderman RS, Voloshin T, Porat Y, Munster M, Blat R, et al. Mitotic Spindle Disruption by Alternating Electric Fields Leads to Improper Chromosome Segregation and Mitotic Catastrophe in Cancer Cells. *Sci Rep* (2015) 5:18046. doi: 10.1038/srep18046
8. Gera N, Yang A, Holtzman TS, Lee SX, Wong ET, Swanson KD. Tumor Treating Fields Perturb the Localization of Septins and Cause Aberrant Mitotic Exit. *PloS One* (2015) 10:e0125269. doi: 10.1371/journal.pone.0125269
9. Voloshin T, Kaynan N, Davidi S, Porat Y, Shteingauz A, Schneiderman RS, et al. Tumor-Treating Fields (TTFields) Induce Immunogenic Cell Death Resulting in Enhanced Antitumor Efficacy When Combined With Anti-PD-1 Therapy. *Cancer Immunol Immunother* (2020) 69(7):1191–204. doi: 10.1007/s00262-020-02534-7
10. Vitale I, Galluzzi L, Castedo M, Kroemer G. Mitotic Catastrophe: A Mechanism for Avoiding Genomic Instability. *Nat Rev Mol Cell Biol* (2011) 12:385–92. doi: 10.1038/nrm3115
11. Fennell DA. Tumour Treating Fields for Mesothelioma: Controversy Versus Opportunity. *Lancet Oncol* (2019) 20:1623–5. doi: 10.1016/S1470-2045(19)30642-4
12. Lassman AB, Joanta-Gomez AE, Pan PC, Wick W. Current Usage of Tumor Treating Fields for Glioblastoma. *Neurooncol Adv* (2020) 2:vdaa069. doi: 10.1093/noajnl/vdaa069
13. Novocure. *Our Pipeline* (2021). Available at: https://www.novocure.com/our-pipeline/#clinical-trials.
14. Giladi M, Schneiderman RS, Porat Y, Munster M, Itzhaki A, Mordechovich D, et al. Mitotic Disruption and Reduced Clonogenicity of Pancreatic Cancer Cells *In Vitro* and *In Vivo* by Tumor Treating Fields. *Pancreatology* (2014) 14:54–63. doi: 10.1016/j.pan.2013.11.009

15. Jo Y, Oh G, Gi Y, Sung H, Joo EB, Lee S, et al. Tumor Treating Fields (TTF) Treatment Enhances Radiation-Induced Apoptosis in Pancreatic Cancer Cells. *Int J Radiat. Biol* (2020) 96:1528–33. doi: 10.1080/09553002.2020.1838658
16. Rivera F, Benavides M, Gallego J, Guillen-Ponce C, Lopez-Martin J, Kung M. Tumor Treating Fields in Combination With Gemcitabine or Gemcitabine Plus Nab-Paclitaxel in Pancreatic Cancer: Results of the PANOVA Phase 2 Study. *Pancreatology* (2019) 19:64–72. doi: 10.1016/j.pan.2018.10.004
17. Novocure. *PANOVA-3 Trial Pancreatic Cancer* (2021). Available at: https://www.novocuretrial.com/panova/.
18. Overgaard J. History and Heritage-an Introduction. In: J Overgaard, editor. *Hyperthermic Oncology*. London: Taylor and Francis (1985). p. 3–8.
19. Kirui DK, Celia C, Molinaro R, Bansal SS, Cosco D, Fresta M, et al. Mild Hyperthermia Enhances Transport of Liposomal Gemcitabine and Improves *In Vivo* Therapeutic Response. *Adv Healthc Mater* (2015) 4:1092–103. doi: 10.1002/adhm.201400738
20. Wang S, Weng J, Fu X, Lin J, Fan W, Lu N, et al. Black Phosphorus Nanosheets for Mild Hyperthermia-Enhanced Chemotherapy and Chemo-Photothermal Combination Therapy. *Nanotheranostics* (2017) 1:208–16. doi: 10.7150/ntno.18767
21. Lu N, Huang P, Fan W, Wang Z, Liu Y, Wang S, et al. Tri-Stimuli-Responsive Biodegradable Theranostics for Mild Hyperthermia Enhanced Chemotherapy. *Biomaterials* (2017) 126:39–48. doi: 10.1016/j.biomaterials.2017.02.025
22. Scutigliani EM, Liang Y, Crezee H, Kanaar R, Krawczyk PM. Modulating the Heat Stress Response to Improve Hyperthermia-Based Anticancer Treatments. *Cancers (Basel)* (2021) 13(6):1243. doi: 10.3390/cancers13061243
23. Ohguri T, Imada H, Yahara K, Moon SD, Yamaguchi S, Yatera K, et al. Re-Irradiation Plus Regional Hyperthermia for Recurrent non-Small Cell Lung Cancer: A Potential Modality for Inducing Long-Term Survival in Selected Patients. *Lung Cancer* (2012) 77:140–5. doi: 10.1016/j.lungcan.2012.02.018
24. Jones EL, Oleson JR, Prosnitz LR, Samulski TV, Vujaskovic Z, Yu DH, et al. Randomized Trial of Hyperthermia and Radiation for Superficial Tumors. *J Clin Oncol* (2005) 23:3079–85. doi: 10.1200/JCO.2005.05.520
25. Harima Y, Nagata K, Harima K, Ostapenko VV, Tanaka Y, Sawada S. A Randomized Clinical Trial of Radiation Therapy Versus Thermoradiotherapy in Stage IIIB Cervical Carcinoma. *Int J Hyperthermia* (2001) 17:97–105. doi: 10.1080/02656730010001333
26. Huilgol NG, Gupta S, Sridhar CR. Hyperthermia With Radiation in the Treatment of Locally Advanced Head and Neck Cancer: A Report of Randomized Trial. *J Cancer Res Ther* (2010) 6:492–6. doi: 10.4103/0973-1482.77101
27. Overgaard J, Gonzalez Gonzalez D, Hulshof MC, Arcangeli G, Dahl O, Mella O, et al. Randomised Trial of Hyperthermia as Adjuvant to Radiotherapy for Recurrent or Metastatic Malignant Melanoma. European Society for Hyperthermic Oncology. *Lancet* (1995) 345:540–3. doi: 10.1016/S0140-6736(95)90463-8
28. Schroeder C, Gani C, Lamprecht U, von Weyhern CH, Weinmann M, Bamberg M, et al. Pathological Complete Response and Sphincter-Sparing Surgery After Neoadjuvant Radiochemotherapy With Regional Hyperthermia for Locally Advanced Rectal Cancer Compared With Radiochemotherapy Alone. *Int J Hyperthermia* (2012) 28:707–14. doi: 10.3109/02656736.2012.722263
29. Coccolini F, Campanati L, Catena F, Ceni V, Ceresoli M, Jimenez Cruz J, et al. Hyperthermic Intraperitoneal Chemotherapy With Cisplatin and Paclitaxel in Advanced Ovarian Cancer: A Multicenter Prospective Observational Study. *J Gynecol Oncol* (2015) 26:54–61. doi: 10.3802/jgo.2015.26.1.54
30. de Jong MA, Oldenborg S, Bing Oei S, Griesdoorn V, Kolff MW, Koning CC, et al. Reirradiation and Hyperthermia for Radiation-Associated Sarcoma. *Cancer* (2012) 118:180–7. doi: 10.1002/cncr.26252
31. van der Horst A, Versteijne E, Besselink MGH, Daams JG, Bulle EB, Bijlsma MF, et al. The Clinical Benefit of Hyperthermia in Pancreatic Cancer: A Systematic Review. *Int J Hyperthermia* (2018) 34:969–79. doi: 10.1080/02656736.2017.1401126
32. Sreedhar AS, Csermely P. Heat Shock Proteins in the Regulation of Apoptosis: New Strategies in Tumor Therapy - A Comprehensive Review. *Pharmacol Ther* (2004) 101:227–57. doi: 10.1016/j.pharmthera.2003.11.004
33. Warters RL, Henle KJ. DNA Degradation in Chinese Hamster Ovary Cells After Exposure to Hyperthermia. *Cancer Res* (1982) 42:4427–32.
34. Kampinga HH, Konings AW. Inhibition of Repair of X-Ray-Induced DNA Damage by Heat: The Role of Hyperthermic Inhibition of DNA Polymerase Alpha Activity. *Radiat. Res* (1987) 112:86–98. doi: 10.2307/3577079
35. Wong RS, Dynlacht JR, Cedervall B, Dewey WC. Analysis by Pulsed-Field Gel Electrophoresis of DNA Double-Strand Breaks Induced by Heat and/or X-Irradiation in Bulk and Replicating DNA of CHO Cells. *Int J Radiat. Biol* (1995) 68:141–52. doi: 10.1080/09553009514551041
36. Wust P, Hildebrandt B, Sreenivasa G, Rau B, Gellermann J, Riess H, et al. Hyperthermia in Combined Treatment of Cancer. *Lancet Oncol* (2002) 3:487–97. doi: 10.1016/S1470-2045(02)00818-5
37. Solimando AG, Summa S, Vacca A, Ribatti D. Cancer-Associated Angiogenesis: The Endothelial Cell as a Checkpoint for Immunological Patrolling. *Cancers (Basel)* (2020) 12(11):3380. doi: 10.3390/cancers12113380
38. Palti Y. Stimulation of Internal Organs by Means of Externally Applied Electrodes. *J Appl Physiol* (1966) 21:1619–23. doi: 10.1152/jappl.1966.21.5.1619
39. Polk C. Therapeutic Applications of Low Frequency Electric and Magnetic Fields. In: Lin JC, editor. *Advances in Electromagnetic Fields in Living Systems*. Boston, MA: Springer US (1994). p. 129–53.
40. Bassett CA. The Development and Application of Pulsed Electromagnetic Fields (PEMFs) for Ununited Fractures and Arthrodeses. *Clin Plast Surg* (1985) 12:259–77. doi: 10.1016/S0094-1298(20)31696-5
41. Chen C, Bai X, Ding Y, Lee I-S. Electrical Stimulation as a Novel Tool for Regulating Cell Behavior in Tissue Engineering. *Biomat Res* (2019) 23:25. doi: 10.1186/s40824-019-0176-8
42. Kirson ED, Dbaly V, Tovarys F, Vymazal J, Soustiel JF, Itzhaki A, et al. Alternating Electric Fields Arrest Cell Proliferation in Animal Tumor Models and Human Brain Tumors. *Proc Natl Acad Sci USA* (2007) 104:10152–7. doi: 10.1073/pnas.0702916104
43. Ravin R, Cai TX, Pursley RH, Garmendia-Cedillos M, Pohida T, Freidlin RZ, et al. A Novel *In Vitro* Device to Deliver Induced Electromagnetic Fields to Cell and Tissue Cultures. *Biophys J* (2020) 119:2378–90. doi: 10.1016/j.bpj.2020.11.002
44. Silginer M, Weller M, Stupp R, Roth P. Biological Activity of Tumor-Treating Fields in Preclinical Glioma Models. *Cell Death Dis* (2017) 8:e2753. doi: 10.1038/cddis.2017.171
45. Hermann PC, Huber SL, Herrler T, Aicher A, Ellwart JW, Guba M, et al. Distinct Populations of Cancer Stem Cells Determine Tumor Growth and Metastatic Activity in Human Pancreatic Cancer. *Cell Stem Cell* (2007) 1:313–23. doi: 10.1016/j.stem.2007.06.002
46. Pelicci PG, Dalton P, Orecchia R. Heating Cancer Stem Cells to Reduce Tumor Relapse. *Breast Cancer Res* (2011) 13:305. doi: 10.1186/bcr2847
47. Dewhirst MW, Lee CT, Ashcraft KA. The Future of Biology in Driving the Field of Hyperthermia. *Int J Hyperthermia* (2016) 32:4–13. doi: 10.3109/02656736.2015.1091093
48. van Oorschot B, Granata G, Di Franco S, Ten Cate R, Rodermond HM, Todaro M, et al. Targeting DNA Double Strand Break Repair With Hyperthermia and DNA-PKcs Inhibition to Enhance the Effect of Radiation Treatment. *Oncotarget* (2016) 7:65504–13. doi: 10.18632/oncotarget.11798
49. Voloshin T, Munster M, Blatt R, Shteingauz A, Roberts PC, Schmelz EM, et al. Alternating Electric Fields (TTFields) in Combination With Paclitaxel Are Therapeutically Effective Against Ovarian Cancer Cells *In Vitro* and *In Vivo*. *Int J Cancer* (2016) 139:2850–8. doi: 10.1002/ijc.30406
50. Joglekar AP. A Cell Biological Perspective on Past, Present and Future Investigations of the Spindle Assembly Checkpoint. *Biol (Basel)* (2016) 5 (4):44. doi: 10.3390/biology5040044
51. Shteingauz A, Porat Y, Voloshin T, Schneiderman RS, Munster M, Zeevi E, et al. AMPK-Dependent Autophagy Upregulation Serves as a Survival Mechanism in Response to Tumor Treating Fields (TTFields). *Cell Death Dis* (2018) 9:1074. doi: 10.1038/s41419-018-1085-9
52. Rausch V, Liu L, Apel A, Rettig T, Gladkich J, Labsch S, et al. Autophagy Mediates Survival of Pancreatic Tumour-Initiating Cells in a Hypoxic Microenvironment. *J Pathol* (2012) 227:325–35. doi: 10.1002/path.3994
53. Apel A, Zentgraf H, Büchler MW, Herr I. Autophagy - a Double-Edged Sword in Oncology. *Int J Cancer* (2009) 125:991–5. doi: 10.1002/ijc.24500
54. Iliakis G, Wu W, Wang M. DNA Double Strand Break Repair Inhibition as a Cause of Heat Radiosensitization: Re-Evaluation Considering Backup Pathways of NHEJ. *Int J Hyperthermia* (2008) 24:17–29. doi: 10.1080/02656730701784782
55. Yin Y, Liu L, Zhao Z, Yin L, Bauer N, Nwaeburu CC, et al. Simvastatin Inhibits Sonic Hedgehog Signaling and Stemness Features of Pancreatic Cancer. *Cancer Lett* (2018) 426:14–24. doi: 10.1016/j.canlet.2018.04.001
56. Fan P, Liu L, Yin Y, Zhao Z, Zhang Y, Amponsah PS, et al. MicroRNA-101-3p Reverses Gemcitabine Resistance by Inhibition of Ribonucleotide Reductase M1 in Pancreatic Cancer. *Cancer Lett* (2016) 373:130–7. doi: 10.1016/j.canlet.2016.01.038

57. Pfeifer T, Bai L, Gladkich J, Gross W, Liu L, Herr I, et al. Therapy of Pancreatic Cancer With Alternating Electric Fields: Limitations of the Method. *Bioelectrochemistry* (2021) 141:107881. doi: 10.1016/j.bioelechem.2021.107881
58. Schneider CA, Rasband WS, Eliceiri KW. NIH Image to ImageJ: 25 Years of Image Analysis. *Nat Methods* (2012) 9:671–5. doi: 10.1038/nmeth.2089
59. Dai M, Wang P, Boyd AD, Kostov G, Athey B, Jones EG, et al. Evolving Gene/Transcript Definitions Significantly Alter the Interpretation of GeneChip Data. *Nucleic Acids Res* (2005) 33:e175. doi: 10.1093/nar/gni179

Conflict of Interest: The authors declare that the research was conducted in the absence of any commercial or financial relationships that could be construed as a potential conflict of interest.

Publisher's Note: All claims expressed in this article are solely those of the authors and do not necessarily represent those of their affiliated organizations, or those of the publisher, the editors and the reviewers. Any product that may be evaluated in this article, or claim that may be made by its manufacturer, is not guaranteed or endorsed by the publisher.

frontiers in Oncology

CORRECTION
published: 31 March 2022
doi: 10.3389/fonc.2022.889215

Corrigendum: Establishment of Tumor Treating Fields Combined With Mild Hyperthermia as Novel Supporting Therapy for Pancreatic Cancer

Liping Bai[1†], Tobias Pfeifer[1], Wolfgang Gross[1], Carolina De La Torre[2], Shuyang Zhao[3], Li Liu[1], Michael Schaefer[1‡] and Ingrid Herr[1‡]*

[1] Molecular OncoSurgery, Section Surgical Research, Department of General, Visceral and Transplantation Surgery, University of Heidelberg, Heidelberg, Germany, [2] Medical Research Center, Medical Faculty Mannheim, University of Heidelberg, Heidelberg, Germany, [3] Department of Hematology, Oncology and Rheumatology, Internal Medicine V, University Hospital of Heidelberg, Heidelberg, Germany

OPEN ACCESS

Edited and reviewed by:
Michael Jon Pishvaian, Johns Hopkins Medicine, United States

***Correspondence:**
Ingrid Herr
i.herr@uni-heidelberg.de

†Present address:
Liping Bai, Department of Gastrointestinal Surgery, The Affiliated Zhongshan Hospital, and Institute of Gastrointestinal Oncology, School of Medicine, Xiamen University, Xiamen, China

‡These authors share last authorship

Specialty section:
This article was submitted to Gastrointestinal Cancers: Hepato Pancreatic Biliary Cancers, a section of the journal Frontiers in Oncology

Received: 03 March 2022
Accepted: 14 March 2022
Published: 31 March 2022

Citation:
Bai L, Pfeifer T, Gross W, De La Torre C, Zhao S, Liu L, Schaefer M and Herr I (2022) Corrigendum: Establishment of Tumor Treating Fields Combined With Mild Hyperthermia as Novel Supporting Therapy for Pancreatic Cancer. Front. Oncol. 12:889215. doi: 10.3389/fonc.2022.889215

Keywords: pancreatic ductal adenocarcinoma, hyperthermia, tumor treating fields, alternative therapies, bioinformatics and computational biology

A Corrigendum on

Establishment of Tumor Treating Fields Combined With Mild Hyperthermia as Novel Supporting Therapy for Pancreatic Cancer

By Bai L, Pfeifer T, Gross W, De La Torre C, Zhao S, Liu L, Schaefer M and Herr I (2021). Front. Oncol. 11:738801. doi: 10.3389/fonc.2021.738801

In the original article, there was a mistake in **Figure 2A** as published. The representative images of colony formation "AsPC-1/CO/38.5°C, 1st generation" and "BxGEM/CO/38.5°C, 2nd generation" were mixed up by mistake. The corrected **Figure 2** appears below.

The authors apologize for this error and state that this does not change the scientific conclusions of the article in any way.

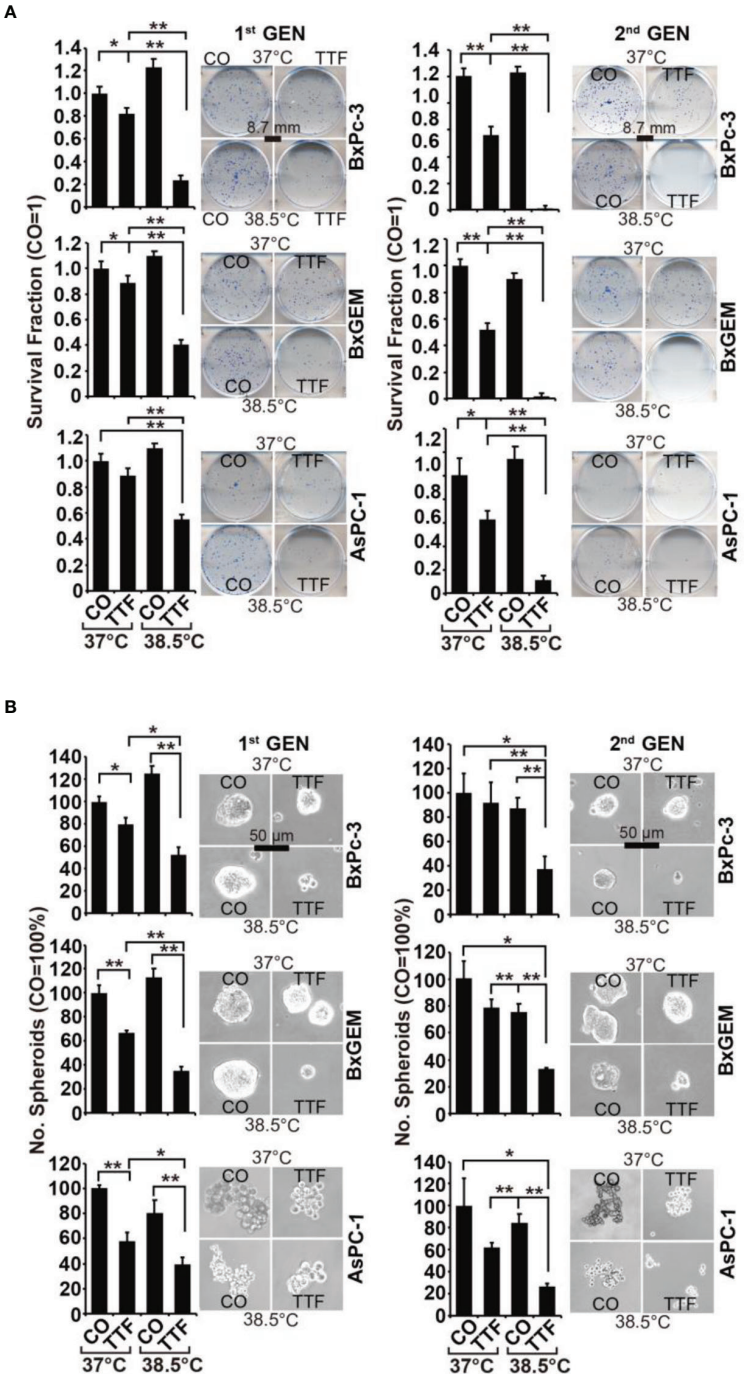

FIGURE 2 | TTField-mediated inhibition of cancer stem cell features is enhanced by hyperthermia. **(A)** The cells were treated as described in Figures 1A, B, **(B)** After 3 days, the cells were detached from the cell culture plates by trypsinization and reseeded at clonal density (AsPC-1: 1,500 cells/well; BxPC-3 and Bx-GEM: 1,000 cells/well) in 6-well plates. The cells were cultured under regular conditions at 37°C without a medium change for 2 weeks, resulting in first-generation colonies (1st GEN). The number of colonies was evaluated by fixing and Coomassie staining, followed by counting colonies with at least 50 cells using a dissecting microscope. The survival fraction and representative images are shown on the left. For the formation of second-generation (2nd GEN) colonies, surviving cells from each group of firstgeneration colonies were collected, reseeded and analyzed as described above. **(B)** After treatment, as described in Figure 1A, the cells were seeded at a clonal density of 500 cells/well in ultralow-attachment 24-well plates in cell growth factor-supplemented serum-free culture medium to induce spheroid formation. Six dayslater, the first generation of spheroids developed, and the percentage of viable spheroids was evaluated by microscopy at 100× magnification and counting. Representative photographs and the means are shown on the left. For the formation of second-generation spheroids (2nd GEN), surviving cells were collected from each group of first-generation spheroids and reseeded and analyzed as described above. The data are presented as the means ± SDs. *$P < 0.05$, **$P < 0.01$.

frontiers in Oncology

ORIGINAL RESEARCH
published: 18 November 2021
doi: 10.3389/fonc.2021.783231

Impact of *TNF-α* Gene Polymorphisms on Pancreatic and Non-Small Cell Lung Cancer-Induced Cachexia in Adult Egyptian Patients: A Focus on Pathogenic Trajectories

Rana Yehia[1], *Mona Schaalan*[1], *Dalaal M. Abdallah*[2], *Amr S. Saad*[3], *Neven Sarhan*[1] *and Samira Saleh*[2]*

[1] Clinical Pharmacy and Pharmacy Practice, Faculty of Pharmacy, Misr International University, Cairo, Egypt, [2] Pharmacology and Toxicology Department, Faculty of Pharmacy, Cairo University, Cairo, Egypt, [3] Oncology Department, Faculty of Medicine, Ain Shams University, Cairo, Egypt

OPEN ACCESS

Edited by:
Nadia M. Hamdy,
Ain Shams University, Egypt

Reviewed by:
Oskan Bahidinov Tasinov,
Medical University of Varna, Bulgaria
Zeinab Shirvani Farsani,
Shahid Beheshti University, Iran

***Correspondence:**
Samira Saleh
samirasaleh7@gmail.com;
samira.saleh@pharma.cu.edu.eg

Specialty section:
This article was submitted to Gastrointestinal Cancers: Hepato Pancreatic Biliary Cancers, a section of the journal Frontiers in Oncology

Received: *25 September 2021*
Accepted: *25 October 2021*
Published: *18 November 2021*

Citation:
Yehia R, Schaalan M, Abdallah DM, Saad AS, Sarhan N and Saleh S (2021) Impact of TNF-α Gene Polymorphisms on Pancreatic and Non-Small Cell Lung Cancer-Induced Cachexia in Adult Egyptian Patients: A Focus on Pathogenic Trajectories. Front. Oncol. 11:783231. doi: 10.3389/fonc.2021.783231

Background: Cachexia is a frequent syndrome in pancreatic and non-small cell lung (NSCL) cancer patients. The storm of cancer-induced inflammatory cytokines, in particular TNF-α, is a crucial pathogenic mechanism. Among the molecular alterations accused of cancer-induced cachexia, *TNF-α 308 G/A* (rs1800629) and *–1031T/C* (rs1799964) are single-nucleotide polymorphisms (SNPs) within the gene encoding this pro-inflammatory cytokine. Recent studies have demonstrated the crucial role of non-coding microRNAs (*miRNAs*) in pathogenesis of different diseases including cachexia. Moreover, the mechanistic cytokine signaling pathway of *miR-155*, as a *TNF-α* regulator, supports the involvement of SOCS1, TAB2, and Foxp3, which are direct targets of *TNF-α* gene.

Aim: A case–control study (NCT04131478) was conducted primarily to determine the incidence of *TNF-α 308 G/A* (rs1800629) and *–1031T/C* (rs1799964) gene polymorphisms in adult Egyptian patients with local/advanced or metastatic pancreatic or NSCL cancer and investigate both as cachexia risk factors. The association of gene polymorphism with cachexia severity and the expression of *miR-155* in cachectic patients were analyzed. A mechanistic investigation of the cytokine signaling pathway, involving SOCS1, TAB2, and Foxp3, was also performed.

Results: In both pancreatic and NSCL cancer cohorts, the mutant *TNF-α* variant of *308 G/A* was positively associated with cachexia; on the contrary, that of 1031T/C was negatively associated with cachexia in the NSCL cancer patients. *MiR-155* was higher in cachexia and in alignment with its severity in the cachectic group as compared with the non-cachectic group in both the pancreatic and NSCL cancer patients. Though TAB2 did not change to any significant extent in cachectic patients, the levels of SOCS1 and Foxp3 were significantly lower in the cachectic group as compared with the non-cachectic group.

Conclusion: Carriers of the A allele *308 G/A* gene and high *miR-155* are at greater risk of cachexia in both the pancreatic and NSCL cancer patients; however, the mutant variant of

1031T/C gene is protective against cachexia in the NSCL cancer patients. Finally, high levels of *miR-155* in the cachectic group lead to negative feedback inhibition of both SOCS1 and Foxp3 in both the pancreatic and NSCL cancer patients.

Keywords: pancreatic and NSCL cancer, cachexia, single-nucleotide polymorphism, *TNF-α* gene, *miR-155*, SOCS1, Foxp3, TAB2

INTRODUCTION

Cachexia is a devastating, multifactorial syndrome that is observed in the majority of end-stage cancer patients (1–3). It is more acute in certain incurable malignancies, such as pancreatic and NSCL cancers (4–6). The current understanding of cancer cachexia indicates that factors secreted by tumors together with factors secreted as a result of the tumor–host interaction initiate systemic inflammation and metabolic disturbances, which in turn trigger muscle wasting. Thus, systemic inflammation is thought to be a major mediator of cancer cachexia (7). TNF-α is probably the most characterized cytokine in cachexia, as it promotes anorexia and skeletal muscle wasting mainly through the NF-κB pathway (8). In a feedforward loop, this cytokine functions in controlling the transcription factor nuclear factor kappa light chain enhancer of activated B cells (NF-κB), which helps in adjusting immune and inflammatory responses and consequently leads to the generation of specific cytokines that have a role in proteolysis and breakdown of myofibrillar proteins (9). Accordingly, TNF-α-mediated NF-κB activation promotes wasting of muscle that leads to bodyweight loss ending with cancer cachexia (10).

In the last few years, several functional single-nucleotide polymorphisms (SNPs) within cytokines' genes have been identified and described as cancer-related genetic alterations. The most important ones seem to be SNPs located within the promoter of *TNF-α* because of their ability to regulate gene expression and, consequently, the expression of the TNF-α protein. Among frequently investigated SNPs, the 308 G/A (rs1800629) and −238 G/A (rs361525) are potentially involved in tumor aggressiveness, prognosis, and risk of malnutrition (11, 12). Notably, there are only few data concerning the role of *TNF-α −1031T/C* SNP (rs1799964) in the regulation of systemic inflammatory response; however, the latest studies have demonstrated the role of this SNP as cachexia-related genetic alteration (13, 14). Accordingly, the significant role of the systemic inflammatory response mediated by TNF-α in the etiopathology of cachexia encourages investigating SNPs of *TNF-α* as cachexia-related risk factors.

MicroRNAs (miRNAs) represent another class of molecules that may be involved in muscle wasting (15). Altered expression of microRNAs has been shown to be involved in skeletal muscle homeostasis in health and disease (16–19). Moreover, several lines of evidence demonstrate that *miR-155* is overexpressed in a number of neoplastic diseases (20), where altered *miRNA* expression has been found in hematological malignancies, thyroid carcinoma breast and colon cancer (21); thus, it is considered to be a marker of poor prognosis (22). Additionally, many studies have highlighted the role of miRNAs in the pathophysiology of cancer cachexia (23) particularly *Mir-155* (24).

Noteworthy, Jiang et al. (25) identified SOCS1 as a novel target of *miR-155* in breast cancer cells (25). The suppressors of cytokine signaling (SOCS) protein family are described as direct regulators of janus kinase (JAK)/signal transducer and activator of transcription (STAT) signaling pathway in cancer. Overexpression of *SOCS* gene and consequently the SOCS proteins were observed in breast cancer; and a higher expression level was significantly associated with high-grade tumors (26). These data provide further evidence for the proto-oncogenic contribution of SOCS protein in cancer. Furthermore, the forkhead transcription factor is an immune regulator where the Foxp3 member is mainly expressed in CD4+ cells, which directly suppress the immune system through suppressing nuclear transcript abundant transcript 1 (NEAT1) and NF-κB and consequently repress interleukin-2 (IL-2) and T-cell cytokines (27). Recently, high expression levels of Foxp3, at genetic and protein levels, are significantly associated with tumor invasion in pancreatic ductal adenocarcinoma (PDAC) and lung adenocarcinoma (28). Moreover, transforming growth factor β binding activated kinase 1 protein 2 (TAB2) is an inflammatory mediator in cancer pathogenesis. Aberrant expression of TAB2 protein is significantly associated with cancer progression through activation of mitogen-activated protein kinase (MAPK) and NF-κB signaling pathway. A higher expression level of TAB2 was observed in ovarian cancer (29).

Genetic studies on cancer-associated cachexia remain highly controversial. Thus, the present study focused on two types of solid cancers with different pathological entities, pancreatic cancer "digestive system cancer" and lung cancer "respiratory system cancer." Cumulative evidences have proven that TNF-α is a pro-cachectic protein; therefore, two SNPs of *TNF-α* gene, as well as *miR-155* expression, have been investigated and correlated the gene genotype with risk of cancer-associated cachexia. The selection of SNPs was based on the global and European minor allele frequency (MAF): *TNF-α 308 G/A* (rs1800629) and *−1031T/C* (rs1799964) SNP. Finally, the involvement of SOCS1, TAB2, and Foxp3 as direct targets for *TNF-α* gene in both cancer types was assessed.

PATIENTS AND METHODS

Study Design and Population

This case–control study was conducted at the Oncology Department, Faculty of Medicine, Ain Shams University

Abbreviations: Foxp3, Forkhead box P3; SOCS1, Suppressor of cytokine signaling 1; TAB2, TAK1-associated Binding Protein 2; *TNF-α*, Tumor necrosis alpha subunit gene.

(Cairo, Egypt). Pancreatic and NSCL cancer patients (n = 203) were recruited in this study; their mean age was 51.45 ± 9.7 and ranged at 20–77 years. They were divided into two subgroups according to the degree of depletion of energy stores, body mass index (BMI), and ongoing weight loss; the first subgroup includes 94 patients who represent the comparative control non-cachectic group. The second subgroup includes 109 cachectic cancer patients who were then classified into pre-cachexia, cachexia, and refractory cachexia according to the cachexia severity index (30) by comparing their current weight with their actual one recorded on first admission. Pre-cachexia is defined as a ≤5% weight loss with anorexia and metabolic change; cachectic patients present with weight loss of >5%, BMI < 20, and weight loss of >2% or sarcopenia and weight loss of >2%; they also often had reduced food intake and systemic inflammation. In refractory cachexia, the cancer is pro-catabolic and not responsive to treatment (1). According to the type of cancer, patients were additionally classified into two groups: 71% of cases were subclassified into cachectic (n = 69) and non-cachectic (n = 76) groups who received *Xeloda* (pancreatic cancer; n = 145), and 29% were also subclassified into cachectic (n = 40) and non-cachectic (n = 18) groups treated with *Gem/Cis* (lung cancer).

Approval and Ethical Considerations

The current study was approved by the Research Ethics Committee of Faculty of Pharmacy, Cairo University (Cairo, Egypt; PT-2387), as well as the Ethical Committee of the Oncology Department, Ain Shams University, and registered in ClinicalTrials.gov (trial registration number NCT04131478). The recruited patients provide the required informed consent.

Inclusion and Exclusion Criteria

Inclusion criteria were based on a thorough history taking, and clinical and pathological examinations. Patients were considered eligible if they meet the following criteria: a medical diagnosis of cancer (e.g., lung or pancreatic), locally, advanced, or metastatic cancer scheduled for first-line cytotoxic chemotherapy; starting or continuing chemotherapy at the time of screening for participants where the duration was set based on standard period of first-line chemotherapy; and age between 18 and 80 years.

On the other hand, patients with the following criteria were excluded from the study: if they planned to have surgical procedures at the time of recruitment, have underwent surgery during the study or in the month prior to the study, and did not have chemotherapy scheduled post-surgery. Also, patients with comorbidities that could affect the interpretation of study findings were excluded, e.g., HIV, Alzheimer's disease, movement disorder, acute myocardial infarction within the last 3 months, hepatitis, open burn sites or infected wounds, esophageal cancer with a swallowing difficulty in mechanical nature, or an uncorrected mechanical digestive obstruction. Pregnant, nursing women or patients with disorders associated with change in *miR-155* level (rheumatic arthritis, osteoarthritis, atopic eczema, Down's syndrome, breast cancer, endometrioid adenocarcinoma, acute myeloid leukemia (AML), chronic lymphocytic leukemia (CLL), and papillary carcinoma thyroid tumors) were excluded too; and finally, patients with inflammatory and autoimmune diseases (multiple sclerosis, psoriasis, and systemic lupus erythematous) were excluded.

Study Outcomes

Primary outcomes: to detect the incidence of *TNF-α 308 G/A* (rs1800629) and *−1031T/C* (rs1799964) gene polymorphism and investigate both as cachexia risk factors in local/advanced/metastatic pancreatic or NSCL cancer in adult Egyptian patients; to determine the association of gene polymorphism with cachexia severity; to assess the expression of *miR-155* in cachectic patients and its association with cachexia severity; and to verify the involvement of the cytokines SOCS1, TAB2, and Foxp3 signaling pathway in pancreatic and NSCL cancers.

Secondary outcomes: to measure the association between *TNF-α 308 G/A* (rs1800629) and *−1031T/C* (rs1799964) gene polymorphism in the selected patient groups and the development of cancer cachexia; and to analyze the correlation between *miR-155* gene expression and SOCS1, TAB2, or Foxp3 in cachectic pancreatic or NSCL cancer patients.

Sample Collection and Genotyping Procedure

A venous blood sample (5 ml) was withdrawn from each participant under complete aseptic conditions and divided into two portions, as follows: 2 ml of blood was placed in an EDTA-containing tube for DNA extraction used for genotyping of the *TNF-α* gene polymorphism, and 3 ml of blood was left at room temperature for 30 min for spontaneous clotting, and then serum was separated by centrifugation at 3,000 rpm for 10 min. The serum samples were used for RNA extraction and for ELISA technique. Both samples were stored at −80°C until analysis.

Clinicopathological Assessments

Blood urea nitrogen (BUN), alanine aminotransferase (ALT), aspartate aminotransferase (AST), total serum bilirubin, and direct serum bilirubin were analyzed by spectrophotometric assay on fully automated clinical chemistry analyzer (Synchron LX® Systems; Beckman Coulter, CA, USA); and hemoglobin, platelets, and total leukocytic count are also measured by the AcT 5diff Cap Pierce hematology analyzer (Beckman Coulter hematology analyzer; CA, USA).

TNF-α Gene Polymorphism by Pharmacogenetics Analysis/Genotyping

Genomic DNA was extracted from peripheral blood leukocytes using the automated QIAcube device (Qiagen, Hilden, Germany) according to the manufacturer's guidelines. The selected polymorphisms were then genotyped by TaqMan allelic discrimination method according to the manufacturer's recommendations (Applied Biosystems, Thermo Fisher Scientific, MA, USA).

Amplification of *MiR-155* Using qRT-PCR Technique

Total *miRNA* was isolated from patients' sera by using the "miRNeasySerum/Plasma Kit" (Qiagen). *MiR-155* was

reversibly transcribed using miScript II RT Kit (Qiagen). In a reverse transcription reaction with miScript HiSpec Buffer, mature miRNAs are polyadenylated by poly(A) polymerase and converted into cDNA by reverse transcriptase with oligo-dT priming; and the cDNA was then used for real-time PCR quantification of mature *miRNA* expression. Relative miRNA expression levels for the candidate *miR-155* were analyzed by *mi*Script SYBR Green PCR Kit (Qiagen) and specific primers (Hs_*miR-155*_2 miScript Primer Assay [cat#: 218300], which target mature *miR-155* (cat#: MS00031486; Qiagen) and Hs_SNORD68_11 miScript Primer Assay cat#: 218300) as housekeeper gene (HK), which targets SNORD68 small nucleolar RNA, C/D box 68 (cat#: MS000337). The amplification was done using 5 Plex Rotor Gene RealTime PCR Analyzer (Qiagen). The relative quantitation of miR-155 was calculated using the equation $2^{-\Delta\Delta Ct}$ test control.

Quantification of SOCS1, TAB2, and Foxp3 Serum Levels Using ELISA Technique

Serum *SOCS1* (cat#: SL3093Hu), *TAB2* (cat#: SL3094Hu), and *Foxp3* (cat#: SL2462Hu) were measured in patients' sera using the corresponding human ELISA Kit (SunLong Biotech Co., Hangzhou, China).

Statistical Analysis

The sample size was calculated using G* program, version 3.1.9.4, setting alpha error at 5% and power at 95% and the allocation ratio for N1/N2 = 1. So assuming an effect size of 0.5 (Cohen's f) between two groups produced a total sample size of not less than 184 subjects. Parametric data were presented as mean ± SD and range, while non-parametric data were presented as median and range; categorical variables were given as numbers (percentage). Data were checked for normality using the Kolmogorov–Smirnov test and homogeneity with chi-squared test, as appropriate. For parametric data, the comparison between the two groups was done by Student's *t*-test, whereas for multiple comparisons, *one-way ANOVA* followed by Bonferroni's post-hoc test was performed. For non-parametric variables, the *Mann–Whitney* test was adopted to compare the two groups, whereas the *Wilcoxon Signed Rank* test assessed the statistical significance differences between two dependent samples. Logistic regression analysis was used for the association between two SNPs and susceptibility to cancer-associated cachexia and was given as odds ratios (ORs) and corresponding 95% CI. The *Hardy–Weinberg equilibrium (HWE)* and the association between *TNF-α* gene polymorphisms and risk of cancer-related cachexia were calculated by SNPstats online software (http://www.snpstats.net/start.htm), which assessed the frequency distribution between cachectic and non-cachectic Egyptian adult cancer patients of four genetic models: codominant, dominant, recessive, and overdominant (31). Spearman's correlation analysis was used between *miR-155* gene expression and serum levels of SOCS1, TAB2, and Foxp3 in cachexia-related with pancreatic and NSCL cancers. The collected data were revised, coded, and tabulated using *SPSS version 24* (IL, USA). All graphs were plotted by *GraphPad Prism Software 8.4.2* (CA, USA). The level of significance is taken at a p-value of <0.05.

Bioinformatics Analysis of *TNF-α* Gene

In order to infer interrelationships among the *TNF-α* gene and cancer cachexia, the SNPs, and *TNF-α* (rs1800629) and (rs1799964), selection was based on global and European MAF published on the National Center for Biotechnology Information in collaboration with the National Human Genome Research Institute (dbSNP) accessed from https://www.ncbi.nlm.nih.gov/snp. The frequency of selected SNPs was double-checked from Pharmacogenomics Knowledgebase (*Pharm GKB*) accessed from https://www.pharmgkb.org.

RESULTS

Clinical and Biochemical Features of Pancreatic and Non-Small Cell Lung Cancer Patients

The current study was conducted on 203 adult Egyptian cancer patients who were sub-classified into two main groups: the cachectic group (n = 109) and non-cachectic group (n = 94) where their baseline characteristics are given in **Table 1**. There was no difference between the cachectic and non-cachectic patients regarding the mean of age, distribution of gender, presence, and number of comorbidities with the majority having only one comorbid disease; the only difference was the type of cancer/chemotherapy. Significant associations existed between cachexia and non-cachexia subgroups for BUN and TLC in the pancreatic cancer patients (**Table S1**) and direct serum bilirubin in the NSCL cancer patients (**Table S2**).

Distribution of *TNF-α 308G/A* or *–1031T/C* Polymorphisms and Genotypes Among Pancreatic and Non-Small Cell Lung Cancer Patients

In the pancreatic cancer group, 69 out of 145 patients were cachectic, whereas in the NSCL cancer group, 40 out of 58 were cachectic. According to the present allele frequency distribution data of all cancer patients, only 27 patients of 203 (13%) had the *TNF-α 308G/A* (rs1800629) mutation, whereas approximately seven times more patients carried the wild-type allele (176 patients, i.e., 87% of the total number). Of the 14 pancreatic cancer patients carrying the mutant *TNF-α 308G/A* (rs1800629) gene, 10 patients were cachectic (15%), and four patients were non-cachectic (5%), showing a significant positive association between *TNF-α 308G/A* gene mutation and cachexia (**Figure 1A**). In the NSCL cancer group, in a total of 13 patients, 11 patients who were cachectic (28%) and only two patients who were non-cachectic (11%) carried this allele, revealing also a significant positive association (**Figure 1B**). No significant association was observed between the polymorphism of *TNF-α 1031T/C* (rs1799964) in pancreatic cancer subgroups (**Figure 1C**), whereas a significant negative association

TABLE 1 | Demographic characteristics in non-cachectic and cachectic cancer patients.

Variable	Cancer patients			F/χ^2
	Total	Non-cachectic	Cachectic	
Number of patients	**203**	**94**	**109**	
Age in years				
Mean ± SD	51.45 ± 9.7	52.0 ± 8.8	50.98 ± 10.4	F = 2.9
Median (Range)	51 (20–77)	52 (30–77)	50 (20–75)	p = 0.46
Gender [n (%)]				
Male	107 (53)	45 (48)	62 (57)	χ^2 = 1.6
Female	96 (47)	49 (52)	47 (43)	p = 0.208
Cancer type [n (%)]				
Pancreatic cancer	145 (71)	76 (81)	69 (63)	χ^2 = 7.6
NSCL cancer	58 (29)	18 (19)	40 (37)	p = 0.008**
Comorbidities [n (%)]				
Negative	100 (49)	50 (54)	50 (46)	χ^2 = 1.2
Positive	103 (51)	44 (46)	59 (54)	p = 0.32
No. of comorbidities [n (%)]				
One	77 (75)	34 (77)	43 (73)	χ^2 = 0.26
>One	26 (25)	10 (23)	16 (27)	p = 0.65
Type of chemotherapy [n (%)]				
Xeloda	145 (71)	76 (81)	69 (63)	χ^2 = 7.6
Gem/Cis	58 (29)	18 (19)	40 (37)	p = 0.008**

*Data are given as mean ± SD, median (minimum–maximum), or n (%). Statistical analysis was carried out using the independent t-test and chi-square test; p ≤ 0.05. Cis, cisplatin; F, independent t-test value; Gem, gemcitabine; n (%), number of cases within the group (percentage); NSCL, non-small cell lung; χ^2, chi-square value. **Significant difference at p ≤ 0.01.*

(**Figure 1D**) was found between *TNF-α 1031T/C* gene mutation and cachexia in the NSCL cancer group. As expected, for an admixed population from Egypt, the frequency of the *TNF-α 308G/A* (χ^2: 5.2, p = 0.001) and *TNF-α 1031T/C* (χ^2: 3.8, p = 0.15) gene polymorphisms were higher than in Africans, Latin Americans, Asians, and Europeans (**Table S3**).

The genotype distribution of *TNF-α 308G/A* polymorphism in each cancer type is presented in **Figure 2**. In the cachectic pancreatic cancer, the heterozygous GA genotype (49%) showed the highest frequency among the three, whereas the homozygous GG genotype (62%) was the most frequently distributed among the non-cachectic group; and the homozygous AA genotype was more frequently distributed in cachectic (15%) than non-cachectic (5%) patients (**Figure 2A**). In the cachectic NSCL cancer patients, the heterozygous GA genotype (55%) showed the highest frequency among the three, whereas the homozygous GG genotype (61%) was the most frequently distributed among the non-cachectic group; and the homozygous AA genotype was more frequently distributed in cachectic (28%) compared with non-cachectic (11%) patients (**Figure 2B**). Similarly the genotype distribution of *TNF-α 1031T/C* is presented also in **Figure 2**. However, the *TNF-α 1031T/C* genotype was not associated with cancer-related cachexia in pancreatic cancer patients (**Figure 2C**). In contrast, in the cachectic NSCL cancer patients, the homozygous CC genotype (45%) showed the highest frequency among the three, whereas the homozygous TT genotype (61%) was the most frequently distributed among the non-cachectic group; and the heterozygous TC genotype was more frequently distributed in cachectic (33%) than non-cachectic (17%) patients (**Figure 2D**).

Impact of *TNF-α 308G/A* or *–1031T/C* Gene Mutation Frequency on Cachexia Severity Score Among Pancreatic and/or Non-Small Cell Lung Cancer Patients

In both pancreatic (**Tables 2** and **S4**) and NSCL (**Tables 3** and **S5**) cancer patients, no significant association existed between *TNF-α 308G/A* or *TNF-α 1031T/C* mutant alleles as well as their allelic genotypes and the severity of cachexia. Similarly, no significant association was reached between *TNF-α 308G/A* or *TNF-α 1031T/C* allelic genotypes and the cachexia severity, regardless of the cancer type (**Table S6**).

Impact of *TNF-α 308G/A* or *–1031T/C* Single-Nucleotide Polymorphisms on Susceptibility to Cancer-Associated Cachexia

After correction for multiple comparisons, both rs1799964 and rs1800629 showed a significant association with cachexia regardless of cancer type. In the unconditional logistic regression analysis, individuals with *TNF-α 308G/A* mutant genotypes had a significantly increased risk of cachexia as compared with those with the wild genotype. On the other hand, individuals with *TNF-α –1031T/C* mutant genotypes had a significantly decreased risk of cachexia as compared with those with the wild genotype. Moreover, the dominant and recessive models were analyzed, and the genotypic models for both SNPs were tested as follows (GG vs. GA and AA) for the SNP rs1800629 and (CC versus TC and TT) for the rs1799964: significant associations with both pancreatic cancer and NSCL cancer-associated cachexia were reached (**Table 4**).

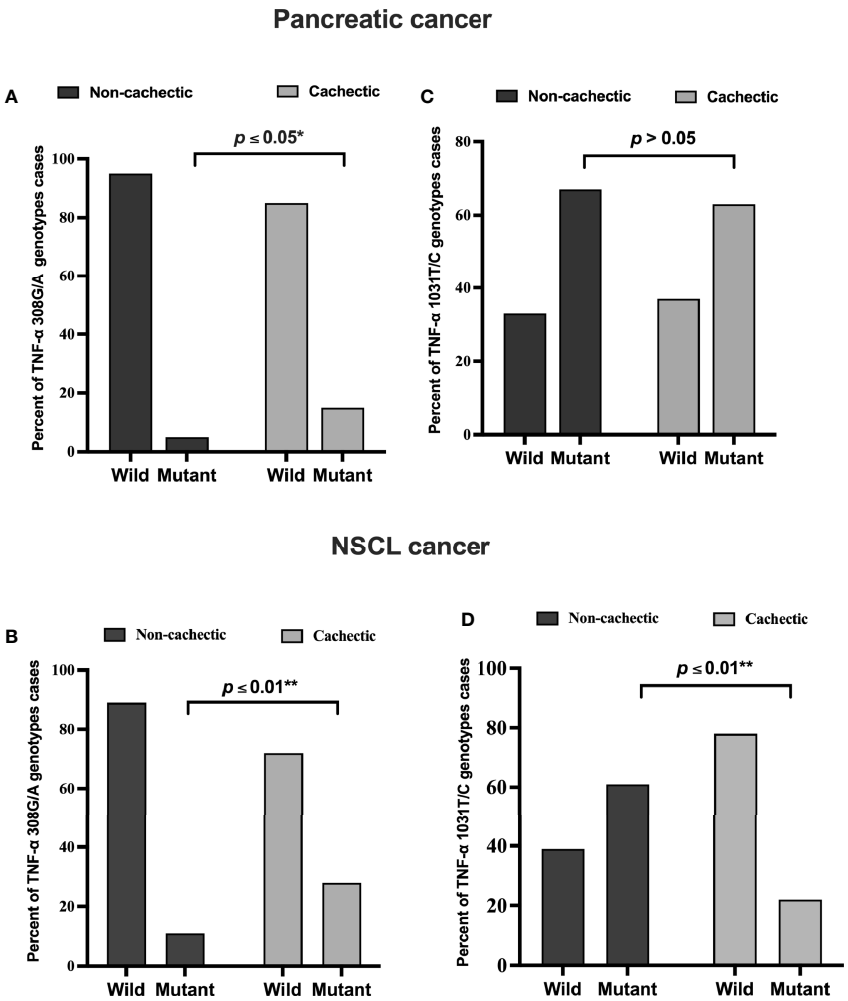

FIGURE 1 | Frequencies of *TNF-α 308 G/A* (rs1800629) wild and mutant alleles among **(A)** pancreatic **(B)** NSCL cancer patients and *TNF-α T/C* 1031 (rs1799964) wild and mutant alleles among **(C)** pancreatic and **(D)** NSCL cancer patients. Comparison between wild and mutant alleles as performed by chi-square test at *p < 0.05. **Significant difference at p ≤ 0.01. NSCL, non-small cell lung.

Serum *MiRNA-155* Is Associated With Cachexia and Its Severity in Patients With Pancreatic or Non-Small Cell Lung Cancer

Circulating miRNAs have recently emerged in cancer cachexia and are a promising class of biomarkers. In the present study, a significant positive association of serum *miR-155* expression level between cachectic and non-cachectic patients existed, where *miR-155* is increased by 424-fold in the cachectic patients compared with the non-cachectic group in pancreatic cancer (**Figure 3A**); and also in NSCL cancer, *miR-155* was upregulated to 4.5-fold with cancer-associated cachexia (**Figure 3B**). This means that patients with cancer who have high *miR-155* have an increased likelihood of developing cancer cachexia than those with low *miR-155*. Overexpression of *miR-155* was even higher in cachectic patients with increasing phases (pre-cachexia, cachexia, refractory cachexia) in both pancreatic (**Figure 3C**) and NSCL (**Figure 3D**) cancers.

Serum Level of SOCS1, TAB2, and Foxp3 in Patients With Pancreatic and Non-Small Cell Lung Cancer

In pancreatic cancer patients, a significant negative association was recorded between serum SOCS1 and Foxp3 with the presence of cachexia. Lower levels of SOCS1 (**Table 5**) and Foxp3 (**Table 5**) were observed in the cachectic group as compared with the non-cachectic one. On the other hand, there was no association between TAB2 and the presence of cachexia (**Table 5**). Regarding the association between the SOCS1, TAB2, and Foxp3 with the severity of cachexia, no significant association was detected except for Foxp3, where lower levels were significantly associated with higher severity of cachexia in patients with pancreatic cancer (**Table 5**).

Regarding the NSCL cancer patients, significantly lower serum levels of SOCS1 and Foxp3 were noted in cachexia as compared with non-cachexia. The median serum level for

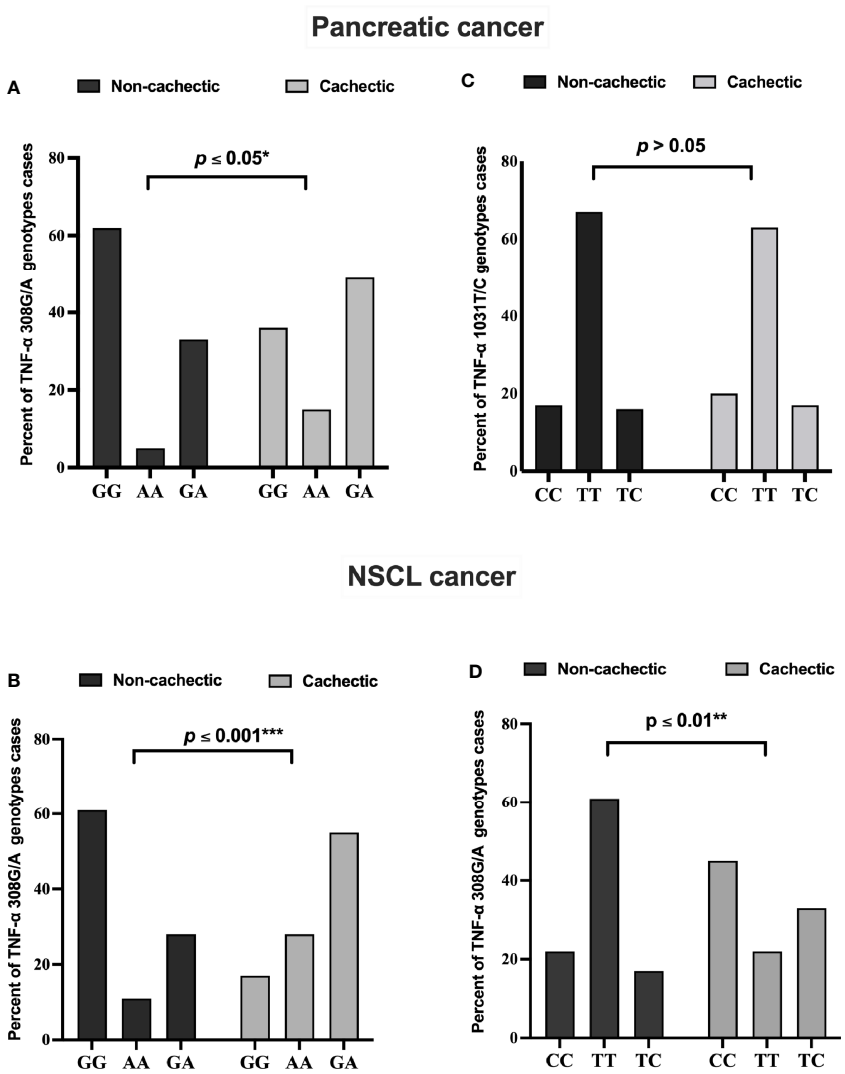

FIGURE 2 | Frequencies of *TNF-α 308 G/A* genotypes among **(A)** pancreatic and **(B)** NSCL cancer patients and *TNF-α 1031 T/C genotypes* among **(C)** pancreatic and **(D)** NSCL cancer patients. Comparison between all genotypes was performed by chi-square test at *p ≤ 0.05. *Significant difference at p ≤ 0.05. **Significant difference at p ≤ 0.01 and *** at p ≤ 0.001. NSCL, non-small cell lung.

TABLE 2 | Distribution of *TNF-α* gene alleles among cachectic pancreatic cancer patients considering the cachexia severity.

Variable	*TNF-α 308G/A* (rs1800629)		*TNF-α 1031T/C* (rs1799964)	
	Wild	**Mutant**	**Wild**	**Mutant**
Cachexia severity				
Pre-cachexia (n = 20)	17 (85)	3 (15)	8 (40)	12 (60)
Cachexia (n = 32)	29 (91)	3 (9)	10 (31)	22 (69)
Refractory (n = 17)	13 (77)	4 (23)	8 (47)	9 (53)
χ^2	1.8		0.19	
	p = 0.42		p = 0.90	

Data are given as n (%). Statistical analysis was carried out using the chi-square test; p ≤ 0.05.
n (%), number (percentage); rs, referred sequence; TNF-α, tumor necrosis alpha subunit gene; χ^2, chi-square value.

TABLE 3 | Distribution of *TNF-α* gene genotype among cachectic NSCL cancer patients considering the cachexia severity.

Variable	*TNF-α 308G/A* (rs1800629)		*TNF-α 1031T/C* (rs1799964)	
	Wild	Mutant	Wild	Mutant
Cachexia severity				
Pre-cachexia (n = 10)	9 (75)	3 (25)	7 (70)	3 (30)
Cachexia (n = 23)	8 (67)	4 (33)	20 (87)	3 (13)
Refractory (n = 7)	12 (75)	4 (25)	4 (57)	3 (43)
χ^2	2.0		3.2	
	p = 0.38		p = 0.2	

Data are given as n (%). Statistical analysis was carried out using the chi-square test; p ≤ 0.05.
n (%), number (percentage); rs, referred sequence; TNF-α, tumor necrosis alpha subunit gene; χ^2, chi-square value; NSCL, non-small cell lung.

TABLE 4 | Risk factors for cachexia associated with cancer by binary logistic regression analysis.

Risk factor	β^0	p-Value	Odds ratio	95% CI for Exp(B)
TNF-α 308G/A, rs1800629				
Wild/mutant regardless of cancer type	–0.355	0.04*	0.701	0.28–1.705
Wild/mutant for pancreatic cancer	–0.215	0.014*	0.414	0.203–0.845
Wild/mutant for NSCL cancer	–0.548	0.0001***	0.5	0.345–0.724
TNF-α 1031T/C, rs1799964				
Wild/mutant regardless of cancer type	0.706	0.02*	2.02	1.12–3.673
Wild/mutant for pancreatic cancer	0.881	0.012*	1.605	1.07–2.39
Wild/mutant for NSCLC	0.916	0.004**	2.5	1.67–751

For rs1800629, GA and AA are coded as 0, while GG carriers are coded as 1. For rs1799964, TC and TT are coded as 0, while CC carriers are coded as 1. Data are presented as odd ratio and 95% CI. p ≤ 0.05.
**Significant difference at p ≤ 0.05.*
***Significant difference at p ≤ 0.01.*
****Significant difference at p ≤ 0.001.*

SOCS1 was 10.9 in the non-cachectic patients and nearly half this value at 5.8 in cachectic patients (**Table 5**). Similarly, Foxp3 was 8.8 in the non-cachectic patients compared with 6.8 in the cachectic patients (**Table 5**). In contrast, no significant association was detected between the TAB2 and the presence of cachexia in the NSCL cancer patients (**Table 5**). Moreover, there was no association between SOCS1, TAB2, and Foxp3 with the cachexia severity in NSCL cancer (**Table 5**).

SOCS1 Correlates Positively With Foxp3 in Cachexia Associated With Pancreatic Cancer

Correlation analyses (**Table 6**) revealed a strong positive correlation between SOCS1 and Foxp3 in the cachectic pancreatic cancer patients. On the other hand, no significant correlation was detected between serum *miR-155* and any of the targeted proteins (SOCS1, TAB2, and Foxp3) or between TAB2 and Foxp3 levels. Similarly, for the NSCL cancer patients with cachexia, no significant correlation was detected among the serum *miR-155* and any of the three targeted proteins (**Table 6**).

Serum *MiRNA-155* Is Associated With the Severity of Cachexia in Cancer Patients Regardless of the Type of Cancer But Not With SOCS1, TAB2, and Foxp3

A significant positive association was detected between serum *miR-155* level and the severity of cachexia in cancer patients regardless of the type of cancer where *miR-155* was increased by approximately sixfold in patients with refractory cachexia compared with cachectic patients, and it was also upregulated to around ninefold in cachectic patients compared with pre-cachectic patients (**Table 7**). In contrast, the severity of cachexia was not associated with the expression of SOCS1, TAB2, and Foxp3 (**Table 7**).

DISCUSSION

Cancer cachexia is a polygenic complex syndrome in which a dysregulated inflammatory response partakes in its development (32). In this study, we first identified the genetic variants of *TNF-α 308G/A* (rs1800629) and *TNF-α 1031T/C* (rs1799964) and their association with cachexia in pancreatic and lung cancer Egyptian patients. To the best of the authors' knowledge, the genotypic and allelic associations of *TNF-α 308G/A* and *TNF-α 1031T/C* gene polymorphisms with cachexia in pancreatic and NSCL cancers have not been unveiled before, especially in the Egyptian population. *TNF-α 308G/A* (rs1800629) gene polymorphism was a significant predictor for cachexia in both the lung and pancreatic cancer patients rather than that of *TNF-α 1031T/C* (rs1799964) gene, which was associated with lower risk of cachexia in the NSCL cancer patients. Of note, the homozygous GG genotype (wild) was mainly distributed among the non-cachectic group, and the homozygous AA

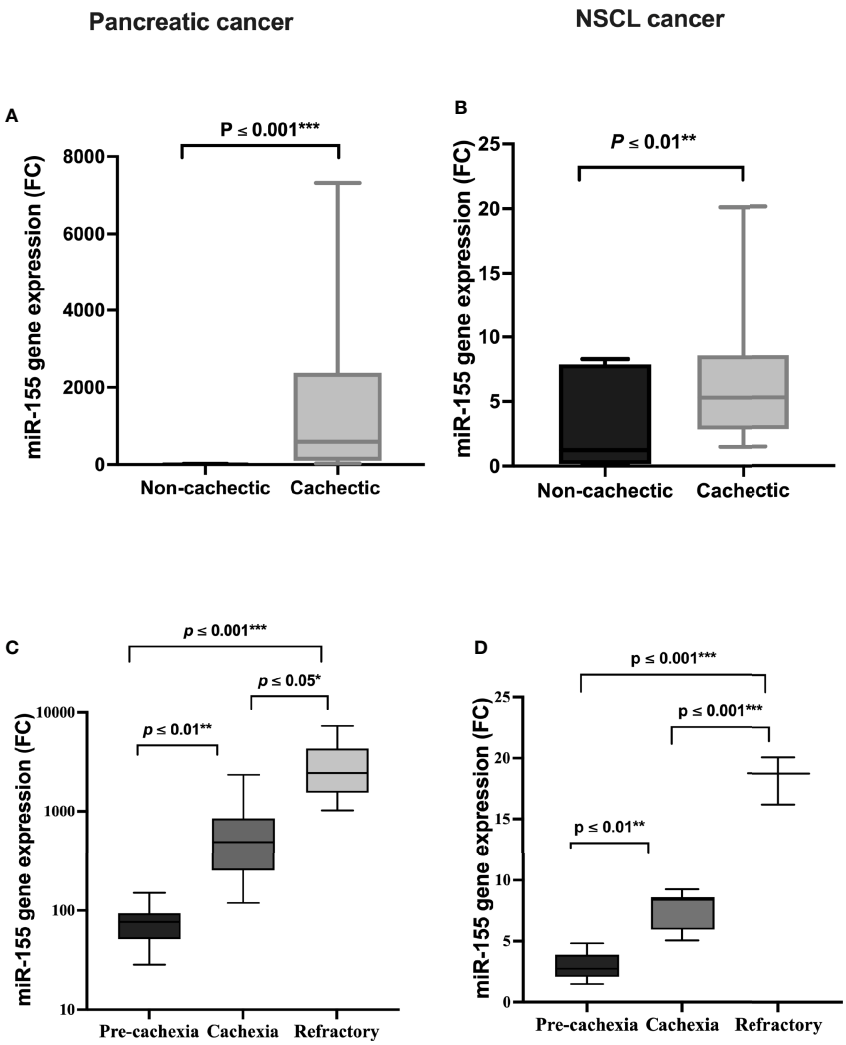

FIGURE 3 | Serum expression of *miR-155* in **(A)** pancreatic and **(B)** NSCL non-cachectic and cachectic cancer patients and its expression in different grades of cachexia severity in **(C)** pancreatic and **(D)** NSCL cancer patients. Comparison between cachectic and non-cachectic groups was performed by chi-square test at *p < 0.05. **Significant difference at p ≤ 0.01 and *** at p ≤ 0.001. Comparison between all cachexia grades was performed by ANOVA test followed by Bonferroni's post-hoc test; at *p < 0.05. **Significant difference at p ≤ 0.01 and *** at p ≤ 0.001. NSCL, non-small cell lung.

(mutant) genotype was more frequently distributed in the cachectic than non-cachectic patients with pancreatic cancer. Regarding *TNF-α 308G/A* gene polymorphism in the NSCL cancer group, the heterozygous GA genotype was frequently detected in patients of the cachectic group, followed by the homozygous AA genotype with the least percent carrying the homozygous GG genotype. Secondly, we attempted to examine the involvement of *miR-155*/SOCS1/Foxp3/*TNF-α* signaling and *TAB2* in the pathogenesis of cachectic cancer patients. In this context, higher serum *miR-155* expressions were correlated with susceptibility to cachexia and were in parallel with its severity in both cancer types. Meanwhile, lower protein expression of SOCS1 and Foxp3 was only evident in both cachectic cancer groups without any association between TAB2 protein expression and the presence of cachexia. Moreover, lower protein expression of Foxp3 was significantly associated with higher severity of cachexia in patients with pancreatic cancer.

Cancer cachexia is a devastating multifactorial and often irreversible syndrome that affects approximately 50%–80% of cancer patients, depending on tumor type. It leads to substantial weight loss, primarily from loss of skeletal muscle and body fat (32, 33). Genetic variations are likely to contribute to the susceptibility or resistance to developing cancer cachexia. The role of TNF-α, one of the important genetic variants of genes encoding pro-inflammatory cytokines, has been reported in cancer cachexia (34). More than 100 gene variants that are linked to development of cachexia in cancer patients have been identified (35). SNPs, the most common type of heritable and evolutionarily stable genetic variations in the population, seem to be an attractive option for the selection of patients with high risk

TABLE 5 | Serum SOCS1, TAB2, and Foxp3 level in cachectic and non-cachectic pancreatic and NSCL cancer patients and cachexia severity.

Variable	SOCS1 (ng/ml)	TAB2 (ng/ml)	Foxp3 (ng/ml)
Pancreatic cancer patients			
Non-cachectic (n = 20)	9.3 (7–26)	6.3 (2.0–8.4)	16 (5–30)
Cachectic (n = 48)	5.6 (3.3–8.6)	6.2 (4.8–13.0)	8.9 (6.5–96.0)
Statistics	U: 185 p = 0.002**	U: 262 p = 0.06	U: 49 p = 0.0001***
Cachexia severity			
Pre-cachexia (n = 14)	5.6 (3.2–6.5)	6.5 (5.2–8.4)	16 (7–35)
Cachexia (n = 17)	5.2 (4.2–8.6)	6.3 (5.9–8.4)	14.5 (6–33)
Refractory (n = 17)	5.8 (3.7–7.4)	5.6 (2.6–7.8)	11.3 (5.6–30)
Statistics	F: 1.1 p = 0.34	F: 0.2 p = 0.8	F: 5.3 p = 0.008**
NSCL cancer patients			
Non-cachectic (n = 10)	10.9 (4.0–14)	9.2 (7.0–20)	8.8 (6.0.11)
Cachectic (n = 18)	5.8 (4.0–9.2)	8.0 (5.6 –29)	6.8 (4.6–9.7)
Statistics	U: 39 p = 0.01**	U: 57 p = 0.12	U: 35 p = 0.03*
Cachexia severity score			
Pre-cachexia (n = 9)	7.2 (4.2–9.2)	10 (5.6–29)	7.4 (4.6–9.7)
Cachexia (n = 7)	5.5 (4.5–6.8)	7.5 (7.0–9.0)	6.9 (4.9–7.8)
Refractory (n = 2)	5.2 (4.8–5.4)	6.4 (6.0–6.8)	NA
Statistics	F: 2.3 p = 0.12	F: 1.2 p = 0.34	F: 1.2 p = 0.33

Data are given as median (minimum–maximum). Statistical analysis was carried out using the Mann–Whitney test and ANOVA test followed by Bonferroni's post-hoc test; p ≤ 0.05. F, ANOVA test value; Foxp3, forkhead box P3; n, number; SOCS1, suppressor of cytokine signaling 1; TAB2, TAK1-associated Binding Protein 2; U, Mann-Whitney; NSCL, non-small cell lung.
**Significant difference at p < 0.05.*
***Significant difference at p ≤ 0.01.*
****Significant difference at p ≤ 0.001.*

TABLE 6 | Correlation analysis between *miR-155* gene expression and SOCS1, TAB2, and Foxp3 in cachectic pancreatic or NSCL cancer patients (Spearman's correlation).

	miR-155 (FC)	SOCS1 (ng/ml)	TAB2 (ng/ml)
Cachectic pancreatic cancer patients			
miR-155 (FC)			
SOCS1 (ng/ml)	0.17 p = 0.3		
TAB2 (ng/ml)	0.002 p = 0.9	–0.17 p = 0.2	
Foxp3 (ng/ml)	0.1 p = 0.56	0.69 p = 0.001***	0.08 p = 0.4
Cachectic NSCL cancer patients			
miR-155 (FC)			
SOCS1 (ng/ml)	–0.3 p = 0.2		
TAB2 (ng/ml)	–0.4 p = 0.09	–0.2 p = 0.1	
Foxp3 (ng/ml)	–0.2 p = 0.3	–0.2 p = 0.6	0.08 p = 0.4

Data are given as r. Statistical analysis was carried out using Spearman's correlation analysis; p ≤ 0.05.
FC, fold change; Foxp3, forkhead box P3; miR-155*, microRNA-155; n, number;* r*, Spearman's correlation coefficient; SOCS1, suppressor of cytokine signaling 1; TAB2, TAK1-associated Binding Protein 2; NSCL, non-small cell lung.*
****Significant difference at p ≤ 0.001.*

of cachexia (35). The *TNF-α 308 G/A* polymorphisms is one of the most frequently related with risk of malnutrition and tumor aggressiveness (33). A study on Tunisian population demonstrated a positive association between the TNF-α (-308 G/A) polymorphism and breast cancer susceptibility (36). Results of the study of Ahmad et al. (37) among an Indian population, suggest that TNF-α-308G/A polymorphism showed significant association with breast cancer patients (37).

TABLE 7 | Expression level of miR-155, SOCS1, TAB2, and Foxp3 in cancer cachectic patients considering the cachexia severity, regardless of the cancer type.

Cachexia severity	*MiR-155* (FC)	SOCS1 (ng/ml)	TAB2 (ng/ml)	Foxp3 (ng/ml)
Pre-cachexia	46.2 (1.4–151)	5.8 (3.3–9.2)	10 (5.6–29)	6.3 (5.2–8.4)
Cachexia	431 (5.1–2348)	5.4 (4.2–8.6)	12 (7–25)	6.6 (4.8–8.4)
Refractory	2688 (16.5–7316)	5.8 (3.7–7.4)	16 (5.2–30)	6 (2.6–10)
Statistics	F: 29	F: 1.2	F: 0.2	F: 1.3
	p = 0.0001***	p = 0.3	p = 0.8	p = 0.3

Data are given as median (minimum–maximum). Statistical analysis was carried out using the ANOVA test followed by Bonferroni's post-hoc test; p ≤ 0.05.
F, ANOVA test value; FC, fold change; Foxp3, forkhead box P3; miR-155*, microRNA-155; SOCS1, suppressor of cytokine signaling 1; TAB2, TAK1-associated Binding Protein 2.*
****Significant difference at p ≤ 0.001.*

Our results show that the mutant *TNF-α* variant of *308 G/A* was significantly associated with increased risk of cachexia in both the pancreatic and NSCL cancer patients. On the contrary, that of 1031T/C was significantly associated with reduced risk of cachexia in the NSCL cancer patients. Notably, Barber et al. (38) have demonstrated that the A allele positivity in 308 gene loci confers approximately to a 3.0-fold increased susceptibility to malnutrition and cachexia in patients with end-stage renal disease (38), to consolidate the present data regarding *TNF-α 308G/A* gene polymorphism in both the pancreatic and NSCL cancer patients. Actually, the findings of the present study showed that the heterozygous GA genotype was detected in 55% of the lung cancer patients of the cachectic group, followed by the homozygous AA genotype (28%) with only 17% carrying the homozygous GG genotype. As for *TNF-α 308G/A* gene polymorphism in pancreatic cancer patients, the heterozygous GA genotype was frequently distributed (49%) in the cachectic group, whereas the wild homozygous GG genotype was frequently distributed (62%) among the non-cachectic group, and the homozygous AA genotype was more frequently distributed in cachectic (15%) than non-cachectic (5%) patients with pancreatic cancer.

Few data are available regarding the association of *TNF-α –1031T/C* genotype variant with cancer-related cachexia or inflammation. Nourian et al. (39), one of the recent studies, studying the role of genetics in Iranian patients with inflammatory bowel diseases (IBDs), reported that CC haplotype was associated with genetic risk of IBD (14). A previous study, however, found no association between the TNF-α polymorphisms at position −1031 and susceptibility to IBD (39). Moreover, in a study conducted on head and neck cancer patients, Powrózek et al. (35), investigating the potential role of *TNF-α 1031T/C* SNP as a risk factor for cachexia after radiotherapy, demonstrated that the C allele represents the unfavorable allele that is significantly associated with higher risk of cachexia, lower BMI, and shorter overall survival as compared with the TT or TC genotype carriers. Besides, the CC genotype carriers had a 9.7- to 13.2-fold higher risk of cachexia with the highest level of plasma TNF-α that directly reflects the alternation in patients' nutritional status due to the underlying inflammatory response (35). In alignment, our results revealed that in the NSCL cancer patients, the homozygous CC genotype of *TNF-α 1031T/C* constitutes 45% of the cachectic patients, 33% for the heterozygous TC, and 22% for the homozygous TT genotype, contrary to pancreatic cancer patients where the homozygous TT is the most frequent genotype constituting 63% of the cachectic patients, followed by the homozygous CC genotype constituting 20% of cachectic patients and 17% for the heterozygous TC.

Our finding on the frequency of genetic polymorphisms in Egyptian pancreatic and NSCL cancer patients reported herein does not match that of Africans, Latin Americans, Asians, or Europeans (**Table S3**). This supports previous reported data related to Egyptians and non-Egyptians (40–43). Indeed, previous studies also revealed such a discrepancy among Asian and non-Asian ethnicity regarding the TNF-308 G/A polymorphisms in hepatocellular carcinoma risk (12). This could be explained by different factors attributed to the unmatched ethnic population and different pathological nature of the disease.

Skeletal muscle metabolism plays a crucial role in the pathogenesis of cachexia in cancer patients (44), where *miRNAs* are abundantly expressed in skeletal muscles and are involved in cancer cachexia. Numerous *miRNAs* are known to modulate skeletal muscle and adipose tissue turnover; therefore, the potential of *miRNAs* as predictor biomarkers and their clinical relevance in cachexia have been previously suggested (45). Indeed, their aberrant expression is associated with impaired myogenesis, consequently promoting the development of cachexia (13, 46). *MiRNAs* are also involved in the pathogenesis of different diseases including cancers and autoimmune diseases (47). *MiR-155* gene was found to be overexpressed in several solid tumors, such as thyroid carcinoma as well as breast and colon cancer (21). Moreover, altered *miRNA* expression has been found in several types of lymphoma and leukemia (19), and their role in cancer-associated cachexia has been earlier documented (47). In the current study, the levels of *miR-155* were significantly higher in the cachectic groups as compared with the non-cachectic groups, which was in alignment with the cachexia severity in both the pancreatic and NSCL cancer patients. This is in accordance with the observations that higher expression of *miR-155* was significantly associated with cancer progression and accelerates the development of cachexia in breast cancer patients (32, 48, 49). Consistent with our results, Wu et al. (50) have demonstrated that tumor-originated exosomal *miR-155* promotes the differentiation and remodels the metabolism of adipocytes in breast cancer (50).

The findings of the present study show lower levels of SOCS1 and Foxp3 together with higher expression of *miR-155* in the cachectic patients of both pancreatic and NSCL cancers in contrast to non-cachectic patients. Of note, the oncogenic role

of *miR-155* in several cancer types has been previously addressed (51, 52). Regarding signaling pathway of *miR-155*, SOCS1 has been identified as a direct functional target of miR-155 (53) by enhancing TNF-α expression *via* SOCS1 suppression (54), hence elevating *TNF-α* cellular levels (55, 56). Therefore, these data delineate SOCS1 reduction in cachectic cancer patients in the present study.

Since *miRNAs* can often feedback to inhibit the transcription factor required for its induction (57), they might function as important epigenetic switches required for the functional maintenance of the cell type (58, 59). In this context, Foxp3, a transcription factor that is required for the maintenance of regulatory T cells (Treg), was shown to drive the high level of *miR-155* expression found in these cells to be followed by *miR-155*-mediated feedback inhibition of its target Foxp3 (58) *via* an *indirect* mechanism (60). This can afford a reasonable explanation for the low levels of Foxp3 with a high expression of *miRNA-155* in cachectic patients of the present study. Additionally, Foxp3 serum level indirectly correlates with cachexia severity only in the pancreatic cancer patients. Such an effect is in alignment with Gerriets et al. (61) who showed that conditions such as inflammation resulting from cachexia provide signals that increase glycolysis and expression of glucose transporter 1 (Glut1) levels in Treg. These metabolic changes directly modify Treg-cell function to downregulate the transcription factor Foxp3 (61). Moreover, there is a significant correlation among SOCS1 and Foxp3 protein in cachectic patients with pancreatic cancer. Similarly, the results of Collins et al. (62) results strongly suggest that SOCS1 contributes to the stability of the $Foxp3^+$ Treg peripheral population under conditions of strong pro-inflammatory environments (62).

Apart from SOCS1 and Foxp3 involved in the oncogenic inflammatory machinery, TAB2 is a signaling molecule downstream of TNF receptor-associated factor 6 (TRAF6) that activates MAPKs (63). Intriguingly, Ceppi et al. (64) supported that TAB2 is considered a direct protein target of *miRNA*s in TLR signaling pathway (64). On the contrary, our results showed no significant association between the TAB2 protein and the presence of higher serum levels of *miR-155* or cachexia in both cancer groups. Since SOCS1, Foxp3, and TAB2 are components of several other TLR signaling pathways, hence, once one TLR is triggered, *miRNA*-mediated targeting of common signaling proteins could silence signaling through multiple TLRs (54, 58).

The authors are aware that the study was conducted on small scale of population that represents the main limitation. Another limitation was the lack of non-treated groups; the current study was also not longitudinal, and it was therefore not possible to follow up the progression of cachexia in the patients. Despite these limitations, this case study shows that carriers of the A allele *308 G/A* gene and high *miR-155* are at greater risk of cachexia in both the pancreatic and NSCL cancer patients; however, the mutant variant of *1031T/C* gene is protective against cachexia in the NSCL cancer patients. Nonetheless, further studies should be carried out on the two *TNF-α* SNPs on larger scale of patients in order to confirm their predictive/prognostic significance. Finally, high levels of *miR-155* in the cachectic group lead to negative feedback inhibition of both SOCS1 and Foxp3 in both the pancreatic and NSCL cancer patients.

DATA AVAILABILITY STATEMENT

The datasets presented in this study can be found in online repositories. The names of the repository/repositories and accession number(s) can be found in the article/**Supplementary Material**.

ETHICS STATEMENT

The studies involving human participants were reviewed and approved by Research Ethics Committee of Faculty of Pharmacy, Cairo University (Cairo, Egypt; PT-2387) as well as the Ethical Committee of the Oncology department, Ain Shams University. The patients/participants provided their written informed consent to participate in this study.

AUTHOR CONTRIBUTIONS

RY and AS performed the research. SS, MS, and DA wrote the research. SS, MS, DA, and AS designed the research. RY, MS, SS, DA, and NS analyzed the data. All authors contributed to the article and approved the submitted version.

SUPPLEMENTARY MATERIAL

The Supplementary Material for this article can be found online at: https://www.frontiersin.org/articles/10.3389/fonc.2021.783231/full#supplementary-material

REFERENCES

1. Fearon K, Strasser F, Anker SD, Bosaeus I, Bruera E, Fainsinger RL, et al. Definition and Classification of Cancer Cachexia: An International Consensus. *Lancet Oncol* (2011) 12(5):489–95. doi: 10.1016/S1470-2045(10)70218-7
2. Daas SI, Rizeq BR, Nasrallah GK. Adipose Tissue Dysfunction in Cancer Cachexia. *J Cell Physiol* (2019) 234(1):13–22. doi: 10.1002/jcp.26811
3. Muscaritoli M, Anker SD, Argiles J, Aversa Z, Bauer JM, Biolo GI, et al. Consensus Definition of Sarcopenia, Cachexia and Pre-Cachexia: Joint Document Elaborated by Special Interest Groups (SIG) "Cachexia-Anorexia in Chronic Wasting Diseases" and "Nutrition in Geriatrics". *Clin Nutr* (2010) 29(2):154–9. doi: 10.1016/j.clnu.2009.12.004
4. Zalite IO, Zykus R, Gonzalez MF, Saygili F, Pukitis A, Gaujoux S, et al. Influence of Cachexia and Sarcopenia on Survival in Pancreatic Ductal Adenocarcinoma: A Systematic Review. *Pancreatology* (2015) 15(1):19–24. doi: 10.1016/j.pan.2014.11.006
5. Yamaguchi O, Kaira K, Hashimoto K, Mouri A, Miura Y, Shiono A, et al. Radiotherapy Is an Independent Prognostic Marker of Favorable Prognosis in Non-Small Cell Lung Cancer Patients After Treatment With the Immune

Checkpoint Inhibitor, Nivolumab. *Thorac Cancer* (2019) 10(4):992–1000. doi: 10.1111/1759-7714.13044
6. Johns N, Hatakeyama S, Stephens NA, Degen M, Degen S, Frieauff W, et al. Clinical Classification of Cancer Cachexia: Phenotypic Correlates in Human Skeletal Muscle. *PLoS One* (2014) 9(1):e83618. doi: 10.1371/journal.pone.0083618
7. Fearon KC, Glass DJ, Guttridge DC. Cancer Cachexia: Mediators, Signaling, and Metabolic Pathways. *Cell Metab* (2012) 16(2):153–66. doi: 10.1016/j.cmet.2012.06.011
8. Cruceriu D, Baldasici O, Balacescu O, Berindan-Neagoe I. The Dual Role of Tumor Necrosis Factor-Alpha (TNF-α) in Breast Cancer: Molecular Insights and Therapeutic Approaches. *Cell Oncol* (2020) 43(1):1–8. doi: 10.1007/s13402-019-00489-1
9. Duzova H, Duzova H. Skeletal Muscle, Myokines and Health. *Med Sci* (2012) 1(3):211–31. doi: 10.5455/medscience.2012.01.8023
10. Mondello P, Mian M, Aloisi C, Famà F, Mondello S, Pitini V. Cancer Cachexia Syndrome: Pathogenesis, Diagnosis, and New Therapeutic Options. *Nutr Cancer* (2015) 67(1):12–26. doi: 10.1080/01635581.2015.976318
11. Liu CJ, Wong YK, Chang KW, Chang HC, Liu HF, Lee YJ. Tumor Necrosis Factor-α Promoter Polymorphism Is Associated With Susceptibility to Oral Squamous Cell Carcinoma. *J Oral Pathol Med* (2005) 34(10):608–12. doi: 10.1111/j.1600-0714.2005.00359.x
12. Hu Q, Lou GG, Liu YC, Qian L, Lv BD. The Tumor Necrosis Factor-α-308 and-238 Polymorphisms and Risk of Hepatocellular Carcinoma for Asian Populations: A Meta-Analysis. *Curr Ther Res* (2014) 76:70–5. doi: 10.1016/j.curtheres.2014.04.001
13. Johns N, Stretch C, Tan BH, Solheim TS, Sørhaug S, Stephens NA, et al. New Genetic Signatures Associated With Cancer Cachexia as Defined by Low Skeletal Muscle Index and Weight Loss. *J Cachexia Sarcopenia Muscle* (2017) 8(1):122–30. doi: 10.1002/jcsm.12138
14. Nourian M, Chaleshi V, Pishkar L, Azimzadeh P, Baradaran Ghavami S, Balaii H, et al. Evaluation of Tumor Necrosis Factor (TNF)-α mRNA Expression Level and the Rs1799964 Polymorphism of the TNF-α Gene in Peripheral Mononuclear Cells of Patients With Inflammatory Bowel Diseases. *Biomed Rep* (2017) 6(6):698–702. doi: 10.3892/br.2017.908
15. Okugawa Y, Toiyama Y, Hur K, Yamamoto A, Yin C, Ide S, et al. Circulating miR-203 Derived From Metastatic Tissues Promotes Myopenia in Colorectal Cancer Patients. *J Cachexia Sarcopenia Muscle* (2019) 10(3):536–48. doi: 10.1002/jcsm.12403
16. Kasinski AL, Slack FJ. MicroRNAs En Route to the Clinic: Progress in Validating and Targeting microRNAs for Cancer Therapy. *Nat Rev Cancer* (2011) 11(12):849–64. doi: 10.1038/nrc3166
17. Roberts TC. The microRNA Biology of the Mammalian Nucleus. *Mol Ther Nucleic Acids* (2014) 3:e188. doi: 10.1038/mtna.2014.40
18. Singh SK, Pal Bhadra M, Girschick HJ, Bhadra U. MicroRNAs–micro in Size But Macro in Function. *FEBS J* (2008) 275(20):4929–44. doi: 10.1111/j.1742-4658.2008.06624.x
19. Calin GA, Liu CG, Sevignani C, Ferracin M, Felli N, Dumitru CD, et al. MicroRNA Profiling Reveals Distinct Signatures in B Cell Chronic Lymphocytic Leukemias. *Proc Natl Acad Sci* (2004) 101(32):11755–60. doi: 10.1073/pnas.0404432101
20. Esquela-Kerscher A, Slack FJ. Oncomirs—microRNAs With a Role in Cancer. *Nat Rev Cancer* (2006) 6(4):259–69. doi: 10.1038/nrc1840
21. Lu J, Getz G, Miska EA, Alvarez-Saavedra E, Lamb J, Peck D, et al. MicroRNA Expression Profiles Classify Human Cancers. *Nature* (2005) 435(7043):834–8. doi: 10.1038/nature03702
22. Volinia S, Calin GA, Liu CG, Ambs S, Cimmino A, Petrocca F, et al. A microRNA Expression Signature of Human Solid Tumors Defines Cancer Gene Targets. *Proc Natl Acad Sci* (2006) 103(7):2257–61. doi: 10.1073/pnas.0510565103
23. Mubaid S, Ma JF, Omer A, Ashour K, Lian XJ, Sanchez BJ, et al. HuR Counteracts miR-330 to Promote STAT3 Translation During Inflammation-Induced Muscle Wasting. *Proc Natl Acad Sci* (2019) 116(35):17261–70. doi: 10.1073/pnas.1905172116
24. Wu Q, Sun S, Li Z, Yang Q, Li B, Zhu S, et al. Tumour-Originated Exosomal miR-155 Triggers Cancer-Associated Cachexia to Promote Tumour Progression. *Mol Cancer* (2018) 17(1):1–7. doi: 10.1186/s12943-018-0899-5
25. Jiang S, Zhang HW, Lu MH, He XH, Li Y, Gu H, et al. MicroRNA-155 Functions as an OncomiR in Breast Cancer by Targeting the Suppressor of Cytokine Signaling 1 Gene. *Cancer Res* (2010) 70(8):3119–27. doi: 10.1158/0008-5472.CAN-09-4250
26. Ghafouri-Fard S, Oskooei VK, Azari I, Taheri M. Suppressor of Cytokine Signaling (SOCS) Genes Are Downregulated in Breast Cancer. *World J Surg Oncol* (2018) 16(1):1–9. doi: 10.1186/s12957-018-1529-9
27. Kim CH. FOXP3 and Its Role in the Immune System. *Forkhead Transcription Factors* (2009) 17–29. doi: 10.1007/978-1-4419-1599-3_2
28. Wang X, Lang M, Zhao T, Feng X, Zheng C, Huang C, et al. Cancer-FOXP3 Directly Activated CCL5 to Recruit FOXP3+ Treg Cells in Pancreatic Ductal Adenocarcinoma. *Oncogene* (2017) 36(21):3048–58. doi: 10.1038/onc.2016.458
29. Cai PC, Shi L, Liu VW, Tang HW, Liu IJ, Leung TH, et al. Elevated TAK1 Augments Tumor Growth and Metastatic Capacities of Ovarian Cancer Cells Through Activation of NF-κb Signaling. *Oncotarget* (2014) 5(17):7549.
30. Argilés JM, Betancourt A, Guàrdia-Olmos J, Peró-Cebollero M, López-Soriano FJ, Madeddu C, et al. Validation of the CAchexia SCOre (CASCO). Staging Cancer Patients: The Use of miniCASCO as a Simplified Tool. *Front Physiol* (2017) 8:92.
31. Liu C, Wang Y, Song H, Li Q, Zhang Y, Chen P, et al. Genetic Association of Interleukin-31 Gene Polymorphisms With Epithelial Ovarian Cancer in Chinese Population. *Dis Marker* (2018) 2018:3503858.
32. Argilés JM, Busquets S, Stemmler B, López-Soriano FJ. Cancer Cachexia: Understanding the Molecular Basis. *Nat Rev Cancer* (2014) 14(11):754–62. doi: 10.1038/nrc3829
33. Baracos VE, Martin L, Korc M, Guttridge DC, Fearon KC. Cancer-Associated Cachexia. *Nat Rev Dis Primers* (2018) 4(1):1–8. doi: 10.1038/nrdp.2017.105
34. Tan BH, Ross JA, Kaasa S, Skorpen F, Fearon KC. European Palliative Care Research Collaborative. Identification of Possible Genetic Polymorphisms Involved in Cancer Cachexia: A Systematic Review. *J Genet* (2011) 90(1):165–77.
35. Powrózek T, Mlak R, Brzozowska A, Mazurek M, Gołębiowski P, Małecka-Massalska T. Relationship Between TNF-α– 1031t/C Gene Polymorphism, Plasma Level of TNF-α, and Risk of Cachexia in Head and Neck Cancer Patients. *J Cancer Res Clin Oncol* (2018) 144(8):1423–34. doi: 10.1007/s00432-018-2679-4
36. Chouchane L, Ahmed SB, Baccouche S, Remadi S. Polymorphism in the Tumor Necrosis Factor-α Promotor Region and in the Heat Shock Protein 70 Genes Associated With Malignant Tumors. *Cancer* (1997) 80(8):1489–96. doi: 10.1002/(SICI)1097-0142(19971015)80:8<1489::AID-CNCR17>3.0.CO;2-1
37. Ahmad MM, Farah Parveen NA, Siddiqui JA, Shukla NK, Husain SA. Genetic Polymorphism in TNF-α-308 G/a and TNF-β+ 252 a/G, as Prognostic Biomarker in Breast Cancer Patients Among Indian Population. *Asian Pac J Cancer Prev* (2020) 21(2):301. doi: 10.31557/APJCP.2020.21.2.301
38. Barber RC, Aragaki CC, Rivera-Chavez FA, Purdue GF, Hunt JL, Horton JW. TLR4 and TNF-α Polymorphisms Are Associated With an Increased Risk for Severe Sepsis Following Burn Injury. *J Med Genet* (2004) 41(11):808–13. doi: 10.1136/jmg.2004.021600
39. Nourian M, Asgharian AM, Asadzadeh Aghdaei H. Lack of Association Between Tumor Necrosis Factor Alpha (Tnfα) Gene-1031C/T Polymorphisms and Susceptibility to Inflammatory Bowel Disease (IBD). *Arak Univ Med Sci J* (2016) 19:71–9.
40. Özçelik T, Kanaan M, Avraham KB, Yannoukakos D, Mégarbané A, Tadmouri GO, et al. Collaborative Genomics for Human Health and Cooperation in the Mediterranean Region. *Nat Genet* (2010) 42(8):641–5.
41. Shahin MH, Khalifa SI, Gong Y, Hammad LN, Sallam MT, El Shafey M, et al. Genetic and Nongenetic Factors Associated With Warfarin Dose Requirements in Egyptian Patients. *Pharmacogenet Genomics* (2011) 21(3):130.
42. Khalil BM, Shahin MH, Solayman MH, Langaee T, Schaalan MF, Gong Y, et al. Genetic and Nongenetic Factors Affecting Clopidogrel Response in the Egyptian Population. *Clin Transl Sci* (2016) 9(1):23–8. doi: 10.1111/cts.12383
43. Sarhan NM, Shahin MH, El Rouby NM, El-Wakeel LM, Solayman MH, Langaee T, et al. Effect of Genetic and Nongenetic Factors on the Clinical Response to Mineralocorticoid Receptor Antagonist Therapy in Egyptians With Heart Failure. *Clin Transl Sci* (2020) 13(1):195–203. doi: 10.1111/cts.12702
44. Petruzzelli M, Wagner EF. Mechanisms of Metabolic Dysfunction in Cancer-Associated Cachexia. *Genes Dev* (2016) 30(5):489–501. doi: 10.1101/gad.276733.115

45. Singh GB, Cowan DB, Wang DZ. Tiny Regulators of Massive Tissue: microRNAs in Skeletal Muscle Development, Myopathies, and Cancer Cachexia. *Front Oncol* (2020) 10:2647. doi: 10.3389/fonc.2020.598964
46. Santos JM, Peixoto da Silva S, Gil da Costa RM, Medeiros R. The Emerging Role of microRNAs and Other Non-Coding RNAs in Cancer Cachexia. *Cancers* (2020) 12(4):1004.
47. Donzelli S, Farneti A, Marucci L, Ganci F, Sacconi A, Strano S, et al. Non-Coding RNAs as Putative Biomarkers of Cancer-Associated Cachexia. *Front Cell Dev Biol* (2020) 8:257. doi: 10.3389/fcell.2020.00257
48. Biswas AK, Acharyya S. Cancer-Associated Cachexia: A Systemic Consequence of Cancer Progression. *Annu Rev Cancer Biol* (2020) 4:391–411. doi: 10.1146/annurev-cancerbio-030419-033642
49. Naito T. Emerging Treatment Options for Cancer-Associated Cachexia: A Literature Review. *Ther Clin Risk Manage* (2019) 15:1253. doi: 10.2147/TCRM.S196802
50. Wu Q, Sun S, Li Z, Yang Q, Li B, Zhu S, et al. Breast Cancer-Released Exosomes Trigger Cancer-Associated Cachexia to Promote Tumor Progression. *Adipocyte* (2019) 8(1):31–45.
51. Merkel O, Hamacher F, Griessl R, Grabner L, Schiefer AI, Prutsch N, et al. Oncogenic Role of miR-155 in Anaplastic Large Cell Lymphoma Lacking the T (2; 5) Translocation. *J Pathol* (2015) 236(4):445–56. doi: 10.1002/path.4539
52. Mattiske S, Suetani RJ, Neilsen PM, Callen DF. The Oncogenic Role of miR-155 in Breast Cancer. *Cancer Epidemiol Prev Biomarkers* (2012) 21(8):1236–43. doi: 10.1158/1055-9965.EPI-12-0173
53. Huffaker TB, O'Connell RM. miR-155-SOCS1 as a Functional Axis: Satisfying the Burden of Proof. *Immunity* (2015) 43(1):3–4. doi: 10.1016/j.immuni.2015.06.020
54. Wang P, Hou J, Lin L, Wang C, Liu X, Li D, et al. Inducible microRNA-155 Feedback Promotes Type I IFN Signaling in Antiviral Innate Immunity by Targeting Suppressor of Cytokine Signaling 1. *J Immunol* (2010) 185 (10):6226–33. doi: 10.4049/jimmunol.1000491
55. Tili E, Michaille JJ, Cimino A, Costinean S, Dumitru CD, Adair B, et al. Modulation of miR-155 and miR-125b Levels Following Lipopolysaccharide/TNF-α Stimulation and Their Possible Roles in Regulating the Response to Endotoxin Shock. *J Immunol* (2007) 179(8):5082–9. doi: 10.4049/jimmunol.179.8.5082
56. Tili E, Michaille JJ, Wernicke D, Alder H, Costinean S, Volinia S, et al. Mutator Activity Induced by microRNA-155 (miR-155) Links Inflammation and Cancer. *Proc Natl Acad Sci* (2011) 108(12):4908–13. doi: 10.1073/pnas.1101795108
57. Martinez NJ, Walhout AJ. The Interplay Between Transcription Factors and microRNAs in Genome-Scale Regulatory Networks. *Bioessays* (2009) 31 (4):435–45. doi: 10.1002/bies.200800212
58. Kohlhaas S, Garden OA, Scudamore C, Turner M, Okkenhaug K, Vigorito E. Cutting Edge: The Foxp3 Target miR-155 Contributes to the Development of Regulatory T Cells. *J Immunol* (2009) 182(5):2578–82. doi: 10.4049/jimmunol.0803162
59. Iliopoulos D, Jaeger SA, Hirsch HA, Bulyk ML, Struhl K. STAT3 Activation of miR-21 and miR-181b-1 *via* PTEN and CYLD Are Part of the Epigenetic Switch Linking Inflammation to Cancer. *Mol Cell* (2010) 39(4):493–506. doi: 10.1016/j.molcel.2010.07.023
60. Gao S, Wang Y, Wang M, Li Z, Zhao Z, Wang RX, et al. MicroRNA-155, Induced by FOXP3 Through Transcriptional Repression of BRCA1, Is Associated With Tumor Initiation in Human Breast Cancer. *Oncotarget* (2017) 8(25):41451. doi: 10.18632/oncotarget.17816
61. Gerriets VA, Kishton RJ, Johnson MO, Cohen S, Siska PJ, Nichols AG, et al. Foxp3 and Toll-Like Receptor Signaling Balance T Reg Cell Anabolic Metabolism for Suppression. *Nat Immunol* (2016) 17(12):1459–66. doi: 10.1038/ni.3577
62. Collins EL, Jager LD, Dabelic R, Benitez P, Holdstein K, Lau K, et al. Inhibition of SOCS1–/– Lethal Autoinflammatory Disease Correlated to Enhanced Peripheral Foxp3+ Regulatory T Cell Homeostasis. *J Immunol* (2011) 187 (5):2666–76. doi: 10.4049/jimmunol.1003819
63. Takaesu G, Kishida S, Hiyama A, Yamaguchi K, Shibuya H, Irie K, et al. TAB2, a Novel Adaptor Protein, Mediates Activation of TAK1 MAPKKK by Linking TAK1 to TRAF6 in the IL-1 Signal Transduction Pathway. *Mol Cell* (2000) 5 (4):649–58. doi: 10.1016/S1097-2765(00)80244-0
64. Ceppi M, Pereira PM, Dunand-Sauthier I, Barras E, Reith W, Santos MA, et al. MicroRNA-155 Modulates the Interleukin-1 Signaling Pathway in Activated Human Monocyte-Derived Dendritic Cells. *Proc Natl Acad Sci* (2009) 106 (8):2735–40. doi: 10.1073/pnas.0811073106

Conflict of Interest: The authors declare that the research was conducted in the absence of any commercial or financial relationships that could be construed as a potential conflict of interest. The handling editor declared a shared affiliation with several of the authors AS and SS at time of review.

Publisher's Note: All claims expressed in this article are solely those of the authors and do not necessarily represent those of their affiliated organizations, or those of the publisher, the editors and the reviewers. Any product that may be evaluated in this article, or claim that may be made by its manufacturer, is not guaranteed or endorsed by the publisher.

frontiers in Oncology

ORIGINAL RESEARCH
published: 09 December 2021
doi: 10.3389/fonc.2021.770022

EUS-FNA Biopsies to Guide Precision Medicine in Pancreatic Cancer: Results of a Pilot Study to Identify *KRAS* Wild-Type Tumours for Targeted Therapy

*Joanne Lundy[1,2,3], Marion Harris[4], John Zalcberg[5,6], Allan Zimet[7], David Goldstein[8,9], Val Gebski[10], Adina Borsaru[11], Christopher Desmond[12], Michael Swan[12], Brendan J. Jenkins[1,2] and Daniel Croagh[1,3,13]**

[1] Centre for Innate Immunity and Infectious Diseases, Hudson Institute of Medical Research, Clayton, VIC, Australia, [2] Department of Molecular and Translational Science, Faculty of Medicine, Nursing and Health Sciences, Monash University, Clayton, VIC, Australia, [3] Department of Surgery, Faculty of Medicine, Nursing and Health Sciences, Monash University, Clayton, VIC, Australia, [4] Department of Oncology, Faculty of Medicine, Nursing and Health Sciences and School of Clinical Sciences, Monash University, Clayton, VIC, Australia, [5] Department of Medical Oncology, Alfred Health, Melbourne, VIC, Australia, [6] Public Health and Preventative Medicine, Monash University, Melbourne, VIC, Australia, [7] Department of Medical Oncology, Epworth Hospital, Melbourne, VIC, Australia, [8] Prince of Wales Clinical School, University of New South Wales, Sydney, NSW, Australia, [9] Department of Medical Oncology, Prince of Wales Hospital, Randwick, NSW, Australia, [10] National Health and Medical Research Council Clinical Trials Centre, University of Sydney, Camperdown, NSW, Australia, [11] Diagnostic Imaging, Monash Health, Melbourne, VIC, Australia, [12] Department of Gastroenterology, Monash Health, Melbourne, VIC, Australia, [13] Department of Surgery, Epworth Healthcare, Melbourne, VIC, Australia

OPEN ACCESS

Edited by:
Sumit Sahni,
Royal North Shore Hospital, Australia

Reviewed by:
Emily K. Colvin,
The University of Sydney, Australia
Aditi Jain,
Thomas Jefferson University, United States

***Correspondence:**
Daniel Croagh
Daniel.Croagh@monashhealth.org

Specialty section:
This article was submitted to Gastrointestinal Cancers: Hepato Pancreatic Biliary Cancers, a section of the journal Frontiers in Oncology

Received: 03 September 2021
Accepted: 18 November 2021
Published: 09 December 2021

Citation:
Lundy J, Harris M, Zalcberg J, Zimet A, Goldstein D, Gebski V, Borsaru A, Desmond C, Swan M, Jenkins BJ and Croagh D (2021) EUS-FNA Biopsies to Guide Precision Medicine in Pancreatic Cancer: Results of a Pilot Study to Identify KRAS Wild-Type Tumours for Targeted Therapy. Front. Oncol. 11:770022. doi: 10.3389/fonc.2021.770022

Background: Pancreatic ductal adenocarcinoma (PDAC) is a leading cause of cancer death and lacks effective treatment options. Diagnostic endoscopic ultrasound-guided fine-needle aspiration (EUS-FNA) biopsies represent an appealing source of material for molecular analysis to inform targeted therapy, as they are often the only available tissue for patients presenting with PDAC irrespective of disease stage. However, EUS-FNA biopsies are typically not used to screen for precision medicine studies due to concerns about low tissue yield and quality. Epidermal growth factor receptor (EGFR) inhibition has shown promise in clinical trials of unselected patients with advanced pancreatic cancer, but has not been prospectively tested in *KRAS* wild-type patients. Here, we examine the clinical utility of EUS-FNA biopsies for molecular screening of *KRAS* wild-type PDAC patients for targeted anti-EGFR therapy to assess the feasibility of this approach.

Patients and Methods: Fresh frozen EUS-FNA or surgical biopsies from PDAC patient tumours were used to screen for *KRAS* mutations. Eligible patients with recurrent, locally advanced, or metastatic *KRAS* wild-type status who had received at least one prior line of chemotherapy were enrolled in a pilot study (ACTRN12617000540314) and treated with panitumumab at 6mg/kg intravenously every 2 weeks until progression or unacceptable toxicity. The primary endpoint was 4-month progression-free survival (PFS).

Results: 275 patient biopsies were screened for *KRAS* mutations, which were detected in 88.3% of patient samples. 8 eligible *KRAS* wild-type patients were enrolled onto the interventional study between November 2017 and December 2020 and treated with panitumumab. 4-month PFS was 14.3% with no objective tumour responses observed. The only grade 3/4 treatment related toxicity observed was hypomagnesaemia.

Conclusions: This study demonstrates proof-of-principle feasibility to molecularly screen patients with pancreatic cancer for targeted therapies, and confirms diagnostic EUS-FNA biopsies as a reliable source of tumour material for molecular analysis. Single agent panitumumab was safe and tolerable but led to no objective tumour responses in this population.

Keywords: pancreatic cancer, endoscopic ultrasound, *KRAS*, molecular analysis, precision medicine

INTRODUCTION

Pancreatic ductal adenocarcinoma (PDAC) ranks as the seventh most lethal cancer worldwide but has been predicted to become the second leading cause of cancer death by 2030 (1, 2). Most patients present with advanced disease, and only 15-20% of tumours are amenable to surgery (3). While the incidence of PDAC continues to steadily increase, the prognosis remains extremely poor with a 5-year survival rate of just 10% (4). For the majority of patients who have unresectable or metastatic disease at diagnosis, treatment options are limited, and median survival is just 6-12 months (5).

Gemcitabine plus nab-paclitaxel and FOLFIRINOX are well established as the first line chemotherapy regimens of choice in patients with advanced PDAC with a good performance status, leading to median survival times of 9-11 months (6, 7). However, recommendations for treatment beyond first line therapy are limited by only a select few phase III clinical trials demonstrating clinical benefit in this setting, and limited head-to-head comparisons using current standards of care (8, 9).

Given the modest effect of chemotherapy in unselected PDAC patients, the prospect of applying precision therapy based on molecular profiling holds great appeal. Unfortunately, clinical trials of targeted therapies in PDAC to date have proved challenging, due to both patient factors (e.g. poor performance status, propensity to rapid clinical deterioration) and practical factors (e.g. poor quality biopsy specimens, delays in processing tissue for molecular analysis, and reliance on surgical biopsies which are not available in the majority of patients) (10, 11). A 2011 review in the US estimated that only 4.5% of patients with PDAC enrolled onto a clinical trial in that year, and identified poor study design, inadequate recruitment, lack of access to suitable trials, and patient factors impeding eligibility to clinical trials as potential barriers to inclusion (12). However, clinical benefit can be demonstrated if actionable molecular alterations are identified and treated with appropriate therapies, such as poly ADP ribose polymerase (PARP) inhibitors for *BRCA* mutant tumours (13).

To overcome the challenges of profiling the molecular and genomic landscape of PDAC in patients from all tumour stages (i.e. I-IV), we have demonstrated the feasibility of endoscopic ultrasound-guided fine needle aspiration (EUS-FNA) biopsy, a common diagnostic procedure, as a reliable source of tissue for genetic profiling (e.g. *KRAS* mutation analysis) (14–16). EUS-FNA using 19 to 25-guage needles is a long-established technique in the diagnosis and staging of pancreatic tumours, and a number of studies have investigated technical aspects to improve the diagnostic performance of the procedure (17, 18). The first generation of FNA biopsy needles provide aspirates of suspicious lesions but often yield lowly cellular specimens lacking in architectural tissue structure, which may be critical for diagnosis as well as for the increasingly desired immunohistochemical and genomic analysis of pancreatic tumours (19, 20). However, newer generation needles allow for larger tissue cores, and have been demonstrated to require fewer needle passes to establish a diagnosis (21, 22). This yields higher volume biopsies with less blood contamination than standard FNA biopsies (23), paving the way for EUS-derived biopsies to play a larger role in molecular profiling in PDAC.

PDAC is typified by significant molecular heterogeneity, and most "actionable" phenotypes such as microsatellite instability, high tumour mutation burden, *BRCA* mutations and *NTRK* fusions occur at a low frequency (24, 25). By contrast, activating mutations of the *KRAS* proto-oncogene can be identified in approximately 80-90% of PDAC patient tumours (24–28). This gene is the focus of ongoing interest as a molecular target for therapy, and although early trials targeting mutant *KRAS* failed to demonstrate any significant survival benefit (29, 30), novel inhibitors are showing more promise in ongoing studies (31).

Epidermal growth factor receptor (EGFR) inhibition has proven to be an effective therapy in *KRAS* wild-type patients with advanced colorectal cancer (32–34). In unselected PDAC patients, the addition of the EGFR inhibitor erlotinib to gemcitabine demonstrated a statistically significant, albeit small improvement in median overall survival (mOS) of 6.3 vs 5.9 months compared to gemcitabine alone (35). However, this finding did not significantly change clinical practice based on minimal benefit and additional toxicity in the erlotinib arm (35). Further studies have reported mixed results using EGFR inhibition in PDAC, albeit largely either without stratification for *KRAS* status, or with *post-hoc* analyses only (35–39). Panitumumab is a recombinant human IgG2 monoclonal antibody that binds specifically to EGFR and has demonstrated

clinical efficacy in colorectal cancer (33). In PDAC, a small phase II study with panitumumab, erlotinib and gemcitabine reported a non-significant increase in overall survival in the first line setting when compared to gemcitabine and Erlotinib for PDAC patients who were not selected by *KRAS* status; however, this combination was associated with significant toxicity and limited by the inclusion of a control arm which is no longer considered the standard of care (40).

Here, we aim to demonstrate that standard-of-care diagnostic biopsies sourced from a large PDAC biobank could be used for timely and accurate assessment of *KRAS* mutation status. Specifically, we identified 8 PDAC patients for enrollment onto a pilot study on the efficacy and tolerability of single agent panitumumab for patients with advanced, *KRAS* wild-type PDAC with progressive disease following first line chemotherapy. To the best of our knowledge, this is one of the first prospective biomarker selected studies to date in PDAC.

PATIENTS AND METHODS

Overall Study Design and Ethics Oversight

This study was designed to verify the clinical utility of EUS-FNA biopsies for molecular screening for targeted therapy, and included an exploratory pilot study of single agent panitumumab in patients with *KRAS* wild-type pancreatic cancer. The overall study aims were:

i. To show that treatment selection *via* genomic sequencing is feasible in a typical clinical setting.
ii. To prospectively identify the prevalence of *KRAS* mutations in patients with locally advanced or metastatic pancreatic adenocarcinoma using standard clinical pathology assays.
iii. To obtain preliminary data on the efficacy of panitumumab in patients with *KRAS* wild-type tumours.

The study was conducted in accordance with the principles of the Declaration of Helsinki. It was approved by the Human Research Ethics Committee at Monash Health (reference number 16-0000-584A) and prospectively registered on the Australian New Zealand Clinical Trials Registry (ACTRN12617000540314). Informed, signed written consent was obtained from all patients prior to initiating study procedures. The study schema is shown in **Figure 1**.

EUS-FNA Biopsies

In addition to the standard diagnostic EUS-FNA biopsy (typically 2-4 needle passes), an additional 1-2 needle passes were employed to obtain tissue for biobanking in the Victorian Pancreatic Cancer Biobank (VPCB; Monash Health HREC reference 15450A). EUS-FNA procedures were carried out in accordance with routine local protocols and needle selection, number of biopsies taken, and suction techniques were at the discretion of each individual physician. The needle type utilised in each case was not recorded as part of this study, but the standard-of-care during the majority of the collection period for

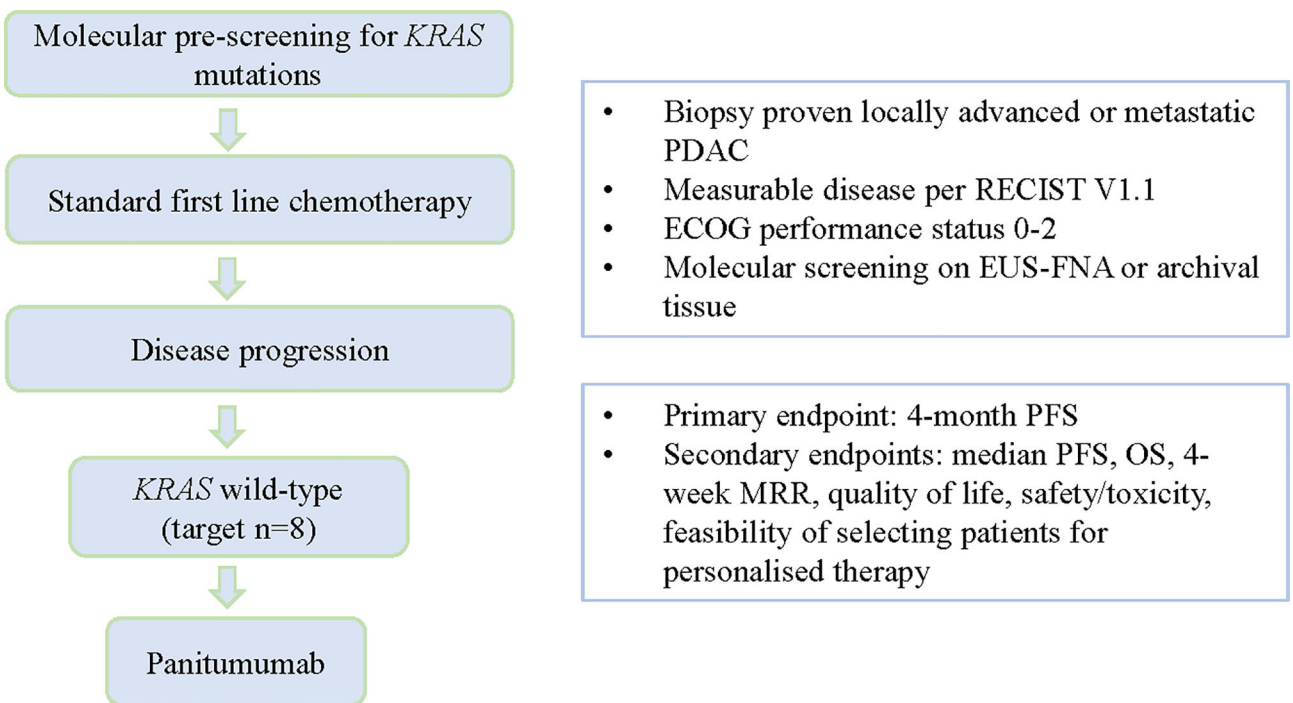

FIGURE 1 | Study schema including key eligibility and response criteria.

this study were the 20 or 22-guage ProCore® Fine Needle Biopsy needles with 10ml negative pressure suction.

KRAS Screening

KRAS mutation analysis was performed in the Genetics and Molecular Pathology Department at Monash Health, using the clinically validated *KRAS* StripAssay™ (ViennaLab Diagnostics) in accordance with manufacturer protocols and standard clinical practice. Where possible, DNA was extracted from fresh frozen EUS-FNA biopsies sourced from the multi-centre VPCB using the AllPrep DNA/RNA Universal Kit (Qiagen), although archival formalin-fixed paraffin embedded (FFPE) tissue was used where fresh frozen biopsy tissue was not available. The isolation of gDNA from FFPE tissue was performed on 5 x 10 micron-thick sections using the ReliaPrep FFPE gDNA Miniprep System (Promega). Prospective tissue testing on diagnostic biopsies was preferred, although archival or previously stored specimens from the VPCB could be used where fresh tissue was not feasible or available. DNA samples were quantified using the Qubit Fluorometer (Life Technologies) and quality assessed by TapeStation (Agilent Technologies). At the time of consent to sample collection for the VPCB, patients could elect for their treating physician to be contacted in the event of a significant genomic finding. *KRAS* wild-type results were notified to treating physicians who were able to offer referral for screening for the study if they deemed it clinically appropriate.

Panitumumab Pilot Study

Patient Selection

Patients were eligible if aged 18 and over, with pathologically-proven unresectable, recurrent or metastatic *KRAS* wild-type PDAC (note that patients with pancreaticobiliary type ampullary tumours may be considered on an individual basis, provided they met all other inclusion criteria); ECOG performance status of 0-2, measurable disease as per RECIST v1.1 criteria; progressive disease following at least one line of chemotherapy (defined as either clear progressive disease on standard CT scans or an increase of CA 19.9 of 30% confirmed on 2 blood draws) or within 12 months of adjuvant chemotherapy; adequate bone marrow function (ANC ≥1500/mcL, platelets ≥100 000/mcL, haemoglobin ≥9g/dL); adequate renal function (CrCl > 50ml/min (Cockcroft-Gault formula) or Creatinine <1.5 XULN); and adequate hepatic function (serum total bilirubin ≤ 1.5 times ULN, ALT/AST ≤ 2.5 times ULN [or ≤ 5 times ULN with documented liver metastases], ALP ≤ 5 times ULN, and INR ≤ 1.5). Exclusion criteria included pregnancy or lactation; active or uncontrolled infection; previous treatment with EGFR inhibitor; previous radiotherapy to the pancreas if the only site of measurable disease (unless there was demonstrated, clear evidence of radiological progression at the site since the completion of radiotherapy); hypersensitivity to study drug; previous or current interstitial lung disease or pulmonary fibrosis; history of another malignancy within 2 years prior to allocation (with the exception of adequately treated carcinoma *in-situ*; curatively treated uterine cervix carcinoma *in-situ* or non-melanoma skin carcinoma or superficial transitional cell carcinoma of the bladder); or any severe or uncontrolled medical conditions within 3 months prior to allocation.

Study Assessments

Screening procedures and study allocation was independently verified by the principal investigator prior to commencement of study therapy. History, physical examination, assessment of adverse events using NCI CTCAE version 4.0, assessment of ECOG performance status, and routine bloods (FBE, EUC, Ca/Mg/phosphate, LFTs and CA 19.9) were performed at screening and before each treatment with panitumumab. Quality of life was assessed at baseline, week 4, week 16 and at the end of study using the EORTC QLQ-C30 version 3.0 questionnaire, with scores calculated using the EORTC QLC-30 Scoring Manual (41). Serum was collected and stored for assessment of circulating tumour DNA (ctDNA) at baseline, 4 and 8 weeks. An FDG-PET scan was performed at baseline and week 4 to assess for early metabolic response, and to identify patients progressing rapidly for whom alternative treatments should be considered. CT or MRI scans of the chest, abdomen, and pelvis were performed every 8 weeks while on treatment and evaluated for tumour response according to RECIST criteria version 1.1. Treatment was stopped if there was evidence of progressive disease, or at any time according to the discretion of the treating clinician and patient. A 30-day safety assessment was performed at the end of treatment.

Treatment

Panitumumab was supplied by Amgen Australia and administered at a standard dose of 6mg/kg by intravenous infusion every 2 weeks. Patients received up to 8 cycles, with the option to continue at the treating physician's discretion if there was evidence of clinical response. Premedication and supportive care were provided in accordance with local institution protocols, with prophylactic antibiotic therapy strongly recommended to reduce the incidence and severity of rash.

Statistical Considerations

This trial was designed as a pilot phase II study, aiming to screen 200 patients to identify the initial cohort of *KRAS* wild-type patients, anticipating a *KRAS* mutation rate of 80-90% and recognizing that some patients would not meet eligibility criteria for the interventional study on the basis of other clinical factors (e.g. poor performance status, inadequate laboratory parameters, clinical decline or death prior to initiation of second line therapy). We deemed that a 50% progression-free survival (PFS) rate at 4 months was considered worthwhile to demonstrate activity of panitumumab, and we planned to enroll 8 patients prior to conducting an assessment to rule out futility (defined as all 8 patients progressing within 4 months, and no metabolic responses seen). In the absence of meeting these criteria, a decision could be made to continue the study and recruit a further 11 patients in a stepwise fashion, guided by the strength of the PFS at 4 months.

The original study design included an observation arm for patients with *KRAS* mutant PDAC receiving physician's choice standard second line chemotherapy. However, the protocol was

amended early in the study to remove this arm due to poor recruitment and lack of perceived benefit of this arm given the small sample size. No patients were recruited onto the initially planned observation cohort prior to the decision to remove this arm.

Study Endpoints

The primary endpoint of the interventional study was PFS at 4 months, with secondary endpoints including 4-week metabolic response rate (MMR; defined as a 30% reduction in SUV max on FDG-PET imaging and/or a 30% reduction in CA19.9 if the FDG-PET scan was not abnormal at baseline and the CA19.9 level was elevated >50% above ULN at baseline); PFS and objective tumour response rate (OTRR) at 6 months; feasibility of selecting patients for personalised therapy; median PFS; median overall survival (OS); safety/toxicity; and quality of life. Exploratory endpoints included measurement of ctDNA at baseline and during therapy.

Monitoring

A trial management committee including study investigators and a statistician was appointed to oversee study planning, monitoring, progress, reviews, and internal audits.

RESULTS

KRAS Screening

We screened 275 PDAC patient tumour biopsies for the presence of *KRAS* mutations. One fresh frozen EUS-FNA and one FFPE biopsy (0.7%) were deemed inadequate for testing due to poor DNA yield, but all 273 other specimens passed quality control testing. The results of the *KRAS* screening are outlined in **Figure 2**. As anticipated based on existing literature (24–28), *KRAS* was detected in 88.3% (241/273) of tumour biopsies, with 32 samples (11.7%) being wild-type. Frozen FNA, frozen surgical biopsies and FFPE-derived surgical biopsy tissues all demonstrated high frequencies of *KRAS* mutation (88.8%, 93.5% and 89.5%, respectively) with poorer results in the very small number of FFPE-derived EUS-FNA biopsies (**Table 1**). Of the 32 results for *KRAS* wild-type status, 24 patients were deemed ineligible due to physician opinion, performance status, rapid disease progression or death. The remaining 8 patients were enrolled onto study treatment.

Patient Characteristics

Between November 2017 and October 2020, 8 patients were enrolled onto the study and treated with panitumumab. The baseline characteristics of the study participants are summarised in **Table 2**. Patients were predominantly male (75%) with an ECOG performance status of 0 or 1 (87.5%) and most had received first line gemcitabine/nab-paclitaxel chemotherapy (62.5%). One patient (12%) had previously undergone a surgical resection and progressed within 12 months of adjuvant gemcitabine/capecitabine. One further patient (12%) had a histological diagnosis of metastatic pancreatic cancer after resection of a previous pancreaticobiliary type tumour of the pancreatic head which was thought to have arisen in the ampulla. After consideration by the principal investigator, this patient was deemed to meet entry criteria for the study. The median time

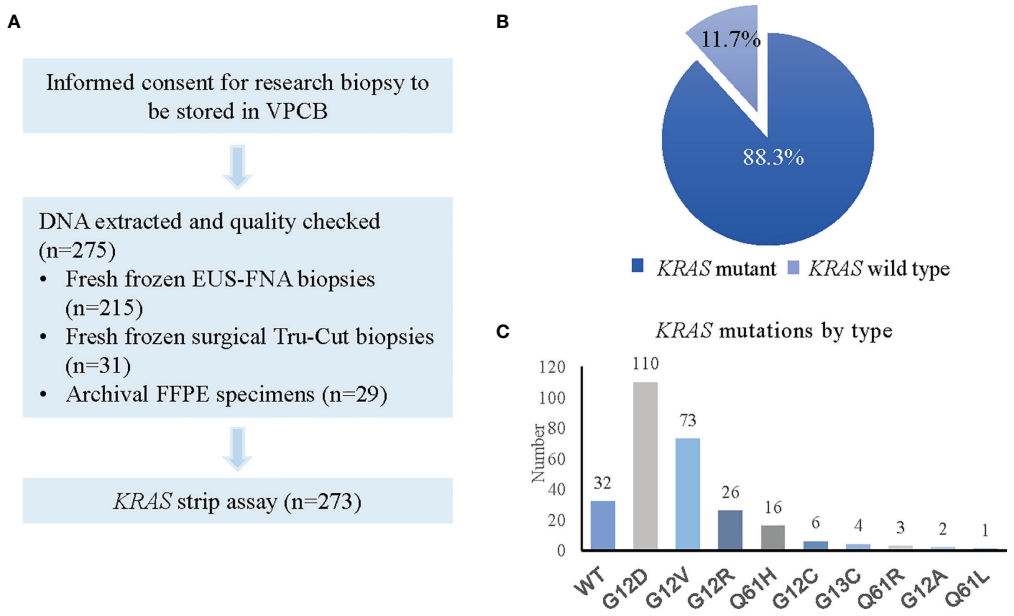

FIGURE 2 | *KRAS* status screening in PDAC patients. **(A)** Flow chart showing process for *KRAS* screening. **(B)** Pie chart representing *KRAS* positivity rate. **(C)** Graph depicting types of *KRAS* mutations detected.

TABLE 1 | *KRAS* mutation rates in fresh frozen EUS-FNA, surgical and FFPE tissue specimens.

Tissue type	*KRAS* wild-type	*KRAS* mutant
Frozen EUS-FNA biopsy	24 (11.2%)	190 (88.8%)
Frozen surgical biopsy	2 (6.5%)	29 (93.5%)
FFPE tissue		
EUS-FNA biopsy	4 (44.4%)	5 (55.5%)
Surgical specimen	2 (10.5%)	17 (89.5%)

from diagnosis of cancer to enrolment onto this study was 66.2 weeks.

Treatment

Patients received a median of 6 cycles of panitumumab (range 2-9). Seven patients (87.5%) were taken off study treatment due to progressive disease. One patient was taken off study treatment after 6 cycles despite RECIST stable disease, after developing acute urinary retention which led to an unexpected diagnosis of comorbid metastatic prostate cancer. A PSMA-PET scan revealed that the biopsy-confirmed locally advanced pancreatic cancer diagnosed three years prior harboured different metabolic expression compared to the metastatic lesions in the liver and bones, which were consistent with the separate pathology of prostate cancer (also subsequently biopsy proven). This patient was considered not evaluable for response but included in analyses of safety and quality of life.

TABLE 2 | Baseline patient characteristics.

Characteristic	Frequency (n=8)
Median age in years (range)	64.5 (51-79)
Sex (%)	
Male	6 (75)
Female	2 (25)
Baseline ECOG (%)	
0	2 (25)
1	5 (62.5)
2	1 (12.5)
TNM stage (%)	
III	2 (75)
IV	6 (75)
Previous systemic therapy (%)	
Gemcitabine	2 (25)
Gemcitabine/nab-paclitaxel	5 (62.5)
Gemcitabine/capecitabine	1 (12.5)
FOLFIRINOX	1 (12.5)
Number of metastatic sites (%)	
0	2 (25)
1	3 (37.5)
≥2	3 (37.5)
Site of metastases (%)	
Liver	4 (50)
Lung	4 (50)
Bone	2 (25)
Lymph nodes	2 (25)
CA 19.9 (%)	
<ULN	2 (25)
>ULN	6 (75)
Median time in weeks from initial diagnosis (range)	66.2 (31.2-308.3)

ECOG, Eastern Oncology Cooperative Group; TNM, Tumour Node Metastasis; ULN, upper limit of normal.

Response Measures

The primary endpoint of PFS at 4 months was 14.3%. No metabolic responses were observed, although one patient was identified as a rapid metabolic progressor at the 4-week FDG-PET scan and taken off study treatment. The best response by RECIST v1.1 criteria was stable disease in 4 patients at the initial 8-week assessment, with no objective tumour responses seen and only one patient demonstrating failure to progress at the 16-week assessment. Median PFS was 12.9 weeks, and median OS was 30.8 weeks (**Figure 3**).

Baseline exploratory analysis of ctDNA included digital droplet PCR screening kit for G12/G13 and Q61 *KRAS* mutations. 7 patients (87.5%) had no detectable *KRAS* in the blood; however, the patient who was taken off study early due to rapid clinical and metabolic progression was unexpectedly found to harbour high level *KRAS* mutant allele fraction in their baseline blood sample.

Safety

Panitumumab was generally well tolerated, in keeping with previous clinical reporting (33). Treatment related adverse events (AEs) are summarised in **Table 3**. The most common treatment related AE was a grade 1 or 2 acneiform rash, occurring in 6/8 patients (75%) and manageable with supportive care. No unexpected or serious drug related toxicity was observed and there were no dose reductions or delays due to toxicity.

Quality of Life

Quality of life questionnaires were employed to assess patient-reported outcome measures during treatment. There were no significant changes observed in total raw quality of life scores, or in calculated global quality of life, functioning, or symptom scores between any of the timepoints recorded (**Figure 4**).

DISCUSSION

This study provides proof-of-principle evidence that EUS-FNA biopsies can be utilised as a source of reliable genetic material to guide timely screening for precision medicine studies in PDAC. The challenges of precision medicine studies in PDAC are well documented, with previous molecularly screened studies failing to achieve recruitment targets due at least in part to tumour specimen inadequacy and processing delays in a patient population requiring timely treatment (10). Here, we demonstrate that selective molecular analysis of EUS-FNA biopsies is sensitive and feasible for patient selection for targeted therapy. Importantly, our reported *KRAS* mutation detection rate was comparable to previous studies which have largely relied on surgical specimens for molecular analysis (24–28). As the majority of patients presenting with PDAC will not undergo surgery, maximizing the use of diagnostic EUS-FNA biopsies for molecular screening and clinical trial selection holds great appeal.

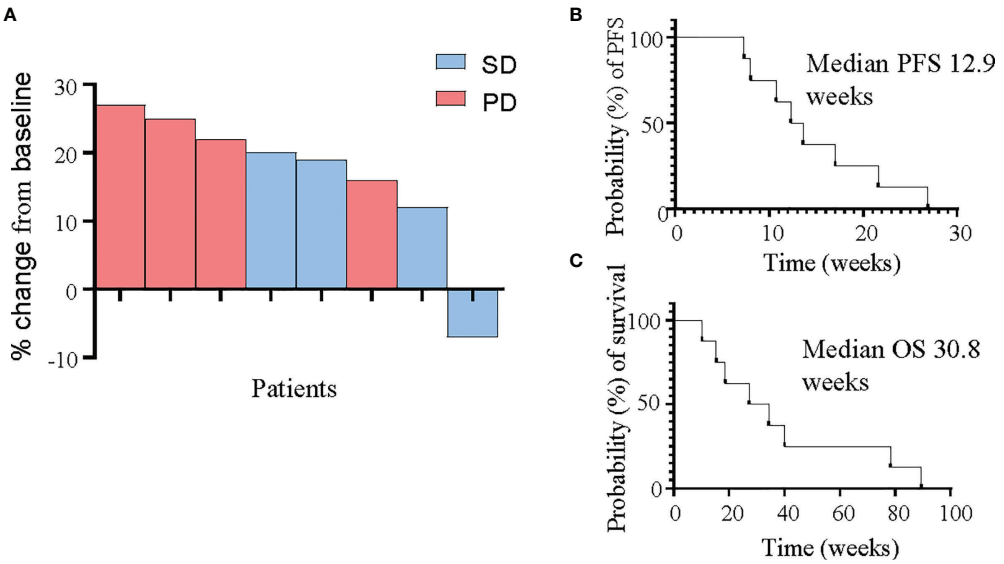

FIGURE 3 | Response of PDAC patients to panitumumab therapy. **(A)** Waterfall plot demonstrating best tumour response as measured by RECIST v1.1 criteria in all 8 patients. **(B, C)** Kaplan-Meier curves for progression-free survival **(B)** and overall survival **(C)**.

TABLE 3 | All treatment related adverse events in 8 patients, according to NCI-CTCAE V4.0 criteria.

AE (related)	G1	G2	G3	G4
Fatigue	2	0	0	0
Acneiform rash	6	2	0	0
Anorexia	2	0	0	0
Diarrhoea	1	1	0	0
Pruritis/dry skin	1	0	0	0
Hypomagnesaemia	0	1	1	0
Hand-foot syndrome	2	0	0	0

While other groups have reported on EUS-FNA for the isolation of genetic material in PDAC, the methodology, selection criteria for "adequate" samples, and sensitivity of *KRAS* analysis has varied widely. One meta-analysis (15) pooling 931 patients across 9 studies evaluating the role of *KRAS* mutation analysis to improve the diagnostic sensitivity of EUS-FNA in PDAC demonstrated significant heterogeneity across studies and reported a pooled sensitivity rate for the detection of *KRAS* mutations in PDAC of only 76.8% and specificity of 93.3%, figures which fall below acceptable standards to use for therapeutic selection in the clinic. Recent studies of precision medicine in PDAC have either completely excluded EUS-FNA biopsies [e.g. IMPaCT (10), COMPASS (42)] or have failed to report on the success rates of molecular testing in the small number of specimens included [e.g. Know Your Tumour (13)], and the prospective validation of these specimens to guide clinical intervention is not yet established.

We were able to identify and treat 8 patients with *KRAS* wild-type PDAC in our pilot study. While panitumumab had an acceptable safety profile and was generally well tolerated, this study did not meet the predefined primary outcome target of 50% PFS at 4 months. It is difficult to draw definitive conclusions based on our small sample size, particularly with one patient deemed not evaluable for response and one other likely returning a false negative *KRAS* tissue result. However, we elected not to expand the study to include further patients due to slow recruitment, changes in standard second line therapy recommendations since initiating the study (43–46), and increasing availability of alternative molecularly selected studies.Treatment beyond first line chemotherapy in PDAC has been historically challenging. Recently, the final survival analysis of the NAPOLI-1 study demonstrated a significant improvement in median OS (6.1 vs 4,2 months, HR 0.67) with liposomal irinotecan plus 5-FU/leucovorin compared to 5-FU/leucovorin alone in patients previously treated with gemcitabine-based chemotherapy (47), establishing this regimen as standard care in this setting. Prior to this, the CONKO III study had demonstrated significant improvement (4.8 vs 2.3 months) in survival in patients treated with the oxaliplatin/5-FU/folinic acid when compared to best supportive care (BSC), although notably the trial closed early due to poor recruitment and poor acceptance of the BSC arm (48), and the findings were not supported by the subsequent PANCREOX study (49).

While it is not feasible to directly compare survival results between trials, historical standards do provide some benchmarks when considering the results of single arm studies in this setting. A recent meta-analysis of 11 randomised controlled trials of second line therapy including 5-FU and oxaliplatin after first line gemcitabine-based therapy in PDAC reported mOS of 6.3 months in patients with good performance status, with an mOS range of 2.6-6.7 months (50).

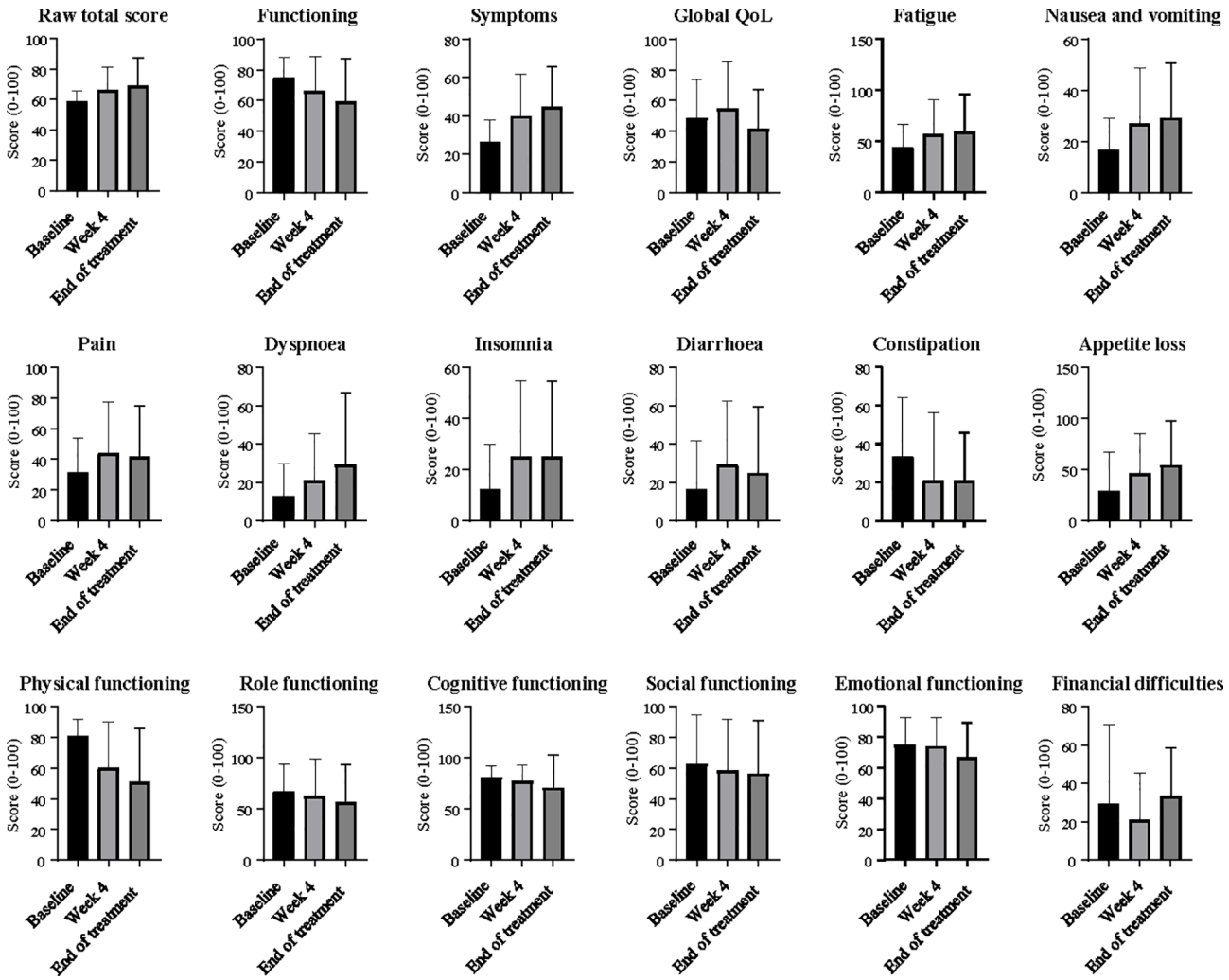

FIGURE 4 | Quality of life scores at baseline, week 4 and end of treatment. Ordinary one-way ANOVA and Tukey's multiple comparisons test were used to compare differences between timepoints. Error bars on column graphs represent the standard deviation from the mean. No significant changes from baseline were seen in any scores.

We note that despite the lack of clear efficacy of the study drug panitumumab, the mOS in our patient group was reasonably long in comparison to these historic standards (47–50), particularly when considering that the median time from diagnosis to enrolment onto study was over 12 months in our cohort, perhaps reflecting the unique biology and prognosis of *KRAS* wild-type disease in PDAC. While pre-clinical studies including one from our group have demonstrated efficacy of EGFR inhibition in patient-derived xenograft models of *KRAS* wild-type PDAC (14, 51, 52), efforts to translate such promising pre-clinical discoveries to the clinic have often yielded underwhelming results in PDAC (53). This is likely due to a number of contributing factors, including tumour heterogeneity and inadequate pre-clinical modelling of the complex tumour microenvironment and stroma which may hamper drug delivery. Patient-derived organoid models are showing promise in overcoming some of these obstacles, although they remain in their infancy as predictors of real-time clinical response in PDAC (54–57).

KRAS has been observed to be a prognostic factor in case series (58) and in *post-hoc* analyses of clinical trials, with a recent meta-analysis including 17 studies of more than 2000 patients reporting a significant association between mutant *KRAS* and overall survival (59). In addition to prognostic significance, it is increasingly clear that *KRAS* wild-type PDAC tumours harbour a distinct clinical and genetic profile when compared to *KRAS* mutant tumours (60, 61). Recently Singhi, et al. reported the results of real-time genome profiling of over 3500 PDAC tumours, including 445 *KRAS* wild-type samples. This study identified potentially targetable genomic changes in 17% of patients, including a number of clinically relevant gene mutations and fusions in the 12% of patients harbouring *KRAS* wild-type tumours (62). In this cohort, 38% of *KRAS* wild-type tumours harboured other alterations with the potential to

activate the Receptor Tyrosine Kinase (RTK)/Ras/MAP Kinase (MAPK) signalling pathway, suggesting that more careful selection of patients who may respond to EGFR inhibitor therapy is required beyond *KRAS* alone. *BRAF* alterations have been shown to be mutually exclusive with *KRAS* mutations, and represent another potential therapeutic target in *KRAS* wild-type tumours (62–64). Interestingly, mismatch repair deficits and kinase fusions are also among the genetic changes reported to occur more commonly among patients with a *KRAS* wild-type phenotype (62, 65, 66). While deeper genomic sequencing was outside of the scope of this study, interrogation of our *KRAS* wild-type tumours for other genetic drivers would be extremely valuable in evaluating the lack of response to EGFR inhibition in our patient cohort. It is very likely that some of these patients may have harboured activating mutations in other RTK/Ras/MAPK pathway genes leading to persistent signal activation downstream of EGFR, while others may have had other mechanisms of primary therapeutic resistance. Our findings suggest that *KRAS* alone does not appear to adequately predict for response to EGFR inhibition in PDAC, and we suggest that broader testing of other activating genes in this pathway would be critical in future studies.

We were able to successfully screen almost 300 biopsies for *KRAS* mutations, relying largely on an active local biobank program. We predominantly utilised EUS-FNA biopsies to screen as many patients as possible, and despite variability in yield of genetic material across samples, our *KRAS* mutation rate was consistent with other published literature (24–28). We did not perform broader molecular sequencing as part of this study, which may require higher quality and quantity genetic material than is required for this highly sensitive assay of a common oncogene (67).

Notably, exploratory analysis of ctDNA revealed a strong positive *KRAS* mutant allele fraction in the patient who only completed 2 cycles of panitumumab due to rapid clinical progression, strongly suggesting that the *KRAS* tissue result was a false negative. The *KRAS* StripAssay™ has high sensitivity to detect mutant *KRAS* occurring in 1-5% of tumour cells, and the discordance between tissue and ctDNA testing is difficult to explain given that the tissue testing for this patient was performed on an archival tissue sample containing 80% tumour cellularity. Our exploratory analysis of ctDNA requires further validation in a larger patient cohort, although to date the concordance between tissue and ctDNA findings, and the specificity of the *KRAS* assay used here appear very high (68), suggesting that the patient in this study was an outlier. However, this finding highlights the need to optimize the accuracy of molecular testing in PDAC, and lends weight to an argument to incorporate liquid biopsies into clinical trial design as another layer of molecular screening to enhance sensitivity and specificity. Our study was performed in a "real-world" setting using standard-of-care biopsies at the discretion of each individual physician, and we did not collect information about the specific types of needles and techniques used to collect the EUS-FNA biopsies. With advancements in technology, the newer-generation core biopsy needles are becoming more commonplace in routine medical practice and in research, and are likely to improve yield and quality of the samples used for genomic analysis. In future studies, we plan to explore the diagnostic accuracy, yield and quality of genetic material obtained with newer generation needles (e.g. Acquire™ or SharkCore™).

EGFR inhibition is not a novel concept in the treatment of PDAC, although results have been mixed. A phase II study of the anti-EGFR monoclonal antibody nimotuzumab in combination with gemcitabine recently demonstrated activity and tolerability in the first line setting, most markedly in *KRAS* wild-type patients. However, the *KRAS* mutation analysis was again performed retrospectively, only available in approximately 50% of participants, and positive in far fewer than expected (37). A previous meta-analysis of 4 randomised control trials of cetuximab revealed no survival benefit, but significant additional toxicity (39), while combined meta-analysis of 24 studies including erlotinib with gemcitabine reported modest evidence of efficacy but did not explore molecular subgroups (38). Notably, a recent systematic review of phase II trials in advanced PDAC reported that of 37 trials investigating biologic agents, just 1 included prospective biomarker enrichment (69). *Post-hoc* analyses have reported conflicting findings with regards to the predictive value of *KRAS* for EGFR pathway inhibition, but are often hampered by incomplete genomic information for study cohorts and lower than expected *KRAS* mutation rates, suggesting the presence of false negative results (36, 60, 70–72).

This study was not designed or powered to detect a benefit of panitumumab over other standard of care agents in PDAC which would require a large multicentre study given the rarity of *KRAS* wild-type tumours and well documented challenges in enrolling patients with PDAC onto clinical trials. We primarily aimed to demonstrate proof-of-principal evidence for routine use of EUS-FNA derived material in real-time molecular screening in PDAC, with a secondary aim to detect preliminary signals of panitumumab efficacy which could be used to justify larger subsequent expansion of the study. Despite the small sample size, we saw no objective responses to therapy, and when examined in the context of previous studies, our study does not offer any convincing evidence that panitumumab demonstrates adequate efficacy to pursue further in this setting.

PDAC is an aggressive malignancy associated with rapid clinical decline, and optimal clinical trial design needs to be carefully considered in this setting. The recent encouraging results of the POLO study demonstrated that maintenance therapy is feasible in this patient population (46). A maintenance approach to anti-EGFR targeted therapy for PDAC patients without *KRAS* or other activating MAPK pathway mutations who achieve disease control on first line chemotherapy may be worthy of exploration in future studies.

As our understanding of the molecular landscape of PDAC has expanded, and with the recent demonstration of a PFS benefit in patients harbouring germline *BRCA* mutations undergoing maintenance olaparib therapy after failure to

progress on platinum-based chemotherapy (46), molecular testing is now routinely recommended in several therapeutic guidelines (8, 73). More recently, several ongoing studies have encouragingly begun to report successful implementation of molecularly matched therapies in PDAC (13, 42), providing ongoing hope for the expansion of precision medicine to improve patient outcomes.

CONCLUSION

In summary, our study confirms that rapid, prospective molecular testing of EUS-FNA diagnostic biopsies can accurately detect *KRAS* mutations in PDAC, and is among the first to prospectively enroll molecularly screened patients onto targeted therapy using EUS-FNA biopsies. Notably, our findings provide key evidence that precision medicine in PDAC can be feasibly applied in clinical trials in the ongoing endeavor to improve outcomes in this deadly disease, and lay the foundation for the continual refinement of targeted therapy approaches in PDAC. Furthermore, our pilot study of single agent panitumumab proved safe and tolerable, but showed no significant signal of efficacy in patients with advanced *KRAS* wild-type PDAC treated after standard chemotherapy. Median survival in the *KRAS* wild-type patient group was longer than historical controls, in keeping with reports from other groups. Importantly, EUS-FNA biopsies proved a feasible source of tissue for rapid *KRAS* analysis of large numbers of patients and highlighted the value of tissue biobanking and the potential utility of these often low-yield biopsies to increase patient access to molecular testing and matched therapies in future studies.

DATA AVAILABILITY STATEMENT

The raw data supporting the conclusions of this article will be made available by the authors, without undue reservation.

ETHICS STATEMENT

The studies involving human participants were reviewed and approved by Human Research Ethics Committee at Monash Health. The patients/participants provided their written informed consent to participate in this study.

AUTHOR CONTRIBUTIONS

Study conception and design: DC, JZ, DG, AZ, VG, and JL. Human tissue acquisition: DC, CD, and MS. Acquisition of study data: DC, MH, and JL. Analysis and interpretation of data: JL, DC, MH, JZ, AZ, DG, VG, AB, and BJ. Writing and/or revision of the manuscript: JL, DC, MH, JZ, AZ, DG, VG, and BJ. Study supervision: DC and BJ. All authors contributed to the article and approved the submitted version.

FUNDING

This study was supported by a Monash Partners Comprehensive Cancer Consortium (MPCCC) Research Grant and an Epworth Medical Foundation (EMF) research grant. Additional funding was obtained from Amgen, who also supplied the study drug, and the Operational Infrastructure Support Program by the Victorian Government of Australia. BJJ is supported by a Senior Research Fellowship from the National Health and Medical Research Council of Australia.

ACKNOWLEDGMENTS

The authors would like to acknowledge the contribution of the Genetics and Molecular Pathology Laboratory at Monash Health for their assistance in performing *KRAS* screening, Zdenka Prodanovic for her oversight of the VPCB, and all the clinicians, scientists and patients who contributed their time and tissues to the VPCB to enable this research.

REFERENCES

1. Sung H, Ferlay J, Siegel RL, Laversanne M, Soerjomataram I, Jemal A, et al. Global Cancer Statistics 2020: GLOBOCAN Estimates of Incidence and Mortality Worldwide for 36 Cancers in 185 Countries. *CA Cancer J Clin* (2021) 71(3):209–49. doi: 10.3322/caac.21660
2. Rahib L, Smith BD, Aizenberg R, Rosenzweig AB, Fleshman JM, Matrisian LM. Projecting Cancer Incidence and Deaths to 2030: The Unexpected Burden of Thyroid, Liver, and Pancreas Cancers in the United States. *Cancer Res* (2014) 74:2913. doi: 10.1158/0008-5472.CAN-14-0155
3. Wade TP, Halaby IA, Stapleton DR, Virgo KS, Johnson FE. Population-Based Analysis of Treatment of Pancreatic Cancer and Whipple Resection: Department of Defense Hospitals, 1989–1994. *Surgery* (1996) 120:680–7. doi: 10.1016/S0039-6060(96)80017-1
4. Siegel RL, Miller KD, Fuchs HE, Jemal A. Cancer Statistics, 2021. *CA Cancer J Clin* (2021) 71:7–33. doi: 10.3322/caac.21654
5. Huang L, Jansen L, Balavarca Y, Babaei M, van der Geest L, Lemmens V, et al. Stratified Survival of Resected and Overall Pancreatic Cancer Patients in Europe and the USA in the Early Twenty-First Century: A Large, International Population-Based Study. *BMC Med* (2018) 16:125–5. doi: 10.1186/s12916-018-1120-9
6. Von Hoff DD, Ervin T, Arena FP, Chiorean EG, Infante J, Moore M, et al. Increased Survival in Pancreatic Cancer With Nab-Paclitaxel Plus Gemcitabine. *N Engl J Med* (2013) 369:1691–703. doi: 10.1056/NEJMoa1304369
7. Conroy T, Desseigne F, Ychou M, Bouche O, Guimbaud R, Becouarn Y, et al. FOLFIRINOX Versus Gemcitabine for Metastatic Pancreatic Cancer. *N Engl J Med* (2011) 364:1817–25. doi: 10.1056/NEJMoa1011923
8. Sohal DPS, Kennedy EB, Cinar P, Conroy T, Copur MS, Crane CH, et al. Metastatic Pancreatic Cancer: ASCO Guideline Update. *J Clin Oncol* (2020) 38:3217–30. doi: 10.1200/jco.20.01364
9. Ducreux M, Cuhna AS, Caramella C, Hollebecque A, Burtin P, Goéré D, et al. Cancer of the Pancreas: ESMO Clinical Practice Guidelines for Diagnosis, Treatment and Follow-Up. *Ann Oncol* (2015) 26 Suppl 5:v56–68. doi: 10.1093/annonc/mdv295
10. Chantrill LA, Nagrial AM, Watson C, Johns AL, Martyn-Smith M, Simpson S, et al. Precision Medicine for Advanced Pancreas Cancer: The Individualized Molecular Pancreatic Cancer Therapy (IMPaCT) Trial. *Clin Cancer Res* (2015) 21:2029–37. doi: 10.1158/1078-0432.CCR-15-0426

11. Ding D, Javed AA, Cunningham D, Teinor J, Wright M, Javed ZN, et al. Challenges of the Current Precision Medicine Approach for Pancreatic Cancer: A Single Institution Experience Between 2013 and 2017. *Cancer Lett* (2021) 497:221–8. doi: 10.1016/j.canlet.2020.10.039
12. Hoos WA, James PM, Rahib L, Talley AW, Fleshman JM, Matrisian LM. Pancreatic Cancer Clinical Trials and Accrual in the United States. *J Clin Oncol* (2013) 31:3432–8. doi: 10.1200/jco.2013.49.4823
13. Pishvaian MJ, Bender RJ, Halverson D, Rahib L, Hendifar AE, Mikhail S, et al. Molecular Profiling of Patients With Pancreatic Cancer: Initial Results From the Know Your Tumor Initiative. *Clin Cancer Res* (2018) 24:5018–27. doi: 10.1158/1078-0432.Ccr-18-0531
14. Berry W, Algar E, Kumar B, Desmond C, Swan M, Jenkins BJ, et al. Endoscopic Ultrasound-Guided Fine-Needle Aspirate-Derived Preclinical Pancreatic Cancer Models Reveal Panitumumab Sensitivity in KRAS Wild-Type Tumors. *Int J Cancer* (2017) 140:2331–43. doi: 10.1002/ijc.30648
15. Fuccio L, Hassan C, Laterza L, Correale L, Pagano N, Bocus P, et al. The Role of K-Ras Gene Mutation Analysis in EUS-Guided FNA Cytology Specimens for the Differential Diagnosis of Pancreatic Solid Masses: A Meta-Analysis of Prospective Studies. *Gastrointest Endosc* (2013) 78:596–608. doi: 10.1016/j.gie.2013.04.162
16. Lundy J, Gao H, Berry W, Masoumi-Moghoddam S, Jenkins BJ, Croagh D, et al. Targeted Transcriptome and KRAS Mutation Analysis Improve the Diagnostic Performance of EUS-FNA Biopsies in Pancreatic Cancer. *Clin Cancer Res* (2021) 27(21):5900–11. doi: 10.1158/1078-0432.Ccr-21-1107
17. Marques S, Bispo M, Rio-Tinto R, Fidalgo P, Devière J. The Impact of Recent Advances in Endoscopic Ultrasound-Guided Tissue Acquisition on the Management of Pancreatic Cancer. *GE Port J Gastroenterol* (2021) 28:185–92. doi: 10.1159/000510730
18. Polkowski M, Jenssen C, Kaye P, Carrara S, Deprez P, Gines A, et al. Technical Aspects of Endoscopic Ultrasound (EUS)-Guided Sampling in Gastroenterology: European Society of Gastrointestinal Endoscopy (ESGE) Technical Guideline – March 2017. *Endoscopy* (2017) 49:989–1006. doi: 10.1055/s-0043-119219
19. Khoury T, Sbeit W, Ludvik N, Nadella D, Wiles A, Marshall C, et al. Concise Review on the Comparative Efficacy of Endoscopic Ultrasound-Guided Fine-Needle Aspiration vs Core Biopsy in Pancreatic Masses, Upper and Lower Gastrointestinal Submucosal Tumors. *World J Gastrointest Endosc* (2018) 10:267–73. doi: 10.4253/wjge.v10.i10.267
20. James T, Baron T. A Comprehensive Review of Endoscopic Ultrasound Core Biopsy Needles. *Expert Rev Med Devices* (2018) 15:127–135. doi: 10.1080/17434440.2018.1425137
21. Alatawi A, Beuvon F, Grabar S, Leblanc S, Chaussade S, Terris B, et al. Comparison of 22G Reverse-Beveled Versus Standard Needle for Endoscopic Ultrasound-Guided Sampling of Solid Pancreatic Lesions. *United European Gastroenterol J* (2015) 3:343–52. doi: 10.1177/2050640615577533
22. Bang JY, Hawes R, Varadarajulu S. A Meta-Analysis Comparing ProCore and Standard Fine-Needle Aspiration Needles for Endoscopic Ultrasound-Guided Tissue Acquisition. *Endoscopy* (2016) 48:339–49. doi: 10.1055/s-0034-1393354
23. Mukai S, Itoi T, Katanuma A, Irisawa A. An Animal Experimental Study to Assess the Core Tissue Acquisition Ability of Endoscopic Ultrasound-Guided Histology Needles. *Endosc Ultrasound* (2018) 7:263–9. doi: 10.4103/eus.eus_16_17
24. Waddell N, Pajic M, Patch AM, Chang DK, Kassahn KS, Bailey P, et al. Whole Genomes Redefine the Mutational Landscape of Pancreatic Cancer. *Nature* (2015) 518:495–501. doi: 10.1038/nature14169
25. Witkiewicz AK, McMillan EA, Balaji U, Baek G, Lin WC, Mansour J, et al. Whole-Exome Sequencing of Pancreatic Cancer Defines Genetic Diversity and Therapeutic Targets. *Nat Commun* (2015) 6:6744. doi: 10.1038/ncomms7744
26. Almoguera C, Shibata D, Forrester K, Martin J, Arnheim N, Perucho M, et al. Most Human Carcinomas of the Exocrine Pancreas Contain Mutant C-K-Ras Genes. *Cell* (1988) 53:549–54. doi: 10.1016/0092-8674(88)90571-5
27. Biankin AV, Waddell N, Kassahn KS, Gingras MC, Muthuswamy LB, Johns AL, et al. Pancreatic Cancer Genomes Reveal Aberrations in Axon Guidance Pathway Genes. *Nature* (2012) 491:399–405. doi: 10.1038/nature11547
28. Jones S, Zhang X, Parsons DW, Lin JC, Leary RJ, Angenendt P, et al. Core Signaling Pathways in Human Pancreatic Cancers Revealed by Global Genomic Analyses. *Science* (2008) 321:1801–6. doi: 10.1126/science.1164368
29. Macdonald JS, McCoy S, Whitehead RP, Iqbal S, Wade JL3rd, Giguere JK, et al. A Phase II Study of Farnesyl Transferase Inhibitor R115777 in Pancreatic Cancer: A Southwest Oncology Group (SWOG 9924) Study. *Invest New Drugs* (2005) 23:485–7. doi: 10.1007/s10637-005-2908-y
30. Marín-Ramos NI, Ortega-Gutiérrez S and López-Rodríguez ML. Blocking Ras Inhibition as an Antitumor Strategy. *Semin Cancer Biol* (2019) 54:91–100. doi: 10.1016/j.semcancer.2018.01.017
31. Hong DS, Kuo J, Sacher AG, Barlesi F, Besse B, Kuboki Y, et al. CodeBreak 100: Phase I Study of AMG 510, a Novel KRASG12C Inhibitor, in Patients (Pts) With Advanced Solid Tumors Other Than Non-Small Cell Lung Cancer (NSCLC) and Colorectal Cancer (CRC). *J Clin Oncol* (2020) 38:3511–1. doi: 10.1200/JCO.2020.38.15_suppl.3511
32. Amado RG, Wolf M, Peeters M, Van Cutsem E, Siena S, Freeman DJ, et al. Wild-Type KRAS Is Required for Panitumumab Efficacy in Patients With Metastatic Colorectal Cancer. *J Clin Oncol* (2008) 26:1626–34. doi: 10.1200/JCO.2007.14.7116
33. Douillard JY, Siena S, Cassidy J, Tabernero J, Burkes R, Barugel M, et al. Randomized, Phase III Trial of Panitumumab With Infusional Fluorouracil, Leucovorin, and Oxaliplatin (FOLFOX4) Versus FOLFOX4 Alone as First-Line Treatment in Patients With Previously Untreated Metastatic Colorectal Cancer: The PRIME Study. *J Clin Oncol* (2010) 28:4697–705. doi: 10.1200/jco.2009.27.4860
34. Van Cutsem E, Köhne CH, Láng I, Folprecht G, Nowacki MP, Cascinu S, et al. Cetuximab Plus Irinotecan, Fluorouracil, and Leucovorin as First-Line Treatment for Metastatic Colorectal Cancer: Updated Analysis of Overall Survival According to Tumor KRAS and BRAF Mutation Status. *J Clin Oncol* (2011) 29:2011–9. doi: 10.1200/jco.2010.33.5091
35. Moore MJ, Goldstein D, Hamm J, Figer A, Hecht JR, Gallinger S, et al. Erlotinib Plus Gemcitabine Compared With Gemcitabine Alone in Patients With Advanced Pancreatic Cancer: A Phase III Trial of the National Cancer Institute of Canada Clinical Trials Group. *J Clin Oncol* (2007) 25:1960–6. doi: 10.1200/JCO.2006.07.9525
36. Boeck S, Jung A, Laubender RP, Neumann J, Egg R, Goritschan C, et al. EGFR Pathway Biomarkers in Erlotinib-Treated Patients With Advanced Pancreatic Cancer: Translational Results From the Randomised, Crossover Phase 3 Trial AIO-Pk0104. *Br J Cancer* (2013) 108:469–76. doi: 10.1038/bjc.2012.495
37. Schultheis B, Reuter D, Ebert MP, Siveke J, Kerkhoff A, Berdel WE, et al. Gemcitabine Combined With the Monoclonal Antibody Nimotuzumab Is an Active First-Line Regimen in KRAS Wildtype Patients With Locally Advanced or Metastatic Pancreatic Cancer: A Multicenter, Randomized Phase IIb Study. *Ann Oncol* (2017) 28:2429–35. doi: 10.1093/annonc/mdx343
38. Wang Y, Hu GF, Zhang QQ, Tang N, Guo J, Liu LY, et al. Efficacy and Safety of Gemcitabine Plus Erlotinib for Locally Advanced or Metastatic Pancreatic Cancer: A Systematic Review and Meta-Analysis. *Drug Des Devel Ther* (2016) 10:1961–72. doi: 10.2147/dddt.S105442
39. Forster T, Huettner FJ, Springfeld C, Loehr M, Kalkum E, Hackbusch M, et al. Cetuximab in Pancreatic Cancer Therapy: A Systematic Review and Meta-Analysis. *Oncology* (2020) 98:53–60. doi: 10.1159/000502844
40. Halfdanarson TR, Foster NR, Kim GP, Meyers JP, Smyrk TC, McCullough AE, et al. A Phase II Randomized Trial of Panitumumab, Erlotinib, and Gemcitabine Versus Erlotinib and Gemcitabine in Patients With Untreated, Metastatic Pancreatic Adenocarcinoma: North Central Cancer Treatment Group Trial N064B (Alliance). *Oncologist* (2019) 24:589–e160. doi: 10.1634/theoncologist.2018-0878
41. Aaronson NK, Ahmedzai S, Bergman B, Bullinger M, Cull A, Duez NJ, et al. The European Organization for Research and Treatment of Cancer QLQ-C30: A Quality-of-Life Instrument for Use in International Clinical Trials in Oncology. *J Natl Cancer Inst* (1993) 85:365–76. doi: 10.1093/jnci/85.5.365
42. Aung KL, Fischer SE, Denroche RE, Jang GH, Dodd A, Creighton S, et al. Genomics-Driven Precision Medicine for Advanced Pancreatic Cancer: Early Results From the COMPASS Trial. *Clin Cancer Res* (2018) 24:1344–54. doi: 10.1158/1078-0432.Ccr-17-2994
43. Mita N, Iwashita T, Uemura S, Yoshida K, Iwasa Y, Ando N, et al. Second-Line Gemcitabine Plus Nab-Paclitaxel for Patients With Unresectable Advanced

Pancreatic Cancer After First-Line FOLFIRINOX Failure. *J Clin Med* (2019) 8 (6):761. doi: 10.3390/jcm8060761
44. Portal A, Pernot S, Tougeron D, Arbaud C, Bidault AT, de la Fouchardière C, et al. Nab-Paclitaxel Plus Gemcitabine for Metastatic Pancreatic Adenocarcinoma After Folfirinox Failure: An AGEO Prospective Multicentre Cohort. *Br J Cancer* (2015) 113:989–95. doi: 10.1038/bjc.2015.328
45. Wang-Gillam A, Li CP, Bodoky G, Dean A, Shan YS, Jameson G, et al. Nanoliposomal Irinotecan With Fluorouracil and Folinic Acid in Metastatic Pancreatic Cancer After Previous Gemcitabine-Based Therapy (NAPOLI-1): A Global, Randomised, Open-Label, Phase 3 Trial. *Lancet (London England)* (2016) 387:545–57. doi: 10.1016/s0140-6736(15)00986-1
46. Golan T, Hammel P, Reni M, Van Cutsem E, Macarulla T, Hall MJ, et al. Maintenance Olaparib for Germline BRCA-Mutated Metastatic Pancreatic Cancer. *N Engl J Med* (2019) 381:317–27. doi: 10.1056/NEJMoa1903387
47. Wang-Gillam A, Hubner RA, Siveke JT, Von Hoff DD, Belanger B, de Jong FA, et al. NAPOLI-1 Phase 3 Study of Liposomal Irinotecan in Metastatic Pancreatic Cancer: Final Overall Survival Analysis and Characteristics of Long-Term Survivors. *Eur J Cancer* (2019) 108:78–87. doi: 10.1016/j.ejca.2018.12.007
48. Pelzer U, Schwaner I, Stieler J, Adler M, Seraphin J, Dörken B, et al. Best Supportive Care (BSC) Versus Oxaliplatin, Folinic Acid and 5-Fluorouracil (OFF) Plus BSC in Patients for Second-Line Advanced Pancreatic Cancer: A Phase III-Study From the German CONKO-Study Group. *Eur J Cancer* (2011) 47:1676–81. doi: 10.1016/j.ejca.2011.04.011
49. Gill S, Ko YJ, Cripps C, Beaudoin A, Dhesy-Thind S, Zulfiqar M, et al. PANCREOX: A Randomized Phase III Study of Fluorouracil/Leucovorin With or Without Oxaliplatin for Second-Line Advanced Pancreatic Cancer in Patients Who Have Received Gemcitabine-Based Chemotherapy. *J Clin Oncol* (2016) 34:3914–20. doi: 10.1200/jco.2016.68.5776
50. Wainberg ZA, Feeney K, Lee MA, Muñoz A, Gracián AC, Lonardi S, et al. Meta-Analysis Examining Overall Survival in Patients With Pancreatic Cancer Treated With Second-Line 5-Fluorouracil and Oxaliplatin-Based Therapy After Failing First-Line Gemcitabine-Containing Therapy: Effect of Performance Status and Comparison With Other Regimens. *BMC Cancer* (2020) 20:633. doi: 10.1186/s12885-020-07110-x
51. Bruns CJ, Solorzano CC, Harbison MT, Ozawa S, Tsan R, Fan D, et al. Blockade of the Epidermal Growth Factor Receptor Signaling by a Novel Tyrosine Kinase Inhibitor Leads to Apoptosis of Endothelial Cells and Therapy of Human Pancreatic Carcinoma. *Cancer Res* (2000) 60:2926–35.
52. Ng SS, Tsao MS, Nicklee T, Hedley DW. Effects of the Epidermal Growth Factor Receptor Inhibitor OSI-774, Tarceva, on Downstream Signaling Pathways and Apoptosis in Human Pancreatic Adenocarcinoma. *Mol Cancer Ther* (2002) 1:777–83.
53. Lieu CH, Tan A-C, Leong S, Diamond JR, Eckhardt SG. From Bench to Bedside: Lessons Learned in Translating Preclinical Studies in Cancer Drug Development. *J Natl Cancer Inst* (2013) 105:1441–56. doi: 10.1093/jnci/djt209
54. Gutierrez-Barrera AM, Menter DG, Abbruzzese JL, Reddy SA. Establishment of Three-Dimensional Cultures of Human Pancreatic Duct Epithelial Cells. *Biochem Biophys Res Commun* (2007) 358:698–703. doi: 10.1016/j.bbrc.2007.04.166
55. Tiriac H, Belleau P, Engle DD, Plenker D, Deschênes A, Somerville TDD, et al. Organoid Profiling Identifies Common Responders to Chemotherapy in Pancreatic Cancer. *Cancer Discov* (2018) 8:1112–29. doi: 10.1158/2159-8290.Cd-18-0349
56. Pasch CA, Favreau PF, Yueh AE, Babiarz CP, Gillette AA, Sharick JT, et al. Patient-Derived Cancer Organoid Cultures to Predict Sensitivity to Chemotherapy and Radiation. *Clin Cancer Res* (2019) 25:5376–87. doi: 10.1158/1078-0432.Ccr-18-3590
57. Frappart P-O, Walter K, Gout J, Beutel AK, Morawe M, Arnold F, et al. Pancreatic Cancer-Derived Organoids – a Disease Modeling Tool to Predict Drug Response. *United European Gastroenterol J* (2020) 8:594–606. doi: 10.1177/2050640620905183
58. Windon AL, Loaiza-Bonilla A, Jensen CE, Randall M, Morrissette JJD. A KRAS Wild Type Mutational Status Confers a Survival Advantage in Pancreatic Ductal Adenocarcinoma. *J Gastrointest Oncol* (2018) 9:1–10. doi: 10.21037/jgo.2017.10.14
59. Tao L-Y, Zhang L-F, Xiu D-R, Yuan C-h, Ma Z-l, Jiang B. Prognostic Significance of K-Ras Mutations in Pancreatic Cancer: A Meta-Analysis. *World J Surg Oncol* (2016) 14:146. doi: 10.1186/s12957-016-0888-3
60. Kim ST, Lim DH, Jang KT, Lim T, Lee J, Choi YL, et al. Impact of KRAS Mutations on Clinical Outcomes in Pancreatic Cancer Patients Treated With First-Line Gemcitabine-Based Chemotherapy. *Mol Cancer Ther* (2011) 10:1993–9. doi: 10.1158/1535-7163.Mct-11-0269
61. Luchini C, Paolino G, Mattiolo P, Piredda ML, Cavaliere A, Gaule M, et al. KRAS Wild-Type Pancreatic Ductal Adenocarcinoma: Molecular Pathology and Therapeutic Opportunities. *J Exp Clin Cancer Res* (2020) 39:227. doi: 10.1186/s13046-020-01732-6
62. Singhi AD, George B, Greenbowe JR, Chung J, Suh J, Maitra A, et al. Real-Time Targeted Genome Profile Analysis of Pancreatic Ductal Adenocarcinomas Identifies Genetic Alterations That Might Be Targeted With Existing Drugs or Used as Biomarkers. *Gastroenterology* (2019) 156:2242–53.e2244. doi: 10.1053/j.gastro.2019.02.037
63. Wrzeszczynski KO, Rahman S, Frank MO, Arora K, Shah M, Geiger H, et al. Identification of Targetable BRAF Δn486_P490 Variant by Whole-Genome Sequencing Leading to Dabrafenib-Induced Remission of a BRAF-Mutant Pancreatic Adenocarcinoma. *Mol Case Stud* (2019) 5(6). doi: 10.1101/mcs.a004424
64. Del Curatolo A, Conciatori F, Cesta Incani U, Bazzichetto C, Falcone I, Corbo V, et al. Therapeutic Potential of Combined BRAF/MEK Blockade in BRAF-Wild Type Preclinical Tumor Models. *J Exp Clin Cancer Res* (2018) 37:140. doi: 10.1186/s13046-018-0820-5
65. Goggins M, Offerhaus GJ, Hilgers W, Griffin CA, Shekher M, Tang D, et al. Pancreatic Adenocarcinomas With DNA Replication Errors (RER+) Are Associated With Wild-Type K-Ras and Characteristic Histopathology. Poor Differentiation, a Syncytial Growth Pattern, and Pushing Borders Suggest RER+. *Am J Pathol* (1998) 152:1501–7.
66. Luchini C, Brosens LAA, Wood LD, Chatterjee D, Shin JI, Sciammarella C, et al. Comprehensive Characterisation of Pancreatic Ductal Adenocarcinoma With Microsatellite Instability: Histology, Molecular Pathology and Clinical Implications. *Gut* (2021) 70:148–56. doi: 10.1136/gutjnl-2020-320726
67. Imaoka H, Sasaki M, Hashimoto Y, Watanabe K, Ikeda M. New Era of Endoscopic Ultrasound-Guided Tissue Acquisition: Next-Generation Sequencing by Endoscopic Ultrasound-Guided Sampling for Pancreatic Cancer. *J Clin Med* (2019) 8:1173. doi: 10.3390/jcm8081173
68. Sellahewa R, Lundy J, Croagh D, Jenkins B. High Circulating Tumour DNA Is a Strong Negative Prognostic Factor in Operable Pancreatic Cancer. *HPB* (2021) 23:S263. doi: 10.1016/j.hpb.2020.11.664
69. Tang M, Chen J, Goldstein D, Links M, Lord S, Marschner I, et al. Evaluation of Phase II Trial Design in Advanced Pancreatic Cancer. *Pancreas* (2019) 48:1274–84. doi: 10.1097/mpa.0000000000001429
70. Infante JR, Somer BG, Park JO, Li CP, Scheulen ME, Kasubhai SM, et al. A Randomised, Double-Blind, Placebo-Controlled Trial of Trametinib, an Oral MEK Inhibitor, in Combination With Gemcitabine for Patients With Untreated Metastatic Adenocarcinoma of the Pancreas. *Eur J Cancer* (2014) 50:2072–81. doi: 10.1016/j.ejca.2014.04.024
71. da Cunha Santos G, Dhani N, Tu D, Chin K, Ludkovski O, Kamel-Reid S, et al. Molecular Predictors of Outcome in a Phase 3 Study of Gemcitabine and Erlotinib Therapy in Patients With Advanced Pancreatic Cancer: National Cancer Institute of Canada Clinical Trials Group Study PA.3. *Cancer* (2010) 116:5599–607. doi: 10.1002/cncr.25393
72. Kullmann F, Hartmann A, Stöhr R, Messmann H, Dollinger MM, Trojan J, et al. KRAS Mutation in Metastatic Pancreatic Ductal Adenocarcinoma: Results of a Multicenter Phase II Study Evaluating Efficacy of Cetuximab Plus Gemcitabine/Oxaliplatin (GEMOXCET) in First-Line Therapy. *Oncology* (2011) 81:3–8. doi: 10.1159/000330194
73. Daly MB, Pilarski R, Yurgelun MB, Berry MP, Buys SS, Dickson P, et al. NCCN Guidelines Insights: Genetic/Familial High-Risk Assessment: Breast, Ovarian, and Pancreatic, Version 1.2020. *J Natl Compr Canc Netw* (2020) 18:380–91. doi: 10.6004/jnccn.2020.0017

Conflict of Interest: The authors declare that the research was conducted in the absence of any commercial or financial relationships that could be construed as a potential conflict of interest.

This study received partial funding from Amgen. The funder had the following involvement with the study: review of study design, provision of study drug and partial funding for study procedures.

The handling editor SS and the reviewer EC have declared a shared parent affiliation with the author VG at the time of review.

Publisher's Note: All claims expressed in this article are solely those of the authors and do not necessarily represent those of their affiliated organizations, or those of the publisher, the editors and the reviewers. Any product that may be evaluated in this article, or claim that may be made by its manufacturer, is not guaranteed or endorsed by the publisher.

frontiers in Oncology

ORIGINAL RESEARCH
published: 05 January 2022
doi: 10.3389/fonc.2021.754104

rs62139665 Polymorphism in the Promoter Region of EpCAM Is Associated With Hepatitis C Virus-Related Hepatocellular Carcinoma Risk in Egyptians

Tarek Mohamed Kamal Motawi[1], *Nermin Abdel Hamid Sadik*[1], *Dina Sabry*[2,3], *Sally Atef Fahim*[4] *and Nancy Nabil Shahin*[1]*

[1] Department of Biochemistry, Faculty of Pharmacy, Cairo University, Cairo, Egypt, [2] Medical Biochemistry and Molecular Biology Department, Faculty of Medicine, Badr University in Cairo, Badr City, Egypt, [3] Medical Biochemistry and Molecular Biology Department, Faculty of Medicine, Cairo University, Cairo, Egypt, [4] Biochemistry Department, School of Pharmacy, Newgiza University (NGU), Cairo, Egypt

OPEN ACCESS

Edited by:
Nadia M. Hamdy,
Ain Shams University, Egypt

Reviewed by:
Zhuqing Shi,
NorthShore University HealthSystem, United States
Oskan Bahidinov Tasinov,
Medical University of Varna, Bulgaria

***Correspondence:**
Nancy Nabil Shahin
nancy.shahin@pharma.cu.edu.eg

Specialty section:
This article was submitted to Gastrointestinal Cancers: Hepato Pancreatic Biliary Cancers, a section of the journal Frontiers in Oncology

Received: *05 August 2021*
Accepted: *06 December 2021*
Published: *05 January 2022*

Citation:
Motawi TMK, Sadik NAH, Sabry D, Fahim SA and Shahin NN (2022) rs62139665 Polymorphism in the Promoter Region of EpCAM Is Associated With Hepatitis C Virus-Related Hepatocellular Carcinoma Risk in Egyptians. Front. Oncol. 11:754104. doi: 10.3389/fonc.2021.754104

Hepatocellular carcinoma (HCC) is a universal health problem that is particularly alarming in Egypt. The major risk factor for HCC is hepatitis C virus (HCV) infection which is a main burden in Egypt. The epithelial cell adhesion molecule (EpCAM) is a stem cell marker involved in the tumorigenesis and progression of many malignancies, including HCC. We investigated the association of -935 C/G single nucleotide polymorphism in EpCAM promoter region (rs62139665) with HCC risk, EpCAM expression and overall survival in Egyptians. A total of 266 patients (128 HCV and 138 HCC cases) and 117 age- and sex-matched controls participated in this study. Genotyping, performed using allelic discrimination and confirmed by sequencing, revealed a significant association between EpCAM rs62139665 and HCC susceptibility, with higher GG genotype and G allele distribution in HCC patients than in non-HCC subjects. Such association was not detected in HCV patients compared to controls. EpCAM gene expression levels, determined in blood by RT-qPCR, and its serum protein expression levels, determined by ELISA, were significantly higher in GG relative to GC+CC genotype carriers in HCV and HCC patients in a recessive model. ROC analysis of EpCAM protein levels revealed significant discriminatory power between HCC patients and non-HCC subjects, with improved diagnostic accuracy when combining α-fetoprotein and EpCAM compared to that of α-fetoprotein alone. Altogether, EpCAM rs62139665 polymorphism is significantly associated with HCC and with EpCAM gene and protein expression levels in the Egyptian population. Moreover, serum EpCAM levels may hold promise for HCC diagnosis and for improving the diagnostic accuracy of α-fetoprotein.

Keywords: epithelial cell adhesion molecule, single nucleotide polymorphism, hepatitis C virus, hepatocellular carcinoma, Egyptians

1 INTRODUCTION

Hepatitis C virus (HCV) infection is a major burden in Egypt, infecting almost 14.7% of the population. HCV in Egypt is considered the highest worldwide. Chronic HCV is the leading cause of liver-related death in Egypt (1).

Hepatocellular carcinoma (HCC) is considered the third cause of cancer-related mortality globally (2). This high mortality rate could be attributed to the late manifestation of HCC symptoms and, hence, its late diagnosis. Such diagnostic inadequacy is particularly prominent in lower resource settings with limited screening tools (3). Approximately 60–80% of HCV patients develop chronic hepatitis, of which 10–20% develop cirrhosis within 20–30 years. About 1–5% of cirrhotic patients may develop HCC (4). Thus, the presence of cirrhosis increases the risk for HCC, however, some patients develop HCC in non-cirrhotic livers and in the absence of inflammation (5). Several studies reported some genetic and epigenetic defects that lead to the onset of HCC (6, 7).

A minor fragment of cancer stem cells (CSCs) are responsible for the tumor initiation, growth, metastasis and relapse after treatment (8, 9). CSCs are mainly responsible for high resistance to both radiation and chemotherapy (10, 11). The epithelial cell adhesion molecule (EpCAM) is a ~ 40kDa transmembrane glycoprotein located on chromosome 2p21, highly expressed in most epithelial cancers except squamous, urothelial and renal cell carcinomas (12). EpCAM is considered as an important marker for hepatic CSCs (13) and it becomes absent once cells are differentiated into mature hepatocytes (14). Poor prognosis was observed in carcinomas with high EpCAM expression (15). The role of EpCAM is not only restricted to cell-cell linkage, but also plays an important role in migration, proliferation, signaling, differentiation, metastasis and renewal of hepatic cells (16). EpCAM acts by the activation of Wnt signaling and increasing the c-Myc expression in highly proliferating tumor cells (17, 18).

Single nucleotide polymorphisms (SNPs) are considered the most common form of genetic diversity scattered throughout the human genome and is responsible for most variabilities in genetic traits between patients as disease vulnerability, prognosis and response to therapy (19). Promoter region SNPs of a gene regulate its expression since transcription factors bind to certain nucleotide sequences within this region, thus modulating translation and predisposing an individual to certain diseases including cancer (20–22). For example, SNP rs1126497 in EpCAM gene is significantly associated with an increased risk of breast cancer and cervical cancer, as well as the overall survival (OS) of non-small cell lung cancer patients and HCC patients who had portal vein tumor thrombus (19, 23–25). These findings suggest that SNPs in the EpCAM gene may play a significant role in the initiation and progression of various types of cancer.

The objective of the present study was to investigate whether -935 C/G SNP (rs62139665) in the EpCAM gene promoter region is associated with its high expression and, hence, with susceptibility to HCC and OS in HCV Egyptian patients.

2 SUBJECTS AND METHODS

2.1 Subjects

The present study was conducted on 266 Egyptian patients categorized into 128 HCV-infected patients and 138 HCV-dependent HCC patients, recruited from the Endemic Medicine and Gastroenterology Department, Faculty of Medicine, Cairo University, from June 2014 until October 2017. The patients were followed-up for 2 years unless they died. Hepatitis C viral RNA was detected in all HCV patients, while HCC patients had HCV infection that was detected by testing positive for anti-HCV antibodies. The medical history of HCC patients is shown in **Table S1**. HCC patients were diagnosed based on pathology, cytology, ultrasound and computed tomography (CT) imaging, in addition to serum levels of alpha-fetoprotein (AFP). Tumor number, lesion size, macroscopic vascular invasion, the TNM stage, portal vein thrombosis, portal hypertension, as well as brain, chest, and total-body bone CT (to rule out extrahepatic metastases) were also evaluated. Model for end-stage liver disease (MELD) and Child-Pugh scores were also determined. HCC patients receiving radiotherapy or chemotherapy or suffering other types of cancer were excluded from the investigation.

One hundred and seventeen apparently healthy volunteers, age- and gender-matched to the patients, joined the study as controls (**Table 1**). They all showed normal liver function profiles, normal hepatobiliary ultrasound, and negative serological results for viral hepatic and autoimmune diseases, with no previous history of liver disease. Liver ultrasound findings in the studied groups are displayed in **Table S2**.

An informed consent form was signed by all the study participants. The study protocol was approved by the Research Ethics Committee, Faculty of Pharmacy, Cairo University (Permit number: BC 1813) and conformed to the ethical guidelines of the 1975 Helsinki Declaration.

Hepatitis B virus (HBV) or human immunodeficiency virus (HIV) antibodies, diabetes, fatty liver, active schistosomiasis, presence of alcohol or heavy metal in blood were considered as exclusion criteria for the study participants.

2.2Methods

2.2.1 Sample Processing and Laboratory Investigations

Ten milliliter-venous blood specimens were obtained from all enrolled subjects by trained laboratory technicians. The collected samples were aliquoted and processed as previously described (22). Briefly, one aliquot was used for RNA and DNA extraction and subsequent gene expression analysis, genotyping and sequencing. A second aliquot was separated into plasma and assayed for albumin as well as prothrombin time-international normalized ratio (PT-INR). A third aliquot was used for serum separation for the assessment of HCV-RNA and antibody titres, AFP and EpCAM levels, alanine aminotransferase (ALT), aspartate aminotransferase (AST) and ALP activities, as well as total and direct bilirubin. The

Abbreviations: AFP, Alpha-fetoprotein; ALP, Alkaline phosphatase; ALT, Alanine aminotransferase; AST, Aspartate aminotransferase; CIs, confidence intervals; CSCs, Cancer stem cells; CT, Computed tomography; EpCAM, Epithelial cell adhesion molecule; HCC, Hepatocellular carcinoma; HCV, Hepatitis C virus; HWE, Hardy-Weinberg equilibrium; MELD, Model for end-stage liver disease; OR, odds ratios; OS, Overall survival; PT-INR, Prothrombin time-international normalized ratio; ROC, Receiver operating characteristic; SNPs, Single nucleotide polymorphisms.

TABLE 1 | Demographic characteristics and laboratory data in the HCV, HCC patients and healthy controls.

	Control (n=117)	HCV (n=128)	HCC (n=138)	*P*-value
Age (years)	49.17 ± 18.69	48.29 ± 13.2	52.28 ± 10.29	0.06
Gender				
Male	62 (52.9%)	76 (59.4%)	83 (60.1%)	0.46
Female	55 (47.1%)	52 (40.6%)	55 (39.9%)	
Hemoglobin	10.82 ± 1.14	13.89 ± 1.48†	12.59 ± 1.67†‡	<0.0001
WBCs (x10^3)	4.16 ± 1.12	6.49 ± 1.96†	5.73 ± 2.15†‡	<0.0001
Platelets (x10^3)	186.4 ± 77.48	238.62 ± 110.22†	138.61 ± 62.31†‡	<0.0001
PC (%)	92.03 ± 5.73	79.72 ± 25.73†	76.86 ± 13.05†	<0.0001
PT-INR	1.09 ± 0.11	1.08 ± 0.11	1.24 ± 0.19†‡	0.002
D Bil (mg/dl)	0.21 ± 0.13	0.39 ± 0.25†	0.51 ± 0.34†‡	<0.0001
T Bil (mg/dl)	0.91 ± 0.22	0.77 ± 0.3†	1.22 ± 0.59†‡	<0.0001
ALT (U/L)	27.55 ± 6.51	46.89 ± 24.07†	59.2 ± 36.13†‡	<0.0001
AST (U/L)	26.82 ± 6.35	54.65 ± 36.31†	70.21 ± 39.11†‡	<0.0001
ALP (U/L)	78.54 ± 29.51	125.72 ± 67.01†	180.89 ± 58.54†‡	<0.0001
Albumin (g/dl)	4.13 ± 0.58	4.22 ± 0.42	3.36 ± 0.52†‡	<0.0001
Creatinine (mg/dl)	0.98 ± 0.63	0.88 ± 0.21	0.86 ± 0.22†	0.038
AFP (ng/ml)	3.95 ± 1.89	6.82 ± 15.81	662.45 ± 1462.1†‡	<0.0001

Data are expressed as mean ± SD, or n (%).

Gender data were compared using Chi square (X^2) test. The rest of the data were analyzed using one-way ANOVA and Tukey's multiple comparisons test.

†Significant difference from the control group.

‡Significant difference from the HCV group.

WBCs, white blood cells; PC, prothrombin concentration; PT-INR, prothrombin time-international normalized ratios; D Bil, direct bilirubin; T Bil, total bilirubin; ALT, alanine aminotransferase; AST, aspartate aminotransferase; ALP, alkaline phosphatase; AFP, alpha-fetoprotein.

extent of cirrhosis in HCC was evaluated on the basis of the Child scoring system that depends on albumin, bilirubin, prothrombin time, ascites and encephalopathy. Child-Pugh grades were assigned to patients according to Child and Turcotte (26).

2.2.2 Designing Primers and Probes

The EpCAM sequence was acquired from the NCBI. Ensembl genome browser 90 was used to display all variants in order to design primers that do not superimpose SNPs. Then, allele-specific primers and probes were designed using Primer3Plus, and their specificity was checked by Blast and MFEprimer-2.0. We chose a SNP, rs62139665, in the 5'UTR with a MAF exceeding 20% and predicted to modulate the promoter binding affinity to various transcription factors, thus modifying EpCAM gene expression.

2.2.3 EpCAM mRNA Expression Analysis

RNA extraction, reverse transcription and qPCR were performed as previously described (22). Briefly, total RNA extraction from blood samples was performed using a total RNA purification kit (Jena Bioscience, Munich, Germany) followed by storage of the isolated RNA at −80°C until analysis. Reverse transcription was performed using cDNA archive kit (Applied Biosystems, Foster City, California, USA). Quantitative real-time PCR (qRT-PCR) was performed using GoTaq PCR master mix (Promega Co., Madison, USA); 1 µL of cDNA was added to 25 µL of master mix, 0.25 µL of CXR Reference Dye, 1 µL of forward and reverse primers and the volume was completed to 50 µL. A protocol comprising an initial denaturation step at 95°C for 10 minutes, followed by 40 cycles of denaturation at 95°C for 15 seconds, and annealing and extension at 60°C for 1 minute, then 60°C for 30 seconds was conducted on a 7500 Real-Time PCR system (Applied Biosystems, Foster City, California, USA). The used primers had the following sequences: 5′-AGTGTAATGGCACGATCTCTG -3' (forward), 5'-GGATCA CCTGAGGTTTGAAGT -3' (reverse) for EpCAM, with β-actin as an internal control.

2.2.4 Genotyping of EpCAM Single Nucleotide Polymorphism rs62139665

DNA extraction and genotyping were carried out as formerly detailed (22), using the primers: 5'- AGTGTAATGGCACGATCTCTG -3' (forward) and 5'- GGATCACCTGAGGTTTGAAGT -3' (reverse), and the two tagged probes: VIC-TAGTAGAGACGGGGTTCCTCC ATGT and FAM- TAGTAGAGACGGCGTTCCTCCATGT. 6-carboxy-X-rhodamine (ROX) was used as a passive reference dye.

2.2.5 Sanger Sequencing

To verify the allelic discrimination results, twenty samples from each genotype were sequenced as previously described by Motawi and co-workers (22). The used primer sequences were as follows: 5'-GGCTCTATGGGAACACCTTT -3' (forward) and 5'- GGATCACC TGAGGTTTGAAGT -3' (reverse). The amplicon size was 240 bp.

2.2.6 Determination of Serum EpCAM Levels

Serum EpCAM protein concentration was determined by an ELISA kit supplied by Boster Biological Technology (Catalogue no. EK0755, Pleasanton, CA, USA) in compliance with its operational guidelines.

2.2.7 Statistical Analysis

Data are presented as mean ± SD, number (percentage) or median (interquartile range). The differences between two groups were statistically analyzed by Student's t-test and Chi square test for numerical and categorical variables, respectively. The variations between the three groups were assessed using one-way ANOVA followed by Tukey's multiple comparisons *post-hoc* test. Receiver operating characteristic (ROC) analysis was performed to calculate

EpCAM and AFP sensitivity and specificity, individually or in combination. The correlation between EpCAM and AFP levels was tested by Spearman's correlation analysis. Four models (dominant, recessive, overdominant and multiplicative) were used to assess the association between each genotype and the risk of HCC. Logistic regression was conducted to estimate the odds ratios (ORs) and 95% confidence intervals (CIs) of the association between EpCAM SNP rs62139665 and HCC risk. For a two-tailed test, a *P*-value lower than 0.05 was considered statistically significant. The Kaplan–Meier method and the log-rank survival test were employed to estimate the OS. The GraphPad Prism 6 (GraphPad Software, CA, USA) and the SPSS software, version 20.0 (SPSS Inc. Chicago, IL, USA) statistical packages were used to perform the statistical analyses. Hardy-Weinberg equilibrium (HWE) was tested online (http://www.oege.org/software/hwe-mr-calc.shtml).

3 RESULTS

3.1 Demographic, Laboratory and Clinical Characteristics of the Study Participants

The demographic features as well as the laboratory and clinical data of the study participants are depicted in **Tables 1**, **S1** and **S2**. Neither age nor gender varied significantly between the studied groups.

3.2 Genotype Distribution and Allele Frequencies of EpCAM rs62139665 Polymorphism in the Studied Groups, and Compliance With Hardy-Weinberg Equilibrium

The genotype frequencies in the control, HCV and HCC groups were in agreement with the assumption of a Hardy–Weinberg equilibrium ($P > 0.05$) as displayed in **Table 2**.

Table 3 and **Figure 1** illustrate the genotype and allele frequencies of EpCAM rs62139665 polymorphism. The GG genotype and G allele frequencies were significantly higher in the HCC group compared to the HCV patients ($P = 0.0005$ and $P < 0.0001$, respectively) and to the control subjects ($P = 0.04$ and $P = 0.001$, respectively), while no significant difference was found between HCV and control groups. According to the genetic model selection strategy (27), a recessive model was chosen as it best fits the analysis of the association between rs62139665 and HCC risk. **Table 4** depicts the association of rs62139665 with HCV and HCC. In HCC cases, the rs62139665 GG genotype carriers displayed a markedly higher distribution than GC+CC genotype carriers relative to the control (OR = 2.86, $P = 0.003$) and HCV (OR = 2.66, $P = 0.004$) groups. Furthermore, the HCC cases exhibited an appreciably higher G allele frequency than in the control (OR = 1.76, $P = 0.002$), and HCV (OR = 2.02, $P = 0.0001$) groups.

The results reported herein accentuate a notable association between EpCAM rs62139665 SNP and HCC susceptibility in Egyptians. Nevertheless, EpCAM rs62139665 was not significantly linked with HCV risk in the tested sample.

3.3 Association of EpCAM rs62139665 Polymorphism With the Clinicopathological Features of HCC Patients

As for the clinicopathological variables, the GG genotype was significantly correlated with higher ALP activity compared to GC + CC genotypes ($P = 0.01$, **Table 5**). In addition, the Kaplan-Meier and log-rank survival tests showed insignificantly lower overall survival and survival time in EpCAM rs62139665 GG genotype carriers compared with GC + CC genotype carriers in

TABLE 2 | Hardy Weinberg equilibrium for EpCAM -935 C/G (rs62139665).

Group	Observed frequency			Expected frequency			*P*-value
Genotype	**CC**	**GC**	**GG**	**CC**	**GC**	**GG**	
Control	45	60	12	48.08	53.85	15.08	0.22
HCV	58	56	14	57.78	56.44	13.78	0.93
HCC	35	69	34	35	69	34	0.99

The Chi square test was used to determine deviation from Hardy-Weinberg equilibrium (HWE).

TABLE 3 | Frequency distribution for genotypes and alleles for EpCAM rs62139665 in patients and control groups.

	Control	HCV	HCC	
CC	45 (0.39)	58 (0.45)	35 (0.25)	
GC	60 (0.51)	56 (0.44)	69 (0.5)	
GG	12 (0.1)	14 (0.11)	34 (0.25)	
P-value	0.04†	0.48‡	0.0005§	0.0006¶
C	150 (0.64)	172 (0.67)	139 (0.51)	
G	84 (0.36)	84 (0.33)	137 (0.49)	
P-value	0.001†	0.47‡	<0.0001§	0.0001¶

Data are expressed as N (%).
†χ^2 *test for difference in the frequency in HCC vs control.*
‡χ^2 *test for difference in the frequency in HCV vs control.*
§χ^2 *test for difference in the frequency in HCC vs HCV.*
¶χ^2 *test for difference in the frequency in the study population.*

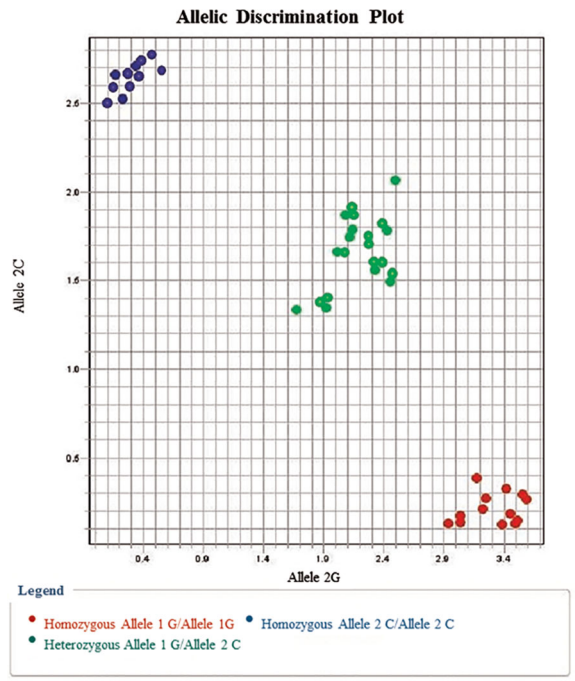

FIGURE 1 | Allelic discrimination plot for EpCAM rs62139665 G/C alleles showing the C/C genotype (represented by upper left dots) near the Y-axis, the G/G genotype (represented by lower right dots) near the X-axis, and the G/C genotype in the middle between both axes.

the HCC group. Moreover, the GC + CC genotype carriers exhibited non-significantly lower MELD score when compared with the GG genotype carriers (**Table 5** and **Figure 2**).

3.4 EpCAM Gene and Protein Expression Levels in the Studied Groups

As illustrated in **Table 6**, the expression of EpCAM at both the gene and protein levels was notably higher in HCV ($P < 0.0001$ and $P < 0.05$, respectively) and HCC ($P < 0.0001$) patients compared to the control group. Moreover, EpCAM protein expression level was appreciably higher in HCC than in HCV patients ($P < 0.0001$), whereas the gene expression level did not vary significantly between the two groups. Comparing the expression of EpCAM between rs62139665 genotypes, we observed a significant link between EpCAM rs62139665 polymorphism and its expression. The GG carriers exhibited significantly higher EpCAM gene and protein expression levels compared to the GC + CC carriers in each of the three studied groups ($P < 0.05$ and $P < 0.0001$ regarding gene and protein expression, respectively, within the control group; $P < 0.0001$ for both gene and protein expression within each of the HCV and HCC groups).

3.5 Serum AFP Level, Correlation With EpCAM Level, and ROC Analysis of Discriminatory Performance of AFP and EpCAM Individually and in Combination

Comparing the serum AFP levels in the three studied groups revealed markedly higher levels in the HCC group than in each of the control and HCV groups ($P < 0.0001$, **Table 1**). As illustrated in **Figure S1**, a strong positive correlation was observed between AFP and EpCAM protein levels (r = 0.99, $P < 0.0001$).

The ROC curves of EpCAM protein expression level depict significant discriminatory power between HCC patients and non-HCC subjects (AUC = 0.92, CI = 0.87-0.97, $P < 0.0001$), as shown in **Figure S2**, suggesting comparable diagnostic

TABLE 4 | Genotype and allele frequency of EpCAM -935 C/G polymorphism in different study groups and its association to HCV and HCC risk by logistic regression analysis.

	Genotype/Allele	Control (117) N(%)	HCV (128) N(%)	HCC (138) N(%)	OR† (95% CI)	*P*-Value†	OR‡ (95% CI)	*P*-Value‡	OR§ (95% CI)	*P*-Value§
Codominant	CC	45 (38.5%)	58 (45.3%)	35 (25.4%)	Ref		Ref		Ref	
	GC	60 (51.3%)	56 (43.8%)	69 (50%)	1.47 (0.84-2.59)	0.2	0.72 (0.42-1.23)	0.28	2.04 (1.18-3.53)	0.01
	GG	12 (10.2%)	14 (10.9%)	34 (24.6%)	3.64 (1.64-8.04)	0.001	0.9 (0.38-2.15)	0.83	4.02 (1.89-8.52)	0.0002
Dominant	GC + GG	72 (61.5)	70 (54.7%)	103 (74.6%)	1.84 (1.07-3.14)	0.03	0.75 (0.45-1.25)	0.3	2.43 (1.45-4.09)	0.0008
Recessive	GC + CC	105 (89.7%)	114 (89.1%)	104 (75.4%)	2.86 (1.4-5.83)	0.003	1.07 (0.47-2.43)	1	2.66 (1.35-5.23)	0.004
Overdominant	CC+GG	57 (48.7%)	72 (56.2%)	69 (50%)	1.05 (0.64-1.72)	0.9	1.35 (0.81-2.24)	0.25	0.78 (0.47-1.26)	0.32
Alleles	C	150 (64.1%)	172 (67.2%)	139 (50.4%)	Ref		Ref		Ref	
	G	84 (35.9%)	84 (32.8%)	137 (49.6%)	1.76 (1.23-2.51)	0.002	0.87 (0.6-1.26)	0.5	2.02 (1.41-2.86)	0.0001

The odds ratios (ORs) and confidence intervals (CIs) of 95 percent were estimated by logistic regression for association analysis.
†HCC vs Control.
‡HCV vs Control.
§HCC vs HCV.
HCC, hepatocellular carcinoma; HCV, hepatitis C virus; OR, odds ratio.

TABLE 5 | The associations of the biochemical parameters and the EpCAM -935 C/G polymorphism in HCC patients.

Genotype/Parameter	GC + CC (n = 104)	GG (n = 34)	*P*-Value
Hemoglobin	12.57 ± 1.58	12.67 ± 1.93	0.75
WBCs (x10^3)	5.82 ± 1.99	5.45 ± 2.62	0.39
Platelets (x10^3)	142 ± 65.18	128.3 ± 65.54	0.27
PC (%)	77.42 ± 13.61	75.16 ± 11.23	0.38
PT-INR	1.23 ± 0.21	1.26 ± 0.14	0.37
D Bil (mg/dl)	0.5 ± 0.37	0.54 ± 0.27	0.58
T Bil (mg/dl)	1.21 ± 0.6	1.27 ± 0.58	0.6
ALT (U/L)	56.42 ± 34.97	67.82 ± 38.81	0.11
AST (U/L)	67.45 ± 38.25	67.73 ± 33.78	0.59
ALP (U/L)	173.7 ± 56.29	205 ± 60.56	0.01*
Albumin (g/dl)	3.33 ± 0.56	3.46 ± 0.39	0.23
Creatinine (mg/dl)	0.86 ± 0.23	0.86 ± 0.19	0.99
Survival period (months)	15.31 ± 9.15	13.03 ± 8.87	0.22
MELD score	9 (6-11)	10 (6-15)	0.2
Child–Pugh score	***A* (n=68); *B* (n=30); *C* (n=6)**	***A* (n=25); *B* (n=9); *C* (n=0)**	0.32
AFP (ng/ml)	238.4 ± 430	1947 ± 2445	<0.0001*

Data are expressed as mean ± SD or median (interquartile range), P < 0.05 was significant. Data were compared using Student's t-test for parametric tests, Mann-Whitney test for non-parametric tests and Chi square test for categorical variables.

WBCs, white blood cells; PC, prothrombin concentration; PT-INR, prothrombin time-international normalized ratios; D Bil, direct bilirubin; T Bil, total bilirubin; ALT, alanine aminotransferase; AST, aspartate aminotransferase; ALP, alkaline phosphatase; MELD, model for end-stage liver disease; A, B and C, Child-Pugh grades A (5 to 6 points, B (7 to 9 points) and C (10 to 15 points) according to the criteria indicated by Child and Turcotte (26); AFP, alpha-fetoprotein.

accuracy to that of AFP (AUC = 0.961, CI = 0.92-0.99, $P < 0.0001$). Combining AFP and EpCAM led to an improved diagnostic accuracy than that of either AFP or EpCAM alone (AUC = 0.99, CI = 0.95-1, $P < 0.0001$).

3.6 Corroboration of EpCAM rs62139665 Genotyping Findings by Sanger Sequencing

Upon comparing the findings of EpCAM rs62139665 genotyping obtained by allelic discrimination with those of Sanger sequencing, both outcomes were perfectly matched for all the genotypes in the tested samples (**Figure 3**).

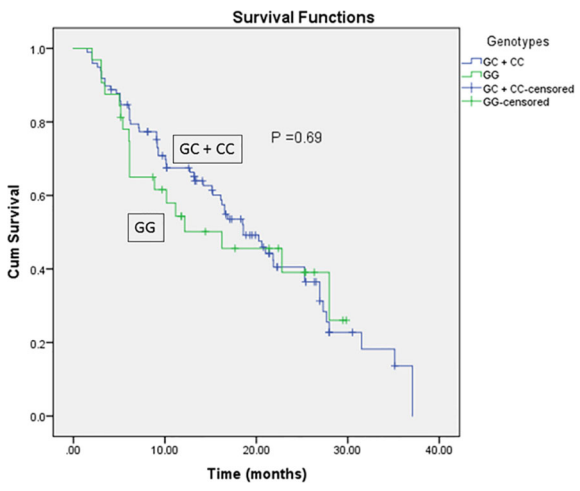

FIGURE 2 | Kaplan-Meier and Log-rank survival curves for HCC patients in relation to EpCAM rs62139665 genotypes in a recessive model.

4 DISCUSSION

Worldwide, Egypt endures the highest incidence of HCV infection that is considered a main predisposing factor for the progression of HCC. This investigation was undertaken to explore the association of -935 C/G (rs62139665) SNP in the promoter region of EpCAM with the risk of HCV-related HCC, EpCAM expression levels and the OS in the Egyptian population.

The present investigation demonstrates, for the first time, the association of EpCAM rs62139665 with HCC risk. rs62139665 is located at 935 upstream in the promoter region and it was reported that the transcriptional activity of 1.1kb upstream of the EpCAM gene is closely associated with the levels of EpCAM 28. Mutations in the EpCAM gene were reported in patients having Lynch syndrome through deletions in the 3'UTR 29 or congenital tufting enteropathy that results in decreasing EpCAM protein level (28).

In the current study, we adopted the allelic discrimination method to examine -935 C/G gene polymorphism (rs62139665) in the promoter region of EpCAM, and we, thereafter, verified the results by direct DNA sequencing. The genotype distribution in the three studied groups agreed with HWE.

It is worthy to note that there is a variation in the incidence of EpCAM rs62139665 SNP that is related to ethnicity, as reported in the NCBI map database for diverse ethnic populations, revealing C and G allele frequencies of C = 0.16 and **G** = 0.83 in African Carribbeans, C = 0.17 and **G** = 0.83 in Han Chinese and **C** = 0.64 and G = 0.36 in Toscani in Italia. The EpCAM rs62139665 C and G allele frequencies disclosed herein in the control group were 0.64 and 0.36, respectively, which are quite in accordance with those reported in the Toscani Italian population, having the C allele as the major allele.

The SNP rs62139665 distribution was significantly different between HCC patients and non-HCC subjects at both genotype and allelic levels. The EpCAM GG genotype and G allele were

TABLE 6 | Gene and protein expression levels of EpCAM in different genotypes of rs62139665.

Groups	Genotype	Gene expression levels		Protein expression levels	
Control	**GG**	2.71 ± 0.42	3.28 ± 0.75	362.8 ± 17.59	281.2 ± 75.3
	GC + CC	3.85 ± 0.54§*		247.2 ± 62.54§**	
HCV	**GG**	1.01 ± 0.21	1.66 ± 0.74†**	819.7 ± 84.05	440.8 ± 247.6†*
	GC + CC	2.08 ± 0.66§**		356.7 ± 183.4§**	
HCC	**GG**	0.95 ± 0.35	1.59 ± 0.56†**	1046 ± 115.1	798.5 ± 243.2†**‡**
	GC + CC	1.95 ± 0.24§**		637.6 ± 148.4§**	

EpCAM gene expression is expressed as ΔCt mean ± SD, where ΔCt = Ct value of EpCAM - Ct value of β-actin; a smaller ΔCt value corresponds to a higher gene expression level.
EpCAM protein expression is expressed as mean ± SD.
The data were analyzed using Student's t-test for comparing 2 groups and one-way ANOVA followed by Tukey's multiple comparisons test for comparing the three studied groups.
†Significant difference from the control group.
‡Significant difference from the HCV group.
§Significant difference from GG within the same group.
**Significant at P < 0.05.*
***Significant at P < 0.0001.*

significantly more frequent in HCC patients than in HCV patients and controls, proposing that the presence of the C allele may have protective effects. By using logistic regression analyses, we found a significant association between HCC risk and the rs62139665 G allele and GG genotype when compared to GC + CC in a recessive model. This association with HCC risk can be explained and evidenced by the significant up-regulatory effect of the GG genotype on EpCAM gene and protein expression levels observed in the present study. Numerous studies showed that SNPs in the promoter region are related to increased gene expression (22, 29, 30).

The HCV group displayed significantly higher gene and protein expression of EpCAM compared to the control group despite the lack of significant difference in rs62139665 genotype and allele frequencies between the two groups. The higher expression of EpCAM observed in the HCV group compared to the control could be linked to the reported HCV-induced elevation of plasminogen activator inhibitor-1 (PAI-1). Increased expression of PAI-1 subsequent to HCV infection promoted the cancer stem-like cells (CSC) state in HCV-infected hepatocytes through the activation of the chief mediator of cell proliferation, protein kinase B, in consort with the increased expression of the CSC marker, EpCAM (31).

Several studies reported the role of EPCAM gene in HCC pathogenesis, as a prognostic marker and in HCC recurrence (32–35). Yet, referring to the TCGA and GEO databases (data compared by GEO2R), it was found that EPCAM gene showed non-significant increase in expression in HCC samples compared to their normal controls (GSE49515), and in HCC patients with and without venous metastasis (GSE5093).

Former studies reported significant association of EpCAM expression in HCC with high tumor grade and AFP level (36, 37). In our current study, the expression levels of AFP and EpCAM were significantly higher in the HCC group relative to the HCV and control groups. Furthermore, a positive correlation was found between AFP and EpCAM protein levels. These results are in line with other published data that also reported the overexpression of EpCAM in cirrhotic and liver tumor tissues compared to normal tissues (38). In addition, AFP level can predict the expression of hepatic progenitor cell markers as EpCAM in HCC (39) and is correlated with tumor metastasis (40). ROC analysis was conducted in the present study to compare the diagnostic performance of AFP and EpCAM. It showed that a combined model of both AFP and EPCAM had a higher specificity than either of them alone at all levels of sensitivity. Previously, AFP^{+}/

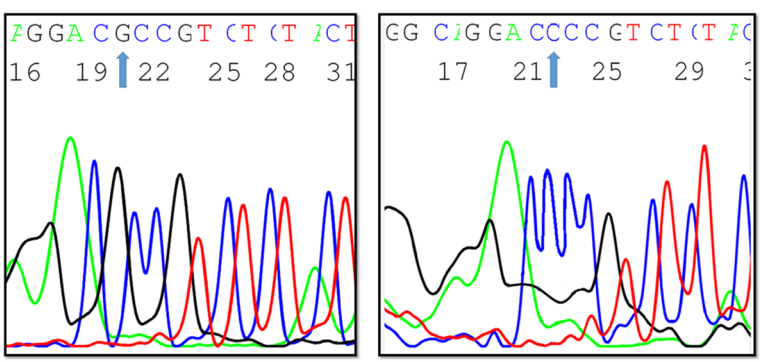

FIGURE 3 | A Sanger sequencing chromatogram depicting EpCAM -935 C/G variants (created by ABI Genetic Analyzer).

$EpCAM^+$ HCC was characterized by poorer prognosis compared to $AFP^-/EpCAM^-$ HCC (35).

By examining the influence of the SNP rs62139665 on the disease outcomes, through correlating the SNP rs62139665 genotypes with several parameters as liver function tests, a significant correlation was detected only between GG genotype frequency, hence high EpCAM expression, and ALP activity. Such association may be attributed to ALP being an embryonic stem cell marker that has been observed during cell reprogramming (41). Furthermore, the inhibition of EpCAM expression resulted in diminished ALP activity (42).

Both OS and the survival period of rs62139665 GG genotype carriers were shorter compared with the GC + CC genotype carriers in HCC patients but did not reach statistical significance. Given the overexpression of EpCAM observed in GG genotype carriers compared to GC + CC genotype carriers, our finding of apparently shorter OS in GG genotype carriers compared with the GC + CC genotype carriers is in accordance with Noh and co-workers' suggestion that patients with positive immunohistochemical expression of EpCAM had reduced OS compared to those who were EpCAM-negative after undergoing surgical resection for HCC (43). Moreover, the detection of EpCAM-positive circulating tumor cells is strongly correlated with the clinical outcome and OS in patients with HCC (39).

In the current study, the MELD score showed no significant difference between GC + CC and GG genotype carriers. Our observation seems to be in agreement with Sancho-Bru and co-workers' report of lack of correlation between EpCAM gene expression and MELD score in patients with alcoholic hepatitis (44). On the other hand, patients with liver cirrhosis who were infused with EpCAM-positive stem cells showed a significant decrease in MELD score and a marked clinical improvement.

In conclusion, the present study accentuates the association of EpCAM rs62139665 SNP, specifically the G allele frequency, with HCC risk. However, no such association was found with HCV infection in the tested sample of Egyptians. In addition, the present findings highlight the association of the rs62139665 GG genotype with increased EpCAM expression at both the gene and protein levels. Further research on larger datasets, other ethnicities and other cancer types are warranted for a comprehensive elucidation of the associations of EpCAM -935 C/G polymorphism with cancer risk.

DATA AVAILABILITY STATEMENT

The datasets presented in this study can be found in online repositories. The name of the repository and accession numbers can be found below: National Center for Biotechnology Information (NCBI) GenBank, https://www.ncbi.nlm.nih.gov/genbank/, MZ826468, MZ826469, MZ826470 and MZ826471.

ETHICS STATEMENT

The studies involving human participants were reviewed and approved by The Research Ethics Committee, Faculty of Pharmacy, Cairo University (Permit number: BC 1813). The patients/participants provided their written informed consent to participate in this study.

AUTHOR CONTRIBUTIONS

TM and NAHS conceived, designed and coordinated the study and revised the manuscript. DS collected the samples and participated in the experimental design and lab work. SF carried out the lab work and the statistical analyses and drafted the manuscript. NNS participated in the experimental design, data analysis and curation, and revised and edited the manuscript. All authors contributed to the article and approved the submitted version.

FUNDING

The present work has been partially funded by the Faculty of Pharmacy, Cairo University (Cairo, Egypt).

SUPPLEMENTARY MATERIAL

The Supplementary Material for this article can be found online at: https://www.frontiersin.org/articles/10.3389/fonc.2021.754104/full#supplementary-material

REFERENCES

1. Polaris Observatory HCV Collaborators. Global Prevalence and Genotype Distribution of Hepatitis C Virus Infection in 2015: A Modelling Study. *Lancet Gastroenterol Hepatol* (2017) 2:161–76. doi: 10.1016/S2468-1253(16)30181-9
2. Bray F, Ferlay J, Soerjomataram I, Siegel RL, Torre LA, Jemal A. Global Cancer Statistics 2018: GLOBOCAN Estimates of Incidence and Mortality Worldwide for 36 Cancers in 185 Countries. *CA Cancer J Clin* (2018) 68:394–424. doi: 10.3322/caac.21492
3. Wang X, Zhang A, Sun H. Power of Metabolomics in Diagnosis and Biomarker Discovery of Hepatocellular Carcinoma. *Hepatology* (2013) 57:2072–7. doi: 10.1002/hep.26130
4. Gomaa A, Allam N, Elsharkawy A, El Kassas M, Waked I. Hepatitis C Infection in Egypt: Prevalence, Impact and Management Strategies. *Hepat Med* (2017) 9:17–25. doi: 10.2147/HMER.S113681
5. Lewis S, Roayaie S, Ward SC, Shyknevsky I, Jibara G, Taouli B. Hepatocellular Carcinoma in Chronic Hepatitis C in the Absence of Advanced Fibrosis or Cirrhosis. *AJR Am J Roentgenol* (2013) 200:W610–6. doi: 10.2214/AJR.12.9151
6. Liu M, Jiang L, Guan X-Y. The Genetic and Epigenetic Alterations in Human Hepatocellular Carcinoma: A Recent Update. *Protein Cell* (2014) 5:673–91. doi: 10.1007/s13238-014-0065-9
7. Dragani TA. Risk of HCC: Genetic Heterogeneity and Complex Genetics. *J Hepatol* (2010) 52:252–7. doi: 10.1016/j.jhep.2009.11.015
8. Bomken S, Fiser K, Heidenreich O, Vormoor J. Understanding the Cancer Stem Cell. *Br J Cancer* (2010) 103:439–45. doi: 10.1038/sj.bjc.6605821

9. Visvader JE. Cells of Origin in Cancer. *Nature* (2011) 469:314–22. doi: 10.1038/nature09781
10. Pajonk F, Vlashi E, McBride WH. Radiation Resistance of Cancer Stem Cells: The 4 R's of Radiobiology Revisited. *Stem Cells* (2010) 28:639–48. doi: 10.1002/stem.318
11. Zhao J. Cancer Stem Cells and Chemoresistance: The Smartest Survives the Raid. *Pharmacol Ther* (2016) 160:145–58. doi: 10.1016/j.pharmthera.2016.02.008
12. Went P, Vasei M, Bubendorf L, Terracciano L, Tornillo L, Riede U, et al. Frequent High-Level Expression of the Immunotherapeutic Target Ep-CAM in Colon, Stomach, Prostate and Lung Cancers. *Br J Cancer* (2006) 94:128–35. doi: 10.1038/sj.bjc.6602924
13. Terris B, Cavard C, Perret C. EpCAM, a New Marker for Cancer Stem Cells in Hepatocellular Carcinoma. *J Hepatol* (2010) 52:280–1. doi: 10.1016/j.jhep.2009.10.026
14. Gires O. EpCAM in Hepatocytes and Their Progenitors. *J Hepatol* (2012) 56:490–2. doi: 10.1016/j.jhep.2011.05.036
15. Ko C-J, Li C-J, Wu M-Y, Chu P-Y. Overexpression of Epithelial Cell Adhesion Molecule as a Predictor of Poor Outcome in Patients With Hepatocellular Carcinoma. *Exp Ther Med* (2018) 16:4810–6. doi: 10.3892/etm.2018.6794
16. Matsumoto T, Takai A, Eso Y, Kinoshita K, Manabe T, Seno H, et al. Proliferating EpCAM-Positive Ductal Cells in the Inflamed Liver Give Rise to Hepatocellular Carcinoma. *Cancer Res* (2017) 77:6131–43. doi: 10.1158/0008-5472.CAN-17-1800
17. Wang M-H, Sun R, Zhou X-M, Zhang M-Y, Lu J-B, Yang Y, et al. Epithelial Cell Adhesion Molecule Overexpression Regulates Epithelial-Mesenchymal Transition, Stemness and Metastasis of Nasopharyngeal Carcinoma Cells *via* the PTEN/AKT/mTOR Pathway. *Cell Death Dis* (2018) 9:2. doi: 10.1038/s41419-017-0013-8
18. Fako V, Yu Z, Henrich CJ, Ransom T, Budhu AS, Wang XW. Inhibition of Wnt/β-Catenin Signaling in Hepatocellular Carcinoma by an Antipsychotic Drug Pimozide. *Int J Biol Sci* (2016) 12:768–75. doi: 10.7150/ijbs.14718
19. Yu X, Ge N, Guo X, Shen S, Liang J, Huang X, et al. Genetic Variants in the EPCAM Gene is Associated With the Prognosis of Transarterial Chemoembolization Treated Hepatocellular Carcinoma With Portal Vein Tumor Thrombus. *PloS One* (2014) 9:e93416. doi: 10.1371/journal.pone.0093416
20. Shoemaker R, Deng J, Wang W, Zhang K. Allele-Specific Methylation is Prevalent and is Contributed by CpG-SNPs in the Human Genome. *Genome Res* (2010) 20:883–9. doi: 10.1101/gr.104695.109
21. Zhang X, Miao X, Tan W, Ning B, Liu Z, Hong Y, et al. Identification of Functional Genetic Variants in Cyclooxygenase-2 and Their Association With Risk of Esophageal Cancer. *Gastroenterology* (2005) 129:565–76. doi: 10.1016/j.gastro.2005.05.003
22. Motawi TMK, Sadik NAH, Sabry D, Shahin NN, Fahim SA. rs2267531, A Promoter SNP Within Glypican-3 Gene in the X Chromosome, Is Associated With Hepatocellular Carcinoma in Egyptians. *Sci Rep* (2019) 9:6868. doi: 10.1038/s41598-019-43376-3
23. Yang Y, Fei F, Song Y, Li X, Zhang Z, Fei Z, et al. Polymorphisms of EpCAM Gene and Prognosis for non-Small-Cell Lung Cancer in Han Chinese. *Cancer Sci* (2014) 105:89–96. doi: 10.1111/cas.12318
24. Hu M, Jian L, Zhang L, Zheng J, You Y, Deng J, et al. Functional Polymorphism in the EpCAM Gene is Associated With Occurrence and Advanced Disease Status of Cervical Cancer in Chinese Population. *Mol Biol Rep* (2012) 39:7303–9. doi: 10.1007/s11033-012-1560-9
25. Jiang L, Zhang C, Li Y, Yu X, Zheng J, Zou P, et al. Zhou Y. A non-Synonymous Polymorphism Thr115Met in the EpCAM Gene is Associated With an Increased Risk of Breast Cancer in Chinese Population. *Breast Cancer Res Treat* (2011) 126:487–95. doi: 10.1007/s10549-010-1094-6
26. Child CG, Turcotte JG. The Liver and Portal Hypertension, in: *Surgery and Portal Hypertension* . Saunders, Philadelphia. Available at: https://www.scirp.org/(S(i43dyn45teexjx455qlt3d2q))/reference/ReferencesPapers.aspx?ReferenceID=1127082 (Accessed July 24, 2020).
27. Horita N, Kaneko T. Genetic Model Selection for a Case-Control Study and a Meta-Analysis. *Meta Gene* (2015) 5:1–8. doi: 10.1016/j.mgene.2015.04.003
28. Sivagnanam M, Schaible T, Szigeti R, Byrd RH, Finegold MJ, Ranganathan S, et al. Further Evidence for EpCAM as the Gene for Congenital Tufting Enteropathy. *Am J Med Genet A* (2010) 152A:222–4. doi: 10.1002/ajmg.a.33186
29. Li Y, Wang J, Jiang F, Lin W, Meng W. Association of Polymorphisms in Survivin Gene With the Risk of Hepatocellular Carcinoma in Chinese Han Population: A Case Control Study. *BMC Med Genet* (2012) 13:1. doi: 10.1186/1471-2350-13-1
30. Buckland PR, Hoogendoorn B, Guy CA, Coleman SL, Smith SK, Buxbaum JD, et al. A High Proportion of Polymorphisms in the Promoters of Brain Expressed Genes Influences Transcriptional Activity. *Biochim Biophys Acta* (2004) 1690:238–49. doi: 10.1016/j.bbadis.2004.06.023
31. Nam D, Angelucci A, Choi D, Leigh A, Seong HC, Hahn YS. Elevation of Plasminogen Activator Inhibitor-1 Promotes Differentiation of Cancer Stem-Like Cell State by Hepatitis C Virus Infection. *J Virol* (2021) 95:e02057–20. doi: 10.1128/JVI.02057-20
32. Li Y, Farmer RW, Yang Y, Martin RCG. Epithelial Cell Adhesion Molecule in Human Hepatocellular Carcinoma Cell Lines: A Target of Chemoresistence. *BMC Cancer 2016 161* (2016) 16:1–10. doi: 10.1186/S12885-016-2252-Y
33. Krause J, von Felden J, Casar C, Fründt TW, Galaski J, Schmidt C, et al. Hepatocellular Carcinoma: Intratumoral EpCAM-Positive Cancer Stem Cell Heterogeneity Identifies High-Risk Tumor Subtype. *BMC Cancer 2020 201* (2020) 20:1–12. doi: 10.1186/S12885-020-07580-Z
34. Yamashita T, Ji J, Budhu A, Forgues M, Yang W, Wang HY, et al. EpCAM-Positive Hepatocellular Carcinoma Cells Are Tumor-Initiating Cells With Stem/Progenitor Cell Features. *Gastroenterology* (2009) 136:1012–24. doi: 10.1053/j.gastro.2008.12.004
35. Yamashita T, Forgues M, Wang W, Kim JW, Ye Q, Jia H, et al. EpCAM and Alpha-Fetoprotein Expression Defines Novel Prognostic Subtypes of Hepatocellular Carcinoma. *Cancer Res* (2008) 68:1451–61. doi: 10.1158/0008-5472.CAN-07-6013
36. Bae JS, Noh SJ, Jang KY, Park HS, Chung MJ, Park CK, et al. Expression and Role of Epithelial Cell Adhesion Molecule in Dysplastic Nodule and Hepatocellular Carcinoma. *Int J Oncol* (2012) 41:2150–8. doi: 10.3892/ijo.2012.1631
37. Lima L do P, Machado CJ, Rodrigues JBSR, Vasconcellos L de S, Junior EP, Vidigal PVT, et al. Immunohistochemical Coexpression of Epithelial Cell Adhesion Molecule and Alpha-Fetoprotein in Hepatocellular Carcinoma. *Can J Gastroenterol Hepatol* (2018) 2018:5970852. doi: 10.1155/2018/5970852
38. Behnke MK, Reimers M, Fisher RA. Stem Cell and Hepatocyte Proliferation in Hepatitis C Cirrhosis and Hepatocellular Carcinoma: Transplant Implications. *Ann Hepatol* (2013) 13:45–53. doi: 10.1016/S1665-2681(19)30903-2
39. Seino S, Tsuchiya A, Watanabe Y, Kawata Y, Kojima Y, Ikarashi S, et al. Clinical Outcome of Hepatocellular Carcinoma can be Predicted by the Expression of Hepatic Progenitor Cell Markers and Serum Tumour Markers. *Oncotarget* (2018) 9:21844–60. doi: 10.18632/oncotarget.25074
40. Lu Y, Zhu M, Li W, Lin B, Dong X, Chen Y, et al. Alpha Fetoprotein Plays a Critical Role in Promoting Metastasis of Hepatocellular Carcinoma Cells. *J Cell Mol Med* (2016) 20:549–58. doi: 10.1111/jcmm.12745
41. Chen H-F, Chuang C-Y, Lee W-C, Huang H-P, Wu H-C, Ho H-N, et al. Surface Marker Epithelial Cell Adhesion Molecule and E-Cadherin Facilitate the Identification and Selection of Induced Pluripotent Stem Cells. *Stem Cell Rev Rep* (2011) 7:722–35. doi: 10.1007/s12015-011-9233-y
42. González B, Denzel S, Mack B, Conrad M, Gires O. EpCAM is Involved in Maintenance of the Murine Embryonic Stem Cell Phenotype. *Stem Cells* (2009) 27:1782–91. doi: 10.1002/stem.97
43. Noh C-K, Wang HJ, Kim CM, Kim J, Yoon SY, Lee GH, et al. EpCAM as a Predictive Marker of Tumor Recurrence and Survival in Patients Who Underwent Surgical Resection for Hepatocellular Carcinoma. *Anticancer Res* (2018) 38:4101–9. doi: 10.21873/anticanres.12700
44. Sancho-Bru P, Altamirano J, Rodrigo-Torres D, Coll M, Millán C, José Lozano J, et al. Liver Progenitor Cell Markers Correlate With Liver Damage and Predict Short-Term Mortality in Patients With Alcoholic Hepatitis. *Hepatology* (2012) 55:1931–41. doi: 10.1002/hep.25614

Conflict of Interest: The authors declare that the research was conducted in the absence of any commercial or financial relationships that could be construed as a potential conflict of interest.

this article, or claim that may be made by its manufacturer, is not guaranteed or endorsed by the publisher.

frontiers in Oncology

ORIGINAL RESEARCH
published: 11 January 2022
doi: 10.3389/fonc.2021.801506

ASF1B Serves as a Potential Therapeutic Target by Influencing Cell Cycle and Proliferation in Hepatocellular Carcinoma

Xiaoxi Ouyang†, Longxian Lv†, Yalei Zhao, Fen Zhang, Qingqing Hu, Zuhong Li, Danhua Zhu and Lanjuan Li**

State Key Laboratory for Diagnosis and Treatment of Infectious Diseases, National Clinical Research Centre for Infectious Diseases, Collaborative Innovation Centre for Diagnosis and Treatment of Infectious Diseases, The First Affiliated Hospital, Zhejiang University School of Medicine, Hangzhou, China

OPEN ACCESS

Edited by:
Jiang Chen,
Zhejiang University, China

Reviewed by:
Wenjie Zheng,
Affiliated Hospital of Nantong University, China
Xiabo Cai,
Shanghai First People's Hospital, China
Huapeng Zhang,
First Affiliated Hospital of Zhengzhou University, China

***Correspondence:**
Danhua Zhu
zhudanhua@zju.edu.cn
Lanjuan Li
ljli@zju.edu.cn

†These authors share first authorship

Specialty section:
This article was submitted to Gastrointestinal Cancers: Hepato Pancreatic Biliary Cancers, a section of the journal Frontiers in Oncology

Received: *09 November 2021*
Accepted: *20 December 2021*
Published: *11 January 2022*

Citation:
Ouyang X, Lv L, Zhao Y, Zhang F, Hu Q, Li Z, Zhu D and Li L (2022) ASF1B Serves as a Potential Therapeutic Target by Influencing Cell Cycle and Proliferation in Hepatocellular Carcinoma. Front. Oncol. 11:801506. doi: 10.3389/fonc.2021.801506

Hepatocellular carcinoma (HCC) is one of the most common malignant tumors with high morbidity and mortality. Therefore, it is very important to find potential biomarkers that can effectively predict the prognosis and progression of HCC. Recent studies have shown that anti-silencing function 1B (ASF1B) may be a new proliferative marker for tumor diagnosis and prognosis. However, the expression and function of ASF1B in hepatocellular carcinoma remain to be determined. In this study, integrated analysis of the Cancer Genome Atlas (TCGA), genotypic tissue expression (GTEx), and Gene Expression Omnibus (GEO) databases revealed that ASF1B was highly expressed in HCC. Kaplan-Meier survival curve showed that elevated ASF1B expression was associated with poor survival in patients with liver cancer. Correlation analysis of immune infiltration suggested that ASF1B expression was significantly correlated with immune cell infiltration in HCC patients. Gene set enrichment analysis (GSEA) indicated that ASF1B regulated the cell cycle, DNA Replication and oocyte meiosis signaling. Our experiments confirmed that ASF1B was highly expressed in HCC tissues and HCC cell lines. Silence of ASF1B inhibited hepatocellular carcinoma cell growth *in vitro*. Furthermore, ASF1B deficiency induced apoptosis and cell cycle arrest. Mechanistically, ASF1B knockdown reduced the expression of proliferating cell nuclear antigen (PCNA), cyclinB1, cyclinE2 and CDK9.Moreover, ASF1B interacted with CDK9 in HCC cells. Taken together, these results suggest that the oncogenic gene ASF1B could be a target for inhibiting hepatocellular carcinoma cell growth.

Keywords: ASF1B, histone chaperone, cell cycle, proliferation, HCC

INTRODUCTION

In global cancer statistics, the incidence of liver cancer ranks sixth and the mortality rate ranks third. In 2020, according to statistics, there are 905,677 new cases of liver cancer worldwide. It is estimated that by 2025, the incidence of liver cancer will exceed 1 million cases, which is a serious threat to human life and health (1–3). Hepatocellular carcinoma (HCC), also known as liver hepatocellular

carcinoma (LIHC), is responsible for 90% of all liver cancers (4). Although clinical HCC treatments, including surgery, interventional therapy, radiotherapy, chemotherapy and immunotherapy, are usually performed, have been significant improvements. However, due to the rapid proliferation, invasion and metastasis of HCC, treatments for patients with HCC are limited and not effective (5–8). Thus, there is an urgent need to identify and develop new molecular targets for hepatocellular carcinoma therapy.

Anti-silence function 1 (ASF1), a chaperone protein of histone H3-H4, plays an important role in DNA replication, DNA damage repair and transcriptional regulation (9, 10). In mammals, ASF1 consists of two homologous proteins, ASF1A and ASF1B. Previous findings indicated that the main function of ASF1A is DNA repair and cell senescence, while the main function of ASF1B is cell proliferation (11). Recently, an increasing number of studies have indicated that the dysregulated expression of ASF1B is associated with many cancer types, such as breast cancer, prostate cancer, cervical cancer, and clear cell renal cell carcinoma (11–14). Therefore, we infer that ASF1B may also be a dysfunctional mediator of HCC. However, the role of ASF1B in HCC remains largely unknown.

In this study, we investigated the expression and prognosis of ASF1B in patients with HCC in The Cancer Genome Atlas (TCGA) and various public databases. Moreover, we analyzed the coexpression genes of ASF1B to explore the potential mechanisms of ASF1B in HCC. Experiments were performed to verify the expression of ASF1B in HCC tissues and cell lines. ASF1B knockdown in HCC cell lines was induced to detect the biological behavior changes *in vitro*. Our data implied that ASF1B was closely associated with proliferation and migration in HCC cells and might be a novel prognostic indicator and therapeutic target in HCC patients.

MATERIALS AND METHODS

Dataset Analyses

We downloaded RNA-seq gene expression data and clinical records from the TCGA database (https://portal.gdc.cancer.gov/), with the GTEx data (https://gtexportal.org/) similarly being downloaded. GSE121248 and GSE33006 datasets was downloaded from Gene expression omnibus (GEO). Oncomine 4.5 database (https://www.oncomine.org/) and HCCDB database were also used in ASF1B expression analysis in pan-cancer and HCC.

In order to study the influence of ASF1B gene and clinical characteristics (such as age, sex, stage, etc.) on HCC prognosis, univariate and multivariate Cox regression analysis and forest map were used to display the p value, HR and 95% CI of each variable through "forestplot" R package. The Kaplan-Meier (KM) survival curve analysis is implemented by R software package "Survival" and "Survminer". Kaplan-Meier Plotter (http://kmplot.com) was used to generate survival curves, including overall survival (OS), progression-free survival (PFS), recurrence-free survival (RFS), and disease-specific survival (DSS), based on gene expression with the log-rank test and the Mantel-Cox test in liver cancer. TimeROC analysis (15–17) was performed to compare the prediction accuracy and risk score of ASF1B gene. The above R software versions are V4.0.3.

Tumor Immune Estimation Resource (TIMER) (https://cistrome.shinyapps.io/Timer) was used to analyze the relationship between ASF1B transcriptional level and immune cell infiltration in patients with HCC. Differentially expressed genes associated with transcription of the ASF1B gene in HCC were analyzed based on the LinkedOmics (http://www.linkedomics.org/login.php) functional module.

Tissues and Cell Lines

This study was approved by the Ethics Committee of the First Affiliated Hospital of Zhejiang University School of Medicine (NO. IIT20210360A), and all patients signed a formal informed consent. Six pairs of HCC and paracancerous tissue samples were obtained from patients who underwent hepatocellular carcinoma resection in the First Affiliated Hospital of Zhejiang University School of Medicine during 2017-2019, and none of them received preoperative radiotherapy or preoperative chemotherapy. All specimens were anonymized in accordance with ethical and legal standards. The MHCC97H cell line was purchased from Guangzhou Cellcook Biology Co., Ltd. (Cellcook, Guangzhou, China), while other cell lines, LO2, Hep3B, HepG2, and Huh7, were purchased from ATCC (ATCC, Manassas, USA).

Western Blot Analysis and Immunohistochemistry

Total protein was obtained with RIPA lysis buffer containing protease inhibitor (Sangon, Shanghai, China) (Genstar, Shenzhen, China), and the protein was quantified with a BCA kit (Biosharp, Anhui, China). The protein was quantified and then used to perform western blot as previously described (18). Antibodies against ASF1B, Cyclin B1, Cyclin E2, CDK9 and GAPDH were purchased from Cell Signaling Technology. The tumor tissue paraffin sections were harvested and treated as previously described (19). Immunohistochemistry primary antibody for anti-human ASF1B (1:300) was purchased from Abcam (#ab235358).

RNA Interference and Transfection

To ensure the inhibition efficiency of ASF1B expression by siRNA, three different ASF1B small interfering RNA were designed.siASF1B-1 (5'-AGGGAGACACAUGUUUGUCUU tt-3' forward, and 5'-AAGACAAACAUGUGUCUCCCU tt-3'reverse). siASF1B-2 (5'-CCUGGAGUGGAAGAUCAUUUA tt-3'forward, and 5' - UAAAUGAUCUUCCACUCCAGG tt-3'reverse). siASF1B-3 (5'-UUAGUUAGUAGGUAGACUUAG tt-3'forward, and 5'- CUAAGUCUACCUACUAACUAA tt-3'reverse) were obtained from Genomeditech Co. Ltd. (Genomeditech, Shanghai, China).And 50 nmol/L siRNA was transfected into MHCC97H or Hep3B cells using INTERFERin (Polyplus transfection, NewYork, USA) according to the manufacturer's protocol.

Reverse Transcription-Quantitative Polymerase Chain Reaction

Total RNA was isolated using RNA fast 2000 kit (Fastagen, Shanghai, China). Reverse transcription of RNA to cDNA was obtained using PrimeScript™ RT Master Mix (Takara,Shiga, Japan). qPCR was performed with QuantStudio 5 Detection System (ABI, Thermo Fisher) in a 10 μl reaction mixture containing SYBR GreenII. Expression of different genes were normalized to GAPDH and were analyzed using the 2−ΔΔCT method.

Cell Counting Kit-8 (CCK-8) Analysis and Cell Invasion Assay

Cell viability was analyzed using cell counting kit-8 (DOJINDO, Kyushu, Japan) according to the manufacturer's protocol. Briefly, MHCC97H and Hep3B were seeded in the 96-well plates with 5000 cells/well and incubated for overnight. At 24 h, 48 h, 72 h, and 120h, 10 μl CCK-8 solution was added to each well, and the cells were incubated for 90 min at 37°C. The absorbance at 450 nm was obtained using an IMARK microplate reader (BIO-RAD).

For cell invasion assay, Matrigel(BD Biosciences, San Jose, USA) was diluted 1:8 with cold serum-free DMEM at 4°C and 50μl was carefully used to coat polycarbonate filters (8 μm; Corning, NY, USA). Incubate at 37°C overnight. Next, 5×10^5 cells were seeded into the upper chamber with 200μl serum-free DMEM. 500μl DMEM with 10% FBS was added to the lower chamber. The cells were cultured at 37°C in a 5% CO2 hydrosphere atmosphere. After 24 hours, the upper chamber was fixed with paraformaldehyde and stained with 0.5% crystal violet. Non-invading cells were removed, and the cells on the lower surface were counted microscopically.

Flow Cytometry for Analysis of the Cell Cycle and Apoptosis

To perform cell cycle assays, $1{\times}10^6$ cells were washed with cold PBS. Cell pellets were suspended with 500μl PI working solution (DOJINDO, Kyushu, Japan), and incubated for 30min at 4°C of light protection. Then the cells were dispersed by vortex oscillation and incubated at 37°C of darkness for 30min. After vortex blending, the cells were filtered by nylon screen for flow cytometry analysis. Cell apoptosis analysis was performed with a FITC Annexin V Apoptosis Detection Kit (BD Biosciences, San Jose, USA) according to the manufacturer's protocol. In brief, after washing with cold PBS twice, the cells were resuspended in binding buffer. A total of 1×10^5 cells (100 μl) were transferred to the flow tube, and 5 μl of FITC Annexin V and 5 μl PI were added. After gentle vortexing and incubation for 15 min at room temperature in the dark, another 400 μl binding buffer was added and then analyzed by flow cytometry.

Protein–Protein Interaction Studies

For co-immunoprecipitation, we used an IP/Co-IP kit from Absin (Absin, Shanghai, China). Co-IP was conducted according to the manufacturer's protocol. Briefly, cells were lysed and incubated on ice, then centrifuged at 14000g for 10 minutes at 4°C. The supernatant was incubated with protein A/G agarose beads for pre-clean. Subsequently, it was immunoprecipitated with an antibody against ASF1B (CST, Boston, USA) or normal rabbit IgG (CST, Boston, USA) overnight at 4°C. Next day, the immunoprecipitated complexes were incubated with protein A/G agarose beads for 1 hour at 4°C. After incubation, the immunoprecipitated complexes were rinsed and analyzed by Western blotting. Input was used as positive control.

Statistical Analysis

Data were analyzed using R v 4.0.3. Wilcoxon tests were used to compare ASF1B expression levels in normal and tumor tissues, while Kruskal-Wallis tests were used to evaluate relationships between ASF1B expression and patient clinical stage. Kaplan-Meier curves were used to assess survival outcomes, and correlations were evaluated with Spearman's correlation coefficients. A two-sided $p < 0.05$ was the threshold of significance.

RESULTS

Elevated Expression of ASF1B in HCC

We used Oncomine to explore the expression levels of ASF1B in normal and various cancer tissues. The results showed that ASF1B was highly expressed in most tumors, and only a few tumors showed low expression (**Figure 1A**). Through the mining of GTEx and TCGA databases, we also found that ASF1B was highly expressed in a variety of tumors, including Cholangiocarcinoma (CHOL), Colon adenocarcinoma (COAD), Esophageal carcinoma (ESCA), Liver hepatocellular carcinoma (LIHC), Pancreatic adenocarcinoma (PADD), Rectum adenocarcinoma(READ), Stomach adenocarcinoma(STAD) (**Figure 1B**). By searching the reported studies, we found that the gene ASF1B was rarely studied in HCC. Therefore, we independently analyzed the expression of ASF1B in LIHC based on the downloaded TCGA data. ASF1B was significantly overexpressed in HCC, as in previous analyses of pan-cancer (**Figure 1C**). Analysis of 11 HCC study cohorts in the HCCDB database showed that mRNA levels of ASF1B in HCC tissues were significantly higher than those in adjacent normal tissues (**Figure 1D**). By analyzing GEO data GSE121248 and GSE33006, we also reached the conclusion that ASF1B was highly expressed in HCC (**Figure 1E**). Overall, our results indicated that ASF1B expression was significantly higher in liver cancer (LIHC) relative to normal tissues.

Evaluation of the Prognostic Relevance of ASF1B in HCC

We used univariate and multivariate cox regression analysis to analyze the relationship between ASF1B expression, clinical factors (such as age, sex, pT stage, pTNM stage, Grade) and OS in HCC patients. Univariate Cox analysis showed that ASF1B expression (*p*.value=0.00034), pT stage (*p*.value<0.0001), pTNM stage (*p*.value=0.00066) were significantly correlated with OS in HCC. ASF1B expression was also significant in multivariate cox

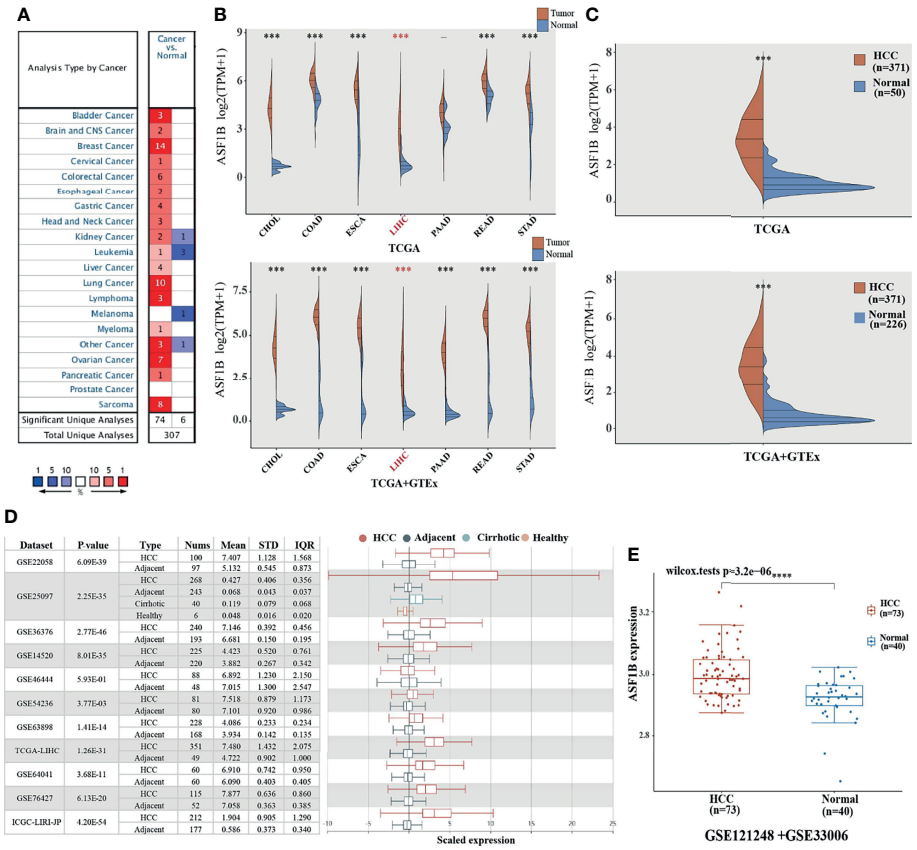

FIGURE 1 | The elevated expression of ASF1B in HCC. **(A, B)** The expression distribution of ASF1B in tumor tissues and normal tissues. **(C)** The expression level of ASF1B gene in HCC patients was up-regulated in TCGA database. **(D)** The transcription of ASF1B was significantly elevated in HCC tissues compared with adjacent normal tissues in HCCDB. **(E)** ASF1B mRNA levels in GE121248 and GSE33006 from GEO database. ***$p < 0.001$, ****$p < 0.0001$.

regression analysis (*p*.value=0.01942), suggesting that ASF1B may be an independent prognostic factor for HCC (**Figure 2A**). According to the results of COX analysis, Kaplan-Meier (KM) plot was used to analyze the overall survival probability of HCC patients with different ASF1B expression, pT stage, pTNM stage and Grade groups (**Figure 2B**). The median value of ASF1B was the cut-off point for ASF1B expression, according to which HCC patients are divided into high expression group and low expression group (**Figure 2F**). The analysis found that those with high ASF1B expression had significantly shorter overall survival. pT stage, pTNM stage and Grade groups' analysis also showed that the overall survival rate of HCC patients decreased with the progression of tumor stage and Grade. Next, we evaluated the relationship between ASF1B expression and HCC cohort survival outcomes based on the Liver Cancer RNA-seq database of Kaplan-Meier Plotter and plotted the Kaplan-Meier survival curve. The results showed that that those with high ASF1B expression had significantly shorter overall survival [OS, n=364, HR=1.71(1.21-2.42), log-rank P=0.002], progression-free survival (PFS, n=370, HR=1.72(1.26-2.35), log-rank P=0.00049), recurrence survival (RFS, n=316, HR=1.74(1.23-2.46), log-rank P =0.0015) and disease-specific survival (DSS, n=362, HR= 2.21 (1.4-3.51) compared with the low expression group in HCC (**Figure 2C**). Through analysis, we also found that the expression of ASF1B increased with the development of HCC grading and staging (**Figure 2D** and **Table 1**). It indicates that ASF1B can be a potential biomarker of HCC disease progression. In addition, timeROC analysis was performed to compare the predictive accuracy and risk score of ASF1B for HCC. It was found that ASF1B could well predict the prognosis of HCC patients at 1, 3 and 5 years, and its AUC under the ROC curve was 0.689, 0.621 and 0.617, respectively (**Figure 2E**). The above results suggest that ASF1B expression predicts adverse outcomes and is associated with disease stage progression in HCC patients.

Correlation of ASF1B Expression With Tumor Purity and Immune Infiltration Level in HCC

We used the TIMER network analysis platform to explore the relationship of ASF1B expression with the immune infiltration level in HCC. The correlation between the expression of ASF1B and the abundances of six immune infiltrates (B cells, CD4+ T cells, CD8+ T cells, neutrophils, macrophages, and dendritic cells) was estimated by purity-corrected partial Spearman's rho.

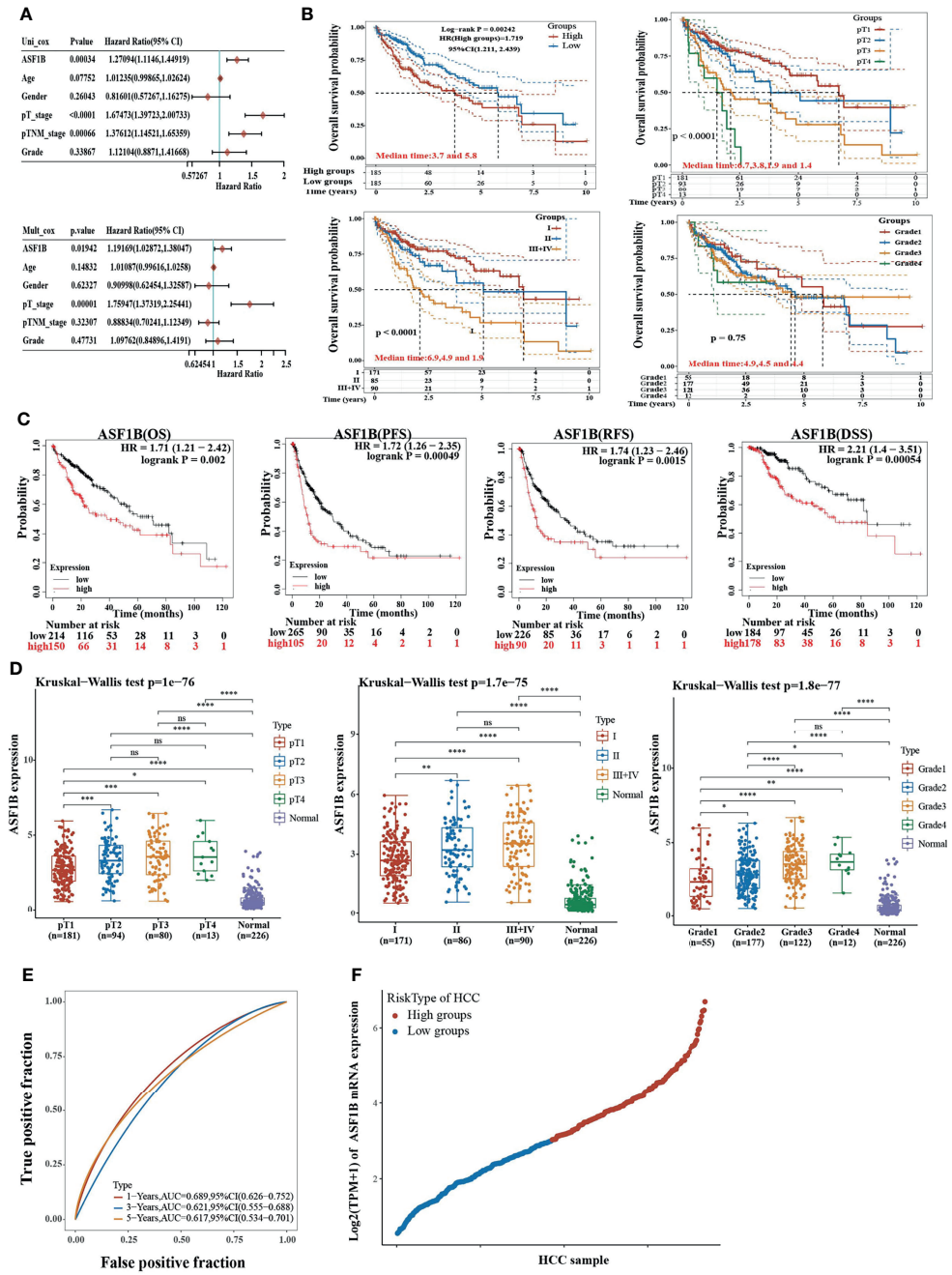

FIGURE 2 | High expression of ASF1B indicates poor survival in patients with HCC. **(A)** The forest plots showed that the risk factors for overall survival of HCC were analyzed by univariate and multivariate COX regression analysis. **(B)** Kaplan-Meier curves were used to analyze the relationship between ASF1B expression, pT stage, pTNM stage, Grade and OS in HCC patients. **(C)** Overall survival (OS), progression-free survival (PFS), relapse-free survival (RFS), and disease-specific survival (DSS) of ASF1B mRNA in the HCC cohort. **(D)** Correlation between ASF1B expression and tumor stage in HCC. **(E)** Time-dependent ROC analysis of ASF1B expression in HCC. **(F)** Scatter diagram of ASF1B mRNA expression from low to high. "ns" represents p≥0.05 *$p < 0.05$, **$p < 0.01$, ***$p < 0.001$, ****$p < 0.0001$.

We found a slightly positive correlation between ASF1B expression and tumor purity (r = 0.191, P = 3.41E-04). In addition, ASF1B expression was positively correlated with the abundance of all six immune infiltrates (**Figure 3A**). We also explored tumor infiltration levels among tumors with different somatic copy number alterations for ASF1B. ASF1B copy number variation (CNV) was significantly correlated with the infiltration levels of CD8+ T cells and macrophages (**Figure 3B**). To broaden our understanding of the interaction between ASF1B and immune genes, we also analyzed the correlation between ASF1B expression and relevant immune cell gene markers. After the correlation coefficients were adjusted by tumor purity, the

TABLE 1 | Relationship between ASF1B expression level and clinicopathological variables and in HCC patients.

	Characteristic	Total	ASF1B Expression		Statistics P
			High	Low	
Status	Alive	241	110	131	
	Dead	130	76	54	0.025
Age	Mean (SD)	59.4 (13.5)	58 (12.5)	60.9 (14.4)	
	Median [MIN, MAX]	61 [16,90]	59 [18,85]	64 [16,90]	0.043
Gender	FEMALE	121	72	49	
	MALE	250	114	136	0.016
Race	AMERICAN INDIAN	2	1	1	
	ASIAN	158	91	67	
	BLACK	17	8	9	
	WHITE	184	83	101	0.145
pT_stage	T1	181	70	111	
	T2	92	54	38	
	T2a	1	1		
	T2b	1	1		
	T3	45	30	15	
	T3a	29	18	11	
	T3b	6	3	3	
	T4	13	9	4	
	TX	1		1	0.001
pN_stage	N0	252	132	120	
	N1	4	3	1	
	NX	114	50	64	0.193
pM_stage	M0	266	141	125	
	M1	4	2	2	
	MX	101	43	58	0.203
pTNM_stage	I	171	67	104	
	II	86	49	37	
	III	3	2	1	
	IIIA	65	42	23	
	IIIB	8	6	2	
	IIIC	9	7	2	
	IV	2	1	1	
	IVB	1	1	1	
	IVA	2		1	0.005
Grade	G1	55	17	38	
	G2	177	76	101	
	G3	122	80	42	
	G4	12	10	2	0

results showed that the ASF1B expression level was significantly correlated with the majority of immune marker sets of various immune cells in HCC (**Table 2**). Of these, the top five gene markers were KIF11 (r=0.904), EXO1 (r=0.886), PRC1 (r=0.885), NUF2 (r=0.874) and CCNB1 (r=0.862). Survival analysis demonstrated that the high risk of ASF1B positively correlated marker genes and the low risk of ASF1B negatively correlated marker genes (**Table 2**).

Co-Expression Networks of ASF1B Indicate the Potential Function of ASF1B in HCC

To understand the biological significance of ASF1B in HCC, we used Linkedomics to analyze the co-expression network of ASF1B in the LIHC cohort. As shown in **Figure 4A**, 5,931 genes (dark red dots) were significantly positively correlated with ASF1B, while 3,077 genes (dark green dots) were significantly negatively correlated with ASF1B (false discovery rate, FDR < 0.01). The top 50 genes positively correlated with ASF1B expression and the top 50 genes negatively correlated with ASF1B expression are shown in the heat map (**Figure 4B**). The expression of ASF1B was strongly positively correlated with the expression of KIFC1 (positive rank #1, r = 0.883, p = 6.54E-120), KIF18B (r = 0.875, p = 2.85E-115) and KIF2C (r = 0.873, p = 4.71E-114). We analyzed the effect of the expression of the top 50 positively and negatively correlated genes on the overall survival of HCC. The top 50 positively correlated genes were highly likely to be high-risk genes for HCC, and all of them had a high hazard ratio (HR) (p <0.05). In contrast, the first 50 negatively correlated genes were most likely to be low-risk genes for HCC, all of which had lower HR values (p <0.05) (**Table 3**). These results further suggest that ASF1B may be related to the upregulation of HCC risk factors and downregulation of HCC protective factors and play a role in promoting the occurrence and development of HCC. Gene set enrichment analysis (GSEA) Gene Ontology (GO) term annotation showed that ASF1B co-expressed genes were mainly involved in DNA replication, chromosome segregation,

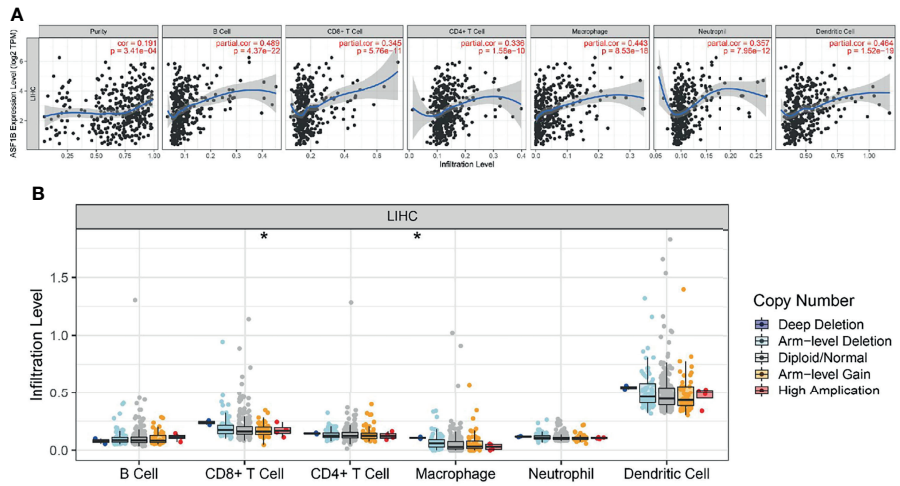

FIGURE 3 | Correlation analysis of the transcript of gene of ASF1B with the immune infiltration in HCC. **(A)** The expression of ASF1B was significantly positively correlated with tumor purity, the level of infiltration of CD8+ T cells, CD4+ T cells, macrophages, neutrophils, and dendritic cells in LIHC. **(B)** ASF1B copy number variation affects the infiltration level of CD8+ T cells, macrophages in HCC. *$p < 0.05$.

mitotic cell cycle phase transition, cell cycle G2/M phase transition and other processes (**Figure 4C**). However, activities such as fatty acid metabolic processes, peroxisome organization and acute inflammatory responses were inhibited. The Kyoto Encyclopedia of Genes and Genomes (KEGG) pathway analysis showed that co-expressed genes were mainly enriched in the cell cycle, DNA replication, oocyte meiosis and other pathways (**Figure 4C**). These results suggest that ASF1B has a wide range of effects on DNA replication and the cell cycle in HCC cells.

ASF1B Expression Was Upregulated in HCC Tissues and Stable Cell Lines

To investigate the role of ASF1B in HCC tumor progression, HCC tissue and corresponding adjacent tissue samples from 6 patients were tested by immunohistochemistry. As shown in **Figure 5A**, positive staining for ASF1B was stronger in HCC tissues than in adjacent tissues. 6 pairs of proteins from liver cancer and adjacent tissues for western blot verification and found that the expression of ASF1B protein was higher in liver cancer tissues than in adjacent normal tissues (**Figure 5B**). We also verified the protein expression of ASF1B in four hepatoma cell lines (Huh7, HepG2, MHCC97H, Hep3B), and the abundance of ASF1B protein was increased in cancer cells compared with immortalized LO2 human hepatocytes (**Figure 5C**).

ASF1B Knockdown Suppressed the Proliferation and Migration of HCC Cell Lines

According to the expression of ASF1B in HCC cells, we selected MHCC97H and Hep3B with relatively high expression of ASF1B

TABLE 2 | Correlation analysis between ASF1B and markers of immune cells in HCC.

Cell Types	Markers	Purity-Adjusted		Cell Types	Markers	Purity-Adjusted	
		Cor	*P*			Cor	*P*
B cell	**CD19**	0.361	0.000	**CD4+ T cell**	**AIM2**	0.409	0.000
	CD79A	0.289	0.000		**CCL4**	0.304	0.000
CD8+ T cell	**ADRM1**	0.424	0.000		**CCNB1**	0.862	0.000
	AHSA1	0.375	0.000		**EXO1**	0.886	0.000
	CD37	0.400	0.000		**KIF11**	0.904	0.000
	CD3D	0.380	0.000		**KNTC1**	0.833	0.000
	CD8A	0.323	0.000		**NUF2**	0.874	0.000
	CETN3	0.368	0.000		**PRC1**	0.885	0.000
	CSE1L	0.636	0.000		**RTKN2**	0.715	0.000
	IL2RB	0.371	0.000	**DC**	**HLA-DPB1**	0.317	0.000
	MPZL1	0.566	0.000		**HLA-DQB1**	0.272	0.000
macrophage	**IRF5**	0.413	0.000		**HLA-DRA**	0.311	0.000
NE	**ITGAM**	0.398	0.000		**HLA-DPA1**	0.285	0.000
	CCR7	0.230	0.000		**ITGAX**	0.425	0.000

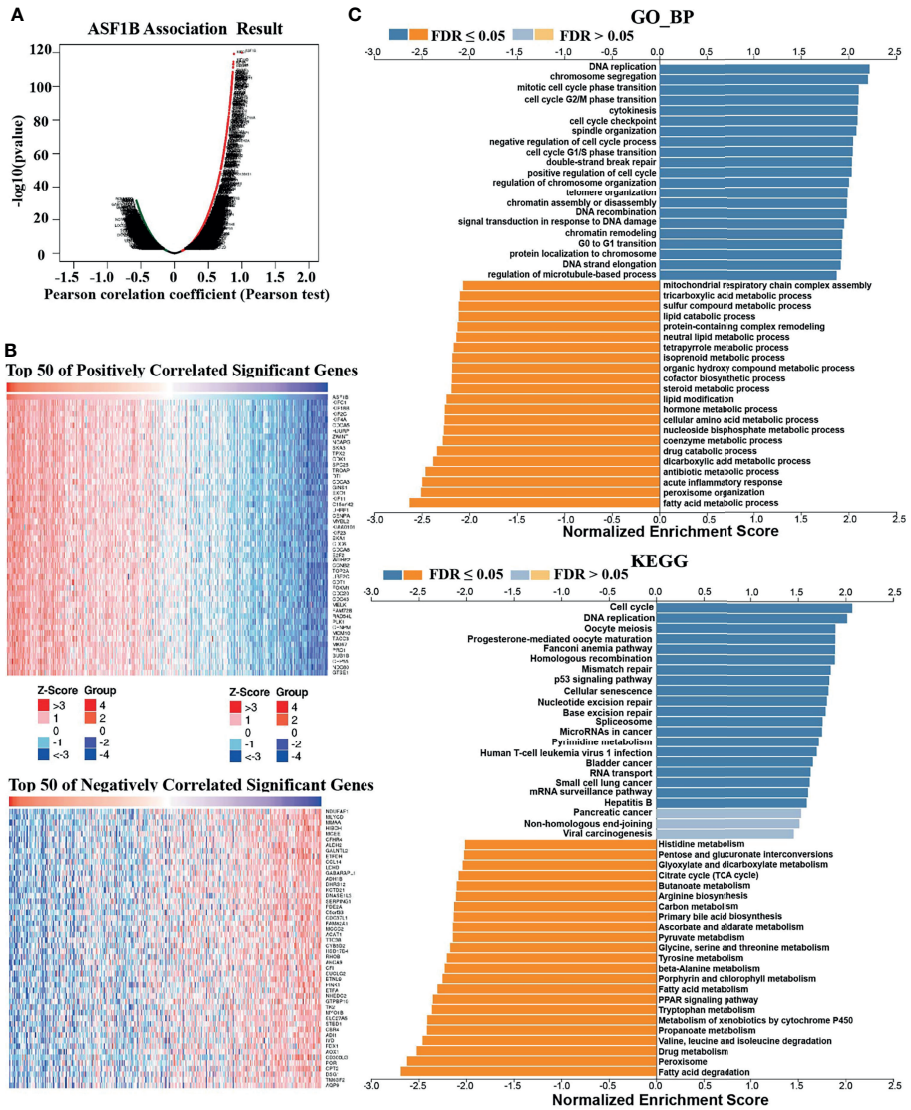

FIGURE 4 | Genes coexpressed with ASF1B in HCC (LinkedOmics). **(A)** All genes coexpressed with ASF1B in HCC. **(B)** The top 50 positively correlated genes and the top 50 negatively correlated genes cotranscript with ASF1B in HCC. **(C)** GO_BP and KEGG pathway analysis (GSEA) of ASF1B correlated genes in HCC.

for functional verification. First, we designed three types of siRNA (siASF1B-1, siASF1B-2, siASF1B-3) based on the ASF1B gene sequence. siRNAs were transfected into MHCC97H and Hep3B, and sicontrol was transfected into control group. The inhibition efficiency of the three siASF1B inhibitors on ASF1B in cells was detected by RT-PCR. The results showed that siASFB-2 had the best inhibition efficiency (**Figure 6A**). A CCK8 assay was conducted to examine cancer cell proliferation. In CCK8 assay, the three siRNA inhibitors of ASF1B expression could significantly inhibit the proliferation of MHCC97H and Hep3B (**Figure 6B**). The proliferation inhibition efficiency of siASF1B-2 and siASF1B-3 groups in MHCC97H was better than that of siASF1B-1 group. Cell invasion assay was used to evaluate the migration ability. In the cell invasion experiment of MHCC97H and Hep3B cells, ASF1B knockdown could significantly reduce the invasion ability of tumor cells (**Figure 6C**). Compared with the scrambled HCC cells, siASFB-2 transfected HCC cells showed significantly decreased invasiveness.

Inhibition of ASF1B Expression Can Promote Apoptosis and Arrest Cell Cycle in HCC Cells

According to knockdown efficiency and cell phenotype, siASF1B-2 was selected as siRNA to inhibit ASF1B expression. Flow cytometry analysis results showed that in MHCC97H, the proportion of cells in FITC positive region in ASF1B knockout group was 9.33%, which was higher than that in control group (9.01%).Similarly, in Hep3B, the proportion of cells in FITC positive region of ASF1B knockout group was 18.67% higher

TABLE 3 | Overall survival analysis of the top 50 genes positively and negatively correlated with ASF1B in HCC.

Pos Genes	HR	logrank P	Neg Genes	HR	logrank P
ASF1B	1.71(1.21-2.42)	0.002	NDUFAF1	0.45(0.31-0.64)	0.000
KIFC1	2.08(1.47-2.93)	0.000	MLYCD	0.66(0.45-0.95)	0.026
KIF18B	2.13(1.49-3.03)	0.000	MMAA	0.36(0.22-0.59)	0.000
KIF2C	2.14(1.66-3.46)	0.000	HIBCH	0.68(0.48-0.97)	0.031
KIF4A	1.94(1.34-2.73)	0.000	MCEE	0.53(0.37-0.77)	0.001
CDCA5	2.32(1.62-3.32)	0.000	CFHR4	0.41(0.29-0.59)	0.000
HJURP	2.14(1.51-3.04)	0.000	ALDH2	0.42(0.29-0.6)	0.000
ZWINT	2.36(1.66-3.36)	0.000	GALNTL2	0.52(0.36-0.74)	0.000
NCAPG	2.19(1.54-3.13)	0.000	ETFDH	0.51(0.36-0.72)	0.000
SKA3	2.07(1.45-2.96)	0.000	CCL14	0.37(0.26-0.53)	0.000
TPX2	2.29(1.62-3.24)	0.000	LDHD	0.55(0.38-0.8)	0.001
CDK1	2.15(1.52-3.06)	0.000	GABARAPL1	0.51(0.36-0.74)	0.000
SPC25	2.13(1.51-3.02)	0.000	ADH1B	0.57(0.4-0.81)	0.002
TROAP	1.84(1.27-2.66)	0.001	DHRS12	0.59(0.41-0.83)	0.003
DTL	1.89(1.33-2.69)	0.000	KCTD21	0.59(0.38-0.93)	0.020
CDCA3	2.21(1.47-3.34)	0.000	DNASE1L3	0.4(0.28-0.57)	0.000
GINS1	2.29(1.6-3.3)	0.000	SERPING1	0.59(0.41-0.85)	0.005
EXO1	2.3(1.63-3.26)	0.000	PDE2A	0.37(0.25-0.53)	0.000
KIF11	2.02(1.42-2.85)	0.000	C5orf33	0.61(0.43-0.87)	0.005
C15orf42	1.95(1.38-2.77)	0.000	CDC37L1	0.56(0.39-0.81)	0.002
UHRF1	1.92(1.34-2.74)	0.000	FAM82A1	0.6(0.42-0.85)	0.003
CENPA	2.33(1.65-3.29)	0.000	MCCC2	0.52(0.36-0.75)	0.000
MYBL2	2.29(1.62-3.24)	0.000	ACAT1	0.41(0.29-0.59)	0.000
KIAA0101	2.09(1.46-3)	0.000	TTC38	0.53(0.37-0.76)	0.000
KIF23	1.92(1.36-2.71)	0.000	CYB5D2	0.45(0.32-0.65)	0.000
SKA1	2.11(1.49-3.01)	0.000	HSD17B4	0.56(0.39-0.79)	0.001
CDC6	2.29(1.6-3.28)	0.000	RHOB	0.63(0.44-0.89)	0.008
CDCA8	2.69(1.89-3.83)	0.000	ABCA9	0.52(0.37-0.74)	0.000
E2F2	2.19(1.52-3.16)	0.000	CFI	0.64(0.45-0.91)	0.013
WDR62	2.38(1.57-3.6)	0.000	SUCLG2	0.56(0.4-0.8)	0.001
CCNB2	1.91(1.28-2.87)	0.001	BTNL9	0.39(0.27-0.56)	0.000
TOP2A	1.99(1.39-2.86)	0.000	PINK1	0.6(0.42-0.87)	0.006
UBE2C	2(1.41-2.83)	0.000	ETFA	0.65(0.46-0.91)	0.013
CDT1	2.05(1.45-2.9)	0.000	NHEDC2	0.62(0.44-0.88)	0.007
FOXM1	1.91(1.33-2.74)	0.000	GTPBP10	0.65(0.46-0.93)	0.016
CDC20	2.49(1.72-3.59)	0.000	TK2	0.53(0.34-0.82)	0.004
CDC45	2.23(1.51-3.28)	0.000	MYO1B	0.5(0.31-0.78)	0.002
MELK	2.22(1.5-3.27)	0.000	SLC27A5	0.52(0.36-0.74)	0.000
FAM72B	2.13(1.44-3.14)	0.000	STBD1	0.69(0.49-0.98)	0.036
RAD54L	2.27(1.59-3.23)	0.000	CBR4	0.53(0.38-0.75)	0.000
PLK1	2.23(1.58-3.15)	0.000	ADI1	0.52(0.36-0.75)	0.000
CENPM	2.09(1.45-3.01)	0.000	IVD	0.47(0.32-0.68)	0.000
MCM10	2.6(1.84-3.69)	0.000	FDX1	0.52(0.37-0.74)	0.000
TACC3	1.8(1.27-2.55)	0.001	AOX1	0.66(0.46-0.96)	0.030
MKI67	1.96(1.38-2.77)	0.000	CD300LG	0.48(0.34-0.69)	0.000
PRC1	1.95(1.36-2.8)	0.000	POR	0.6(0.42-0.85)	0.004
BUB1B	2.01(1.42-2.86)	0.000	CPT2	0.7(0.49-1)	0.047
CEP55	2.62(1.83-3.75)	0.000	DSG1	0.6(0.42-0.85)	0.003
NDC80	2.14(1.5-3.05)	0.000	TM6SF2	0.5(0.33-0.76)	0.001
GTSE1	2(1.41-2.85)	0.000	AQP9	0.52(0.36-0.75)	0.000

than that of control group 17.08%. The results showed that more cells were apoptotic in ASF1B-siRNA HCC cells than in scrambled cells (**Figure 7A**). Through KEGG enrichment analysis of ASF1B in HCC, it has been known that ASF1B is mainly involved in cell cycle regulation. By flow cytometry analysis, we found that the PROPORTION of G2 phase in MHCC97H knockout ASF1B group was 17.4% higher than that in control group (11.3%). In Hep3B, the proportion of S stage in knockout ASF1B group was 37.8%, while that in control group was 35.6%.Combining the two results, it is suggested that ASF1B knockdown can lead to cell cycle S and G2 phase arrest of HCC cells (**Figure 7B**).

ASF1B Knockdown Affected Cell Proliferation and Cell Cycle Pathways

To explore the molecular mechanism of ASF1 knockdown inhibiting HCC cell proliferation and arresting cell cycle, a panel of well-characterized signaling molecules of cell proliferation and the cell cycle were detected in ASF1B-siRNA cells and control cells by western blot. As shown in **Figure 8A**,

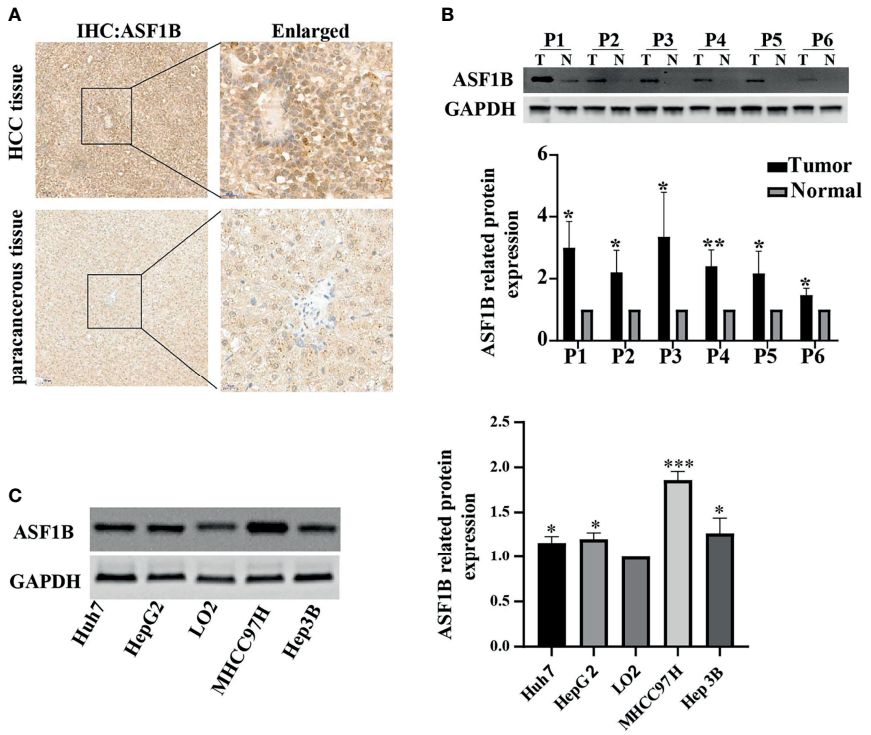

FIGURE 5 | **(A)** HCC tissue and paracancerous tissue samples from HCC patients were tested by immunohistochemistry (IHC). **(B)** The protein expression of ASF1B in 6 pairs of liver cancer tissues. **(C)** The protein expression of ASF1B in four liver cancer cell lines. *$p < 0.05$; **$p < 0.01$; ***$p < 0.001$.

weaker bands for the Proliferating cell nuclear antigen (PCNA), cyclin B1 cyclin E2 and CDK9 proteins were shown in siASF1B cells compared to those in control cells. These results indicated that knockdown of ASF1B induced cell cycle arrest, which mediated the inhibition of HCC cell growth. In Hela cells, ASF1B can bind to CDK9, and knockdown ASF1B reduces the expression of CDK9 protein (12). However, whether ASF1B can bind to CDK9 in HCC cells has not been studied yet. In our study, ASF1B knockdown was found to reduce CDK9 protein expression. Co-IP was then performed with anti-ASF1B antibodies using normal MHCC97H and Hep3B cells. **Figure 8B** showed that endogenous ASF1B formed stable complexes with CDK9 (**Figure 8B**).

DISCUSSION

At present, HCC remains a global medical problem with poor prognosis and high mortality. The main causes of death of patients with liver cancer are a high rate of late diagnosis, metastasis and rapid malignant progression (20). Early diagnosis and effective treatment may significantly improve survival in patients with HCC. Therefore, on the one hand, early diagnosis and characteristic identification of HCC tumor progression are urgently needed (21). On the other hand, it is crucial to find new therapeutic targets and develop new therapeutic strategies (22). In recent years, the development of sequencing and omics technology has provided more opportunities to further understand the mechanism of HCC and explore diagnostic and therapeutic targets (23). Previous studies evaluating the effect of ASF1B on cancer have shown that ASF1B, as an oncogenic gene, promotes tumor growth in breast cancer, cell renal cell carcinoma, cervical cancer, prostate cancer and lung cancer (11–13, 24, 25). These studies suggest that high ASF1B expression is associated with increased tumor incidence, tumor progression, and metastasis. A recent study reported that ASF1B was involved in the immune regulation of HCC (26). However, the role of ASF1B in HCC tumor proliferation and migration has not been systematically studied. ASF1B was rarely described as a key oncogene regulating hepatocellular carcinoma growth.

In this research, we used bioinformatics and multiple databases to comprehensively analyze the expression of ASF1B in pan-cancer, and found that ASF1B was abnormally expressed in most cancers, including liver cancer, which is consistent with current literature reports (27–29). In order to explore the relationship between ASF1B and HCC in detail, RNA-seq data and corresponding clinical data of HCC in TCGA were analyzed separately. We found that the high expression of ASF1B was associated with poor prognosis of HCC patients. COX regression analysis showed that ASF1B was an independent risk factor for HCC prognosis, and ROC curve analysis showed that ASF1B expression had certain predictive value for survival evaluation of HCC patients at 1, 3 and 5 years.ASF1B expression in HCC patients increased with tumor stage and grade progression,

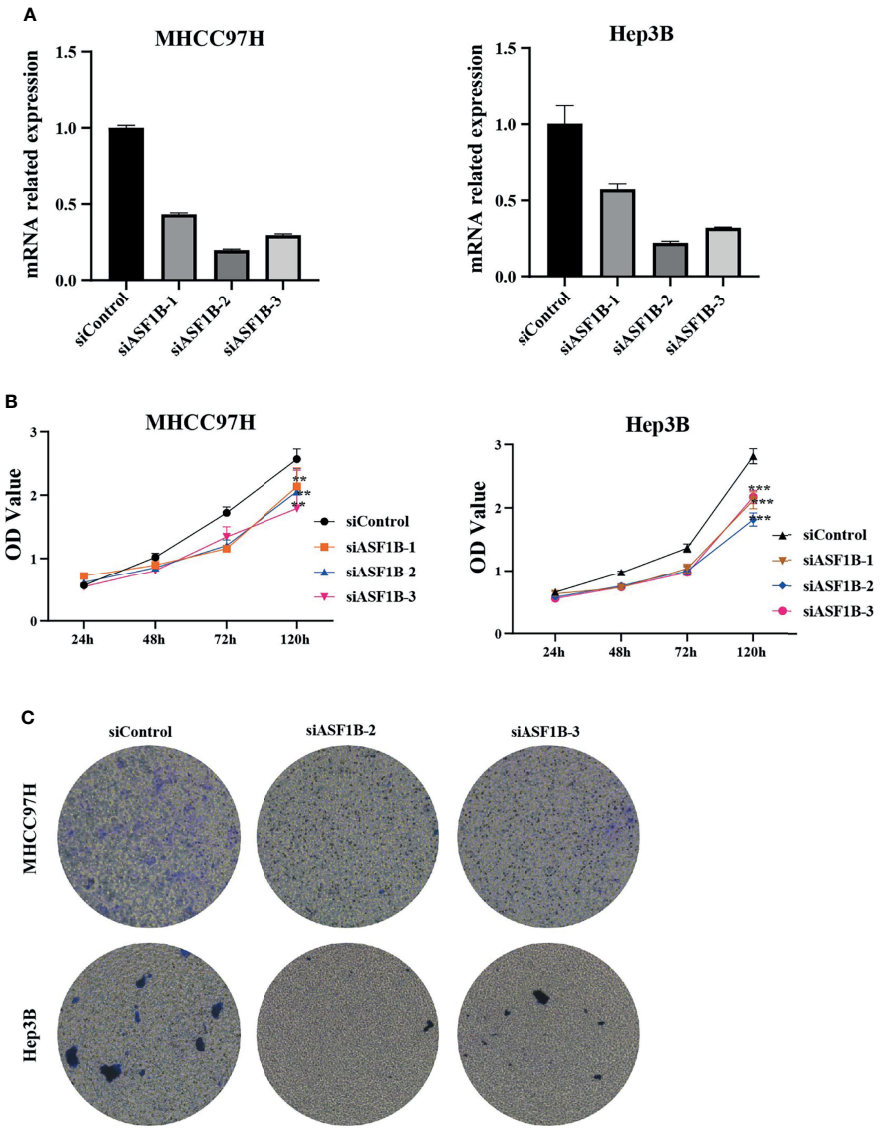

FIGURE 6 | **(A)** Silencing efficiency of ASF1B in two hepatoma cell lines MHCC97H and Hep3B **(B)** Cell viability assay of MHCC97H and Hep3B cells. **(C)** Cell invasion assay of MHCC97H and Hep3B cells. $^{**}p < 0.01$; $^{***}p < 0.001$.

suggesting that ASF1B is associated with HCC disease progression. Recently, an increasing number of studies have found a correlation between cancer progression and tumor immune infiltration (30, 31). Through public data mining, we also found a certain correlation between the expression of ASF1B and the immune infiltration of HCC, which is consistent with the conclusions of current reports (28, 29). But the specific experiments need to be further verified.

To comprehensively analyze the function of ASF1B in HCC, we analyzed the genes that were significantly related to ASF1B expression in HCC. Similar to ASF1B, these genes are abnormally expressed in HCC, most of which are related to the overall survival of HCC. ASF1B may form a regulatory network with these genes to promote the occurrence and development of HCC. These genes coexpressed with ASF1B were enriched by GSEA, and it was found that the regulatory network mainly promoted the cell cycle and DNA replication while inhibiting energy consumption processes such as lipid and glucose metabolism, which was consistent with the pathological characteristics of highly proliferative cancers, such as HCC (32).

Experiments were conducted to further verify the expression of ASF1B in HCC and further study its role and function in HCC. Immunohistochemical analysis of ASF1B expression in HCC tumor tissues and adjacent tissues showed strong ASF1B staining in tumor tissues, and protein western blot analysis also showed stronger ASF1B bands in tumor tissues, thus confirming the high expression of ASF1B in HCC tumor tissues. We also compared the levels of ASF1B protein in normal liver cell line

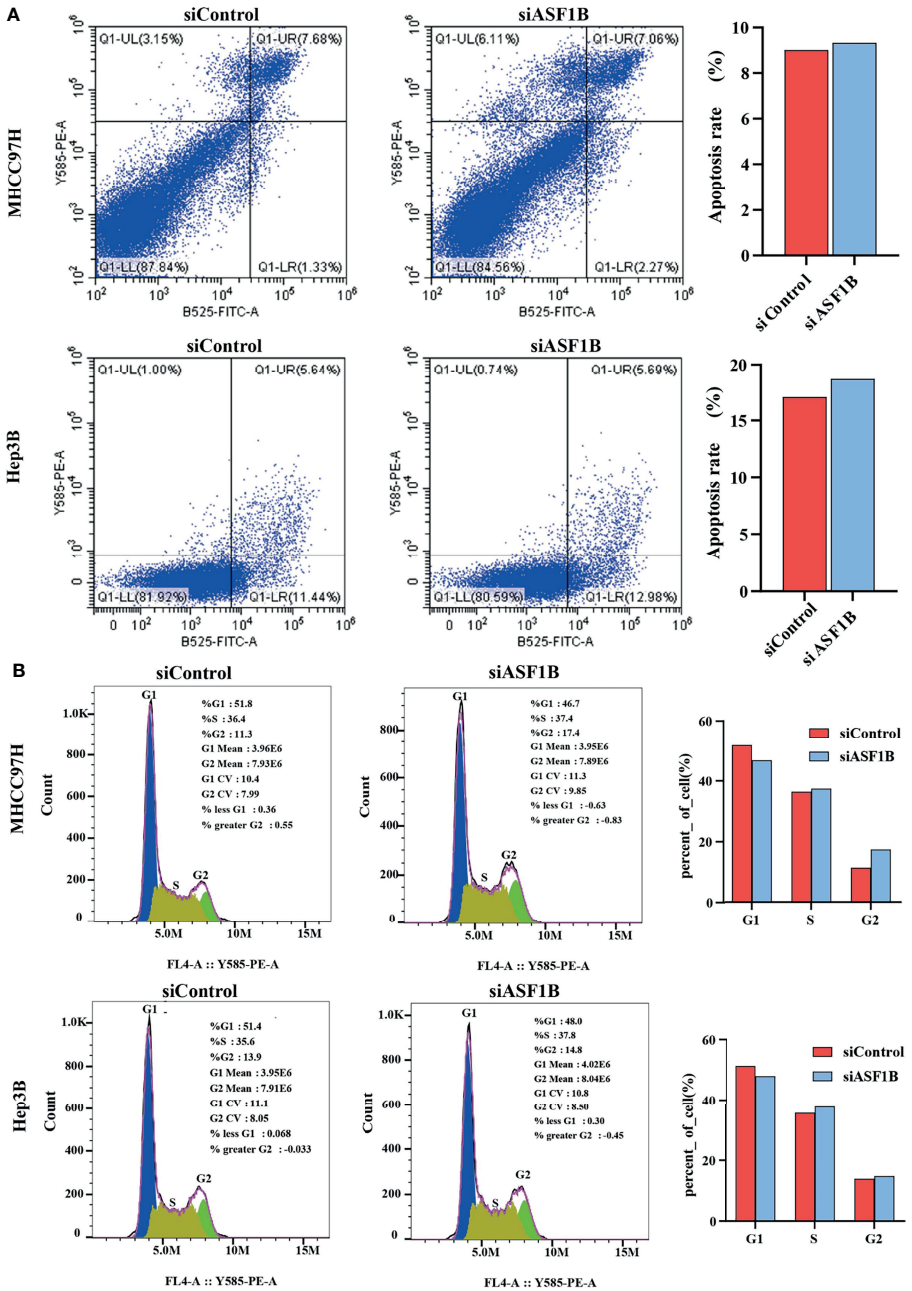

FIGURE 7 | ASF1B knockdown influence apoptosis and cell cycle. **(A)** Flow cytometry was used to detect apoptosis changes in MHCC97H and Hep3B; **(B)** Flow cytometry was used to detect the cell cycle changes in MHCC97H and Hep3B.

LO2 with four hepatocellular carcinoma cell lines such as Huh7, HepG2, MHCC97H and Hep3B. It was found that the protein level of ASF1B in HCC cells was higher than that of LO2, but there were some differences, among which the highest expression was found in MHCC97H.

Subsequently, we induced ASF1B silencing through transfection siRNAs in two HCC cell lines with high ASF1B expression (MHCC97H and Hep3B) to investigate the role of ASF1B in the biological function of HCC cells. The results confirmed that knocking down ASF1B impaired proliferation, induced cell apoptosis and altered cell cycle progression in HCC cells. These results suggest that ASF1B is crucial for maintaining tumorigenic activity of HCC cells *in vitro*. To elucidate the molecular mechanism of ASF1B knockdown-mediated suppression of HCC cells, PCNA, cyclinB1, cyclinE2 and CDK9 proteins were detected in MHCC97H and Hep3B cells after ASF1B knockdown. PCNA is an indispensable factor in DNA replication (33). CyclinB1 is a regulatory protein involved in mitosis and a key protein in G2/M

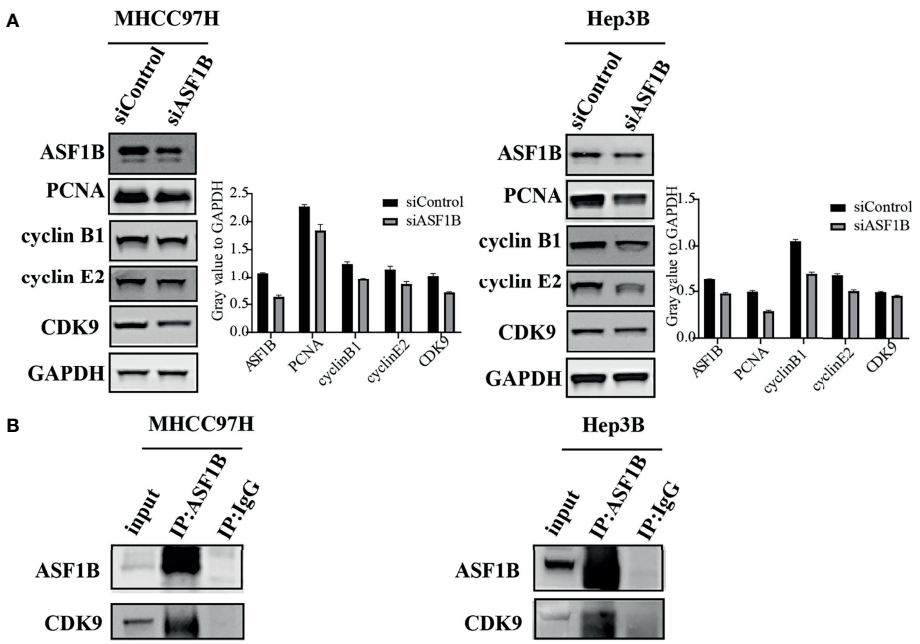

FIGURE 8 | **(A)** Western blots were performed to detect ASF1B, PCNA, cyclin B1, cyclin E2 and CDK9. **(B)** Co-immunoprecipitation results of ASF1B and CDK9 in MHCC97H and Hep3B cells.

phase regulation (34). It has been reported that cyclinB1 depletion constrains proliferation and induces apoptosis in human tumor cells (35). CyclinE2 is also an important cell cycle regulating protein, and abnormal expression of cyclinE2 can affect tumor proliferation (36). Unlike other CDKs, CDK9 not only regulates the cell cycle, but also promotes RNA synthesis in the genetic programmes of cell growth, differentiation, and viral pathogenesis (37). According to our results, knockdown of ASF1B can reduce the protein levels of PCNA, cyclinB1, cyclinE2 and CDK9 in HCC cells. These results suggest that knockout ASF1B may inhibit the proliferation of HCC cells by affecting the expression of these four genes. To further explore the interaction proteins of ASF1B in HCC cells, protein-protein interaction studies were performed by IP and Western blot. According to the literature, ASF1B interacts with CDK9 in cervical cancer cells, but it has not been reported in liver cancer cells (12). We demonstrated the interaction between ASF1B and CDK9 in hepatocellular carcinoma cells. Recently, some studies have shown that CDK9 plays a key role in prostate cancer (38), breast cancer (39), acute myeloid leukemia (40), hepatocellular carcinoma (41). Shao et al. reported that inhibition of CDK9 impaired proliferation and induced apoptosis in HCC cells (41). CDK9 was involved in cancer progression through BRD4-dependent recruitment of p-TEFb involving transcription of the MYC gene, and that MYC is a proto-oncogene that controls cell growth and cell cycle processes (42). These results suggest that ASF1B may affect HCC cell proliferation and cell cycle regulation through its interaction with CDK9.

In conclusion, this study provided multi-level evidence for the significance of ASF1B in HCC development and its potential as a biomarker for HCC disease progression. We figured out the important role of ASF1B as a regulator in cell proliferation, apoptosis induction and cell cycle progression. Interference with ASF1B can significantly inhibit the growth of HCC by regulating cell cycle and apoptosis pathways. These findings proposed a potential target for the development of anti-cancer strategies in HCC.

DATA AVAILABILITY STATEMENT

The original contributions presented in the study are included in the article/**Supplementary Material**. Further inquiries can be directed to the corresponding authors.

ETHICS STATEMENT

The studies involving human participants were reviewed and approved by Clinical Research Ethics Committee of the First Affiliated Hospital, Zhejiang University School of Medicine. The patients/participants provided their written informed consent to participate in this study.

AUTHOR CONTRIBUTIONS

LJL and DZ contributed to conception and design of the study. XO completed the experiment and analyzed the data. XO and LXL drafted the manuscript and prepared diagrams. YZ, FZ, QH, and ZL participated in the material preparation and manuscript

review. All authors have read and approved the manuscript for publication.

FUNDING

This study was funded by the National Key Research and Development Program of China (2016YFC110130413, 2019YFC0840600, 2019YFC08400609, 2021YFC2301800) and by the Zhejiang Provincial Natural Science Foundation of China (LY17H030005).

SUPPLEMENTARY MATERIAL

The Supplementary Material for this article can be found online at: https://www.frontiersin.org/articles/10.3389/fonc.2021.801506/full#supplementary-material

REFERENCES

1. World Health Organization. Cancer Today. Available at: https://gco.iarc.fr/today/home.
2. Singal A, Lampertico P, Nahon P. Epidemiology and Surveillance for Hepatocellular Carcinoma: New Trends. *J Hepatol* (2020) 72(2):250–61. doi: 10.1016/j.jhep.2019.08.025
3. Siegel RL, Miller KD, Jemal A. Cancer Statistics, 2020. *CA Cancer J Clin* (2020) 70(1):7–30. doi: 10.3322/caac.21590
4. Llovet J, Kelley R, Villanueva A, Singal A, Pikarsky E, Roayaie S, et al. Hepatocellular Carcinoma. *Nat Rev Dis Primers* (2021) 7(1):6. doi: 10.1038/s41572-020-00240-3
5. Rebouissou S, Nault J. Advances in Molecular Classification and Precision Oncology in Hepatocellular Carcinoma. *J Hepatol* (2020) 72(2):215–29. doi: 10.1016/j.jhep.2019.08.017
6. Pillai A, Ahn J, Kulik L. Integrating Genomics Into Clinical Practice in Hepatocellular Carcinoma: The Challenges Ahead. *Am J Gastroenterol* (2020) 115(12):1960–9. doi: 10.14309/ajg.0000000000000843
7. Petrowsky H, Fritsch R, Guckenberger M, De Oliveira ML, Dutkowski P, Clavien P-A. Modern Therapeutic Approaches for the Treatment of Malignant Liver Tumours. *Nat Rev Gastroenterol Hepatol* (2020) 17 (12):755–72. doi: 10.1038/s41575-020-0314-8
8. Faivre S, Rimassa L, Finn R. Molecular Therapies for HCC: Looking Outside the Box. *J Hepatol* (2020) 72(2):342–52. doi: 10.1016/j.jhep.2019.09.010
9. Groth A, Corpet A, Cook AJ, Roche D, Bartek J, Lukas J, et al. Regulation of Replication Fork Progression Through Histone Supply and Demand. *Science* (2007) 318(5858):1928–31. doi: 10.1126/science.1148992
10. Messiaen S, Guiard J, Aigueperse C, Fliniaux I, Tourpin S, Barroca V, et al. Loss of the Histone Chaperone ASF1B Reduces Female Reproductive Capacity in Mice. *Reprod (Cambr Engl)* (2016) 151(5):477–89. doi: 10.1530/rep-15-0327
11. Corpet A, De Koning L, Toedling J, Savignoni A, Berger F, Lemaître C, et al. Asf1b, The Necessary Asf1 Isoform for Proliferation, Is Predictive of Outcome in Breast Cancer. *EMBO J* (2011) 30(3):480–93. doi: 10.1038/emboj.2010.335
12. Liu X, Song J, Zhang Y, Wang H, Sun H, Feng X, et al. ASF1B Promotes Cervical Cancer Progression Through Stabilization of CDK9. *Cell Death Dis* (2020) 11(8):705. doi: 10.1038/s41419-020-02872-5
13. Han G, Zhang X, Liu P, Yu Q, Li Z, Yu Q, et al. Knockdown of Anti-Silencing Function 1B Histone Chaperone Induces Cell Apoptosis *via* Repressing PI3K/Akt Pathway in Prostate Cancer. *Int J Oncol* (2018) 53(5):2056–66. doi: 10.3892/ijo.2018.4526
14. Jiangqiao Z, Tao Q, Zhongbao C, Xiaoxiong M, Long Z, Jilin Z, et al. Anti-Silencing Function 1B Histone Chaperone Promotes Cell Proliferation and Migration *via* Activation of the AKT Pathway in Clear Cell Renal Cell Carcinoma. *Biochem Biophys Res Commun* (2019) 511(1):165–72. doi: 10.1016/j.bbrc.2019.02.060
15. Liu Z, Zhang Y, Dang Q, Wu K, Jiao D, Li Z, et al. Genomic Alteration Characterization in Colorectal Cancer Identifies a Prognostic and Metastasis Biomarker: FAM83A|Ido1. *Front Oncol* (2021) 11:632430. doi: 10.3389/fonc.2021.632430
16. Liu Z, Lu T, Li J, Wang L, Xu K, Dang Q, et al. Clinical Significance and Inflammatory Landscape of Anovel Recurrence-Associated Immune Signature in Stage II/III Colorectal Cancer. *Front Immunol* (2021) 12:702594. doi: 10.3389/fimmu.2021.702594
17. Liu Z, Liu L, Guo C, Yu S, Meng L, Zhou X, et al. Tumor Suppressor Gene Mutations Correlate With Prognosis and Immunotherapy Benefit in Hepatocellular Carcinoma. *Int Immunopharmacol* (2021) 101(Pt B):108340. doi: 10.1016/j.intimp.2021.108340
18. Zhao Y, Xue C, Xie Z, Ouyang X, Li L. Comprehensive Analysis of Ubiquitin-Specific Protease 1 Reveals its Importance in Hepatocellular Carcinoma. *Cell Proliferation* (2020) 53(10):e12908. doi: 10.1111/cpr.12908
19. Zhao Y, Chen E, Huang K, Xie Z, Zhang S, Wu D, et al. Dynamic Alterations of Plasma Metabolites in the Progression of Liver Regeneration After Partial Hepatectomy. *J Proteome Res* (2020) 19(1):174–85. doi: 10.1021/acs.jproteome.9b00493
20. Vo Quang E, Shimakawa Y, Nahon P. Epidemiological Projections of Viral-Induced Hepatocellular Carcinoma in the Perspective of WHO Global Hepatitis Elimination. *Liver Int: Off J Int Assoc Study Liver* (2021) 41 (5):915–27. doi: 10.1111/liv.14843
21. Llovet J, Montal R, Sia D, Finn R. Molecular Therapies and Precision Medicine for Hepatocellular Carcinoma. *Nat Rev Clin Oncol* (2018) 15 (10):599–616. doi: 10.1038/s41571-018-0073-4
22. Pan Y, Chen H, Yu J. Biomarkers in Hepatocellular Carcinoma: Current Status and Future Perspectives. *Biomedicines* (2020) 8(12):576. doi: 10.3390/biomedicines8120576
23. Dhanasekaran R, Nault J, Roberts L, Zucman-Rossi J. Genomic Medicine and Implications for Hepatocellular Carcinoma Prevention and Therapy. *Gastroenterology* (2019) 156(2):492–509. doi: 10.1053/j.gastro.2018.11.001
24. Feng Z, Zhang J, Zheng Y, Wang Q, Min X, Tian T. Elevated Expression of ASF1B Correlates With Poor Prognosis in Human Lung Adenocarcinoma. *Per Med* (2021) 18(2):115–27. doi: 10.2217/pme-2020-0112
25. Carrion A, Ingelmo-Torres M, Lozano JJ, Montalbo R, D'Anna M, Mercader C, et al. Prognostic Classifier for Predicting Biochemical Recurrence in Localized Prostate Cancer Patients After Radical Prostatectomy. *Urol Oncol* (2021) 39(8):493. doi: 10.1016/j.urolonc.2020.10.075
26. Zhan T, Gao X, Wang G, Li F, Shen J, Lu C, et al. Construction of Novel lncRNA-miRNA-mRNA Network Associated With Recurrence and Identification of Immune-Related Potential Regulatory Axis in Hepatocellular Carcinoma. *Front Oncol* (2021) 11:626663. doi: 10.3389/fonc.2021.626663
27. Zhang W, Gao Z, Guan M, Liu N, Meng F, Wang G. ASF1B Promotes Oncogenesis in Lung Adenocarcinoma and Other Cancer Types. *Front Oncol* (2021) 11:731547. doi: 10.3389/fonc.2021.731547
28. Hu X, Zhu H, Zhang X, He X, Xu X. Comprehensive Analysis of Pan-Cancer Reveals Potential of ASF1B as a Prognostic and Immunological Biomarker. *Cancer Med* (2021) 10(19):6897–916. doi: 10.1002/cam4.4203
29. Ma J, Han W, Lu K. Comprehensive Pan-Cancer Analysis and the Regulatory Mechanism of ASF1B, a Gene Associated With Thyroid Cancer Prognosis in the Tumor Micro-Environment. *Front Oncol* (2021) 11:711756. doi: 10.3389/fonc.2021.711756
30. Leone V, Ali A, Weber A, Tschaharganeh DF, Heikenwalder M. Liver Inflammation and Hepatobiliary Cancers. *Trends Cancer* (2021) 7(7):606–23. doi: 10.1016/j.trecan.2021.01.012
31. Wang J, Wang Y, Chu Y, Li Z, Yu X, Huang Z, et al. Tumor-Derived Adenosine Promotes Macrophage Proliferation in Human Hepatocellular Carcinoma. *J Hepatol* (2021) 74(3):627–37. doi: 10.1016/j.jhep.2020.10.021
32. Couri T, Pillai A. Goals and Targets for Personalized Therapy for HCC. *Hepatol Int* (2019) 13(2):125–37. doi: 10.1007/s12072-018-9919-1

33. Wang S. PCNA: A Silent Housekeeper or a Potential Therapeutic Target? *Trends Pharmacol Sci* (2014) 35(4):178–86. doi: 10.1016/j.tips.2014.02.004
34. Lv S, Ning H, Li Y, Wang J, Jia Q, Wen H. Inhibition of Cyclinb1 Suppressed the Proliferation, Invasion, and Epithelial Mesenchymal Transition of Hepatocellular Carcinoma Cells and Enhanced the Sensitivity to TRAIL-Induced Apoptosis. *OncoTargets Ther* (2020) 13:1119–28. doi: 10.2147/ott.S225202
35. Xie X, Lin W, Zheng W, Chen T, Yang H, Sun L, et al. Downregulation of G2/Mitotic-Specific Cyclinb1 Triggers Autophagy *via* AMPK-ULK1-Dependent Signal Pathway in Nasopharyngeal Carcinoma Cells. *Cell Death Dis* (2019) 10 (2):94. doi: 10.1038/s41419-019-1369-8
36. Ng S, Ohshima K, Selvarajan V, Huang G, Choo S, Miyoshi H, et al. Prognostic Implication of Morphology, Cycline2 and Proliferation in EBV-Associated T/NK Lymphoproliferative Disease in Non-Immunocompromised Hosts. *Orphanet J Rare Dis* (2014) 9:165. doi: 10.1186/s13023-014-0165-x
37. Wang S, Fischer P. Cyclin-Dependent Kinase 9: A Key Transcriptional Regulator and Potential Drug Target in Oncology, Virology and Cardiology. *Trends Pharmacol Sci* (2008) 29(6):302–13. doi: 10.1016/j.tips.2008.03.003
38. Hu Q, Poulose N, Girmay S, Helevä A, Doultsinos D, Gondane A, et al. Inhibition of CDK9 Activity Compromises Global Splicing in Prostate Cancer Cells. *RNA Biol* (2021), 1–8. doi: 10.1080/15476286.2021.1983287
39. Wei D, Wang H, Zeng Q, Wang W, Hao B, Feng X, et al. Discovery of Potent and Selective CDK9 Degraders for Targeting Transcription Regulation in Triple-Negative Breast Cancer. *J Med Chem* (2021) 64(19):14822–47. doi: 10.1021/acs.jmedchem.1c01350
40. Han X, Song N, Saidahmatov A, Wang P, Wang Y, Hu X, et al. Rational Design and Development of Novel CDK9 Inhibitors for the Treatment of Acute Myeloid Leukemia. *J Med Chem* (2021) 64(19):14647–63. doi: 10.1021/acs.jmedchem.1c01148
41. Shao Y, Li Y, Hsu H, Lin H, Wang H, Wo R, et al. Potent Activity of Composite Cyclin Dependent Kinase Inhibition Against Hepatocellular Carcinoma. *Cancers* (2019) 11(10):1433. doi: 10.3390/cancers11101433
42. Franco L, Morales F, Boffo S, Giordano A. CDK9: A Key Player in Cancer and Other Diseases. *J Cell Biochem* (2018) 119(2):1273–84. doi: 10.1002/jcb.26293

Conflict of Interest: The authors declare that the research was conducted in the absence of any commercial or financial relationships that could be construed as a potential conflict of interest.

The handling editor JC declared a shared parent affiliation with the authors at the time of the review.

Publisher's Note: All claims expressed in this article are solely those of the authors and do not necessarily represent those of their affiliated organizations, or those of the publisher, the editors and the reviewers. Any product that may be evaluated in this article, or claim that may be made by its manufacturer, is not guaranteed or endorsed by the publisher.

frontiers in Oncology

ORIGINAL RESEARCH
published: 11 January 2022
doi: 10.3389/fonc.2021.761030

Prognostic and Predictive Value of BGN in Colon Cancer Outcomes and Response to Immunotherapy

Zi-Xuan He[1†], Sheng-Bing Zhao[1†], Xue Fang[1†], Ji-Fu E[2†], Hong-Yu Fu[1†], Yi-Hang Song[1], Jia-Yi Wu[1], Peng Pan[1], Lun Gu[1], Tian Xia[1], Yi-Long Liu[3], Zhao-Shen Li[1], Shu-Ling Wang[1*] and Yu Bai[1*]*

[1] Department of Gastroenterology, Changhai Hospital, Second Military Medical University/Naval Medical University, Shanghai, China, [2] Department of Colorectal Surgery, Changhai Hospital, Second Military Medical University/Naval Medical University, Shanghai, China, [3] College of Basic Medicine Sciences, Second Military Medical University/Naval Medical University, Shanghai, China

OPEN ACCESS

Edited by:
Yuming Jiang,
Stanford University, United States

Reviewed by:
Yona Keisari,
Tel Aviv Universit, Israel
Milladur Rahman,
Lund University, Sweden

***Correspondence:**
Yu Bai
baiyu1998@hotmail.com
Shu-Ling Wang
wangshuling0000@126.com
Zhao-Shen Li
li.zhaoshen@hotmail.com

[†]These authors have contributed equally to this work and share first authorship

Specialty section:
This article was submitted to Gastrointestinal Cancers: Hepato Pancreatic Biliary Cancers, a section of the journal Frontiers in Oncology

Received: 19 August 2021
Accepted: 15 December 2021
Published: 11 January 2022

Citation:
He Z-X, Zhao S-B, Fang X, E J-F, Fu H-Y, Song Y-H, Wu J-Y, Pan P, Gu L, Xia T, Liu Y-L, Li Z-S, Wang S-L and Bai Y (2022) Prognostic and Predictive Value of BGN in Colon Cancer Outcomes and Response to Immunotherapy. Front. Oncol. 11:761030. doi: 10.3389/fonc.2021.761030

Background: Colon cancer is one of the most frequent malignancies and causes high mortality worldwide. Exploring the tumor-immune interactions in the tumor microenvironment and identifying new prognostic and therapeutic biomarkers will assist in decoding the novel mechanism of tumor immunotherapy. BGN is a typical extracellular matrix protein that was previously validated as a signaling molecule regulating multiple processes of tumorigenesis. However, its role in tumor immunity requires further investigation.

Methods: The differentially expressed genes in three GEO datasets were analyzed, and BGN was identified as the target gene by intersection analysis of PPIs. The relevance between clinical outcomes and BGN expression levels was evaluated using data from the GEO database, TCGA and tissue microarray of colon cancer samples. Univariable and multivariable Cox regression models were conducted for identifying the risk factors correlated with clinical prognosis of colon cancer patients. Next, the association between BGN expression levels and the infiltration of immune cells as well as the process of the immune response was analyzed. Finally, we predicted the immunotherapeutic response rates in the subgroups of low and high BGN expression by TIS score, ImmuCellAI and TIDE algorithms.

Results: BGN expression demonstrated a statistically significant upregulation in colon cancer tissues than in normal tissues. Elevated BGN was associated with shorter overall survival as well as unfavorable clinicopathological features, including tumor size, serosa invasion and length of hospitalization. Mechanistically, pathway enrichment and functional analysis demonstrated that BGN was positively correlated with immune and stromal scores in the TME and primarily involved in the regulation of immune response. Further investigation revealed that BGN was strongly expressed in the immunosuppressive phenotype and tightly associated with the infiltration of multiple immune cells in colon cancer, especially M2 macrophages and induced Tregs. Finally, we demonstrated that high BGN expression presented a better immunotherapeutic response in colon cancer patients.

Conclusion: BGN is an encouraging predictor of diagnosis, prognosis and immunotherapeutic response in patients with colon cancer. Assessment of BGN expression represents a novel approach with great promise for identifying patients who may potentially benefit from immunotherapy.

Keywords: BGN, colon cancer, tumor microenvironment, immunosuppression, immunotherapy

INTRODUCTION

Global Cancer Statistics of 2020 demonstrates that colorectal cancer (CRC) ranks 3rd in terms of the most frequent malignancy and 2nd in terms of tumor-related death. CRC accounts for 9.8% of the total cancer incidence with nearly 1.9 million new cases and 9.2% of the total case mortality with 935,000 deaths annually (1, 2). Although diagnosis of CRC has improved due to early detection through colonoscopy screening and advances in imaging techniques such as CT colonography or PET-CT, approximately 25% of patients still experience advanced diseases (3), which only achieve modest benefits from conventional therapeutic strategies, including surgery, chemotherapy, and radiotherapy (4–6). Immunotherapy holds promise in cancer treatment, providing a novel treatment tool for patients with advanced or drug-resistant colorectal cancer (7). However, responses to immunotherapy vary significantly among different types of colorectal cancer patients (8, 9). Therefore, predicting the efficacy of immunotherapy and finding efficacy-related biological markers are of particular importance for the treatment of colorectal cancer (10, 11).

Recent advances have emphasized the significance of the tumor microenvironment (TME), accounting for approximately 90% of the gross tumor volume. In fact, nontumoral cells including immune cells, cancer-associated fibroblasts (CAFs) or extracellular matrix (ECM) exist in the great majority of solid tumors (12, 13). Within this intratumor microenvironment, both tumor cells and stroma contribute to non-cellular components, such as extracellular matrix, which are largely characterized and associate with tumor invasiveness and metastatic abilities (14, 15). Exploring the impact of cellular composition in the TME would assist in decoding the regulation of the microenvironment by tumors.

BGN is a classic type of extracellular matrix protein that is essential role in mediating the morphology, growth, differentiation and migration of epithelial cells (16). The function of the BGN depends on its microenvironmental context as a structural or signaling molecule. Initially, the function of BGN was mainly to maintain the structural integrity of the ECM (17). In recent years, however, BGN has been regarded as a signaling molecule mediating various steps of tumorigenesis within recent years (16). Aberrant expression of BGN in tumors indicate its promoting effects in migration and invasion abilities of tumor cells (18). Previous studies have found that the up-regulation of BGN in a variety of solid tumors (19–21) and its potential diagnostic and prognostic value in ovarian cancer (21), prostate cancer (22), gastric cancer (23) and colorectal cancer (24, 25). However, a paucity of studies have systematically assessed the function of BGN in tumor immunity. In our current work, which combines data from TCGA and GEO public databases as well as tissue microarrays, we validated the clinical implication of BGN expression in colon cancer samples and utilized multiple bioinformatics approaches to investigate the underlying immunosuppressive mechanisms of BGN in the TME as well as its potential role in predicting immune checkpoint blocker (ICB) immunotherapy responses in colon cancer patients.

RESULTS

Identification of DEGs

First, three GEO datasets including 44 colon cancer tissues and 35 normal tissues were enrolled to identify differential genes. According to the cutoff criteria, 1039, 396, and 256 differentially expressed genes were extracted from GSE4107, GSE110224, and GSE4183 by the GEO2R online tool, respectively. As shown in **Figure 1A**, 14 differentially expressed genes with overlapping expression were screened. Subsequently, a protein-protein interaction network was constructed by the STRING tool (**Figure 1B**) and then uploaded the common PPI network into Cytoscape software. Based on the degree scores generated by the CytoHubba module, seven genes, ABCG2, CXCL8, CXCL12, BGN, SULF1, THBS2, and FAP, were identified as potential hub genes (**Figure 1C**). Among them, BGN had the highest degree score and was identified as the target gene for subsequent functional analysis and validation.

Assessment of BGN Expression in Colon Cancer and Normal Tissues

We compared the mRNA expression levels of BGN among 435 colon cancer samples and 41 normal samples in TCGA. In patients with colon cancer, the transcriptional levels of BGN were markedly upregulated (**Figure 2A**). To investigate the protein expression patterns of BGN, an IHC assay was performed in tumor microarray (TMA) sections. BGN showed an extracellular matrix staining pattern (**Figures 2B, D**). The expression levels of BGN protein were significantly elevated in tumor tissues, as compared with in the adjacent noncancerous tissues (MOD = 0.140 ± 0.023 *vs* 0.133 ± 0.026, p = 0.003) (**Figure 2C**). We then analyzed the association between the upregulation of BGN and clinicopathological variables. As shown in **Table 1**, a total of 84 patients (58.3%) stained positive for BGN expression in tumor tissues. Upregulation of BGN was markedly correlated with tumor size (p = 0.023), serosa invasion (p = 0.002) and surprisingly, length of hospitalization (p = 0.038). These findings above indicate

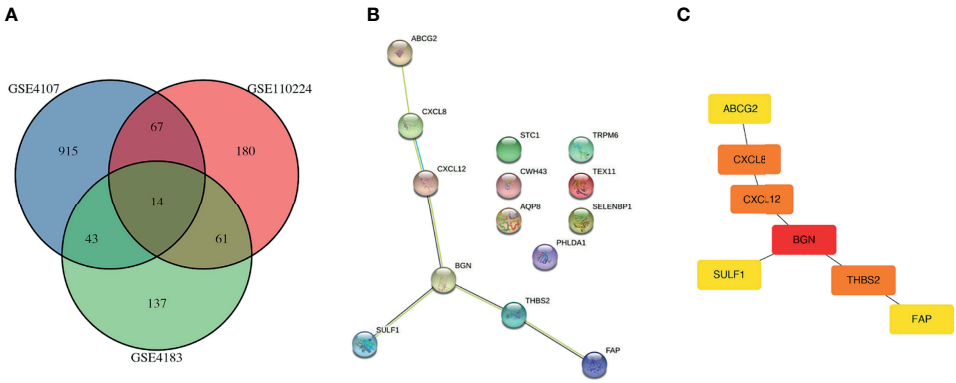

FIGURE 1 | Identification of overlapping DEGs. **(A)** Venn plots of overlapping DEGs in GSE4107 dataset, GSE110224 dataset and GSE4183 dataset. **(B)** PPI of 14 DEGs using the STRING database (https://string-db.org). **(C)** PPI network of DEGs were constructed and visualized by Cytoscape software. PPI, protein-protein interaction; DEG, differentially expressed gene.

that upregulation of BGN might be a potential biomarker for assessing the degree of malignancy in colon cancer.

Prognostic Value of BGN in Colon Cancer Patients

We next explored the association between BGN expression levels and outcomes of colon cancer patients in TCGA and GEO database. Our results manifested that higher BGN expression was linked to poorer overall survival (OS) in patients with colon cancer in TCGA ($p = 0.007$) and GSE17536 dataset ($p < 0.001$) (**Figures 3A, D**). Additionally, univariable and multivariable Cox regression analyses were conducted for identifying the relevant clinicopathological factors of colon cancer patients in TCGA and GSE17536, respectively. As a result, BGN was determined to be an independent prognostic biomarker that could be applied to predict poor OS in GSE17536 ($p = 0.006$) (**Figures 3E, F**). In the

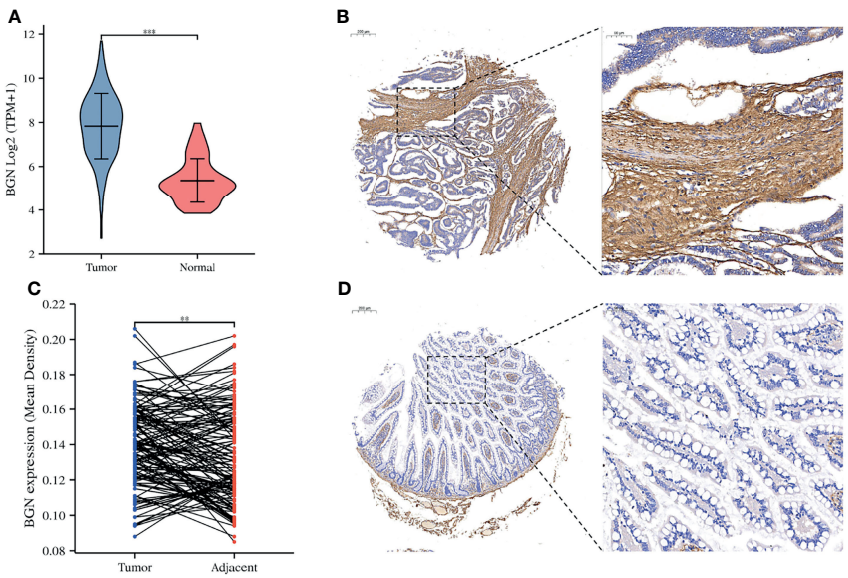

FIGURE 2 | The expression levels of BGN were significantly upregulated in patients with colon cancer. **(A)** The mRNA expression of BGN in the normal and tumor samples in TCGA. Data are represented as the mean ± SD. The Y-axis represents log2 (TPM+1) transformed RNA seq expression data. Wilcoxon rank sum test served as the statistical significance test. **(B, D)** Immunohistochemistry staining of example colon cancer patients with positive BGN staining in tumor tissues and the negative BGN staining in adjacent tissues. **(C)** Paired differentiation analysis for mean density of BGNs detected by immunohistochemistry staining sin tumor and paired adjacent tissues deriving from tumor microarray. The Wilcoxon signed rank test was used for comparison. Significant differences referred ass: $^{**}p < 0.01$, $^{***}p < 0.001$.

TABLE 1 | Association between BGN expression and clinicopathological factors of colon cancer patients.

Variables	Number of cases	Up-regulation of Biglycan numbers (%)		p value
		Positive (N=84)	Negative (N=60)	
Gender				
Male	99	58(69.05%)	41(68.33%)	0.927
Female	45	26(30.95%)	19(31.67%)	
Age (years)				
>=60	89	53(63.10%)	36(60.00%)	0.706
<60	55	31(36.90%)	24(40.00%)	
Tumor location				
Colon	83	52(61.90%)	31(51.67%)	0.220
Rectum	61	32(38.10%)	29(48.33%)	
Tumor size				
T1/T2	28	11(13.10%)	17(28.33%)	**0.023**
T3/T4	116	73(86.90%)	43(71.67%)	
Lymph node metastasis				
N0	68	41(48.81%)	27(45.00%)	0.652
N1/N2	76	43(51.19%)	33(55.00%)	
Distant metastasis				
M0	112	62(73.81%)	50(83.33%)	0.175
M1	32	22(26.19%)	10(16.67%)	
length of hospitalization				
< 10 days	44	20(23.81%)	24(40.00%)	**0.038**
<=10 days	100	64(76.19%)	36(60.00%)	
Tumor type				
ulcerative	33	18(21.43%)	15(25.00%)	0.615
Non-ulcerative	111	66(78.57%)	45(75.00%)	
Tumor differentiation				
Well to moderate	128	76(92.68%)	52(89.66%)	0.528
Poor	12	6(7.32%)	6(10.34%)	
Tumor stage				
I	19	8(9.52%)	11(18.33%)	0.124
II/III/IV	125	76(90.48%)	49(81.67%)	
Disease duration				
>3 months	45	28(33.73%)	17(29.31%)	0.580
<=3 months	96	55(66.27%)	41(70.69%)	
Serosa invasion				
Yes	115	73(86.90%)	42(70.00%)	**0.002**
No	29	11(13.10%)	18(30.00%)	

Length of stay was defined as the number of days the patient was hospitalized for surgical treatment of colon cancer. One day was defined as a hospital stay crossing midnight and was determined by independent physician review from medical records and patient reports. The p value was calculated by the Chi-square test. Bold numbers indicate statistically significant values (p < 0.05).

TCGA database, the prognostic significance of BGN as an independent prognostic factor was not statistically significant (p = 0.080) (**Figures 3B, C**).

The Correlation Between BGN Expression Levels and the TME Immune and Stromal Scores

Interactions of the TME and tumor cells are of great importance for tumor progression and the effect of immunotherapy. Based on the transcriptome data of TCGA, immune and stromal proportions of colon cancer tissues were calculated by a well-established ESTIMATE algorithm. Higher immune or stromal score represent a greater proportion of immune or stromal components in the TME, while ESTIMATE score represent the combined proportion of them. Through Kaplan–Meier analysis, we found that higher ESTIMATE score and immune score were both associated with poor OS (both p = 0.012) in colon cancer patients, except for the stromal score (p = 0.064) (**Figures 4A–C**), which is consistent with previously reported results (26). Moreover, correlation analysis demonstrated that BGN expression correlated with the immune score, stromal score and ESTIMATE score (Pearson r = 0.474, 0.733 and 0.648, respectively, all p < 0.001) in colon cancer (**Figure 4D**). Further analysis suggested that this association presented in a stage-independent mode (**Supplementary Figure 1**). These results suggested that the independent prognostic role of BGN in colon cancer might be associated with alterations in the TME.

The Role of BGN in Modulating Macrophage Polarization in Colon Cancer

For further investigation of the relationship between BGN and the subtypes of immune cell in colon cancer tissues, the proportion of tumor-infiltrating immune cells (TIICs) was segmented by using quanTIseq in TCGA. Among these TIIC subtypes, macrophages (M1 + M2) accounted for approximately 38%, neutrophils accounted for approximately 32%, CD4+ T cells accounted for 10% and NK cells accounted for 7% in colon cancer tissues (**Figure 5A**). The association between BGN

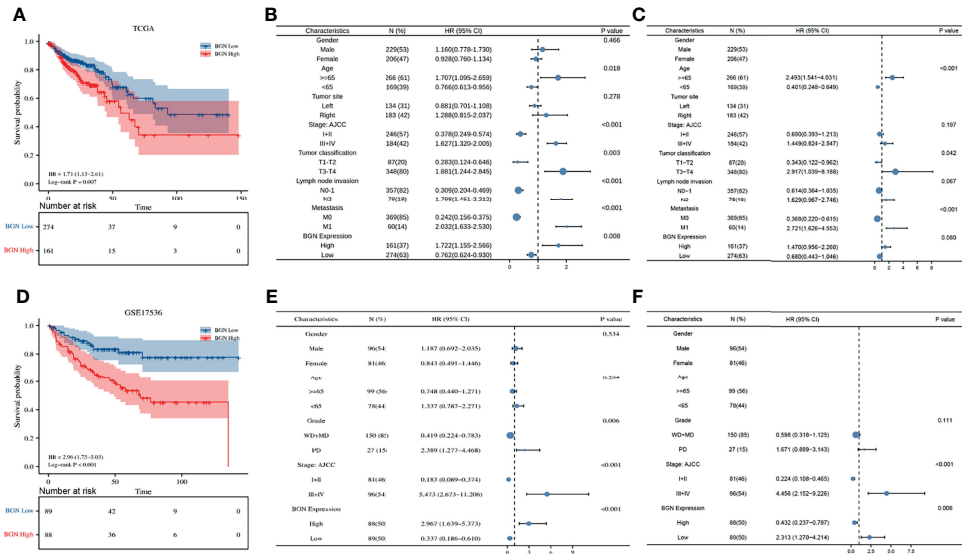

FIGURE 3 | The expression levels of BGN are correlated with overall survival and clinicopathological characteristics of colon cancer patients in TCGA and GSE17536 dataset. **(A, D)** Kaplan-Meier analysis of overall survival in colon cancer patients with different BGN expression. The significance was calculated by the Log-rank test. Number of patients remaining in follow-up at each time point is reported in the box below the figure for each group. **(B, C)** Univariate and multivariate cox regression analysis of clinicopathological characteristics and BGN expression with overall survival in TCGA. **(E, F)** Univariate and multivariate cox regression analysis of clinicopathological characteristics and BGN expression with overall survival in GSE17536. $p < 0.05$ was considered statistically significant. Whiskers represent the 95% confidence interval of the HR value, and dots represents the values of HR.

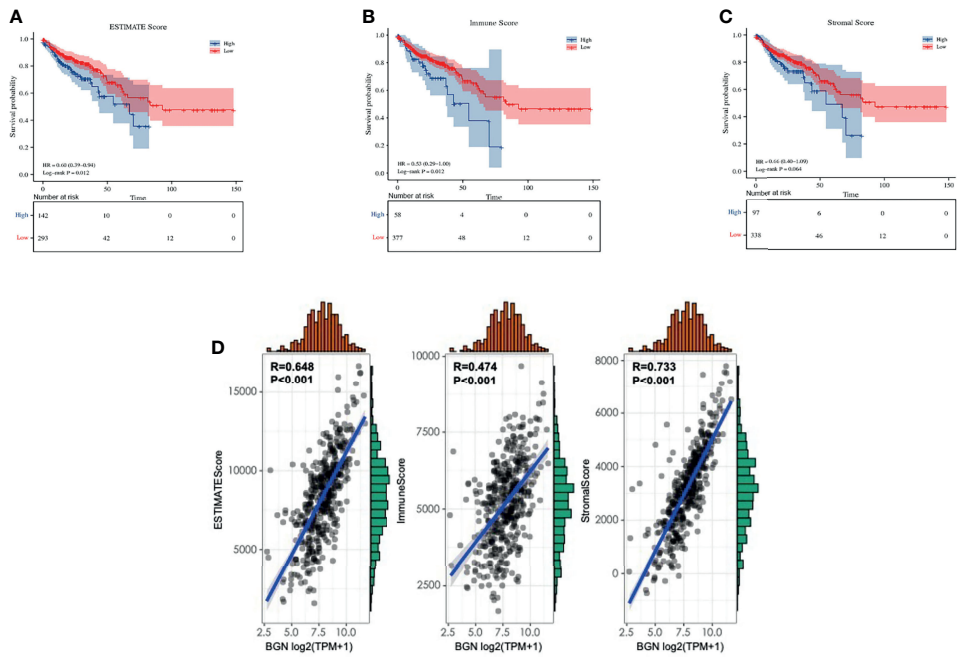

FIGURE 4 | The correlation between BGN expression and tumor microenvironment scores in colon cancer. **(A–C)** ESTIMATE score, immune score and stromal score in predicting overall survival of colon cancer based on Kaplan-Meier analysis. The significance was calculated by the Log-rank test. **(D)** BGN expression is strongly associated with estimate score, immune score and stromal score in colon cancer based on Pearson correlation analysis. $p < 0.05$ was considered statistically significant. The above analysis were based on TCGA expression data.

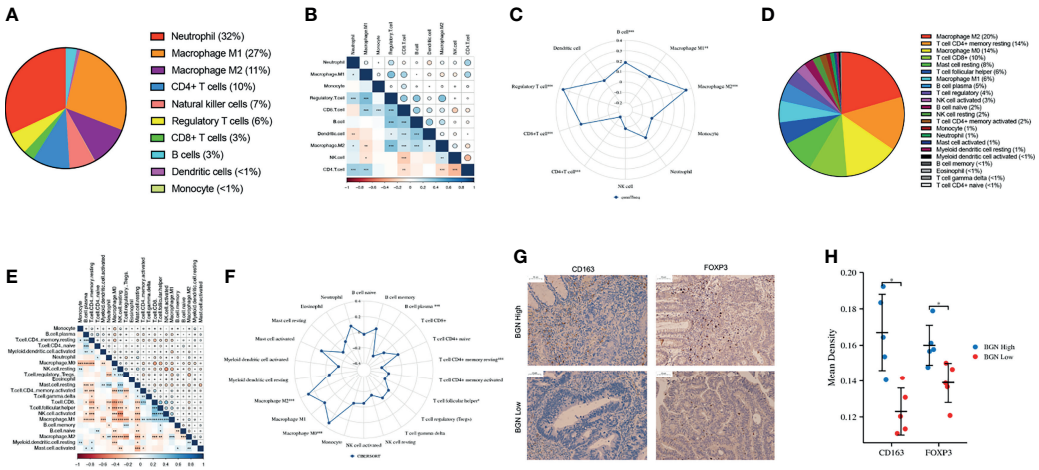

FIGURE 5 | TIIC profile in colon cancer samples and correlation analysis. **(A, D)** Pieplots showing the estimated proportion of different kinds of TIICs in colon tumor samples prediceted by **(A)** quanTIseq and **(D)** CIBERSORT. **(B, E)** Pearson correlation matrix of the different TIIC proportions in the colon cancer microenvironment quantified by **(B)** quanTIseq and **(E)** CIBERSORT. The size of each bubble and shadow of each tiny color box both represented a corresponding correlation value between two cells. Asterisks in each tiny box, indicating the p-value of the correlation between two cells. **(C, F)** Radar chart showing the correlation between BGN expression and different proportions of TIIC analyzed by **(C)** quanTIseq and **(F)** CIBERSORT. **(G)** Representative images of IHC staining for CD163 and FOXP3 in BGN high and low expression groups. **(H)** Quantification of IHC staining intensity for CD163 and FOXP3 in BGN high and low expression groups. Wilcoxon rank sum test served as the statistical significance test. *p < 0.05, **p < 0.01. ***p < 0.001.

expression levels and immune cell infiltration in colon cancer was explored (**Figure 5B**). Pearson correlation analysis indicated that BGN expression exhibited the most significantly related to the macrophage M2 population and regulatory T cell (Tregs) population (r = 0.34, 0.36, respectively, both p < 0.001) (**Figure 5C**). Next, we utilized the CIBERSORT method to validate the association of BGN expression and immune components by constructing 22 types of immune cell profiles in colon cancer and analyzed the proportion of TIICs (**Figures 5D, E**). The top three largest fractions of immune cells were macrophage M2 (20%), CD4+ memory resting T cell (14%) and macrophage M0 (14%) (**Figure 5D**), which revealed that macrophages may play a potential role in tumor immunity. Subsequent correlation analysis revealed that a total of five types of TIICs were strongly associated with BGN expression. Two of the TIICs (M0 macrophages and M2 macrophages) were in positive correlation with BGN expression. Three TIICs were correlated with BGN expression negatively, comprising plasma B cells, follicular helper T cells and resting memory CD4+ T cells (**Figure 5F**). Moreover, association between BGN expression and cell surface markers of diverse types of TIICs were assessed. Pearson correlation coefficients were calculated, and the results indicated that BGN presented the strongest correlations with TIIC markers for monocytes (CD86, CD115), tumor-associated macrophages (TAMs) (IL-10, CCL2, CD68), M2 macrophages (CD163, VSIG4, and MS4A4A) and Tregs (FOXP3, CCR8, TGFβ) (**Table 2**). In addition, the protein expression levels of M2 macrophage marker (CD163) and Tregs marker (FOXP3) were further validated in patient-derived tissue samples. Colon cancer samples with high BGN expression (n = 5) and low BGN expression (n = 5) were used for IHC analyses. As expected, in comparison with low BGN expression samples, both CD163 and FOXP3 were significantly upregulated in high BGN expression samples (**Figures 5G, H**). The above results demonstrated that high BGN expression might facilitate the polarization of M2 although further efforts are required to verify the underlying mechanisms.

Identification of the Potential Interaction of BGN in Colon Cancer Immune Responses

We then analyzed the differentially expressed genes (DEGs) between the high and low expression subgroups by the median level of BGN expression. A total of 1483 upregulated genes and 50 downregulated genes were obtained (adj.p-value < 0.05, fold change > 1.5 or < -1.5, **Figure 6A** and **Supplementary Table 1**). In subsequent GO enrichment analysis, DEGs were predominantly concentrated in extracellular organization as well as in immune-related functions, comprising regulation of leukocyte migration and regulation of T cell activation (**Figure 6B** and **Supplementary Table 2**). KEGG analysis results demonstrated that cell adhesion molecules (CAMs), cytokine-cytokine receptor interactions together with the PI3K–Akt signaling pathway were significantly enriched (**Figure 6C** and **Supplementary Table 3**). Moreover, a gene set enrichment analysis (GSEA) was implemented. For HALLMARK gene sets defined by MSigDB, the DEGs in BGN high-expression group showed significant enrichment for immunological activities, such as inflammatory response or complement and interferon response (**Figure 6D** and **Supplementary Table 4**). For the C7 collection, which was defined as an immunologic gene set, multiple functional gene sets that were involved in immunosuppression were enriched

TABLE 2 | Correlation analysis between BGN and related surface markers of immune cells.

Description	Gene markers	Cor	P
CD8+T cell	CD8A	0.307	***
	CD8B	0.177	***
T cell(general)	CD3D	0.277	***
	CD3E	0.384	***
	CD2	0.340	***
B cell	CD19	0.243	***
	CD79A	0.338	***
Monocyte	CD86	0.614	***
	CD115(CSF1R)	0.642	***
TAM	CCL2	0.632	***
	CD68	0.531	***
	IL10	0.434	***
M1 Macrophage	INOS(NOS2)	-0.153	**
	IRF5	0.323	***
	COX2(PTGS2)	0.198	***
M2 Macrophage	CD163	0.646	***
	VSIG4	0.628	***
	MS4A4A	0.582	***
Neutrophils	CD66b(CEACAM8)	-0.198	***
	CD11b(ITGAM)	0.703	***
	CCR7	0.377	***
Natural killer cell	KIR2DL1	0.180	***
	KIR2DL3	0.157	***
	KIR2DL4	0.157	***
	KIR3DL1	0.244	***
	KIR3DL2	0.223	***
	KIR3DL3	0.020	0.6649
	KIR2DS4	0.158	***
Dendritic cell	HLA-DPB1	0.544	***
	HLA-DQB1	0.339	***
	HLA-DRA	0.451	***
	HLA-DPA1	0.496	***
	BCDA-1(CD1C)	0.353	***
	BCDA-4(NRP1)	0.765	***
	CD11c(ITGAX)	0.711	***
Th1	T-bet(TBX21)	0.388	***
	STAT4	0.291	***
	STAT1	0.388	***
	IFN-γ(IFNG)	0.185	***
	TNF-α(TNF)	0.309	***
Th2	GATA3	0.488	***
	STAT6	0.062	0.1874
	STAT5A	0.311	***
	IL13	0.270	***
Tfh	BCL6	0.560	***
	IL21	0.221	***
Th17	STAT3	0.304	***
	IL17A	-0.236	***
Treg	FOXP3	0.567	***
	CCR8	0.529	***
	STAT5B	0.316	***
	TGFβ(TGFB1)	0.723	***

*The p value was calculated by the Pearson correlation analysis. Significant differences referred as: ***p < 0.001.*

(**Figure 6E** and **Supplementary Table 4**). These above results implied that BGN may act as a potential index for the immune status of the TME. To examine this further, we clarified the potential impact of BGN in the tumor immune response process. Manually curated gene sets associated with innate or adaptive immune responses were applied to quantify the immune status (**Figure 6F**). As a result, the immune response regulated by a series of immune cells tended to be "suppressive" with increasing of BGN expression, implying that BGN might also be involved in a negative interaction with the immune responses of colon cancer (**Figure 6G**).

Potential Role of BGN Expression in Predicting Immunotherapy Responses in Colon Cancer

Primarily, LAG3, SIGLEC15, CD274, PDCD1LG2, PDCD1, TIGIT, HAVCR2 and CTLA4 were selected as immune

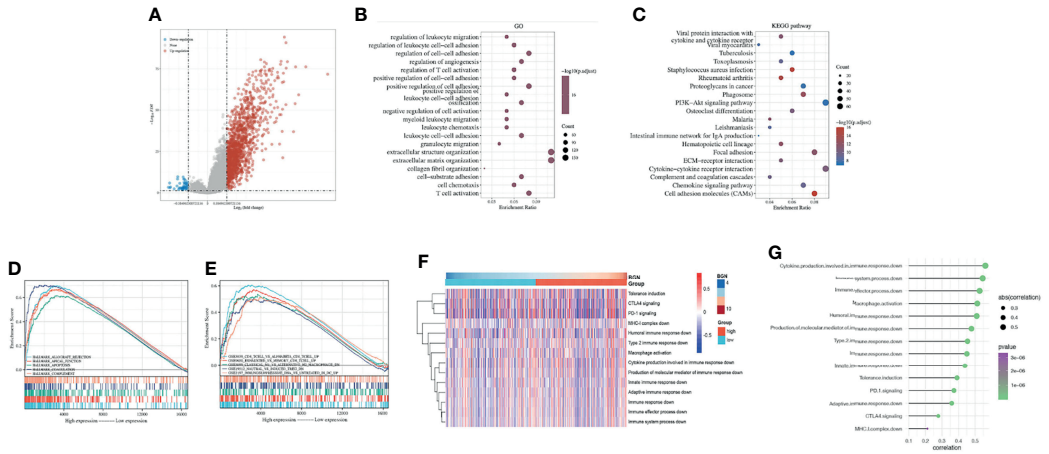

FIGURE 6 | Identification of the correlation between BGN and the regulation of immune responses in colon cancer. **(A)** Volcano plot of the DEGs expression between BGN high and low subgroups. The blue and red dots represented the significantly downregulated and upregulated genes, respectively; The gray dots represented the genes without differential expression. **(B, C)** GO and KEGG results for differential expression genes. The X-axis represents gene ratio and the Y-axis represents different enriched pathways. **(D, E)** The enriched gene sets in HALLMARK and C7 collections by samples of DEGs. Each line representing one particular gene set with unique color. Only gene sets with NOM p-value < 0.05 and FDR q-value < 0.05 were considered significant. **(F)** Heatmap showing BGN-associated GSVA scores of 14 innate and adaptive immunity-related gene sets. **(G)** Pearson correlation between the GSVA scores of 14 innate and adaptive immunity-related gene sets and the expression level of BGN in colon cancer.

checkpoint signature genes (27). Comparing with the BGN low-expression subgroup, all these genes exhibited elevated expression levels in the BGN high-expression subgroup (**Figure 7A**). Subsequently, we quantified the relative abundance of 24 TIICs in the TME using ImmuCellAI. As shown in **Figure 7B**, the correlation heatmap revealed various degrees of correlation between different TIIC subgroups. Notably, the proportion of TIICs varied significantly between the high and low expression subgroups of BGN (**Figure 7C**). Among them, we focused on two subgroups of Treg cells, induced Treg cells (iTregs) and natural Treg cells (nTregs). A positive correlation between BGN expression and the number of iTreg cells was found (**Figure 7D**), while it was the opposite with the number of nTreg cells (**Figure 7E**). To further investigate the

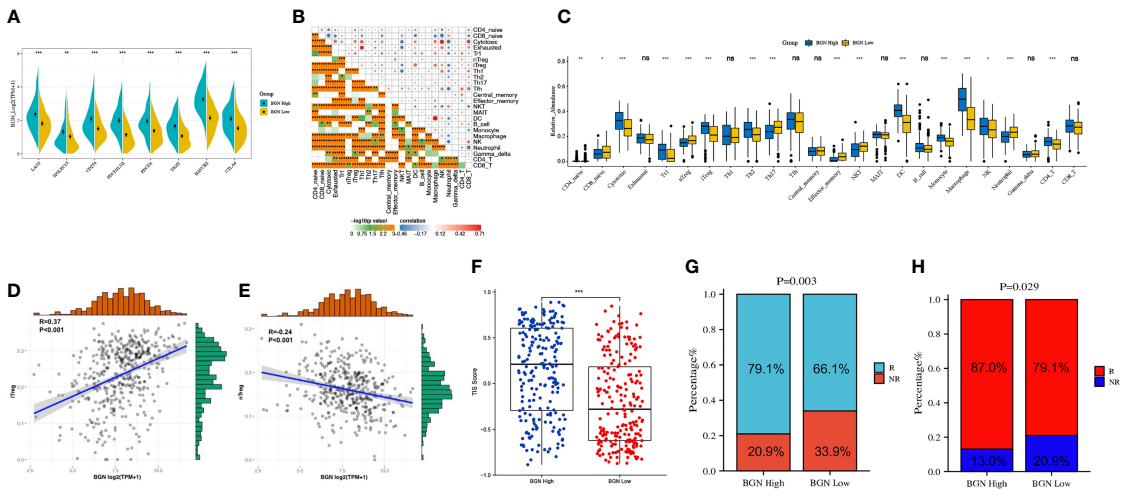

FIGURE 7 | Subgroups divided by levels of BGN expression predict potential immunotherapy responses of colon cancer. **(A)** Immune-checkpoint-relevant genes expressed in high and low BGN subgroups. Wilcoxon rank sum test served as the statistical significance test. **(B)** Pearson correlation matrix of the different TIIC proportions in the colon cancer microenvironment quantified by the ImmuCellAI. **(C)** The fraction of TILCs in BGN high and low subgroups. Wilcoxon rank sum test served as the statistical significance test. **(D, E)** The correlation between the abundance of **(D)** iTreg cells or **(E)** nTreg cells and the expression level of BGN. **(F)** T-cell inflammatory signature (TIS) scores across BGN subgroups. (Wilcoxon rank sum test, $p < 0.001$) **(G, H)** Response rates to immunotherapy of patients with colon cancer from the TCGA cohort predicted by the **(G)** ImmunCellAI (Chi-square test, $p = 0.003$) and **(H)** Tumor Immune Dysfunction and Exclusion (TIDE) web program (Chi-square test, $p = 0.029$) in the high or low BGN subgroups. *$p < 0.05$; **$p < 0.01$; ***$p < 0.001$; ns: $p > 0.05$ no significance.

potential contribution of BGN in predicting immunotherapy response of colon cancer, T-cell inflammatory signaling (TIS) scores were calculated in both high and low BGN expression subgroups. Patients with high BGN expression presented higher TIS score ($p < 0.001$), which was previously reported to correlate with the efficacy of anti-PD-1 inhibitor pembrolizumab (28) (**Figure 7F**). Moreover, immunotherapy response rates in patients with colon cancer were predicted by ImmuCellAI and TIDE algorithms. Patients with high BGN levels were more likely to respond to immunotherapy (79.1%) than those with low BGN levels (66.1%), as predicted by ImmuCellAI (**Figure 7G**). The TIDE algorithm similarly reached the conclusion that the immunotherapy response rates in patients with high and low BGN expression subgroups were 87% and 79.1%, respectively (**Figure 7H**). Collectively, BGN might be a promising indicator for quantifying the TME and predicting the response to ICB immunotherapy in colon cancer.

METHODS

Patients and Tissue Samples

144 pairs of cancer and adjacent normal tissues in total were included in this study. Tissue samples were obtained from patients with primary colon cancer who had undergone surgical resection at Changhai Hospital. This study was approved by the Clinical Research Ethics Committee of Changhai Hospital. The diagnoses for all patients were confirmed histopathologically of surgically resected tumors. TNM stage was defined according to the AJCC TNM Classification and histopathological classification of the resected tumors was performed. All fresh tissue samples were fixed with formalin and paraffinized for subsequent study. This study was conducted in compliance with the Declaration of Helsinki.

Tissue Microarray and Immunochemistry

The tissues were made into formalin-fixed paraffin-embedded tissue microarrays and slides, after which we performed dewaxing using xylene and hydration using a grade alcohol series. After citric acid solution or EDTA buffer (pH 9.0) were used for antigen retrieval, 3% H_2O_2 was applied for the inhibition of endogenous peroxidase. Then the sections were incubated with 5% BSA for 30 min. Next, HRP-conjugated goat anti-rabbit IgG (1:200, Servicebio) was incubated as the secondary antibody for 50 min. Sections were then stained with 3,3-diaminobenzidine (DAB) (Dako). The primary antibodies used were listed as follows: The anti-biglycan primary antibody (diluted 1:2000, Abcam), anti-CD163 primary antibody (diluted 1:500, Servicebio), anti-FOXP3 primary antibody (diluted 1:500, Abcam). Protein expression was assessed with the value of the mean optical density (MOD) using Image-Pro Plus 6.0 software. The definition of BGN positivity was that the ratio of the value of MOD in the tumor tissue to that in the tumor-adjacent tissue of the same patient was greater than 1. Conversely, if the ratio was less than or equal to 1, it was considered BGN negative.

Acquisition of Gene Expression Profiles

We downloaded the mRNA expression profiles of 435 colon adenocarcinoma (COAD) cases, 41 normal sample cases and the corresponding clinical data from TCGA (https://portal.gdc.cancer.gov/). The microarray datasets GSE4107, GSE110224, GSE4183 and GSE17536 were collected from GEO (Gene Expression Omnibus, http://www.ncbi.nlm.nih.gov/geo/). DEGs with upregulated or downregulated expression levels in GEO microarrays were analyzed with $|\log \text{fold change (FC)}| \geq 1.5$, and adjusted p-value < 0.05 as threshold. Gene expression data in these datasets were converted to transcripts per million (TPM) and processed for log (x + 1) normalization.

Human Protein-Protein Interaction Analysis

The STRING database (http://string-db.org) was utilized to construct PPI networks of coexpressed genes with interaction scores > 0.4. For visualization, CytoHubba, a plugin from the open-source platform Cytoscape (version 3.8.2) (http://www.cytoscape.org/), was employed to analyze and calculate the network structure and weighted reconnections between potential hub gene nodes by built-in algorithms. Darker nodes represent higher scores, and proteins with high scores are more likely to be key proteins.

Estimation and Bioinformatic Analysis of TIICs

The proportion of stromal-immune components in the TME of each sample was calculated with the ESTIMATE packages in R (29). The status of immune cell infiltration was acquired with the quanTIseq package in R, which performs an absolute quantification of 10 immune cell types from gene expression profiles (30). The results obtained were then validated by analysis with the 'CIBERSORT' R package (http://cibersort.stanford.edu/) (31), which has a preset LM22 leukocyte gene signature matrix to distinguish the proportion of immune cells. For in-depth exploration of the association between BGN expression and potential biological functions and pathways, we conducted GSVA analysis *via* the R package GSVA (32). In total, 14 immunity-related gene sets, which covered different processes of innate and adaptive response, were derived from the Molecular Signatures Database (MSigDB).

Quantification of the Relative Abundance of TIICs and Prediction of the Response to Immunotherapy

The Immune Cell Abundance Identifier (ImmuCellAI) (33) (http://bioinfo.life.hust.edu.cn/ImmuCellAI#!/analysis) represents a new algorithm capable of estimating of the abundance of 24 TIICs and predicting the response of patients to immune checkpoint blockers therapy based on gene expression datasets. Colon cancer samples in TCGA were calculated with the GSVA analysis using the T-cell inflammatory (TIS) signature, which has been reported to be a genetic profile that effectively predicts the clinical response to pembrolizumab in various tumor types (34). Tumor immune

dysfunction and exclusion (TIDE) (http://tide.dfci.harvard.edu/login/) (35), a computational algorithms that integrates data to assess mechanisms of two tumor immune escape. Patients with higher TIDE scores are more likely to experience from antitumor immune escape and consequently exhibit lower response rates to immune checkpoint blockers. In this study, TIS, ImmuCellAI and TIDE were performed for predicting the efficacy of ICBs in patients with colon cancer.

Survival Analysis

The R package "survival and survminer" was used for the survival analysis We plotted survival curves by the Kaplan-Meier method, and utilized log rank test generated p-values with $p < 0.05$ considered significant.

GO and KEGG Enrichment Analysis

DEGs was obtained by limma package (version: 3.40.2) of R software. GO and KEGG analyses were conducted by use of the ClusterProfiler package (version: 3.18.0) in R. Only terms with both p-values<0.05 and q-values<0.05 were considered significantly enriched.

Gene Set Enrichment Analysis

Hallmark and C7 gene set v7.2 collections downloaded from the Molecular Signatures Database (MsigDB) were selected as the target sets, with which GSEA performed *via* gsea-4.1.0 software. The pathways were considered statistically enriched with p-values < 0.05 and false discovery rate (FDR q-value < 0.05).

Statistical Analyses

Statistical analyses and figure generation were all executed in R (version 3.6.3), GraphPad Prism 8.0 and SPSS 25. Pearson's correlation analysis was used to gauge the degree of correlation between variables. For all statistical analyses, p-values < 0.05 was considered statistically significant.

DISCUSSION

Given the safety and efficacy of tumor immunotherapy, A variety of ICBs have been approved by the FDA for the treatment of colorectal cancer. However, the process of mobilizing autoimmunity to achieve tumor eradication is delicate and complex, involving antigen presentation, T cell activation, tumor targeting, overcoming local suppression and tumor killing (36). The completion of these key steps determines the efficacy of immunotherapy. Thus, identifying new biomarkers that accurately indicate immune status and patient prognosis is of great value to make more robust therapeutic decisions in colorectal cancer.

Previous study has identified BGN as one of CNV-mRNA-protein correlated molecules in colorectal cancer patients with liver metastasis by integrative analysis of multi-omics data (37). In our study, three GEO datasets that included colon cancer tissue and normal tissue were examined for identifying differentially expressed genes. The PPI network subsequently showed that BGN was at the core of the filtered differential genes. Furthermore, in agreement with previously published findings (37, 38), we discovered the average mRNA expression of BGN was higher in colon cancer tissues comparing with normal tissues in TCGA as well as in our own sample set. In addition, our results reaffirm that BGN could serve as a potential informative molecule in the prognosis of colon cancer. Notably, BGN expression levels were also observed to be strongly correlated with tumor size and serosa invasion in our sample set. Interestingly, although prognostic information was not available for these patients, days of hospitalization for surgical treatment of colon cancer was calculated, as this might be a potential metric for clinical benefit that has been used in other studies (39, 40). Correlation analysis of the length of hospitalization suggested that patients with higher BGN expression experienced a correspondingly longer hospitalization stay. The above results again highlight the potential value of BGN and disease prognostic biomarkers.

The TME, which comprises multiple cell types and extracellular components, plays an indispensable role in tumorigenesis and progression and triggers immune escape (36, 41). Previous studies demonstrated that both immune and stromal infiltration were associated with prognosis in cancers (11, 26). Our findings revealed that higher immune infiltration was associated with worse clinical outcomes in colon cancer. Furthermore, BGN expression levels were found positively related to ESTIMATE, stromal and immune scores. As a pivotal component of the extracellular matrix, laboratory data provide evidence that BGN acts as a crucial role in driving chronic inflammation and promoting proliferation, migration, and angiogenesis in tumor progression (23, 42, 43). Our findings indicate that BGN-based outcome prediction in colon cancer may be related to the stroma and immune cells of the TME.

TAM infiltration contributes significantly to the immunosuppressive tumor microenvironment (44, 45). TAMs are the predominant TIICs and are commonly polarized into an immunosuppressive and tumor-promoting M2-like phenotype (46, 47). A recent study showed that M2 macrophages were the only cell type that notably predicted the prognosis of colon cancer with a hazard ratio (HR) > 100 (48). Thus, in tumors with large macrophage infiltrates, altering immune-suppressive characteristics into immune-promoting properties represents a promising approach for colon cancer treatment, as various strategies including targeting the anti-inflammatory cytokine IL-10, targeting pathogen recognition receptors and exogenous Beta-1,6 glucan supplementation have been reported in previous studies (49–51). The present investigation suggests that BGN might act as a potentially essential modulator of macrophages in colon cancer, which is evidenced by quanTIseq and CIBERSORT analysis of the proportion of TIICs. Moreover, BGN expression was found to be positively associated with the typical markers of M2 macrophages, but not significantly with M1 markers. Accordingly, BGN may be involved in initiation and maintenance of M2 polarization in macrophages of colon cancer. Translationally, targeting BGN represents a possible strategy to reorient TAMs toward the antitumor M1 phenotype. Treg cells are another vital group of immunosuppressive cells that mediate immune tolerance,

inhibition of Tregs by targeting pivotal molecules could reverse tumor immunosuppression (52–54). In our present study, BGN-mediated immunosuppression may also involve Treg cells, which are functionally categorized into nTregs and iTregs (55). nTreg cells can interfere with cancer progression by reducing inflammation, while iTreg cells are the main suppressor cell subpopulation present at the tumor site that are responsible for suppressing the antitumor immune response (56). Interestingly, in our study, we found a contrasting correlation between these two subpopulations of Treg cells and BGN expression in colon cancer, with iTregs showing a positive trend distribution with BGN expression. These results illustrate a possible immunosuppressive role of BGN in the TME of colon cancer.

To obtain further insight into the underlying mechanisms and signaling pathways, DEGs between the high and low BGN expression groups were analyzed. As a result of GO and KEGG analyses, DEGs were concentrated in immune-related functions. Furthermore, GSEA and GSVA analyses showed that various immune response-suppressive gene sets and pathways were enriched in the BGN high expression group. Interestingly, a prior study has shown that BGN can significantly promote the expression of MHC-I molecules, enhance immunogenicity and thus promote the immune response in tumors (57). Conversely, in our study, high expression of BGN was proved to be implicated in the repression of both innate and adaptive immune responses in colon cancer. In particular, patients with high BGN expression similarly shared higher expression of immune checkpoint genes, since these molecules act as major negative regulators that inhibit T-cell proliferation and maintain T cells in an inactivated status (58, 59).

Currently, experiences from clinical studies and practices have demonstrated the clinical benefits of ICBs in a subset of patients with colon cancer, yet a substantial proportion of patients still rarely benefit from immunotherapy or relapse after a short-term benefit. The variation on the number, type and function of different immune cells in the TME might be critical factors in regulating the response to ICBs. It is thus hypothesized that the immune status of the TME, known as "cold" immunodesert tumors and "hot" inflammatory immunoinfiltrative tumors, correlates with the response of immunotherapy in cancer patients (34, 60). Consistent with this concept, high immune cell infiltration and high expression of immune checkpoints presented in BGN high expression subgroup suggested its potential clinical implication for predicting immunotherapeutic responsiveness. Moreover, patients in the high BGN subgroup attained higher TIS scores, which was reported to be related to the response to pembrolizumab. The response rate to immunotherapy in colon cancer patients was predicted by the ImmuCellAI and TIDE algorithms, both of which revealed that patients with high expression levels of BGN expression tended to be more likely to respond to immunotherapy.

Despite these promising findings, limitations still remain in this work. First, sample data were obtained from public sources as a result of lacking adequate clinical information to verify the prognostic impact of BGN and its predictive value on immunotherapy response in patients with colon cancer. Second, correlation analysis merely provides preliminary information of a relationship without identifying a causality between BGN and TIICs. BGN may display versatile and complex roles in the tumor immune response, which may depend on the cellular context according to previous reports and our study. Hence, *in vitro* and *in vivo* experiments will be needed to further elucidate the precise underlying molecular mechanisms of BGN in the tumor immune response.

In summary, this study provides preliminary evidence that BGN could serve as a valid biomarker for diagnosis, prognosis, and immunotherapy response prediction in patients with colon cancer. As each human tumor creates its own unique microenvironment, assessment of BGN expression represents a promising approach for identifying patients with the greatest potential to benefit from immunotherapy and a new venture into personalized therapy for cancer patients.

DATA AVAILABILITY STATEMENT

The datasets presented in this study can be found in online repositories. The names of the repository/repositories and accession number(s) can be found in the article/**Supplementary Material**.

ETHICS STATEMENT

The studies involving human participants were reviewed and approved by the Clinical Research Ethics Committee of Changhai Hospital. The patients/participants provided their written informed consent to participate in this study.

AUTHOR CONTRIBUTIONS

ZH, SZ and XF conceived and designed the study. JE, HF, YS, JW, PP, LG, TX and YL collected and analyzed the data. ZH, SZ and JE wrote the original draft. ZH and HF revised the manuscript. YB, SW and ZL reviewed and edited the manuscript. All authors contributed to the article and approved the submitted version. All authors contributed to the article and approved the submitted version.

FUNDING

YB is supported by the National Natural Science Foundation of China (grant 81873546 and 82170567), "Shu Guang" project of Shanghai Municipal Education Commission and Shanghai Education Development Foundation (grant 19SG30), the National Key R&D Program of China (grant 2018YFC1313103) and 234 Discipline Climbing Plan of Changhai Hospital, Second Military Medical University/Naval Medical University (grant 2019YXK004). S-LW is supported by the National Natural Science Foundation of China (no. 82100587), the Shanghai Sailing Program (grant 21YF1458700) and the Youth Star-tup Fund of Changhai

Hospital, Second Military Medical University/Naval Medical University (grant 2019QNB02). TX is supported by grants from the National Natural Science Foundation of China (grant 81702373). XF is supported by grants from the National Natural Science Foundation of China (grant 81800479).

SUPPLEMENTARY MATERIAL

The Supplementary Material for this article can be found online at: https://www.frontiersin.org/articles/10.3389/fonc.2021.761030/full#supplementary-material

REFERENCES

1. Sung H, Ferlay J, Siegel RL, Laversanne M, Soerjomataram I, Jemal A, et al. Global Cancer Statistics 2020: GLOBOCAN Estimates of Incidence and Mortality Worldwide for 36 Cancers in 185 Countries. *CA Cancer J Clin* (2021) 71(3):209–49. doi: 10.3322/caac.21660
2. Arnold M, Sierra MS, Laversanne M, Soerjomataram I, Jemal A, Bray F. Global Patterns and Trends in Colorectal Cancer Incidence and Mortality. *Gut* (2017) 66(4):683–91. doi: 10.1136/gutjnl-2015-310912
3. Ganesh K, Stadler ZK, Cercek A, Mendelsohn RB, Shia J, Segal NH, et al. Immunotherapy in Colorectal Cancer: Rationale, Challenges and Potential. *Nat Rev Gastroenterol Hepatol* (2019) 16(6):361–75. doi: 10.1038/s41575-019-0126-x
4. Dekker E, Tanis PJ, Vleugels JLA, Kasi PM, Wallace MB. Colorectal Cancer. *Lancet* (2019) 394(10207):1467–80. doi: 10.1016/s0140-6736(19)32319-0
5. Siegel RL, Miller KD, Fuchs HE, Jemal A. Cancer Statistics, 2021. *CA Cancer J Clin* (2021) 71(1):7–33. doi: 10.3322/caac.21654
6. Sveen A, Kopetz S, Lothe RA. Biomarker-Guided Therapy for Colorectal Cancer: Strength in Complexity. *Nat Rev Clin Oncol* (2019) 17(1):11–32. doi: 10.1038/s41571-019-0241-1
7. Procaccio L, Schirripa M, Fassan M, Vecchione L, Bergamo F, Prete AA, et al. Immunotherapy in Gastrointestinal Cancers. *BioMed Res Int* (2017) 2017:4346576. doi: 10.1155/2017/4346576
8. Barbee MS, Ogunniyi A, Horvat TZ, Dang TO. Current Status and Future Directions of the Immune Checkpoint Inhibitors Ipilimumab, Pembrolizumab, and Nivolumab in Oncology. *Ann Pharmacother* (2015) 49(8):907–37. doi: 10.1177/1060028015586218
9. Garon EB, Rizvi NA, Hui R, Leighl N, Balmanoukian AS, Eder JP, et al. Pembrolizumab for the Treatment of non-Small-Cell Lung Cancer. *N Engl J Med* (2015) 372(21):2018–28. doi: 10.1056/NEJMoa1501824
10. Overman MJ, McDermott R, Leach JL, Lonardi S, Lenz HJ, Morse MA, et al. Nivolumab in Patients With Metastatic DNA Mismatch Repair-Deficient or Microsatellite Instability-High Colorectal Cancer (Checkmate 142): An Open-Label, Multicentre, Phase 2 Study. *Lancet Oncol* (2017) 18(9):1182–91. doi: 10.1016/S1470-2045(17)30422-9
11. Wu X, Qu D, Weygant N, Peng J, Houchen CW. Cancer Stem Cell Marker DCLK1 Correlates With Tumorigenic Immune Infiltrates in the Colon and Gastric Adenocarcinoma Microenvironments. *Cancers* (2020) 12(2):274. doi: 10.3390/cancers12020274
12. Pickup MW, Mouw JK, Weaver VM. The Extracellular Matrix Modulates the Hallmarks of Cancer. *EMBO Rep* (2014) 15(12):1243–53. doi: 10.15252/embr.201439246
13. Henke E, Nandigama R, Ergün S. Extracellular Matrix in the Tumor Microenvironment and its Impact on Cancer Therapy. *Front Mol Biosci* (2020) 6:160. doi: 10.3389/fmolb.2019.00160
14. Wei R, Liu S, Zhang S, Min L, Zhu S. Cellular and Extracellular Components in Tumor Microenvironment and Their Application in Early Diagnosis of Cancers. *Anal Cell Pathol* (2020) 2020:1–13. doi: 10.1155/2020/6283796
15. Crotti S, Piccoli M, Rizzolio F, Giordano A, Nitti D, Agostini M. Extracellular Matrix and Colorectal Cancer: How Surrounding Microenvironment Affects Cancer Cell Behavior? *J Cell Physiol* (2017) 232(5):967–75. doi: 10.1002/jcp.25658
16. Schulz GB, Grimm T, Sers C, Riemer P, Elmasry M, Kirchner T, et al. Prognostic Value and Association With Epithelial-Mesenchymal Transition and Molecular Subtypes of the Proteoglycan Biglycan in Advanced Bladder Cancer. *Urol Oncol* (2019) 37(8):530.e9–e18. doi: 10.1016/j.urolonc.2019.05.011
17. Guo D, Zhang W, Yang H, Bi J, Xie Y, Cheng B, et al. Celastrol Induces Necroptosis and Ameliorates Inflammation *via* Targeting Biglycan in Human Gastric Carcinoma. *Int J Mol Sci* (2019) 20(22):5716. doi: 10.3390/ijms20225716
18. Wang B, Li G-X, Zhang S-G, Wang Q, Wen Y-G, Tang H-M, et al. Biglycan Expression Correlates With Aggressiveness and Poor Prognosis of Gastric Cancer. *Exp Biol Med* (2011) 236(11):1247–53. doi: 10.1258/ebm.2011.011124
19. Kocbek V, Hevir-Kene N, Bersinger NA, Mueller MD, Rizner TL. Increased Levels of Biglycan in Endometriomas and Peritoneal Fluid Samples From Ovarian Endometriosis Patients. *Gynecol Endocrinol* (2014) 30(7):520–4. doi: 10.3109/09513590.2014.898055
20. Zhou Y, Bian S, Zhou X, Cui Y, Wang W, Wen L, et al. Single-Cell Multiomics Sequencing Reveals Prevalent Genomic Alterations in Tumor Stromal Cells of Human Colorectal Cancer. *Cancer Cell* (2020) 38(6):818–28.e5. doi: 10.1016/j.ccell.2020.09.015
21. Zhao SF, Yin XJ, Zhao WJ, Liu LC, Wang ZP. Biglycan as a Potential Diagnostic and Prognostic Biomarker in Multiple Human Cancers. *Oncol Lett* (2020) 19(3):1673–82. doi: 10.3892/ol.2020.11266
22. Jacobsen F, Kraft J, Schroeder C, Hube-Magg C, Kluth M, Lang DS, et al. Up-Regulation of Biglycan Is Associated With Poor Prognosis and PTEN Deletion in Patients With Prostate Cancer. *Neoplasia* (2017) 19(9):707–15. doi: 10.1016/j.neo.2017.06.003
23. Pinto F, Santos-Ferreira L, Pinto MT, Gomes C, Reis CA. The Extracellular Small Leucine-Rich Proteoglycan Biglycan Is a Key Player in Gastric Cancer Aggressiveness. *Cancers (Basel)* (2021) 13(6):1330. doi: 10.3390/cancers13061330
24. Liang B, Zheng B, Zhou Y, Lai ZQ, Zhang C, Yan Z, et al. Characterization of a Tumor-Microenvironment-Relevant Gene Set Based on Tumor Severity in Colon Cancer and Evaluation of its Potential for Dihydroartemisinin Targeting. *Evid Based Complement Alternat Med* (2021) 2021:4812068. doi: 10.1155/2021/4812068
25. Liu J, Sun GL, Pan SL, Qin MB, Ouyang R, Huang JA. Identification of Hub Genes in Colon Cancer *via* Bioinformatics Analysis. *J Int Med Res* (2020) 48(9):300060520953234. doi: 10.1177/0300060520953234
26. Liu W, Ye H, Liu YF, Xu CQ, Zhong YX, Tian T, et al. Transcriptome-Derived Stromal and Immune Scores Infer Clinical Outcomes of Patients With Cancer. *Oncol Lett* (2018) 15(4):4351–7. doi: 10.3892/ol.2018.7855
27. Zhang X, Shi M, Chen T, Zhang B. Characterization of the Immune Cell Infiltration Landscape in Head and Neck Squamous Cell Carcinoma to Aid Immunotherapy. *Mol Ther Nucleic Acids* (2020) 22:298–309. doi: 10.1016/j.omtn.2020.08.030
28. Danaher P, Warren S, Lu R, Samayoa J, Sullivan A, Pekker I, et al. Pan-Cancer Adaptive Immune Resistance as Defined by the Tumor Inflammation Signature (TIS): Results From the Cancer Genome Atlas (TCGA). *J Immunother Cancer* (2018) 6(1):63. doi: 10.1186/s40425-018-0367-1
29. Yoshihara K, Shahmoradgoli M, Martinez E, Vegesna R, Kim H, Torres-Garcia W, et al. Inferring Tumour Purity and Stromal and Immune Cell Admixture From Expression Data. *Nat Commun* (2013) 4:2612. doi: 10.1038/ncomms3612
30. Finotello F, Mayer C, Plattner C, Laschober G, Rieder D, Hackl H, et al. Molecular and Pharmacological Modulators of the Tumor Immune Contexture Revealed by Deconvolution of RNA-Seq Data. *Genome Med* (2019) 11(1):34. doi: 10.1186/s13073-019-0638-6
31. Newman AM, Liu CL, Green MR, Gentles AJ, Feng W, Xu Y, et al. Robust Enumeration of Cell Subsets From Tissue Expression Profiles. *Nat Methods* (2015) 12(5):453–7. doi: 10.1038/nmeth.3337
32. Hanzelmann S, Castelo R, Guinney J. GSVA: Gene Set Variation Analysis for Microarray and RNA-Seq Data. *BMC Bioinf* (2013) 14:7. doi: 10.1186/1471-2105-14-7
33. Miao YR, Zhang Q, Lei Q, Luo M, Xie GY, Wang H, et al. Immucellai: A Unique Method for Comprehensive T-Cell Subsets Abundance Prediction

and its Application in Cancer Immunotherapy. *Adv Sci (Weinh)* (2020) 7 (7):1902880. doi: 10.1002/advs.201902880
34. Garcia-Mulero S, Alonso MH, Pardo J, Santos C, Sanjuan X, Salazar R, et al. Lung Metastases Share Common Immune Features Regardless of Primary Tumor Origin. *J Immunother Cancer* (2020) 8(1):e000491. doi: 10.1136/jitc-2019-000491
35. Jiang P, Gu S, Pan D, Fu J, Sahu A, Hu X, et al. Signatures of T Cell Dysfunction and Exclusion Predict Cancer Immunotherapy Response. *Nat Med* (2018) 24(10):1550–8. doi: 10.1038/s41591-018-0136-1
36. Joyce JA, Fearon DT. T Cell Exclusion, Immune Privilege, and the Tumor Microenvironment. *Science* (2015) 348(6230):74–80. doi: 10.1126/science.aaa6204
37. Ma YS, Huang T, Zhong XM, Zhang HW, Cong XL, Xu H, et al. Proteogenomic Characterization and Comprehensive Integrative Genomic Analysis of Human Colorectal Cancer Liver Metastasis. *Mol Cancer* (2018) 17 (1):139. doi: 10.1186/s12943-018-0890-1
38. Chen D, Qin Y, Dai M, Li L, Liu H, Zhou Y, et al. BGN and COL11A1 Regulatory Network Analysis in Colorectal Cancer (CRC) Reveals That BGN Influences CRC Cell Biological Functions and Interacts With MiR-6828-5p. *Cancer Manag Res* (2020) 12:13051–69. doi: 10.2147/CMAR.S277261
39. Filippatos G, Teerlink JR, Farmakis D, Cotter G, Davison BA, Felker GM, et al. Serelaxin in Acute Heart Failure Patients With Preserved Left Ventricular Ejection Fraction: Results From the RELAX-AHF Trial. *Eur Heart J* (2014) 35 (16):1041–50. doi: 10.1093/eurheartj/eht497
40. Thomas R, Fysh ETH, Smith NA, Lee P, Kwan BCH, Yap E, et al. Effect of an Indwelling Pleural Catheter vs Talc Pleurodesis on Hospitalization Days in Patients With Malignant Pleural Effusion: The AMPLE Randomized Clinical Trial. *JAMA* (2017) 318(19):1903–12. doi: 10.1001/jama.2017.17426
41. Chen DS, Mellman I. Elements of Cancer Immunity and the Cancer-Immune Set Point. *Nature* (2017) 541(7637):321–30. doi: 10.1038/nature21349
42. Roedig H, Damiescu R, Zeng-Brouwers J, Kutija I, Trebicka J, Wygrecka M, et al. Danger Matrix Molecules Orchestrate CD14/CD44 Signaling in Cancer Development. *Semin Cancer Biol* (2020) 62:31–47. doi: 10.1016/j.semcancer.2019.07.026
43. Cong L, Maishi N, Annan DA, Young MF, Morimoto H, Morimoto M, et al. Inhibition of Stromal Biglycan Promotes Normalization of the Tumor Microenvironment and Enhances Chemotherapeutic Efficacy. *Breast Cancer Res* (2021) 23(1):51. doi: 10.1186/s13058-021-01423-w
44. Ricketts TD, Prieto-Dominguez N, Gowda PS, Ubil E. Mechanisms of Macrophage Plasticity in the Tumor Environment: Manipulating Activation State to Improve Outcomes. *Front Immunol* (2021) 12:642285. doi: 10.3389/fimmu.2021.642285
45. Wang YC, Wang X, Yu J, Ma F, Li Z, Zhou Y, et al. Targeting Monoamine Oxidase a-Regulated Tumor-Associated Macrophage Polarization for Cancer Immunotherapy. *Nat Commun* (2021) 12(1):3530. doi: 10.1038/s41467-021-23164-2
46. Noy R, Pollard JW. Tumor-Associated Macrophages: From Mechanisms to Therapy. *Immunity* (2014) 41(1):49–61. doi: 10.1016/j.immuni.2014.06.010
47. Magkouta SF, Vaitsi PC, Pappas AG, Iliopoulou M, Kosti CN, Psarra K, et al. CSF1/CSF1R Axis Blockade Limits Mesothelioma and Enhances Efficiency of Anti-PDL1 Immunotherapy. *Cancers (Basel)* (2021) 13(11):2546. doi: 10.3390/cancers13112546
48. Zhang X, Quan F, Xu J, Xiao Y, Li X, Li Y. Combination of Multiple Tumor-Infiltrating Immune Cells Predicts Clinical Outcome in Colon Cancer. *Clin Immunol* (2020) 215:108412. doi: 10.1016/j.clim.2020.108412
49. Guiducci C, Vicari AP, Sangaletti S, Trinchieri G, Colombo MP. Redirecting *In Vivo* Elicited Tumor Infiltrating Macrophages and Dendritic Cells Towards Tumor Rejection. *Cancer Res* (2005) 65(8):3437–46. doi: 10.1158/0008-5472.CAN-04-4262
50. Vogelpoel LT, Hansen IS, Rispens T, Muller FJ, van Capel TM, Turina MC, et al. Fc Gamma Receptor-TLR Cross-Talk Elicits Pro-Inflammatory Cytokine Production by Human M2 Macrophages. *Nat Commun* (2014) 5:5444. doi: 10.1038/ncomms6444
51. Cheng H, Sun L, Shen D, Ren A, Ma F, Tai G, et al. Beta-1,6 Glucan Converts Tumor-Associated Macrophages Into an M1-Like Phenotype. *Carbohydr Polym* (2020) 247:116715. doi: 10.1016/j.carbpol.2020.116715
52. Kim M, Min YK, Jang J, Park H, Lee S, Lee CH. Single-Cell RNA Sequencing Reveals Distinct Cellular Factors for Response to Immunotherapy Targeting CD73 and PD-1 in Colorectal Cancer. *J Immunother Cancer* (2021) 9(7): e002503. doi: 10.1136/jitc-2021-002503
53. Zhan Y, Zheng L, Liu J, Hu D, Wang J, Liu K, et al. PLA2G4A Promotes Right-Sided Colorectal Cancer Progression by Inducing CD39+Gammadelta Treg Polarization. *JCI Insight* (2021) 6(16):e148028. doi: 10.1172/jci.insight.148028
54. Doleschel D, Hoff S, Koletnik S, Rix A, Zopf D, Kiessling F, et al. Regorafenib Enhances Anti-PD1 Immunotherapy Efficacy in Murine Colorectal Cancers and Their Combination Prevents Tumor Regrowth. *J Exp Clin Cancer Res* (2021) 40(1):288. doi: 10.1186/s13046-021-02043-0
55. Whiteside TL, Schuler P, Schilling B. Induced and Natural Regulatory T Cells in Human Cancer. *Expert Opin Biol Ther* (2012) 12(10):1383–97. doi: 10.1517/14712598.2012.707184
56. Mandapathil M, Szczepanski MJ, Szajnik M, Ren J, Jackson EK, Johnson JT, et al. Adenosine and Prostaglandin E2 Cooperate in the Suppression of Immune Responses Mediated by Adaptive Regulatory T Cells. *J Biol Chem* (2010) 285(36):27571–80. doi: 10.1074/jbc.M110.127100
57. Subbarayan K, Leisz S, Wickenhauser C, Bethmann D, Massa C, Steven A, et al. Biglycan-Mediated Upregulation of MHC Class I Expression in HER-2/Neu-Transformed Cells. *Oncoimmunology* (2018) 7(4):e1373233. doi: 10.1080/2162402X.2017.1373233
58. Wang C, Feng H, Cheng X, Liu K, Cai D, Zhao R. Potential Therapeutic Targets of B7 Family in Colorectal Cancer. *Front Immunol* (2020) 11:681. doi: 10.3389/fimmu.2020.00681
59. Acharya N, Sabatos-Peyton C, Anderson AC. Tim-3 Finds its Place in the Cancer Immunotherapy Landscape. *J Immunother Cancer* (2020) 8(1): e000911. doi: 10.1136/jitc-2020-000911
60. Janji B, Hasmim M, Parpal S, De Milito A, Berchem G, Noman MZ. Lighting Up the Fire in Cold Tumors to Improve Cancer Immunotherapy by Blocking the Activity of the Autophagy-Related Protein PIK3C3/VPS34. *Autophagy* (2020) 16(11):2110–1. doi: 10.1080/15548627.2020.1815439

Conflict of Interest: The authors declare that the research was conducted in the absence of any commercial or financial relationships that could be construed as a potential conflict of interest.

Publisher's Note: All claims expressed in this article are solely those of the authors and do not necessarily represent those of their affiliated organizations, or those of the publisher, the editors and the reviewers. Any product that may be evaluated in this article, or claim that may be made by its manufacturer, is not guaranteed or endorsed by the publisher.

frontiers in Oncology

ORIGINAL RESEARCH
published: 09 February 2022
doi: 10.3389/fonc.2022.759403

Clinicopathological Features, Prognostic Factors and Survival in Patients With Pancreatic Cancer Bone Metastasis

Ying Ren[1,2,3†], *Shicheng Wang*[4†], *Bo Wu*[5†] *and Zhan Wang*[1,2,3*]

[1] Department of Orthopedic Surgery, The Second Affiliated Hospital, Zhejiang University School of Medicine, Hangzhou, China, [2] Orthopedics Research Institute of Zhejiang University, Hangzhou, China, [3] Key Laboratory of Motor System Disease Research and Precision Therapy of Zhejiang Province, Hangzhou, China, [4] Department of Orthopedics, Ningbo No.6 Hospital, Ningbo, China, [5] Department of Orthopedic Oncology, Affiliated Hangzhou Cancer Hospital, Zhejiang University School of Medicine, Hangzhou, China

OPEN ACCESS

Edited by:
Nadia M. Hamdy,
Ain Shams University, Egypt

Reviewed by:
Bethany A. Kerr,
Wake Forest School of Medicine, United States
Hideo Baba,
Kumamoto University, Japan

***Correspondence:**
Zhan Wang
wangzhanhz@zju.edu.cn

[†]These authors have contributed equally to this work

Specialty section:
This article was submitted to Gastrointestinal Cancers: Hepato Pancreatic Biliary Cancers, a section of the journal Frontiers in Oncology

Received: 16 August 2021
Accepted: 19 January 2022
Published: 09 February 2022

Citation:
Ren Y, Wang S, Wu B and Wang Z (2022) Clinicopathological Features, Prognostic Factors and Survival in Patients With Pancreatic Cancer Bone Metastasis. Front. Oncol. 12:759403. doi: 10.3389/fonc.2022.759403

Purpose: The purpose of this study is to reveal the clinicopathological features and identify risk factors of prognosis among patients with pancreatic cancer bone metastasis (PCBM).

Patients and Methods: Patients with PCBM were retrieved from the Surveillance, Epidemiology, and End Results (SEER) database between 2010 and 2016. Independent predictors for survival of those patients were determined by the univariate and multivariate Cox regression analysis. Forest plots were drawn by GraphPad 8.0.1 and used to visually display the results of multivariate analysis.

Results: We identified 2072 eligible PCBM patients, of which 839 patients (40.5%) were female. Patients with age >60 years accounted for 70.6%. Multivariable Cox regression analysis indicated that age, pathological type, chemotherapy, liver metastasis, lung metastasis, and marital status were independent prognostic factors for both overall survival (OS) and cancer-specific survival (CSS). Kaplan–Meier survival curves showed that for patients with PCBM, age ≤60 years, non-ductal adenocarcinoma type, chemotherapy, no liver metastasis, no lung metastasis, and married status were correlated with increased survival. This population-based study showed that 1-year OS and CSS were 13.6% and 13.7%, respectively.

Conclusion: The present study identified six independent predictors of prognosis in PCBM, including age, pathological type, chemotherapy, liver metastasis, lung metastasis, and marital status. Knowledge of these survival predictors is helpful for clinicians to accelerate clinical decision process and design personalized treatment for patients with PCBM.

Keywords: pancreatic cancer, bone metastasis, prognosis, risk factor, clinicopathological features

INTRODUCTION

Pancreatic cancer (PC) is a highly aggressive and metastatic malignancy, characterized by a high mortality. It has an extremely poor survival, with 5-year survival rate of less than 8% (1–3). Even if the diagnosis and treatment technology of PC improve, its prognosis has improved marginally over the past decades (4). The majority of PC patients develop metastasis either at the time of initial diagnosis or after initial diagnosis, which posts a new challenge for clinicians (3). He et al. (5) reported that liver and peritoneum metastases accounted for 45.1% and 49.9% of metastatic PC patients, respectively, which may be due to their anatomical sites (6). Other less common sites are the lung (11.4%), brain (0.4%), and bone (3.8%) (5). Although some previous studies focused on liver or lung metastasis of PC (7–9), studies on bone metastasis are scarce. The prevalence of bone metastasis in PC patients ranges from 5% to 20% (10, 11). Bone metastasis can result in skeletal related events (SREs), including hypercalcemia, bone pain, pathological fractures, spinal cord compression, and radiotherapy or surgery to the bone, which not only decreases the quality of life but also contributes to an unfavorable prognosis (12–14). Additionally, most bone metastases caused by pancreatic cancer are lytic lesions (15).

Previous studies reported that age, gender, tumor size, tumor location, histological type, T and N stages, histologic differentiation, radiotherapy, and chemotherapy were independent prognostic factors for PC (16, 17). Liu et al. (18) reported that age, gender, tumor size, alanine aminotransferase level (ALT) and CA19-9 were correlated with distant metastasis. Current therapeutic options for PC included surgical resection, radiotherapy, chemotherapy, immunotherapy, and et al. (19). However, there are few studies on the treatment of metastatic PC. To our knowledge, there are few studies reporting the pancreatic cancer bone metastasis (PCBM). Therefore, the present study was conducted to define the clinicopathological features and identify independent survival predictors of PCBM. To obtain insight into PCBM, we conducted a large-scale study by analyzing data of PCBM from the Surveillance, Epidemiology, and End Results (SEER) database.

MATERIALS AND METHODS

Patient Selection

Data of patients diagnosed with PCBM, were extracted from the SEER*Stat version 8.3.9 software between 2010 and 2016. The SEER database collects malignant cancer information from 18 population-based cancer registries, representing approximately a third of the U.S. population (20). As the SEER database is public available and contains no patient-identified information, ethnic approval is not needed.

We first used the case-listing session to select the Site recode ICD-O-3/WHO 2008 "Pancreas". Meanwhile, we set the SEER Combined Mets at DX-bone (2010+) to be YES. Thus, a total of 2842 patients with PCBM were enrolled. 764 patients diagnosed not by pathology were excluded. Additionally, six patients where the cancer was found upon autopsy or necropsy were excluded. **Figure 1** showed the flow chart for selection of study population.

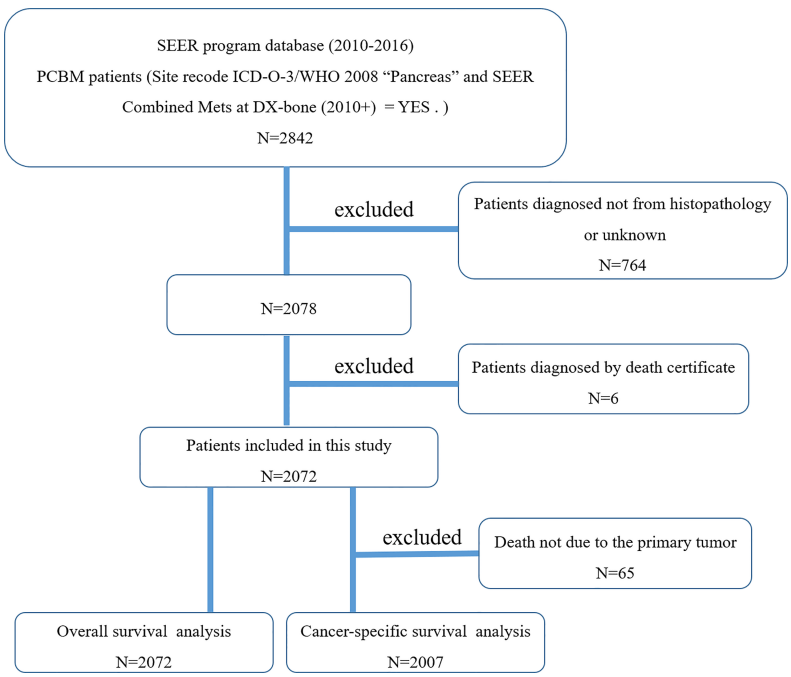

FIGURE 1 | The flow chart for selection of study population. (SEER, Surveillance, Epidemiology, and End Results; ICD-O-3, international classification of diseases for oncology, 3rd edition; PCBM, pancreatic cancer bone metastasis).

Variables obtained from the SEER database were race, gender, age at diagnosis, primary tumor site, pathological type, tumor size, surgery, radiotherapy, chemotherapy, organ metastases, marital status, vital status, survival time, and cause of death. Surgery or radiotherapy in the present study refers to treatment for primary tumor site. Overall survival (OS) was defined as the time from the date of diagnosis to the time of death from any cause (21, 22). Cancer-specific survival (CSS) was defined as the time from the date of diagnosis to the date of death from PC (21, 22).

Statistical Methods

Univariate and multivariable Cox regression models were used to identify independent predictors of OS and CSS. Meanwhile, hazard ratio (HR) and their 95% confidence interval (95% CIs) were presented in both univariate and multivariate analysis. Kaplan–Meier survival curves were applied to compare the differences among these groups by the log-rank test. Chi-square test is used to compare the rates of two groups. SPSS 21.0 software was used to conduct all above statistical tests and risk factors of $p<0.05$ were considered as significant predictors. Additionally, we drew Forest plots by GraphPad 8.0.1 to visually display the results of multivariate analysis.

RESULTS

Clinicopathologic Characteristics

We identified 2072 eligible patients with PCBM. The baseline characteristics of all patients in the current study were summarized in the **Table 1**. Among the population, 79.5%, 11.4%, and 9.1% of patients were white, black, and other races, respectively. More than half of the patients (n=1233, 59.5%) were males. As for age, more patients with age > 60 years (n=1463, 70.6%) were observed. There were 518(25.0%), 285(13.8%), and 503(24.3%) of cases located in head of pancreas, body of pancreas, and tail of pancreas, respectively. Ductal adenocarcinoma accounted for 75.1% of all pathological type. 899(43.4%) of patients presented with tumor size <5 cm, and 511 (24.7%) of patients presented with tumor size ≥ 5 cm. Regarding the treatment, more than half of the patients (51.9%) received chemotherapy, while only 24.7% and 1.4% of patients received radiotherapy and surgery, respectively. As for visceral metastasis, only 3.3% of patients presented with brain metastasis, while 28.7% and 38.8% of patients developed liver and lung metastases, respectively. In addition, more than half of the patients (n=1233, 59.5%) got married. The 1-year OS and CSS rates of the population were 13.6% and 13.7%, respectively.

TABLE 1 | Characteristics of 2072 patients with pancreatic cancer bone metastasis.

Variable	Value
Race	
White	1647 (79.5%)
Black	237 (11.4%)
Others	188 (9.1%)
Gender	
Female	839 (40.5%)
Male	1233 (59.5%)
Age (years)	
≤60	609 (29.4%)
>60	1463 (70.6%)
Mean	66
Median	67
Primary site	
Head of pancreas	518 (25.0%)
Body of pancreas	285 (13.8%)
Tail of pancreas	503 (24.3%)
Others*	766 (37.0%)
Pathological type	
Ductal adenocarcinoma	1557 (75.1%)
Non-ductal adenocarcinoma	515 (24.9%)
Tumor size (cm)	
<5	899 (43.4%)
≥5	511 (24.7%)
Unknown	662 (31.9%)
Surgery	
Yes	28 (1.4%)
No	2044 (98.6%)
Radiotherapy	
Yes	512 (24.7%)
No	1560 (75.3%)
Chemotherapy	
Yes	1075 (51.9%)
No	997 (48.1%)
Brain metastasis	
No	1906 (92.0%)
Yes	69 (3.3%)
Unknown	97 (4.7%)
Liver metastasis	
No	1445 (69.7%)
Yes	594 (28.7%)
Unknown	33 (1.6%)
Lung metastasis	
No	1266 (61.1%)
Yes	804 (38.8%)
Unknown	2 (0.1%)
Marital status	
Married	1137 (54.9%)
Others	843 (40.7%)
Unknown	92 (4.4%)
Dead	
Yes	1874 (90.4%)
No	198 (9.6%)
1-year OS rate	13.60%
1-year CSS rate	13.70%

*OS, overall survival; CSS, cancer-specific survival. *Others: C25.3-Pancreatic duct, and C25.4-Islets of Langerhans, C25.7-Other specified parts of pancreas, C25.8-Overlapping lesion of pancreas, C25.9-Pancreas, NOS.*

Univariate Cox Regression Analysis

Potential risk factors for the OS and CSS by univariate analysis are summarized in **Table 2**. The results showed that age (>60 years vs. ≤60 years, HR=1.265; 95% CI, 1.143-1.399; $p<0.001$), primary site (Body of pancreas vs. Head of pancreas, HR=0.918, 95% CI, 0.787-1.071, $p=0.277$; Tail of pancreas vs. Head of pancreas, HR=1.078, 95% CI, 0.947-1.226, $p=0.254$; Others vs. Head of pancreas, HR=1.159, 95% CI, 1.031-1.302, $p=0.014$), pathological type (Non-ductal adenocarcinoma vs. Ductal adenocarcinoma, HR=0.689; 95% CI, 0.618-0.769; $p<0.001$), local radiotherapy (No vs. Yes, HR=1.236; 95% CI, 1.112-

TABLE 2 | Univariate Cox analysis of variables in pancreatic cancer bone metastasis.

Variable	OS		CSS	
	HR (95% CI)	*p*	HR (95% CI)	*p*
Race				
White	1		1	
Black	1.005 (0.870-1.160)	0.948	0.982 (0.847-1.139)	0.808
Others	1.007 (0.858-1.183)	0.929	1.007 (0.844-1.168)	0.932
Gender				
Female	1		1	
Male	1.075 (0.980-1.179)	0.124	1.071 (0.975-1.177)	0.152
Age (years)				
≤60	1		1	
>60	1.265 (1.143-1.399)	<0.001	1.264 (1.141-1.400)	<0.001
Primary site				
Head of pancreas	1		1	
Body of pancreas	0.918 (0.787-1.071)	0.277	0.912 (0.779-1.068)	0.254
Tail of pancreas	1.078 (0.947-1.226)	0.254	1.086 (0.952-1.238)	0.219
Others	1.159 (1.031-1.302)	0.014	1.157 (1.027-1.304)	0.016
Pathological type				
Ductal adenocarcinoma	1		1	
Non-ductal adenocarcinoma	0.689 (0.618-0.769)	<0.001	0.681 (0.609-0.762)	<0.001
Tumor size (cm)				
<5	1		1	
≥5	1.087 (0.969-1.220)	0.156	1.082 (0.962-1.216)	0.188
Radiotherapy				
Yes	1		1	
No	1.236 (1.112-1.374)	<0.001	1.228 (1.103-1.366)	<0.001
Chemotherapy				
Yes	1		1	
No	2.334 (2.125-2.565)	<0.001	2.367 (2.150-2.606)	<0.001
Brain metastasis				
No	1		1	
Yes	1.064 (0.827-1.368)	0.629	1.117 (0.863-1.445)	0.4
Liver metastasis				
No	1		1	
Yes	1.301 (1.176-1.440)	<0.001	1.293 (1.166-1.434)	<0.001
Lung metastasis				
No	1		1	
Yes	1.288 (1.174-1.414)	<0.001	1.288 (1.171-1.416)	<0.001
Marital status				
Married	1		1	
Others	1.195 (1.088-1.313)	<0.001	1.181 (1.073-1.299)	<0.001

1.374; p<0.001), systemic chemotherapy (No vs. Yes, HR=2.334; 95% CI, 2.125-2.565; *p*<0.001), liver metastasis (Yes vs. No, HR=1.301; 95% CI, 1.176-1.440; *p*<0.001), lung metastasis (Yes vs. No, HR=1.288; 95% CI, 1.174-1.414; *p*<0.001), and marital status(Others vs. Married, HR=1.195; 95% CI, 1.088-1.313; *p*<0.001), were significantly associated with OS. In terms of CSS, age (>60 years vs. ≤60 years, HR=1.264; 95% CI, 1.141-1.400; *p*<0.001), primary site (Body of pancreas vs. Head of pancreas, HR=0.912, 95% CI, 0.779-1.068, *p*=0.254; Tail of pancreas vs. Head of pancreas, HR=1.086, 95% CI, 0.952-1.238, *p*=0.219; Others vs. Head of pancreas, HR=1.157, 95% CI, 1.027-1.304, *p*=0.016), pathological type (Non-ductal adenocarcinoma vs. Ductal adenocarcinoma, HR=0.681; 95% CI, 0.609-0.762; *p*<0.001), local radiotherapy (No vs. Yes, HR=1.228; 95% CI, 1.103-1.366; p<0.001), systemic chemotherapy (No vs. Yes, HR=2.367; 95% CI, 2.150-2.606; *p*<0.001), liver metastasis (Yes vs. No, HR=1.293; 95% CI, 1.166-1.434; *p*<0.001), lung metastasis (Yes vs. No, HR=1.288; 95% CI, 1.171-1.416; *p*<0.001), and marital status(Others vs. Married, HR=1.181; 95% CI, 1.073-1.299; *p*<0.001), were significant predictors.

Multivariate Cox Regression Analysis

Multivariate analysis of the OS and CSS among patients with PCBM presented in **Table 3** and **Figure 2**. Multivariable Cox regression analysis indicated that age (>60 years vs. ≤60 years, HR=1.193; 95% CI, 1.077-1.321; *p*<0.001), pathological type (Non-ductal adenocarcinoma vs. Ductal adenocarcinoma, HR=0.615; 95% CI, 0.549-0.688; *p*<0.001), systemic chemotherapy (No vs. Yes, HR=2.512; 95% CI, 2.277-2.771; *p*<0.001), liver metastasis (Yes vs. No, HR=1.414; 95% CI, 1.275-1.568; *p*<0.001), lung metastasis (Yes vs. No, HR=1.318; 95% CI, 1.198-1.450; *p*<0.001), and marital status(Others vs. Married, HR=1.150; 95% CI, 1.046-1.265; *p*=0.004) were independent prognostic factors for OS. In terms of CSS, age (>60 years vs. ≤60 years, HR=1.190; 95% CI, 1.072-1.320; *p*<0.001), pathological type (Non-ductal adenocarcinoma vs.

TABLE 3 | Multivariate Cox analysis of variables in pancreatic carcinoma bone metastasis.

Variable	OS		CSS	
	HR (95% CI)	*p*	HR (95% CI)	*p*
Age (years)				
≤60	1		1	
>60	1.193 (1.077-1.321)	0.001	1.190 (1.072-1.320)	0.001
Primary site				
Head of pancreas	1		1	
Body of pancreas	0.893 (0.765-1.043)	0.153	0.881 (0.752-1.033)	0.118
Tail of pancreas	1.029 (0.902-1.173)	0.673	1.032 (0.903-1.179)	0.647
Others	1.069 (0.949-1.205)	0.273	1.063 (0.942-1.201)	0.322
Pathological type				
Ductal adenocarcinoma	1		1	
Non-ductal adenocarcinoma	0.615 (0.549-0.688)	<0.001	0.606 (0.539-0.681)	<0.001
Radiotherapy				
Yes	1		1	
No	1.109 (0.997-1.234)	0.057	1.110 (0.996-1.237)	0.059
Chemotherapy				
Yes	1		1	
No	2.512 (2.277-2.771)	<0.001	2.537 (2.295-2.804)	<0.001
Liver metastasis				
No	1		1	
Yes	1.414 (1.275-1.568)	<0.001	1.401 (1.261-1.556)	<0.001
Lung metastasis				
No	1		1	
Yes	1.318 (1.198-1.450)	<0.001	1.302 (1.181-1.434)	<0.001
Marital status				
Married	1		1	
Others	1.150 (1.046-1.265)	0.004	1.134 (1.030-1.250)	0.011

Ductal adenocarcinoma, HR=0.606; 95% CI, 0.539-0.681; p<0.001), systemic chemotherapy (No vs. Yes, HR=2.537; 95% CI, 2.295-2.804; p<0.001), liver metastasis (Yes vs. No, HR=1.401; 95% CI, 1.261-1.556; p<0.001), lung metastasis (Yes vs. No, HR=1.302; 95% CI, 1.181-1.434; p<0.001), and marital status(Others vs. Married, HR=1.134; 95% CI, 1.030-1.250; p=0.011) were independent risk factors. Additionally, we drew Kaplan–Meier survival curves to visually show these independent prognostic factors. Patients with age ≤ 60 years were significantly associated with better outcomes (**Figure 3**). Patients with ductal adenocarcinoma type exhibited worse survival outcomes (**Figure 4**). Chemotherapy had a positive effect on prolonging the life of patients (**Figure 5**). Liver and lung metastases were associated with poor survival in patients with PCBM (**Figure 6**). Notably, longer OS and CSS were observed in married patients (**Figure 7**). The survival curves of patients in different groups decreased with time. In the first 20 months, the survival curve of patients in each group dropped rapidly.

DISCUSSION

Although treating PC has made remarkable progress over the past century, the prognosis remains poor mainly due to difficulties in its early diagnosis and metastasis (23). Bone metastasis represents an underappreciated site of metastasis among PC patients. As indicated in the present study, patients with PCBM experienced quite poor survival with 1-year OS and CSS rates of less than 15%. However, factors influencing their

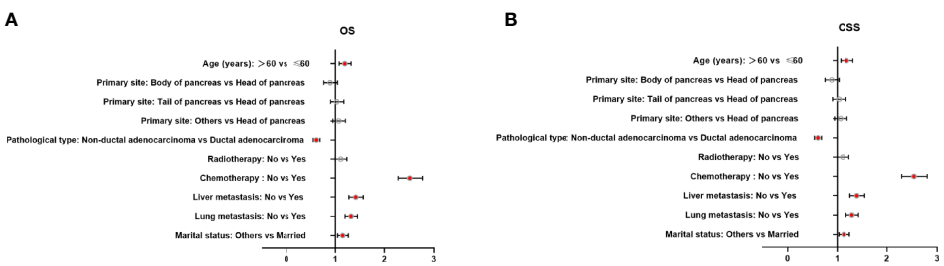

FIGURE 2 | Forest plots of the predictors of OS **(A)** and CSS **(B)** in patients with PCBM. (PCBM, pancreatic cancer bone metastasis; OS, overall survival; CSS, cancer-specific survival).

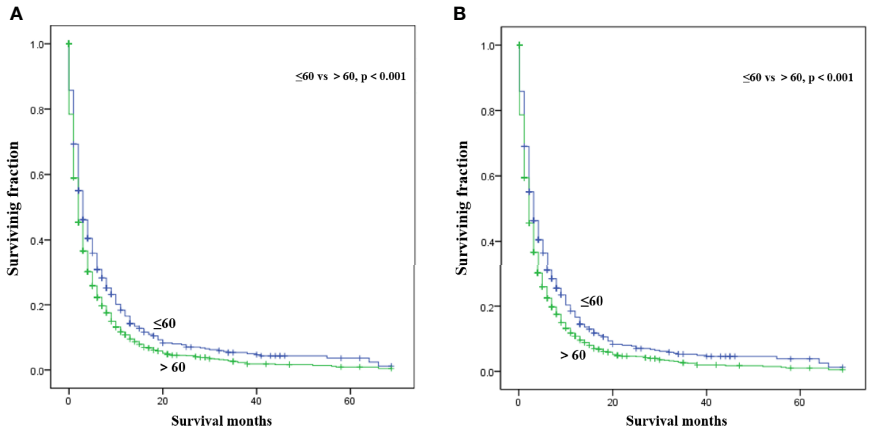

FIGURE 3 | Kaplan-Meier survival curves for estimating OS **(A)** and CSS **(B)** in patients with PCBM based on age.

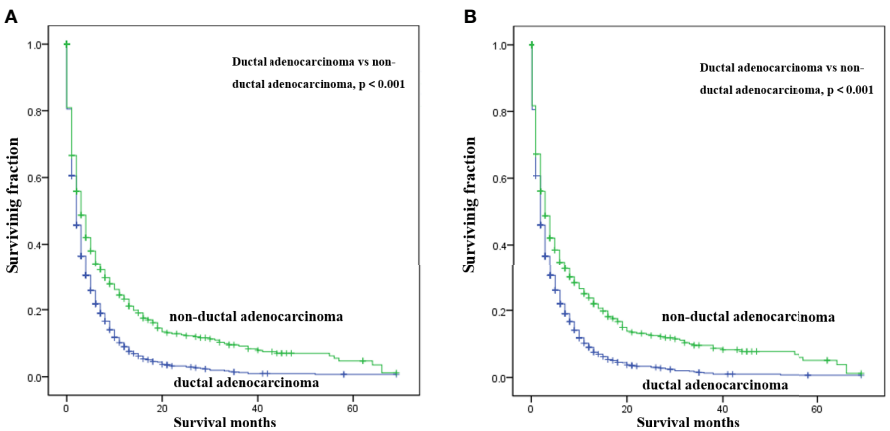

FIGURE 4 | Kaplan-Meier survival curves for estimating OS **(A)** and CSS **(B)** in patients with PCBM based on pathological type.

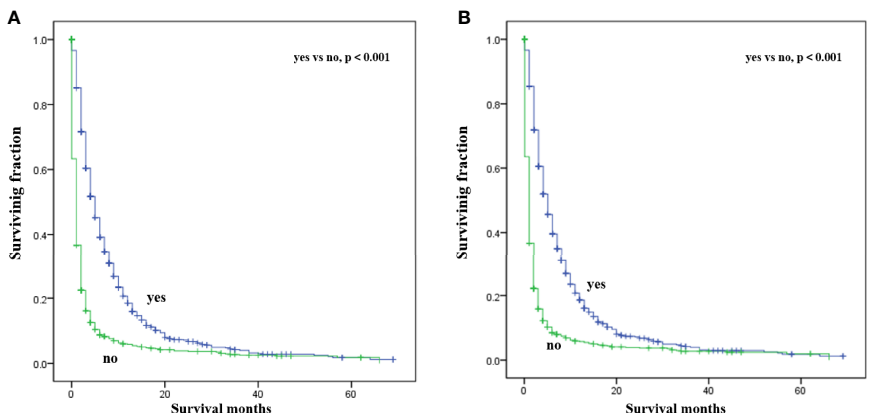

FIGURE 5 | Kaplan-Meier survival curves for estimating OS **(A)** and CSS **(B)** in patients with PCBM based on chemotherapy.

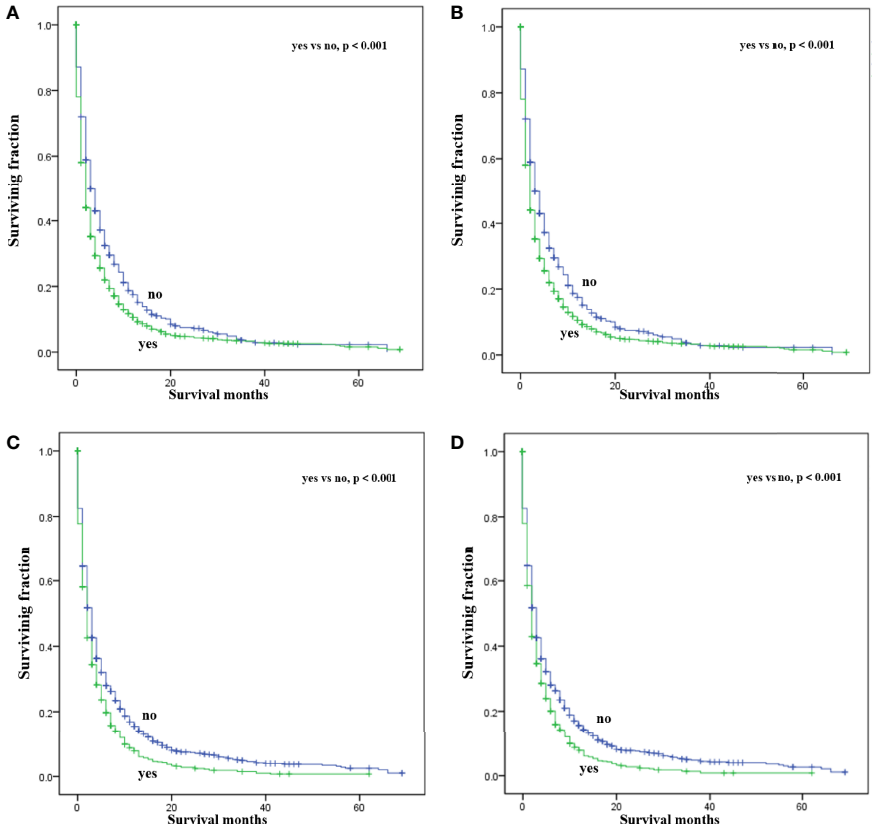

FIGURE 6 | Kaplan-Meier survival curves for estimating OS and CSS in patients with PCBM based on liver **(A, B)** and lung **(C, D)** metastasis.

survival remain poorly understood. Previous studies of metastatic PC have been limited by small sample sizes, lack of population-based data. To our knowledge, the present study is the first population-based analysis to explore the survival predictors for patients with PCBM.

In this observational study, age at diagnosis was proved to be an independent survival predictor for patients with PCBM, which was consistent with previous findings among all PC patients (24–26). Patients over 60 years old are generally considered the elderly. Based on previous literature (27, 28), we divided the patients' age into >60

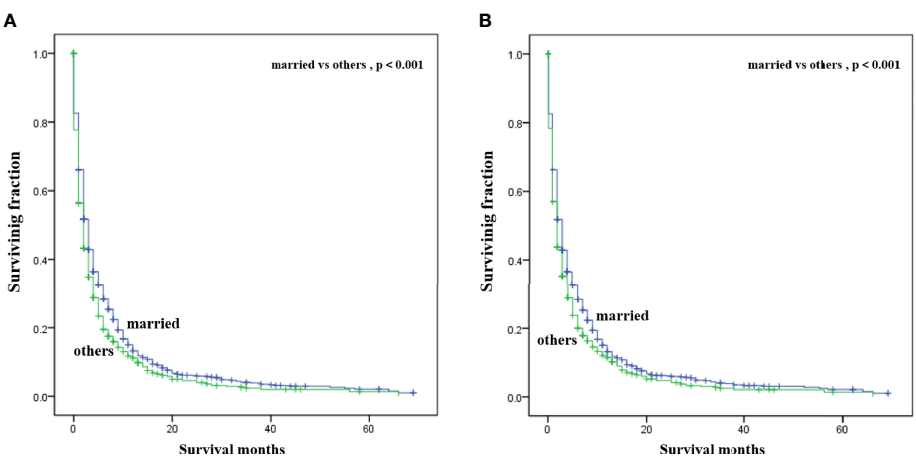

FIGURE 7 | Kaplan-Meier survival curves for estimating OS **(A)** and CSS **(B)** in patients with PCBM based on marital status.

years old and ≤60 years old for convenient analysis. Although some researchers reported tumor site was an independent survival predictor of PC (29–31), our multivariate Cox regression analysis showed that tumor site was not correlated with OS or CSS in patients with PCBM. For convenient analysis, patients' tumor size were divided into<5 and ≥5 cm based on previous literature (21, 28). However, univariate Cox regression analysis showed tumor size was not correlated with survival. Pancreatic ductal adenocarcinomas (PDACs) account for approximately 95% of all PC pancreatic cancers (32). In our study, ductal adenocarcinoma subtype (75%) also represented most histological subtype of patients with PCBM. Moreover, ductal adenocarcinoma subtype was an important independent predictor for worse CSS and OS of patients with PCBM. Maybe non-ductal tumors have unique morphology and biology that is distinct from that of ductal neoplasms of the pancreas (33). Further researches are needed to clarify its specific mechanism. Lung or liver metastasis worsens the prognosis of patients with PCBM, which were in line with previous studies on PC (34, 35). Interestingly, better prognosis was observed in married patients, which may be associated with family social support. Similar results were supported by other studies on PC patients (36, 37). In **Supplement Table 1**, we found that among married patients, the proportions of white patients, male patients, patients with age>60 years, patients undergoing surgery and chemotherapy were higher.

The impact of chemotherapy to increase survival of PCBM remains unknown. This retrospective data analysis using a large cancer database suggests that use of chemotherapy could improve survival in patients with PCBM. Additionally, chemotherapy can stabilize health-related quality of life and improve pain control among advanced PC patients (38, 39). As for radiotherapy, our study did not find its survival benefits for patients with PCBM. Surgery is the mainstay of treatment for non-metastatic PC patients (40). Due to the small number of patients with PCBM receiving surgery in the current study, we did not analyze the its effect on survival. Additionally, previous studies indicated that surgical resection of oligometastatic disease after PDAC might have benefit for prolonging survival (41–43). Thus, research efforts should focus on exploring the role of surgery in patients with PCBM in the future. In summary, this study provides support for the selection of clinical treatment for patients with PCBM.

Although the SEER database provides a large amount of clinical data, there are still many limitations in our research. First, we need to further conduct a follow-up clinical trial to verify this result. Second, the role of surgery on prognosis were not analyzed due to the small number of cases who received surgery. Finally, the performance status, lymph node metastasis, and CEA or CA19-9 levels, were not available in the SEER database, which need to be further studied.

CONCLUSION

Our population-based study showed that age ≤60, non-ductal adenocarcinoma type, chemotherapy, no liver metastasis, no lung metastasis, and married status were independent predictors for better OS and CSS, which may have implications for future clinical practice. However, further studies are warranted to validate these results.

DATA AVAILABILITY STATEMENT

The raw data supporting the conclusions of this article will be made available by the authors, without undue reservation.

ETHICS STATEMENT

Ethical review and approval was not required for the study on human participants in accordance with the local legislation and institutional requirements. Written informed consent for participation was not required for this study in accordance with the national legislation and the institutional requirements.

AUTHOR CONTRIBUTIONS

ZW conceived and designed the study. YR, SW, and BW collected the data. YR and SW performed the statistical analysis. YR wrote the manuscript. ZW and BW revised it. All authors read and approved the final manuscript.

FUNDING

This work was supported by the China Postdoctoral Science Foundation (2021M692792), National Natural Science Foundation of China (82103499), and Zhejiang Provincial Natural Science Foundation (LQ22H160040).

SUPPLEMENTARY MATERIAL

The Supplementary Material for this article can be found online at: https://www.frontiersin.org/articles/10.3389/fonc.2022.759403/full#supplementary-material

REFERENCES

1. Siegel RL, Miller KD, Jemal A. Cancer Statistics, 2018. *CA: Cancer J Clin* (2018) 68(1):7–30. doi: 10.3322/caac.21442
2. Deplanque G, Demartines N. Pancreatic Cancer: Are More Chemotherapy and Surgery Needed? *Lancet (Lond Engl)* (2017) 389(10073):985–6. doi: 10.1016/s0140-6736(17)30126-5
3. Ayres Pereira M, Chio IIC. Metastasis in Pancreatic Ductal Adenocarcinoma: Current Standing and Methodologies. *Genes* (2019) 11(1):6. doi: 10.3390/genes11010006
4. Hall BR, Cannon A, Atri P, Wichman CS, Smith LM, Ganti AK, et al. Advanced Pancreatic Cancer: A Meta-Analysis of Clinical Trials Over Thirty Years. *Oncotarget* (2018) 9(27):19396–405. doi: 10.18632/oncotarget.25036

5. He C, Huang X, Zhang Y, Lin X, Li S. The Impact of Different Metastatic Patterns on Survival in Patients With Pancreatic Cancer. *Pancreatol: Off J Int Assoc Pancreatol (IAP) [et al]* (2021) 21(3):556–63. doi: 10.1016/j.pan.2021.01.014
6. Tao L, Yuan C, Ma Z, Jiang B, Xiu D. Surgical Resection of a Primary Tumor Improves Survival of Metastatic Pancreatic Cancer: A Population-Based Study. *Cancer Manag Res* (2017) 9:471–9. doi: 10.2147/cmar.S145722
7. Tagawa T, Ito K, Fukuzawa K, Okamoto T, Yoshimura A, Kawasaki T, et al. Surgical Resection for Pulmonary Metastasis From Pancreatic and Biliary Tract Cancer. *Anticancer Res* (2017) 37(3):1413–6. doi: 10.21873/anticanres.11464
8. Zhou W, Wang D, Lou W. Current Role of Surgery in Pancreatic Cancer With Synchronous Liver Metastasis. *Cancer Control: J Moffitt Cancer Center* (2020) 27(1):1073274820976593. doi: 10.1177/1073274820976593
9. Morimoto D, Yamada S, Sonohara F, Takami H, Hayashi M, Kanda M, et al. Characteristics of Lung Metastasis as an Initial Recurrence Pattern After Curative Resection of Pancreatic Cancer. *Pancreas* (2020) 49(5):699–705. doi: 10.1097/mpa.0000000000001559
10. Hatfield DR, DeLand FH, Maruyama Y. Skeletal Metastases in Pancreatic Carcinoma: Study by Isotopic Bone Scanning. *Oncology* (1976) 33(1):44–7. doi: 10.1159/000225100
11. Borad MJ, Saadati H, Lakshmipathy A, Campbell E, Hopper P, Jameson G, et al. Skeletal Metastases in Pancreatic Cancer: A Retrospective Study and Review of the Literature. *Yale J Biol Med* (2009) 82(1):1–6.
12. Wu C, Jiang H, Chen J. A Systematic Review and Meta-Analysis About the Effect of Bisphosphonates on the Risk of Skeletal-Related Event in Men With Prostate Cancer. *Anti-cancer Agents Med Chem* (2020) 20(13):1604–12. doi: 10.2174/1871520620666200521114815
13. Hong S, Youk T, Lee SJ, Kim KM, Vajdic CM. Bone Metastasis and Skeletal-Related Events in Patients With Solid Cancer: A Korean Nationwide Health Insurance Database Study. *PloS One* (2020) 15(7):e0234927. doi: 10.1371/journal.pone.0234927
14. Howard LE, De Hoedt AM, Aronson WJ, Kane CJ, Amling CL, Cooperberg MR, et al. Do Skeletal-Related Events Predict Overall Survival in Men With Metastatic Castration-Resistant Prostate Cancer? *Prostate Cancer Prostatic Dis* (2016) 19(4):380–4. doi: 10.1038/pcan.2016.26
15. Saif MW, Galanina N, Ravage-Mass L, Kaley K, Cornfeld D, Lamb L, et al. Bone Metastasis as the Only Metastatic Site in a Patient With Pancreatic Cancer Following Distal Pancreatectomy. *Case Rep Med* (2010) 2010:634975. doi: 10.1155/2010/634975
16. Kang JS, Mok L, Heo JS, Han IW, Shin SH, Yoon YS, et al. Development and External Validation of Survival Prediction Model for Pancreatic Cancer Using Two Nationwide Databases: Surveillance, Epidemiology and End Results (SEER) and Korea Tumor Registry System-Biliary Pancreas (KOTUS-Bp). *Gut Liver* (2021) 15(6):912–21. doi: 10.5009/gnl20306
17. Zhang W, Xu L, Che X. Nomogram for Predicting the Prognoses of Patients With Pancreatic Head Cancer After Pancreaticoduodenectomy: A Population-Based Study on SEER Data. *Front Oncol* (2021) 11:766071:766071. doi: 10.3389/fonc.2021.766071
18. Liu X, Fu Y, Chen Q, Wu J, Gao W, Jiang K, et al. Predictors of Distant Metastasis on Exploration in Patients With Potentially Resectable Pancreatic Cancer. *BMC Gastroenterol* (2018) 18(1):168. doi: 10.1186/s12876-018-0891-y
19. Raufi AG, Manji GA, Chabot JA, Bates SE. Neoadjuvant Treatment for Pancreatic Cancer. *Semin Oncol* (2019) 46(1):19–27. doi: 10.1053/j.seminoncol.2018.12.002
20. Lin S, Liu C, Tao Z, Zhang J, Hu X. Clinicopathological Characteristics and Survival Outcomes in Breast Carcinosarcoma: A SEER Population-Based Study. *Breast (Edinburgh Scotland)* (2020) 49:157–64. doi: 10.1016/j.breast.2019.11.008
21. Wang Z, Cheng Y, Chen S, Shao H, Chen X, Wang Z, et al. Novel Prognostic Nomograms for Female Patients With Breast Cancer and Bone Metastasis at Presentation. *Ann Trans Med* (2020) 8(5):197. doi: 10.21037/atm.2020.01.37
22. Wang Z, Wu B, Zhou Y, Huang X, Pan W, Liu M, et al. Predictors of the Survival of Primary and Secondary Older Osteosarcoma Patients. *J Cancer* (2019) 10(19):4614–22. doi: 10.7150/jca.32627
23. Torphy RJ, Fujiwara Y, Schulick RD. Pancreatic Cancer Treatment: Better, But a Long Way to Go. *Surg Today* (2020) 50(10):1117–25. doi: 10.1007/s00595-020-02028-0
24. Exarchakou A, Papacleovoulou G, Rous B, Magadi W, Rachet B, Neoptolemos JP, et al. Pancreatic Cancer Incidence and Survival and the Role of Specialist Centres in Resection Rates in England, 2000 to 2014: A Population-Based Study. *Pancreatol: Off J Int Assoc Pancreatol (IAP) [et al]* (2020) 20(3):454–61. doi: 10.1016/j.pan.2020.01.012
25. Sugiura T, Okamura Y, Ito T, Yamamoto Y, Ashida R, Uesaka K. Impact of Patient Age on the Postoperative Survival in Pancreatic Head Cancer. *Ann Surg Oncol* (2017) 24(11):3220–8. doi: 10.1245/s10434-017-5994-0
26. Loveday BPT, Lipton L, Thomson BN. Pancreatic Cancer: An Update on Diagnosis and Management. *Aust J Gen Pract* (2019) 48(12):826–31. doi: 10.31128/ajgp-06-19-4957
27. Liu Y, Zhang P, Zhang Y, Zheng L, Xu W, Hou D, et al. Clinical Characteristics and Overall Survival Nomogram of Second Primary Malignancies After Prostate Cancer, a SEER Population-Based Study. *Sci Rep* (2021) 11(1):1293. doi: 10.1038/s41598-020-80534-4
28. Hu H, Wang Z, Zhang M, Niu F, Yu Q, Ren Y, et al. Clinicopathological Characteristics and Prognosis in Endometrial Cancer With Bone Metastasis: A SEER-Based Study of 584 Women. *Front Oncol* (2021) 11:694718:694718. doi: 10.3389/fonc.2021.694718
29. Zheng Z, Wang M, Tan C, Chen Y, Ping J, Wang R, et al. Disparities in Survival by Stage After Surgery Between Pancreatic Head and Body/Tail in Patients With Nonmetastatic Pancreatic Cancer. *PloS One* (2019) 14(12):e0226726. doi: 10.1371/journal.pone.0226726
30. Yadav S, Sharma P, Zakalik D. Comparison of Demographics, Tumor Characteristics, and Survival Between Pancreatic Adenocarcinomas and Pancreatic Neuroendocrine Tumors: A Population-Based Study. *Am J Clin Oncol* (2018) 41(5):485–91. doi: 10.1097/coc.0000000000000305
31. Chen J, Yang Y, Liu Y, Kan H. Prognosis Analysis of Patients With Pancreatic Neuroendocrine Tumors After Surgical Resection and the Application of Enucleation. *World J Surg Oncol* (2021) 19(1):11. doi: 10.1186/s12957-020-02115-z
32. Grossberg AJ, Chu LC, Deig CR, Fishman EK, Hwang WL, Maitra A, et al. Multidisciplinary Standards of Care and Recent Progress in Pancreatic Ductal Adenocarcinoma. *CA: Cancer J Clin* (2020) 70(5):375–403. doi: 10.3322/caac.21626
33. Dhillon J. Non-Ductal Tumors of the Pancreas. *Monogr Clin Cytol* (2020) 26:92–108. doi: 10.1159/000455737
34. Lianyuan T, Deyu L, Haibo Y, Yadong D, Guanjing T. Clinical Features and Prognostic Factors of Elderly Patients With Metastatic Pancreatic Cancer: A Population-Based Study. *Aging* (2021) 13(5):7133–46. doi: 10.18632/aging.202570
35. Ni X, Li D, Dai S, Pan H, Sun H, Ao J, et al. Development and Evaluation of Nomograms to Predict the Cancer-Specific Mortality and Overall Mortality of Patients With Hepatocellular Carcinoma. *BioMed Res Int* (2021) 2021:1658403. doi: 10.1155/2021/1658403
36. Zhou H, Zhang Y, Song Y, Tan W, Qiu Z, Li S, et al. Marital Status is an Independent Prognostic Factor for Pancreatic Neuroendocrine Tumors Patients: An Analysis of the Surveillance, Epidemiology, and End Results (SEER) Database. *Clinics Res Hepatol Gastroenterol* (2017) 41(4):476–86. doi: 10.1016/j.clinre.2017.02.008
37. Song W, Miao DL, Chen L. Nomogram for Predicting Survival in Patients With Pancreatic Cancer. *OncoTargets Ther* (2018) 11:539–45. doi: 10.2147/ott.S154599
38. Kristensen A, Vagnildhaug OM, Grønberg BH, Kaasa S, Laird B, Solheim TS. Does Chemotherapy Improve Health-Related Quality of Life in Advanced Pancreatic Cancer? A Systematic Review. *Crit Rev Oncol Hematol* (2016) 99:286–98. doi: 10.1016/j.critrevonc.2016.01.006
39. Laquente B, Macarulla T, Bugés C, Martín M, García C, Pericay C, et al. Quality of Life of Patients With Metastatic Pancreatic Adenocarcinoma Initiating First-Line Chemotherapy in Routine Practice. *BMC Palliat Care* (2020) 19(1):103. doi: 10.1186/s12904-020-00610-4
40. Heinrich S, Lang H. Neoadjuvant Therapy of Pancreatic Cancer: Definitions and Benefits. *Int J Mol Sci* (2017) 18(8):1622. doi: 10.3390/ijms18081622
41. Ilmer M, Schiergens TS, Renz BW, Schneider C, Sargut M, Waligora R, et al. Oligometastatic Pulmonary Metastasis in Pancreatic Cancer Patients: Safety and Outcome of Resection. *Surg Oncol* (2019) 31:16–21. doi: 10.1016/j.suronc.2019.08.010

42. Lopez-Lopez V, Robles-Campos R, López-Conesa A, Brusadin R, Carbonel G, Gomez-Ruiz A, et al. Surgical Resection of Liver Metastasis in Pancreatic and Periampullary Carcinoma. *Minerva Chir* (2019) 74(3):253–62. doi: 10.23736/s0026-4733.18.07972-5
43. Su BB, Bai DS, Yu JQ, Zhang C, Jin SJ, Zhou BH, et al. Can Patients With Pancreatic Cancer and Liver Metastases Obtain Survival Benefit From Surgery? A Population-Based Study. *J Cancer* (2021) 12(2):539–52. doi: 10.7150/jca.51218

Conflict of Interest: The authors declare that the research was conducted in the absence of any commercial or financial relationships that could be construed as a potential conflict of interest.

Publisher's Note: All claims expressed in this article are solely those of the authors and do not necessarily represent those of their affiliated organizations, or those of the publisher, the editors and the reviewers. Any product that may be evaluated in this article, or claim that may be made by its manufacturer, is not guaranteed or endorsed by the publisher.

Advantages of publishing in Frontiers

OPEN ACCESS
Articles are free to read for greatest visibility and readership

FAST PUBLICATION
Around 90 days from submission to decision

HIGH QUALITY PEER-REVIEW
Rigorous, collaborative, and constructive peer-review

TRANSPARENT PEER-REVIEW
Editors and reviewers acknowledged by name on published articles

Frontiers
Avenue du Tribunal-Fédéral 34
1005 Lausanne | Switzerland

Visit us: www.frontiersin.org
Contact us: frontiersin.org/about/contact

REPRODUCIBILITY OF RESEARCH
Support open data and methods to enhance research reproducibility

DIGITAL PUBLISHING
Articles designed for optimal readership across devices

FOLLOW US
@frontiersin

IMPACT METRICS
Advanced article metrics track visibility across digital media

EXTENSIVE PROMOTION
Marketing and promotion of impactful research

LOOP RESEARCH NETWORK
Our network increases your article's readership